Blood Platelet Behavior on Structured Substrates

- From Spreading Dynamics to Cell Morphology

Dissertation
for the award of the degree
"Doctor rerum naturalium"
of the Georg-August-Universität Göttingen
within the doctoral program
Göttingen Graduate School for Neurosciences,
Biophysics, and Molecular Biosciences (GGNB)
of the Georg-August University
School of Science (GAUSS)
submitted by

Rabea Sandmann

from Lemgo (Germany)

Göttingen, 2015

Thesis Committee:

Prof. Dr. Sarah Köster

Physics Department

Institute for X-Ray Physics

Georg-August-Universität Göttingen

Dr. Florian Rehfeldt

Physics Department

Third Institute of Physics - Biophysics

Georg-August-Universität Göttingen

Prof. Dr. Oskar Hallatschek

Max-Planck Institute for Dynamic and Self-Organization,

Department for Biological Physics and Evolutionary Dynamics

Members of the Examination Board:

Referee: Prof. Dr. Sarah Köster

Physics Department

Institute for X-Ray Physics

Georg-August-Universität Göttingen

2nd referee: Dr. Florian Rehfeldt

Physics Department

Third Institute of Physics - Biophysics

Georg-August-Universität Göttingen

Further members of the Examination Board:

Prof. Dr. Oskar Hallatschek

Max-Planck Institute for Dynamic and Self-Organization,

Department for Biological Physics and Evolutionary Dynamics

Prof. Dr. Andreas Janshoff

Chemistry Department

Institute for Physical Chemistry

Georg-August-Universität Göttingen

Prof. Dr. Detlev Schild

Department of Neurophysiology and Cellular Biophysics

University Medical Center Göttingen

Dr. Iwan Schaap

Physics Department

Third Institute of Physics - Atomic Force Microscopy

Georg-August-Universität Göttingen

Date of Oral Examination:

13.03.2015

Contents

Abbreviations, Definitions and Symbols

Abbreviations

BSA	bovine serum albumin	20
CCD	charge-coupled device	38
DMS	demarcation membrane system	7
FA	formaldehyde	36
FWHM	full width half maximum	38
HT buffer	HEPES Tyrode buffer	32
MCP	microcontact printing	27
NA	numerical aperture	38
OCS	open canalicular system	9
PBS	phosphate buffered saline	27
PDMS	poly(dimethylsiloxane)	16
PGE_1	prostaglandin E_1	33
PSG	PIPES-Saline-Glucose	32
ROI	region of interest	50
rpm	rotations per minute	24
WD	working distance	38

Most Important Definitions and Variables

patterned substrates	chemically patterned substrates
structured substrates	topographically structured substrates
relative perimeter	ratio of perimeter of the platelet to perimeter of an ellipse that has the same area, orientation and eccentricity as the platelet
$\vec{v}_{\text{cell-ellipse}}(\beta, t)$	vector between platelet outline and corresponding ellipse, with β being the angle it encloses with the x-axis and t the time point of the image in the time lapse series
$l_{\text{cell-ellipse}}(\beta, t)$	signed length of vector $\vec{v}_{cell-ellipse}(\beta, t)$
var_{dir}	variance between the moving average of signed lengths $l_{\text{cell-ellipse}}(\beta, t)$ in different directions
var_{time}	variance between the moving average of signed lengths $l_{\text{cell-ellipse}}(\beta, t)$ in time
adapted platelets (as defined in chapter 6)	platelets on structured substrates that show a mean var_{dir} of larger than $0.18\,\mu\text{m}^2$
unadapted platelets (as defined in chapter 6)	platelets on structured substrates that show a mean var_{dir} of smaller than $0.18\,\mu\text{m}^2$

1

Introduction

Blood platelets are life-saving for mammals, since they prevent excessive blood loss upon injury [80]. When attempting to close a wound platelets encounter differently structured substrates with length scales ranging from the nanoscale up to the macroscale, originating for example from exposed extracellular matrix proteins [49] or missing or partly destroyed cells. Not only the wounds themselves, but also artificial materials, *e.g.* implants that are placed inside the body present different structures to platelets [71]. With the emergence of new experimental techniques like photolithography [10, 82, 112] and microcontact printing [82], it is now possible to study the reaction of cells to topographically structured and chemically patterned substrates and this field has received growing interest [4, 26, 39, 50, 61]. The underlying mechanisms of topography sensing and cellular reaction are however very complex and thus cellular reaction to structured substrates is still not completely understood [61]. For platelets, the current scientific knowledge is more limited than for other cells concerning the influence of topographic features on cellular behavior, despite of accumulating evidence that different substrate cues, *e.g.* stiffness [76] or distribution of binding sites [25, 52], have a great impact on platelet behavior. In part this may be due to experimental difficulties such as the tiny size of platelets. Studies of platelet reaction to to-

pographical features of the substrates mostly focus on coarse-grained effects like number of adhering cells [51, 71, 115] or degree of activation [51, 71].
An example for such a study is shown in figure 1.1 where the influence of differently structured titanium surfaces on platelet adhesion is displayed. Park *et al.* [71] show in this study that the more structured a titanium surface is, the more platelets adhere. Thus, it is obvious that substrate topography has an effect on platelet behavior.

In order to deepen the understanding of platelet reaction to structured substrates, the studies carried out in the context of this thesis aim at investigating *single* platelet behavior on microstructured substrates. In these studies more global parameters like cell morphology, cell area and number of cellular protrusions as well as more local parameters like spreading dynamics at different positions and the dynamics of cellular protrusions are examined. Please note that we will use the term filopodium here to describe elongated thin cellular protrusions.
Chapter 2 briefly summarizes the existing literature and gives an overview about the function, formation and buildup of blood platelets. Furthermore, the role and emergence of cellular protrusions as well as current findings for cell spreading in general, and platelet spreading in particular are detailed. Finally, different techniques to topographically structure and chemically pattern substrates and the influence of patterned and structured substrates on cell behavior and especially on platelets are summarized.
Chapter 3 describes the experimental techniques used here to structure and coat substrates, isolate and stain platelets and image both fixed and non-fixed platelets. In order to analyze platelet behavior, several analysis methods have been developed and implemented. These methods are described in chapter 4. The results can be found in chapters 5, 6 and 7. These chapters also include a discussion of the findings with respect to existing literature and a discussion of the experimental techniques and analysis methods. Chapter 5 shows how the morphology of platelets is altered by the topography and the coating of the underlying substrate. In chapter 6 the question of how differences in spreading lead to the observed changes in cell morphology is examined further and chapter 7 details how cellular protrusions influence the spreading on structured substrates.
Finally, in chapter 8, the most important results are summarized, the implications for the understanding of cellular reaction to structured substrates and for implant design are detailed and experiments are proposed to examine the system under more physiological conditions as well as to test the influence of thrombin on the

system in more detail.

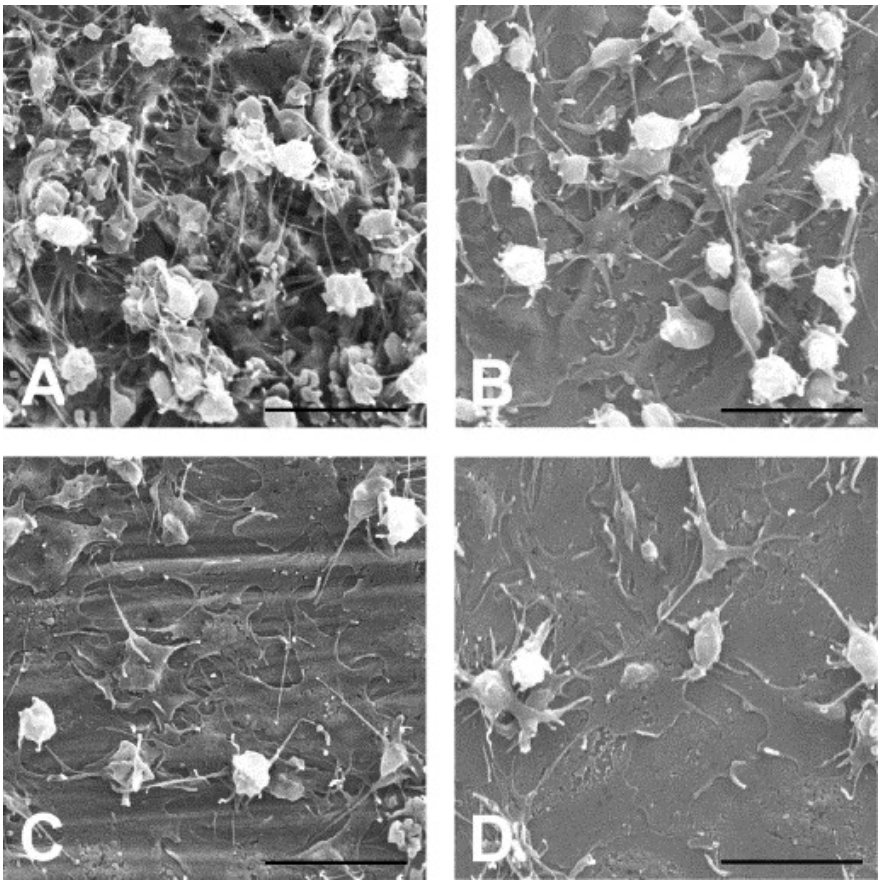

Figure 1.1.: Scanning electron micrographs showing blood platelet reaction to differently structured titanium. The scale bars indicate $6\,\mu$m.
(A) Dual acid-etched titanium is highly structured and shows higher levels of platelet adhesion than the substrates shown in (C) and (D).
(B) 320 grit abraded titanium is less structured than dual acid-etched but more structured than machined (C) or polished (D) titanium. Levels of platelet activation are higher than on substrates shown in (C) and (D).
(C) Machined titanium is less structured than the substrates presented in (A) and (B) and fewer platelets attach to it.
(D) Polished titanium is least structured and shows less platelet adhesion than the structures presented in (A) and (B).
Information given in this caption has been obtained from [71].
With permission from J.Y. Park, C.H. Gemmell, J.E. Davies, Platelet interactions with titanium: modulation of platelet activity by surface topography, Biomaterials, Vol. 22, pp. 2671-2682. [71] Elsevier, 2001.

2

State of the Art

In instances where the following references [9, 38, 44, 47, 59, 108] are cited, note that the citation also refers to references in those chapters.
In the following, the term *patterned substrate* describes a substrate that is chemically patterned while the term *structured substrate* signifies that the substrate is topographically patterned.
In sections 2.3.1, 2.2 and 2.5 spreading, filopodia and lamellipodia formation and the role of lamellipodia/filopodia as well as the cellular reaction to structured and patterned substrates are described in general. Although the results presented in these sections have not been obtained studying blood platelets, most of them are likely applicable to blood platelets. In the sections 5.1, 6.1 and 7.1 similarities and differences between results for other cell types and the ones obtained in this work for blood platelets are discussed. This enables us to show general aspects of cell spreading on microstructured substrates while also pointing out in which aspects blood platelets are special.

2.1 Function, Origin and Buildup of Blood Platelets

2.1.1 Function of Blood Platelets

Quiescent human blood platelets are discoid [44] with a diameter of about $2.0 - 5.0\,\mu$m[i] and a thickness of about $0.5\,\mu$m [108]. Human blood platelets lack a nucleus [59]. During their short lifespan of about 7 to 10 days [108] the blood platelets play an important role in hemostasis [80]. Due to their size and shape, blood platelets flow close to the vessel walls in the blood stream [44]. Platelet reaction can be triggered by exposed proteins on vessel walls like linearized von Willebrand factor that is bound to collagen but also soluble factors can cause platelets to leave their quiescent state [44]. One of the activators of blood platelets is thrombin [11]. When platelets leave their quiescent state, they first bind to the surface, then they spread and thus cover the damaged surface [44]. Furthermore, platelets are able to attract other platelets by secreting chemicals, forming filopodia and by recruiting more and activating receptors on their plasma membrane [44]. Individual platelets covering the wounded site are then cross-linked by fibrinogen [9]. A sketch of the different steps of blood clot formation is shown in figure 2.1.

2.1.2 Origin of Blood Platelets

In the previous section the importance of platelets in hemostasis is discussed. In this section the formation of blood platelets is explained.
In mammals, blood platelets originate from polyploid precursor cells - the megakaryocytes [59]. Several models have been suggested in order to explain platelet formation by megakaryocytes [47]. The outline of the models follows the description in [47].
Megakaryocytes arise from hematopoietic stem cells, which in adults are mostly situated in the bone marrow [47]. Since megakaryocytes can also translocate from the bone marrow into the blood stream, platelet formation is speculated to not only take place in the bone marrow but also among other places in the blood or in the lungs [47].
Preceding to platelet production, megakaryocytes undergo several cycles of DNA replication [47]. This DNA replication, however, takes place during a process termed endomitosis and is not accompanied by cell divisions [47]. The increased amount of DNA is thought to help the megakaryocytes to increase their protein

[i] As described in section 2.1.2 the larger platelets may also be pre-platelets.

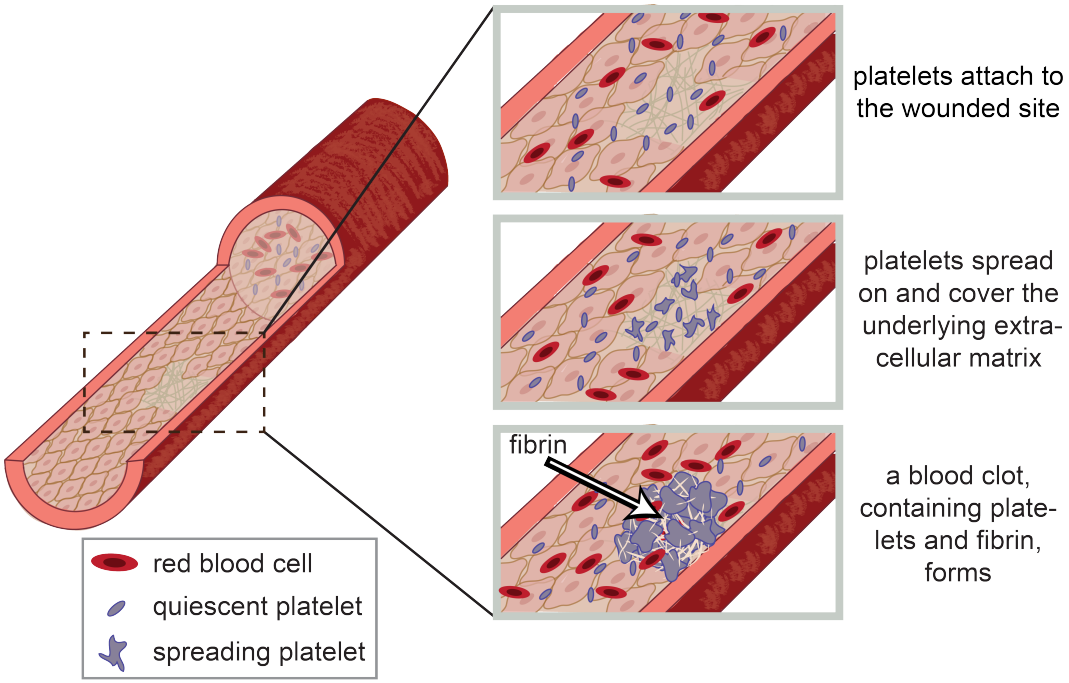

Figure 2.1.: Sketch of different steps of blood clot formation.
(left) Sketch of an injured blood vessel.
(right) More detailed view of the injured vessel wall and the attachment of platelets to the wounded site (upper), spreading platelets (middle) and the formed blood clot (lower).
The sketch builds on general details of hemostasis as described in [23, 44].

synthesis and to grow [77]. The cytoplasm of megakaryocytes contains proteins, organelles and membrane systems that are passed on to platelets [47]. One of these membrane systems is the demarcation membrane system (DMS), which is thought to supply the cells with further membrane material needed in the process of platelet formation [47]. The DMS is the basis of one of the model that explains the process of platelet formation [47]. This model suggests that the cytoplasm of megakaryocytes fragments along the membrane lines provided by the DMS [47]. However, several findings argue against this theory: the domains separated by the DMS do not show the distinct microtubule coils[ii] found at the periphery of platelet cytoplasm and platelet production through fragmentation along the DMS lines has never been shown directly [47]. A second model suggests blebbing of megakaryocytes as a mechanism for platelet formation [47]. However, the blebs lack the organelles found in platelets [47].

[ii]The buildup of platelets including the circumferential microtubule coil present in quiescent platelets will be described in section 2.1.3.

The third model is based on the observation that megakaryocytes can form thin cytoplasmic protrusions (the so-called proplatelets) which are suggested to be precursors of platelets [47]. Studies have shown these protrusions extending through gaps in the endothelial lining of blood vessels in the bone marrow from where they are speculated to be released into the blood stream [47].
Formation of platelets from megakaryocytes through proplatelets *in vitro* has been shown by Italiano jr. *et al.* [48]. In this process megakaryocytes transform into a great number of proplatelets whose final appearance is that of beads interspersed by thin strands of cytoplasm [48]. In the final stage of proplatelet production, the megakaryocyte retracts, which frees proplatelets from the remaining cell body [48]. The end of a proplatelet is formed like a teardrop and comprises a microtubule coil [48]. As this coil is similar to the one found in blood platelets, platelets are thought to be formed at the ends of proplatelets [48].
In vitro, an intermediate form between platelets and proplatelets has been recognized and termed preplatelet [95]. These preplatelets have been shown to backconvert to proplatelets in an *in vitro* mouse model [95]. The fission into platelets is thought to be at least partly due to shear forces since shear forces *in vitro* accelerate release of platelets from proplatelets [95].
Experiments with human blood cells have shown that platelets stored *ex vivo* can generate new platelets which seem to be identical in appearance and behavior to normal platelets [89]. The generation of new platelets takes place with an increase in volume, protein content and increased protein synthesis in the parent platelets [89]. During storage, platelets occasionally form proplatelet-like structures of two or several platelet-sized swellings being interconnected by thin cytoplasmic parts [89]. These thin cytoplasmic parts fracture easily during pipetting or centrifugation [89]. The break-down of this cytoplasmic connection is thus speculated to lead to conversion into single platelets by shear stresses in the blood stream and by this indicate an ongoing platelet production in the blood stream [89].
The upper diameter of platelets is thought to be the diameter at which the preplatelets are not able to undergo the transition from preplatelet to proplatelet anymore and thus cannot divide any longer into single platelets [96]. By analysis of human platelet-rich plasma, platelets were found to have a diameter of about $1.5 - 3\,\mu$m (quiescent) while preplatelets were found to have a diameter of about $3 - 10\,\mu$m [96].
Since proplatelets have been found in the blood [96] and direct evidence of megakaryocytes extending proplatelets into the blood vessels has been provided [47],

platelet production via proplatelets seems the most promising explanation.

2.1.3 Buildup of Blood Platelets

In section 2.1.1 the size and shape of quiescent blood platelets are described. Here, the buildup of quiescent and activated platelets is described in more detail. A sketch of the general buildup of quiescent platelets as described here is shown in figure 2.2.

The plasma membrane of a quiescent platelet appears wrinkled and additionally has several small openings which result from an internal membrane system called open canalicular system (OCS) [109]. The OCS is composed of invaginations of the plasma membrane and is thought to be responsible for both uptake of substances from the blood plasma and release of substances into the blood plasma [105]. Furthermore, the OCS provides additional membrane for spreading by evagination [107]. The wrinkled plasma membrane of platelets also comprises additional membrane that can be used for spreading [109]. During complete spreading, the exposed surface area of a platelet can enlarge up to 420 % [108].

Attachment of platelets to substrates is achieved by proteins in the plasma membrane [108]. One protein in the plasma membrane of platelets, which is important for our studies, is the glycoprotein GPIIb-IIIa (also known as integrin αIIbβ3) capable of binding fibrinogen [108]. It has been shown by binding of fibrinogen-coated gold particles to GPIIb-IIIa that GPIIb-IIIa can move into the channels of the OCS in early spreading cells (dendritic) while in completely spread cells the receptors move to the cell center [108]. However, there are indications for a nearly endless number of GPIIb-IIIa receptors [106]. The mobility of GPIIb-IIIa receptors is thought to be important for spreading, since the GPIIb-IIIa/fibrinogen-complexes are rather immobile [108]. Thus, the receptors will have to move in the plasma membrane and the OCS-channels to allow for spreading without breaking the connections between fibrinogen and GPIIb-IIIa [108]. A spectrin-based skeleton is situated directly underneath the plasma membrane [44] and is connected to the actin cortex [41].

Inside the actin cortex lies a circumferential microtubule coil consisting of several loops of microtubuli [44, 108]. Recently, it has been shown by Diagouraga *et al.* [30] that the microtubule coil is extended during platelet activation which is thought to result from dyneins moving the microtubuli apart. Induced by the coiling of the microtubuli coil, the platelets obtain a spherical form typical for activated platelets [30]. Tension exerted by actomyosin elements compresses the coil

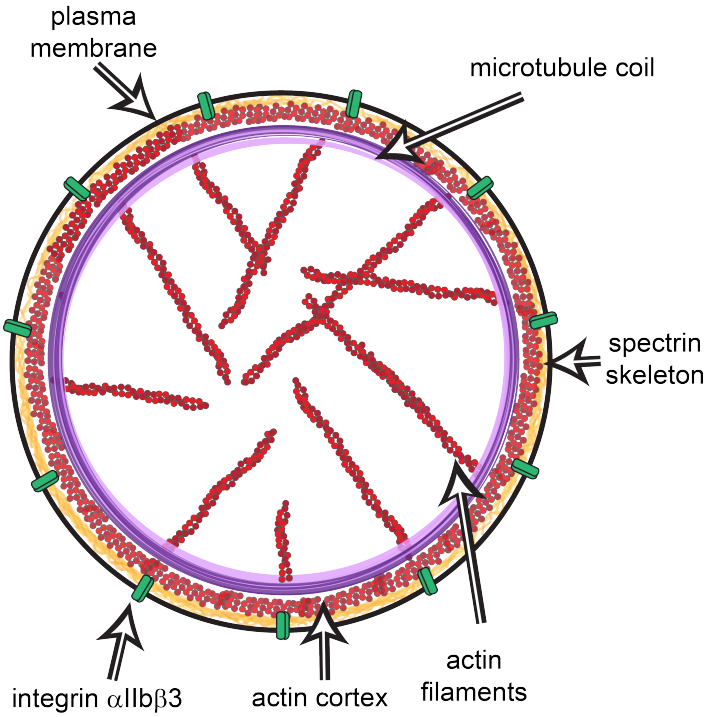

Figure 2.2.: Sketch of the buildup of a quiescent platelet. This sketch and caption are based on the descriptions of the platelet cytoskeleton in [44].
The platelet is composed of a plasma membrane (shown in black) that comprises membrane proteins like integrin αIIbβ3 (green). Underneath this plasma membrane lies a spectrin-skeleton (orange) that is connected to the actin cortex (red). Still further inside lies a microtubule coil (purple) and actin filaments (red) fill the cytoplasm of the platelet.

and polymerization of new microtubuli leads to a smaller microtubule ring [30]. Beneath the microtubule coil, a network of actin filaments is situated which runs through the cytoplasm of the quiescent platelet [44]. While the platelet is quiescent, approximately 40 % of the actin is polymerized [40]. The changes the actin skeleton undergoes during spreading are detailed in section 2.3.2.
Platelets contain myosin in the form of nonmuscle myosin IIA and IIB and most likely also other nonfilamentous myosin types [44]. The function of myosin in platelets includes force generation to contract the blood clot [24, 44] as well as maintenance of morphology during spreading [13]. Formation of holes has been observed in platelets spreading on collagen caused by addition of Y27632 or blebbistatin and thus inhibiting ROCK or myosinII, respectively [13]. ROCK inhibits myosin light chain phosphatase and thus activates myosinII [13].
Additionally, platelets contain a few mitochondria, which are involved in the energy metabolism and secretory organelles [108]. Platelets display some heterogeneity both in their size (see also section 2.1.1) as well as in their granule content [44].

2.2 Filopodia and Lamellipodia Formation

In figure 2.3 an electron microscopy image (taken from [113], for copyright notice see figure caption) of the actin cytoskeleton is shown depicting the buildup of lamellipodia and filopodia.

Lamellipodia play an important role, *e.g.* in cell spreading, migration and adhesion formation [90] while filopodia are known to sense the extracellular environment [8].

In keratinocytes, filopodia have also been shown to play a role in the formation of adhesion sites [85]. Focal adhesions are located behind[iii] stable filopodia, whereas no focal adhesions are located behind unstable filopodia [85]. Schäfer *et al.* [85] suggested that filopodia search for binding sites on the substrates and upon finding them establish adhesion complexes. When the lamellipodium reaches these adhesion complexes they grow and become focal adhesions [85].

Whether filopodia or lamellipodia are formed by a cell is thought to depend on the presence or absence of proteins that cap actin filaments or stimulate elonga-

[iii] *i.e.* further inside of the cell

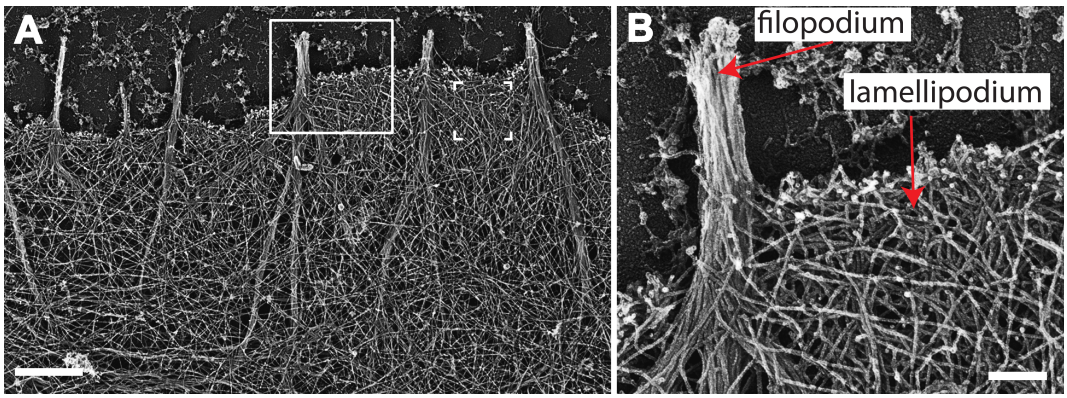

Figure 2.3.: Platinum replica electron microscopy image of the actin cytoskeleton in B16F1 mouse melanoma cells. A branched network of actin can be seen in lamellipodia and the protruding filopodia show bundles of long actin filaments. The image shown in B comprises a magnification of the region marked with a box in A and the scale bars indicate $1\,\mu$m in A and $0.2\,\mu$m in B. Information given in this caption have been obtained from [113]. The image has been cropped from the original image to show only the panels A and B and a filopodium as well as a lamellipodium have been marked by arrows. The image has been reproduced from Yang *et al.* (2007), Novel roles of formin mDia2 in lamellipodia and filopodia formation in motile cells. PloS Biology, 5(11): e317. doi: 10.1371/journal.pbio.0050317 [113], Copyright (2007) Yang *et al.* The article is open-access under the terms of the Creative Commons Attribution License (CC By).

tion [63]. Mejillano *et al.* [63] suggested that the capping protein regulates whether filopodia or lamellipodia are being formed with capping protein depletion inducing increased filopodia formation. Ena/VASP[iv] is essential for filopodia formation when capping protein is depleted, since lack of Ena/VASP leads to ruffling instead of filopodia formation [63]. It is hypothesized that more involvement of capping protein leads to formation of shorter filaments in a branched network, whereas less capping protein involvement leads to longer filaments and with the help of Ena/VASP to filopodia [63]. However, also other proteins are thought to be involved in the competing formation of filopodia and lamellipodia [5]. Bilancia *et al.* [5] found that Ena (Enabled) and Dia (Diaphanous, a formin) together regulate filopodia formation. Ena forms short, more dynamic filopodia while Dia leads to longer filopodia with longer lifetimes [5]. Thus, it is proposed that Dia is regulated by Ena, since localization of both Ena and Dia in the tips of filopodia leads to retraction, back folding or resting of filopodia [5]. This interaction is assumed to help the cells changing their protrusions from filopodia to a mixture of lamellipodia and filopodia [5].

Tsygankov *et al.* [97] have recently described a software to detect the tips of filopodia and analyze filopodia behavior as well as examine the movement of the cell body excluding the filopodia. The program named *CellGeo* describes cell outlines by a tree graph [97]. This tree graph originates at the cell center and extends branches to convex and concave edges on the cell outline [97]. The tips of filopodia can then be detected by finding the local maxima of the lengths of the branches and the bases are found by assigning a maximal width to the filopodia [97]. Additionally, filopodia are tracked by computing the distances of all points on the branches inside the filopodium to those in the successive frame [97]. Thus, the tracking does not rely only on the position of the tip [97]. If no precursor of a filopodium can be found, the program searches for precursors in preceding frames [97]. By excluding the points belonging to filopodia from the whole cell outline, the cell body is defined and its dynamics can be described by comparing the positions of cell outlines over time [97].

[iv] Ena/VASP proteins attach to barbed ends (+-ends) of actin filaments, counteract capping by CapZ, bind profilin and diminish the density of filaments originating by Arp2/3 branching [55].

2.3 Molecular Details and Mechanisms of Spreading

2.3.1 General Aspects and Possible Mechanisms of Cellular Spreading

In this section, possible mechanisms for cellular spreading, which may be applicable to our findings, are detailed. However, there are many more models existing in the literature which are not discussed here for the sake of clarity.
The findings described below have been obtained in studies of spreading of immortalized embryonic mouse fibroblasts and show that actin polymerization at the outer edge of the cell and rearward actin movement govern spreading [31, 42, 43]. It has been shown for several cell types that actin polymerization occurs predominantly near the cell membrane while the actin network inside lamellipodia moves rearward [75, 101, 102]. Furthermore, the speed of protrusion of the cell's outer edge shows a negative correlation with the rate of rearward actin movement [14]. Giannone *et al.* [42] and Dubin-Thaler *et al.* [31] found two different spreading behaviors in immortalized embryonic mouse fibroblasts which, however, have no influence on the final cell area or final morphology [31]. Anisotropic spreading in fibroblasts involves filopodia, while isotropically spreading fibroblasts show no filopodia [42]. Furthermore, in isotropically spreading fibroblasts little or no membrane ruffling is observed, while anisotropically spreading fibroblasts do show membrane ruffles [31]. The speed of actin rearward movement increases for isotropic spreading when the cell has nearly completely spread [31]. For anisotropic spreading the speed of actin rearward movement is at a constant high level (similar to that of isotropic spreading at the endphase of spreading) from the onset of spreading [31]. Furthermore, there are indications for a non-constant actin polymerization [31]. Thus, protrusion of the cell edge is thought to be dictated by the speed of actin polymerization and the speed of rearward movement of the actin network [31].
Isotropic spreading for the same cell type shows a three-phased spreading behavior [42]. In the beginning, fibroblasts spread fast at a constant rate that decreases in the second spreading phase [42]. During the second phase, the fibroblasts show periodic interruptions/retractions and the next and last phase is characterized by either a transition to anisotropic spreading behavior or maintenance of isotropic spreading [42]. The periodic interruptions/retractions are explained by an increase in rearward actin movement [42]. Thus, Dubin-Thaler *et al.* [31] and Giannone *et al.* [42] showed that differences in actin rearward movement can account

for different spreading behaviors in one cell type.
A mechanism to explain periodic retractions as well as membrane ruffling in spreading was proposed by Giannone *et al.* [43]. In this proposed mechanism, myosin activity leads to a rearward force (towards the cell center) being applied on the lamellipodium [43]. These forces lead to upwards bending of the lamellipodium as well as formation of adhesion sites at the lamellipodial tip [43]. Subsequently, the lamellipodium detaches from the plasma membrane leaving the machinery for actin polymerization in place [43]. Thus, newly polymerizing actin can reconstitute the lamellipodium network [43]. A new cycle of edge retraction can be initiated by the rearward moving actin in the lamellipodium that reaches the myosin in the back of the lamellipodium [43]. In contrast, membrane ruffling occurs when no or not stable enough adhesions can be formed during force application on the lamellipodium leading to detachment of the cell from the substrate [43].

2.3.2 Details of Spreading in Platelets

When a platelet spreads on a surface, its discoid shape is first converted into a rounded/spheroid shape [44]. Further spreading includes filopodia or is conducted simply with lamellipodia [2]. The authors (Allen *et al.* [2]) used the termini pseudopodia and hyalomer, respectively. However, from the description they gave and the images they provided hyalomers are most likely lamellipodia and pseudopodia are most likely filopodia. They also stated that hyalomers resemble lamellipodia in their dynamics [2]. Thus, the terms filopodia and lamellipodia will be used in the following instead of pseudopodia and hyalomer.
Different types of spreading have been described for platelets seeded on siliconized glass at 29° C [2]. For platelets spreading via contribution of filopodia, the filopodia extend before the onset of lamellipodial spreading in between the filopodia [2]. The lamellipodium can also extend laterally from an extended filopodium [2]. Spreading via lamellipodia is achieved by outwards spreading of these lamellipodia which either occurs symmetrically or asymmetrically [2]. Filopodia are not needed for spreading via lamellipodia [2]. Furthermore, a single platelet can display more than one of these types of spreading in different regions of its periphery [2]. Platelet spreading on siliconized glass is accomplished within as little as $10 - 12$ minutes and seldomly takes more than 30 minutes [2]. On smooth glass coverslips covered with fibrinogen, filopodia are observed to develop spatially isotropic for murine platelets [56]. Spreading is achieved via polymerization of

actin filaments [44, 100] which is driven by either uncapping of barbed ends of existing actin filaments [44] or by nucleation via Arp2/3 [36]. In activated platelets $60 - 85\,\%$ of the total actin content is integrated into the cytoskeleton [17]. The role of the wrinkled plasma membrane of quiescent platelets and of the OCS in spreading has been detailed above (section 2.1.3).
During spreading the platelet becomes flat and granules as well as organelles are translocated to the cell center [44]. The extended lamellipodia can then ruffle and retract [2, 44] and filopodia emerge from the center of the cell [44]. Lamellipodia are filled with a dense network consisting of actin filaments that are about $0.5\,\mu$m long [44] and in a completely spread platelet the lamellipodium is only $50 - 100$ nm thick [2]. Filopodia consist of bundles of long actin filaments [44] and contain microtubuli [44, 73].
Park *et al.* [72] examined platelet area over time for spreading on fibrinogen-coated glass at room temperature. In this study, platelets reach an area of about $50\,\mu\text{m}^2$ after approximately 1 hour of spreading [72]. Additionally, they examined platelet circularity and showed that at low fibrinogen concentrations of smaller than $0.16\,\mu\text{g/cm}^2$ circularity depends on fibrinogen concentration whereas for higher concentrations the area of platelets is elevated and the circularity stays constant [72]. Lee *et al.* [56] investigated spreading of murine blood platelets on fibrinogen coated glass coverslips. This spreading shows a fast first, isotropic spreading phase that lasts about 2 minutes [56]. Thereafter, spreading slows down and is thought to be accompanied by formation of stable adhesions [56].
PAR4 is a thrombin receptor [11]. If this thrombin receptor is activated, platelets start spreading nearly instantaneously upon contact with the surface and filopodia only persist for 4 minutes after the onset of spreading while lamellipodia form during the whole spreading process [56]. These findings indicate a spreading via lamellipodia upon activation of PAR4 [56]. The onset of lamellipodia formation depends on the amount of fibrinogen on the substrate with more fibrinogen ($100\,\mu$g/ml compared to $1\,\mu$g/ml) leading to faster lamellipodia formation [56]. Without activation of PAR4 the number of filopodia is increased to about 5 compared to about 2 with receptor activation [56]. The duration of filopodia formation is increased if PAR4 is not activated and the filopodia number reaches a plateau after about 4 minutes [56]. Spreading speed seems to be neither influenced by the protein coating of coverslips nor by activation of PAR4 [56]. However, the shape changes of platelets seem to be influenced by fibrinogen, since additional fibrinogen coating on dimethyldichlorosilane coated glass leads to decreases in

circularity which are not seen without fibrinogen coating [72].
While platelets spread on fibrinogen coated surfaces, they can interact with the fibrinogen and redistribute it with thrombin accelerating this redistribution [37]. It was observed by Feuerstein *et al.* [37] that platelets shrink after they have reached their maximal area and that the regions of the redistributed fibrinogen have a size resembling the maximal platelet area.
Newly arrived platelets which only attach to other already spread platelets but not the underlying substrate, i.e. coverslip, extend filopodia until these filopodia come in contact with the substrate and subsequently start to spread on the substrate [2]. The lamellipodia of neighboring platelets in contact with the substrate often show an overlap but spreading is not hindered [2].

2.4 Microstructuring and Micropatterning Surfaces

Several lithographic techniques are available to structure substrates in the micro- and nanometer range [112]. One of these techniques is photolithography in which a layer of photoresist is patterned by selective exposure [10, 82, 112]. The photoresist is deposited on a substrate via spincoating and then baked to evaporate remaining solvent [10, 82] and consolidate the resist layer [10]. Afterwards, the resist is exposed through a mask using UV light [82]. Thereafter, the sample is developed [10, 82] and baked again to further consolidate the resist, harden the resist or increase the attachment to the underlying substrate [10]. Smaller structures can be created employing extreme UV light, soft X-rays, electrons, ions or proximal probe lithography [112]. Starting from an already patterned elastomer several other techniques can be employed to either pattern or structure a substrate [112]. Patterning can be achieved using microcontact printing [82, 112] in which a stamp is soaked with material that will be transferred onto a substrate [82]. The surface that shall be patterned has to be energetically favorable over the stamp for the transfer to take place [82]. Liang *et al.* [60] patterned an array of poly(dimethylsiloxane) (PDMS) posts with fibrinogen by ozone treatment of the posts.
In order to structure a substrate by an already patterned elastomer (*e.g.* PDMS) substrate, different micromolding techniques can be used [112]. For the molding, prepolymers are filled into the elastomer stamp and cured by UV light or heat [112]. Before curing, the elastomer/prepolymer-sample can be placed onto a substrate so that the mold later on is directly attached to the substrate [112].

Attachment of the mold to a substrate can also be achieved by exploiting capillary forces and thus filling channels between substrate and elastomer with prepolymer and then curing the prepolymer [112]. Finally, thermoplastic polymers can also be structured by pressing a stamp into the polymer that has been softened by heat [112]. This technique is called embossing [112].

2.5 Cell Reaction to Micro-Patterned and Micro-Structured Substrates

On micropatterened substrates and on topographically structured substrates, it has been observed that cells can span non-adhesive regions and indentations, respectively (for micropatterned substrates: *e.g.* [6, 52, 81]; for microstructured substrates: *e.g.* [22, 69, 91]). Rossier *et al.* [81] examined the underlying mechanisms of this behavior further by characterizing cellular bridges that are formed by immortalized mouse embryonic fibroblasts over non-adhesive regions between micropatterned stripes of protein. Fibroblast spreading over adhesive areas is enhanced but spreading also occurs over non-adhesive areas [81]. Focal adhesions are only present at adhesive regions and are concentrated at the edges of adhesive stripes [81].
After the first, fast spreading phase, myosin II caused contraction is initiated and induces retraction over non-adhesive regions thus leading to concave shaped cell edges [81]. Area growth is afterwards achieved by alternating protrusions and contractions with bridges extending when the fibroblasts spread further on adhesive regions [81]. During further spreading, ruffling can be observed over non-adhesive regions [81]. Cellular bridges are thought to be maintained by ongoing assembly of actin and myosin filaments at focal adhesion sites and subsequent movement of actin and myosin filaments towards the non-adhesive regions [81]. However, for the initial spreading over adhesive as well as non-adhesive regions myosin II does not seem to be crucial, as myosin inhibition does not block intial spreading [81]. Interestingly, 3T3 fibroblasts spanning an array of grooves and ridges [91] show similar morphologies as described by Rossier *et al.* [81] on micropatterned substrates. Furthermore, Rossier *et al.* [81] showed that fibroblasts on lines of PDMS pillars display bridges with the same morphology as on micropatterned substrates. Thus, the mechanism of cellular bridge formation as described by Rossier *et al.* [81] is transferable to structured substrates.
Lim and Donahue [61] pointed out that chemical patterns also present a topographical pattern to the cells, as the protein layers also have a certain height.

Charest *et al.* [19] and Britland *et al.* [12] examined whether micropatterns or microtopographies determine cell behavior. Alignment to both micropatterned lanes as well as ridges and grooves can be seen when pattern and topography are presented individually to MC3T3-E1 osteoblast-like cells [19]. When lanes are printed perpendicularly to the ridges on topographically structured substrates and thus result in no patterns at the bottom of the grooves, the cells align to the underlying topography rather than to the micropattern [19]. However, when micropatterned lines also extend to the grooves the alignment of BHK21 C13 cells is dominated by the direction of the micropattern except for very narrow and deep grooves (5 μm width, 6 μm depth) [12]. When the topography as well as micropattern are oriented in the same direction, the alignment effect is significantly stronger than to topography alone except for very deep grooves (depth=3 μm and 6 μm) [12]. Thus, cells can detect different guidance cues at the same time and adapt their reaction to them [12].

The ability of 3T3 fibroblasts to bridge grooves depends on the ridge height and spacings of the ridge [91]. Thus, Stevenson *et al.* [91] proposed a maximal length that the fibroblasts are still able to bridge, while for bending into the grooves they suggested, in agreement with previous suggestions by Dunn and Heath [33], a critical angle that the cellular protrusions are still able to form. To form these connections, the fibroblasts furthermore likely must have enough space to form adhesions at the bottom of the groove and the top of a ridge that can support the bending into the groove [91]. Chick heart fibroblasts sense the curvature of a glass fiber as well as that of a glass prism edge and respond to glass fibre radii of under 100 μm and prism edge angles of over $4 - 8^{\circ}$ [33]. Influences of topography are strongest when cells encounter the discontinuities perpendicularly [33]. However, Stevenson *et al.* [91] observed most connections between ridges and grooves nearly perpendicular to the direction of ridges. It is hypothesized that cytoskeletal bundles in the lamellipodium cannot form or function if the cell has to bend under the length scale of these fibers and thus fibroblasts on structured substrates opt for unrestricted regions [33]. However, although actin filaments have a persistence length of about 10 μm, the actin filaments can bend below this length [7]. Supporting the idea of restricted bending of cytoskeletal filaments, Dunn and Heath [33] as well as Britland *et al.* [12] found adhesions near topographic discontinuities where new bundles originate that do not cross the edge. A further support of this idea may lie in the finding that macrophages show increased levels of actin at the edges of grooves/ridges in the substrate [110].

Ohara and Buck [69] suggested that the area available for focal adhesion formation alters the cells behavior with respect to topographic discontinuities. Alignment perpendicularly to the ridges/grooves restricts the maximal size of focal adhesions to the size of the ridge, while parallel alignment to the ridges/grooves allows for unrestricted focal adhesions and these differences are speculated to alter the reaction of cells [69]. This argument was revisited by Stevenson *et al.* [91] who proposed the need of a certain size of the attached parts to allow for bending into grooves. However, for all findings it has to be considered that the reaction to topographic discontinuities may depend on the specific cell types, since, *e.g.*, rabbit neutrophils do not react as strongly to 5 μm high steps as chick heart fibroblasts react to the structure [21]. Furthermore, Clark *et al.* [21] stated that protrusions at edges in the topography are in neither case (different structure heights) completely blocked, instead the probability of occurrence is reduced. The angle and the height of ridges are thought to be unimportant once the cell bridges the discontinuities [91].

Von Recum and van Kooten [78] pointed out the importance of curvature at topographic discontinuities to trigger cell reaction. It is speculated that cells may be able to sense the curvature of micrometer sized pits and thus adapt their reaction to the pit size [3]. Berry *et al.* [3] found that fibroblasts enter larger pits (diameter 25 μm) while covering smaller holes (diameter 7 μm) in quartz surfaces. On substrates with nanopits of 75 nm and 120 nm in diameter, fibroblasts have been shown to detect nanosized pits, interact via filopodia with the pits and form more filopodia than on flat substrates [27]. On substrates with 35 nm sized pits the number of filopodia is not elevated, although the cells seem to sense the structures [27]. Thus, Dalby *et al.* [27] speculated that filopodia are able to sense the pit sizes by determining the curvature of the pits. Filopodia oriented perpendicular to ridges and grooves are speculated to take place less often than filopodia parallel to ridges and grooves, since the stress formation is hypothesized to be different for the two cases [4].

Even if one fibroblast alone is not able to span a pore, a group of fibroblasts is able to cover it in a collective attempt [83]. However, cell reaction is influenced strongly by the cell type, since endothelial cells are not able to cover larger pores together [83]. Salem *et al.* [83] speculated that the differences in behavior for the two different cell types may be caused by different amounts of available actin. Endothelial cells show concentrated actin and thus focal adhesions at the edges of pores and may therefore not be able to reorientate around the pore [83]. Also,

cell area seems to be influenced by the underlying substrate topography in different ways for different cell types [32, 86, 110]. P388D1 macrophages (cell line) spread to a larger area on grooved substrates (0.5 μm or 5 μm deep, 10 μm wide) compared to smooth substrates [110]. A different study on murine peritoneal macrophages showed that the cells are smallest on silicone substrates with 5 μm features compared to other structure sizes, glass and smooth silicone substrates [86]. Chick heart fibroblasts on grooved substrates adapt a smaller cell area than on unstructured substrates [32]. Lehnert *et al.* [58] found a dependence of spread area on the amount of substrate covered with adhesive proteins. An amount of above 15 % is sufficient to achieve 80 % of the maximal spreading for mouse B16F1 melanoma cells and NIH 3T3 fibroblasts on fibronectin coated substrates regardless of the details of the micropattern [58]. At the border between patterned and homogeneously coated substrate it is obvious that the mouse B16F1 melanoma cells adapt the distribution of their integrin receptors on the patterned part of the substrate [58]. An adaptation of cell shape to the patterns can be observed, if adhesive patches lie 5 μm or more apart, but not for distances of 2 μm and less [58].

2.6 Blood Platelets on Artificial Surfaces

Several studies have investigated the behavior of both single platelets [25, 52, 111] as well as ensembles of platelets [29, 111] on micropatterned substrates. On microcontact-printed stripes of collagen or fibrinogen interspersed with bovine serum albumin (BSA) single platelets adapt both their shape as well as their cytoskeleton to the underlying pattern [52]. Actin is concentrated at the edges of fibrinogen/collagen stripes but tubulin distribution is not influenced [52].
In the following, platelet reactions to patterns with different sizes are detailed. Platelets are able to span non-adhesive regions of up to $4 - 5\,\mu$m [52]. Furthermore, platelets are thought to use their filopodia to search for binding sites and then spread on the regions where filopodia find binding sites [52]. The amount of substrate that is covered with fibrinogen influences the degree of spreading in platelets as was shown by Corum *et al.* [25]. Platelets adapt to the underlying pattern if about 50 % of the surface is covered with fibrinogen, while almost no spreading occurs at 20 % coverage and at surface coverages over about 85 %, spreading is not restricted to fibrinogen coated parts of the substrate [25]. Platelets adhering to 6 μm wide fibrinogen-printed circles on coverslips do not show any

differences in spread area or height to platelets attaching to homogeneously fibrinogen coated coverslips without micropattern [111]. PAR1 is a thrombin receptor [11]. Activation of this receptor results in thrombus formation on the printed circles and the area of the clots increases with increasing amounts of stimulation of PAR1 and exceeds the printed patterns [111]. Larger patterns of 17 μm wide von Willebrand factor-printed squares on glass lead to completely spread platelets with several platelets adhering to one pattern [29]. Furthermore, platelets avoid the uncoated glass next to the printed squares resulting in an adaptation of platelets to the printed pattern at the border between pattern and glass [29]. More platelets attach to the pattern than to the glass [29].

Platelet studies on topographically structured surfaces are fewer and often conducted on biomaterials [51, 53, 71]. Reactions of blood platelets to those implant surfaces are important, since, for example, blood (and thus platelets) will come directly into contact with implants that are placed into the bone [28]. Thus, the blood modifies the implant surfaces and by this may alter the behavior of osteogenic cells which may in turn influence the integration of the implant into the bone [71]. When comparing titanium surfaces with different microstructures, it is evident that blood platelet activation is influenced more by the underlying structure than by chemically modifying the surfaces with calcium and phosphate [51]. Titanium surfaces that show a higher degree of structuring display higher platelet adhesion than more smooth substrates [51, 71]. Furthermore, several layers of platelets are present on the more structured substrates and the findings suggest that also subsequent layers of platelets are influenced by the structures [71].

Studies of platelets on defined micro- and nanostructures show a dependence of platelet adhesion on these structures [20, 53, 115]. Platelets from platelet rich plasma adhere more to uncoated flat than to uncoated micro- or nanostructured PDMS surfaces with substrates being more hydrophobic inducing less platelet adhesion [115]. Furthermore, platelets align to nanogrooves [115]. Chen *et al.* [20] and Koh *et al.* [53] examined how surface patterns alter platelet reaction as well as protein adsorption. The differences in protein adsorption is thought to be responsible for platelet reaction but mechanical features of the substrates also play a role [53]. Micropatterned PDMS substrates show an increase in protein adsorption compared to flat PDMS substrates [20]. Fibrinogen mostly adheres at the flanks and valleys of protrusions in the substrate and platelets adhere as well to these regions suggesting a relation between protein adsorption and platelet response [20]. A higher adsorption of fibrinogen and higher platelet reaction has been observed

for microstructured compared to nanostructured poly(lactic-co-glycolic-acid) films [53].

3

Materials and Methods

Parts of this chapter have been published in [84].
In this chapter, methods as well as materials used to perform the experiments are presented. First, a description of structured wafer production is given (3.1). Then, the substrate production from these wafers, coating of substrates with protein and the characterization of substrates is detailed (section 3.2.1, section 3.2.2 and section 3.3). Afterwards, platelet isolation (section 3.4), staining (in section 3.5.1 for the experimental data on which chapter 5 is based and in section 3.5.2 for the experimental data on which chapters 6 and 7 are based) and imaging (section 3.6) are described.

3.1 Fabrication of Structured Silicon Wafers

In order to produce masters for the cast of poly(dimethylsiloxane) (PDMS) substrates, silicon wafers were structured via conventional photolithography ([112], [10]) in a class 100 cleanroom. Working in a cleanroom is necessary for this step, since even small impurities like dust particles can hinder the production of structured wafers. The process of wafer structuring via photolithography is sketched in figure 3.1. This protocol follows the one described in chapter 3 of [68].

Prior to deposition of photoresist onto the silicon wafer, the wafer had to be cleaned (figure 3.1 a)). In a first step, dust particles were removed by rinsing the wafer with isopropanol and subsequently drying it with dry nitrogen. Afterwards, the wafer was baked for about 10 minutes at 200 °C on a hotplate to evaporate all liquid residues. The photoresist used for producing the structures is a mixture of 1 volume part of SU-8 2001 (MicroChem, Newton, Massachusetts, USA) and 1 volume part of SU-8 2000 Thinner (MicroChem). This mixture was spin coated onto the wafer in a spin coater (Optispin SB 20, ATM Group, Salem/Beuren, Germany), first for a total duration of 10 seconds at a final speed of 500 rotations per minute (rpm) and a ramp of $100\frac{\text{rpm}}{\text{s}}$, and later at a final speed of 3000 rpm and a ramp of $300\frac{\text{rpm}}{\text{s}}$ for a total duration of 30 seconds. This procedure deposits the resist smoothly onto the wafer with a thickness of about 500 nm (figure 3.1 b)). In section 3.3.1 the exact values of structure height are given.
After spin coating, the wafer was baked for 60 seconds at 95 °C on a hotplate. Then, the wafer was exposed to UV-light through a quartz-chromium mask (ML&C Masken Lithographie & Consoluting GmbH, Jena, Germany) (figure 3.1 c)). The quartz-plate is selectively coated with chromium such that light passes through

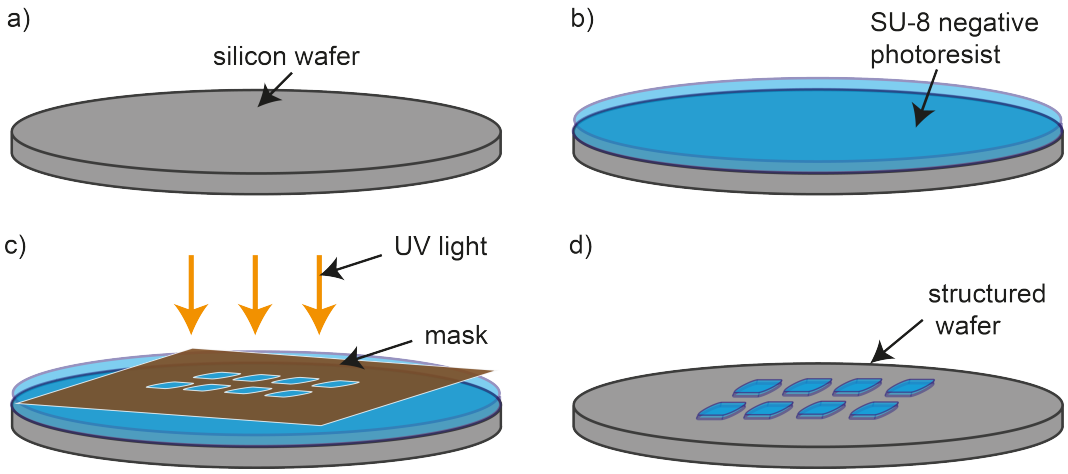

Figure 3.1.: Steps in production of structured silicon wafers via photolitography.
a) A silicon wafer was cleaned by rinsing with isopropanol, drying with dry nitrogen, and baking on a hotplate.
b) A negative photoresist (mixture of 1 volume part SU-8 2001 photoresist and 1 volume part SU-8 2000 thinner) was spin coated onto the wafer to obtain a smooth, thin layer of photoresist.
c) Exposure to UV light through a mask led to cross-linking of the illuminated parts of the photoresist.
d) The non-exposed parts were dissolved while in contact with a developer and then washed away with isopropanol. Subsequently, the resulting structured wafer was dried via nitrogen.

the non-coated parts and is blocked by the chromium-coated parts. Hence, one can control which parts of the photoresist are illuminated and thus cross-linked. In order to produce the small structures needed for the experiments, it is necessary that the mask is in direct contact with the wafer during illumination in a mask aligner (MJB4, SÜSS MicroTec AG, Garching, Germany). Therefore "vacuum contact mode" was employed and a stable vacuum was created through a 30 seconds long mode of "pre-vacuum" and a 15 second long period of "main vacuum" during which the exposure took place. Exposure was performed for 3 seconds with $22\frac{\mathrm{mW}}{\mathrm{cm}^2}$ at a wavelength of 365 nm.
The following baking step cross-links the exposed parts of the resist further and was conducted at 95 °C for 120 seconds on a hotplate. Thereafter, non-exposed parts of the resist were removed with a developer (mr-Dev 600, microresist technology, Berlin, Germany) by submerging the wafer in developer solution for 1 minute. Remaining developer was rinsed off with isopropanol and the wafer was dried with dry nitrogen. Lastly, the wafer was baked for 10 minutes at 150 °C or left as it was. The resulting structure is sketched in figure 3.1 d). To ensure an easier lift-off of the PDMS-cast from the wafer, the wafer was then coated with fluorosilane ((heptafluoropropyl)trimethylsilane, Aldrich, Steinheim, Germany)) for at least 1 hour.

3.2 Substrate Production

3.2.1 Casting of Polydimethylsiloxane (PDMS) Substrates

For the studies presented here, an inverted research microscope equipped with objectives with a working distance between 200 and 300 μm (see section 3.6 for details) was used. As a consequence, it was necessary to use a substrate thin enough to allow for focusing on the top plane of the substrate in the case of live imaging of platelet spreading. Furthermore, a thin substrate also facilitated the mounting of fixed samples.
To obtain such thin substrates, a mixture of 10 parts PDMS-elastomer (Sylgard® 184 Silicone Elastomer Base, Dow Corning, Midland, Michigan, USA) and 1 part of the corresponding cross-linker (Sylgard® Silicone Elastomer Curing Agent, Dow Corning) was spin coated onto the structured silicon wafer (see figure 3.2 a)). The spin coating was carried out for 2 minutes at a speed of 1000 rpm with a ramp time of 2 seconds (Spincoat G3P-8, Specialty Coating Systems (SCS), Surrey,

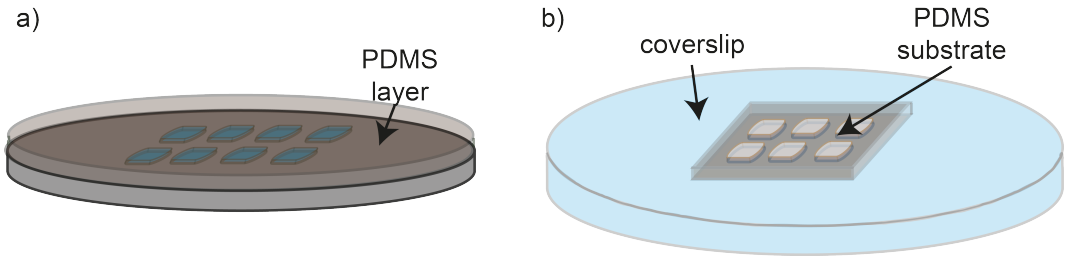

Figure 3.2.: Sketch of PDMS-substrate casting.
a) A base/cross-linker-mixture for PDMS was spin coated onto the structured wafer and cured afterwards for 1 hour at 80 °C on a hotplate.
b) The desired structure was cut from the PDMS cast and transferred with the structured side facing up onto a cover slip.

United Kingdom). Afterwards, wafer and PDMS were baked for 1 hour at 80 °C on a hotplate. After being cured, the desired structure was cut out and transferred (structured site to the top) onto a cover slip (see figure 3.2 b)). For the experiments with fixed, actin-stained platelets, No.1 (24 × 60 mm, VWR, Darmstadt, Germany) cover slips were used, whereas for the experiments with non-fixed, membrane-stained platelets, No.1 round cover slips (∅ 50 mm, VWR) were used due to different requirements during imaging.

3.2.2 Substrate Coating with Fibrinogen

Completely Coated Substrates

Complete fibrinogen coating of substrates, produced as described in section 3.2.1, was accomplished by activation in a plasma-cleaner (Plasma Cleaning, PDC-32 G, Harrick Plasma, Ithaca, New York, USA) at level "medium" for 1.5 minutes. The plasma-cleaning renders the substrate hydrophilic and therefore allows for complete coating. Afterwards, a square of approximate size of 18 × 18 mm was drawn around the substrate (onto the cover slip) with a mini PAP pen (Invitrogen, Darmstadt, Germany). The drawn boundary prevented liquid from running down the substrate and thus kept the later applied fibrinogen solution in place. 500 μl of Alexa Fluor® 488 conjugated fibrinogen solution (concentration of 0.05 $\frac{\text{mg}}{\text{ml}}$, fibrinogen from human plasma, Alexa Fluor® 488 conjugate, excitation approximately 495 nm, emission approximately 519 nm, Invitrogen) were added to the activated substrate and incubated for 1 hour at room temperature in dark (see figure 3.3 a)). Afterwards, the fibrinogen solution was removed and the substrate was washed

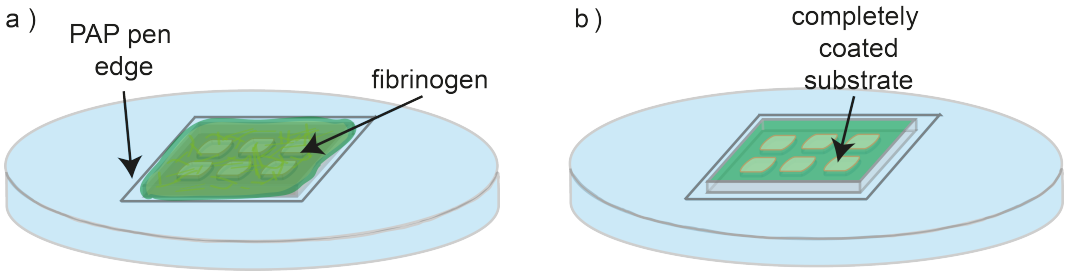

Figure 3.3.: Sketch of different steps in complete substrate coating.
a) The substrate was activated in a plasma-cleaner and thus rendered hydrophilic. This procedure allowed complete coverage of the substrate with fibrinogen by incubation for 1 hour with fibrinogen solution. A 18×18 mm square drawn with a mini PAP pen around the substrate prevented the fluid from running down the substrate.
b) The substrate was washed three times with PBS and either let dry or kept in PBS.

three times with phosphate buffered saline (PBS)[i]. A sketch of the resulting coated substrate is shown in figure 3.3 b). The substrate was either stored in PBS or left to dry.[ii] Dry storage only took place for some of the substrates used to obtain the data presented in chapter 5. Usually, the substrates were prepared one day prior to the experiment and stored at $4 - 8\,^{\circ}\mathrm{C}$ until usage.

Selectively Coated Substrates

Selective coating of PDMS-substrates was here achieved by microcontact printing (MCP) [82]. The method explained below has been adapted from the method described by Liang *et al.* in [60].
A sketch of the different steps in selective coating of the substrates is shown in figure 3.4. Transfer of protein onto the substrate was achieved by a stamp made of PDMS. This stamp was produced by mixing 10 parts PDMS-elastomer (Sylgard® 184 Silicone Elastomer Base, Dow Corning) and 1 part of the corresponding cross-linker (Sylgard® Silicone Elastomer Curing Agent, Dow Corning) and pouring the mixture into a petri-dish. Then the mixture was degassed in a desiccator before being baked in an oven (DryLine, VWR) for 1.5 hours at $65\,^{\circ}\mathrm{C}$. Afterwards, a piece was cut from the PDMS-layer and coated with Alexa Fluor® 488 conjugated fibrinogen solution (concentration of $0.05\frac{\mathrm{mg}}{\mathrm{ml}}$, Invitrogen) by incubating the stamp for 1 hour with the solution at room temperature in dark (see figure 3.4 a)). Then, the solution was removed from the stamp, which subsequently was washed twice,

[i] 0.137 M NaCl, 2.7 mM KCl, 4.3 mM $Na_2HPO_4 \cdot 12\ H_2O$, 1.4 mM KH_2PO_4
[ii] The differences in substrate coating resulting from wet or dry storage are shown in figure 3.5.

each time for about 5 seconds in fresh MilliQ water and the remaining liquid was blown off with dry nitrogen as described in [74].
A structured substrate, produced as described above (see section 3.2.1), was activated using plasma-cleaning (Plasma Cleaning, PDC-32 G, Harrick Plasma) at level "medium" for 1.5 minutes. The dried stamp was then placed and briefly pressed onto the activated substrate so that the side of the stamp coated with fibrinogen touched the structured side of the substrate (see figure 3.4 b)). The stamp was kept on the substrate for 15 minutes, during which a weight of about 15 g was placed on top of the stamp. The stamp and the weight were taken off and the selectively coated substrate was stored at $4 - 8\,^{\circ}\mathrm{C}$.[iii] To prevent the liquid running down the substrate, a square of the approximate size of 18×18 mm was drawn around the substrate (onto the cover slip) with a mini PAP pen (Invitrogen) (see

[iii] The substrates were usually produced one day prior to the experiments.

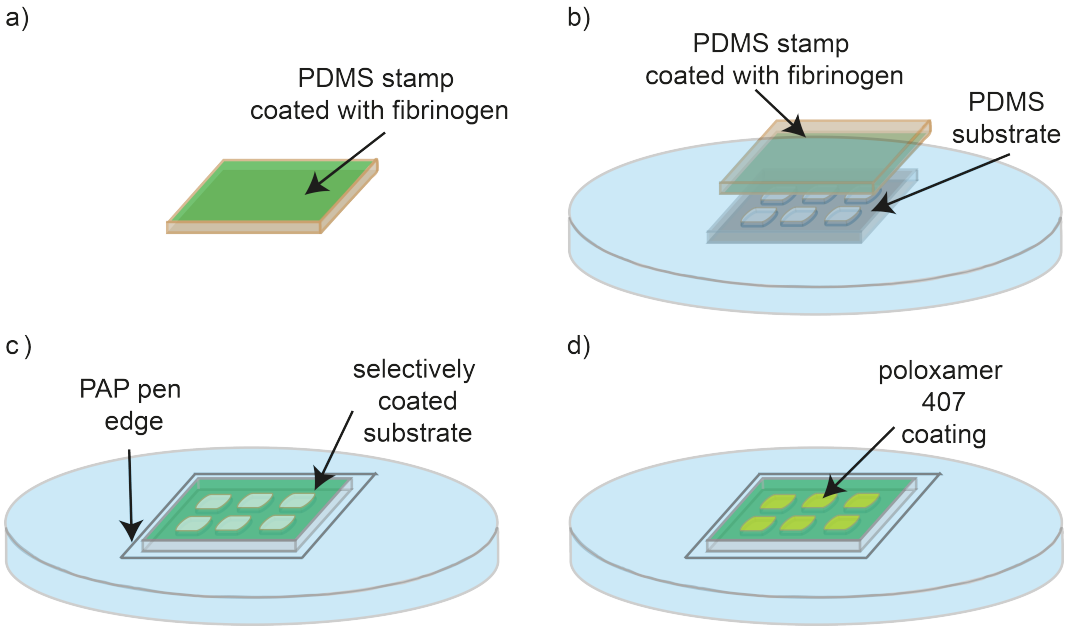

Figure 3.4.: Sketch of different steps in selective substrate coating.
a) A PDMS stamp was coated by incubation with fibrinogen solution for 1 hour. Afterwards it was washed twice in MilliQ water and dried with dry nitrogen.
b) Activation of the substrate in a plasma-cleaner rendered it hydrophilic and allowed for protein transfer when the stamp was placed onto the substrate.
c) The stamp was removed and a 18×18 mm square was drawn around the substrate with a mini PAP pen in order to keep liquid from running down the substrate.
d) Poloxamer 407 was added to the substrate to block unspecific binding sites and incubated for 2 hours. Thereafter, the substrate was washed again three times with PBS.

figure 3.4 c)).
Unspecific binding sites were blocked by incubation of the substrate with 0.2% Poloxamer 407[iv] (Sigma-Aldrich, St. Louis, Missouri, USA) for 2 hours on the day of the experiment. Afterwards, the liquid was removed and the substrate was washed three times with PBS. The resulting coating is sketched in figure 3.4 d).

3.3 Characterization of Substrates

3.3.1 Height Measurements of Structures with a Profilometer

In order to measure the height of the structures on the wafers produced as described in a previous section (section 3.1), a profilometer (Veeco Dektak 6M Stylus Profiler, Veeco Instruments Inc., Plainview, New York, USA) was employed. The structures used here were too small in diameter (for the largest holes about 3 μm) to be measured by this profilometer, since it uses a 5 μm-stylus to measure the height of structures. However, during the structuring of the wafer, labels lying next to the structures were produced to differentiate between different kinds of structures. These labels are created simultaneously with all structures on a wafer. Thus, the labels can be measured instead of the structures to determine the height of the structures. Measurements of the height of these labels show an average height of about 505 ($\pm$25) nm for the static data shown in chapter 5 and 540 ($\pm$10) nm for the dynamic data shown in chapters 6 and 7.

3.3.2 Quality of Fibrinogen Coating

In figure 3.5 the quality of fibrinogen coating on selectively (a)) and completely coated substrates (b) and c)) is depicted.
The fibrinogen coating on selectively coated substrates is mostly even with some brighter spots which are presumably clusters of fibrinogen (figure 3.5 a)). If the completely coated substrates are stored dry, the fibrinogen coating becomes uneven as is shown in figure 3.5 b). However, when the completely coated substrates are stored wet, the fibrinogen coating is mostly even as is depicted in figure 3.5 c). As is explained in more detail in section 4.2 and figure 4.2 b), platelets lying on very uneven fibrinogen coating were excluded from further analysis. The slight unevenness seen in figure 3.5 b) does not seem to influence the results and thus

[iv] 0.2 g Poloxamer 407 filled up to 100 ml with MilliQ water

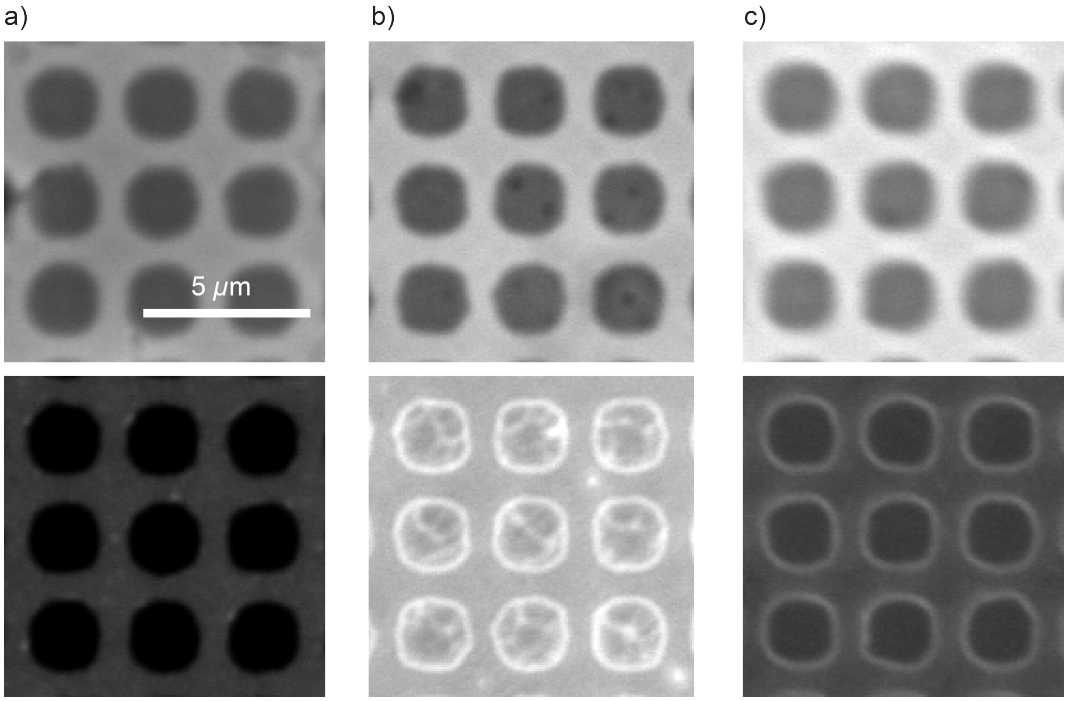

Figure 3.5.: Micrographs depicting the quality of fibrinogen coating for selectively (a)) and completely coated substrates (b) and c)). The upper images show phase contrast micrographs, while the lower images show fluorescence images of the fibrinogen coating.
a) The fibrinogen coating is even except for small, brighter spots that most likely show small clusters of fibrinogen.
b) The substrate shown here has been stored dry after coating and shows some irregularities in coating.
c) This substrate has been stored wet after coating and in contrary to b) does not show large irregularities in coating on the length scale of the resolution. The micrographs shown in b) have been adapted from [84] - Reproduced by permission of The Royal Society of Chemistry.

platelets from both types of substrates - stored wet and stored dry - have been included into the analysis.

3.3.3 Imaging with an Atomic Force Microscope

An image taken as described below with an atomic force microscope of a substrate with 2.1 μm wide holes (see figure A.1 in the appendix (chapter A) and section 4.4 for the hole size) is shown in figure 3.6. A PDMS-cast, produced as described in section 3.2.1 was activated for 1.5 minutes at level "medium" in a plasma cleaner (Plasma Cleaning, PDC-32 G, Harrick Plasma) and subsequently immersed in PBS. Measurements were taken with a MFP-3D (Asylum Research, Santa Barbara, California, USA) atomic force microscope equipped with an Olympus OMCL-AC-240-

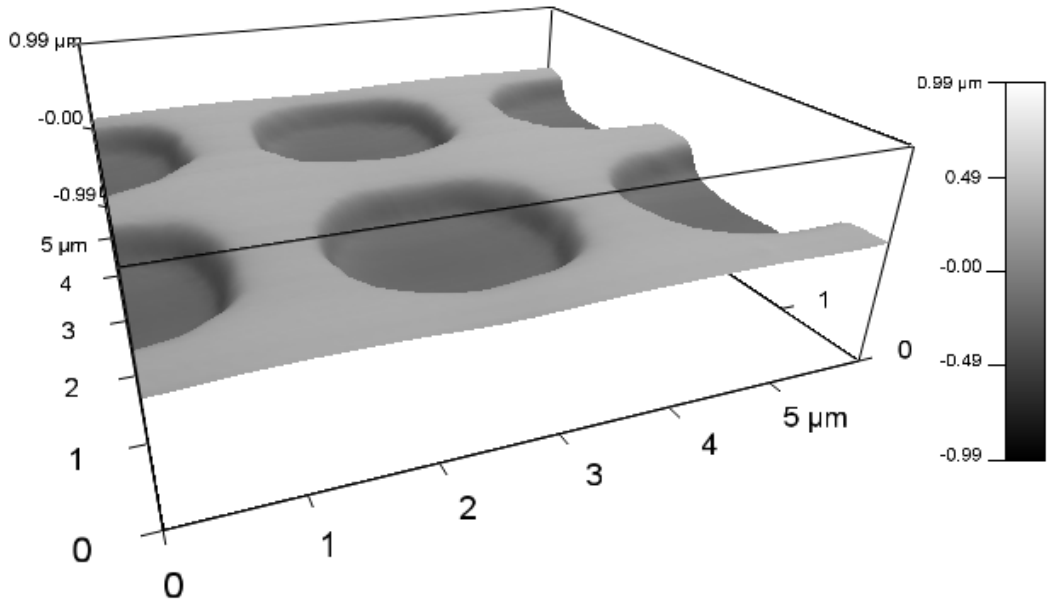

Figure 3.6.: Atomic force microscopy image of a substrate containing holes of approximately 2.1 μm in width and interspaces about 0.9 μm wide. The holes are quite shallow. Figure has been adapted from [84] - Reproduced by permission of The Royal Society of Chemistry.

TS cantilever (Atomic Force F&E GmbH, Mannheim, Germany). A total field of $9 \times 9\,\mu$m with a resolution of 256×256 points was imaged at a scan rate of 0.25 Hz in AC mode.

3.3.4 Measurements of Substrate Height

The height of substrates was measured at the border of PDMS to underlying cover slip with an inverted research microscope (IX81, Olympus, Hamburg, Germany). The z-position while focusing on the upper layer of the PDMS and while focusing on the upper layer of the glass were denoted. The difference of these positions was given as the height of the PDMS layer. The average height of the PDMS layer was measured as 45 ($\pm$6) μm.

3.4 Platelet Isolation

Platelet isolation was performed similarly as previously described in chapter III of [88] and details of the procedure are described below.
Blood platelets were obtained from platelet concentrates provided by the Department of Transfusion Medicine of the University Medical Center Göttingen. The experiments were conducted in agreement with the ethical vote of the Ethic Committee (University of Göttingen, votum 11/11/09). The used concentrates were no longer valid for transfusion, as they were typically $5-6$ days old (day zero is the day of blood donation). However, since blood platelets circulate $7-10$ days in humans [108], the concentrates still contained many undestroyed platelets and thus could be used for the experiments.
In order to prevent uncontrollable influences from blood plasma, which constitutes the platelet concentrates together with the platelets, platelets were purified by separating them from the plasma. The platelet concentrates also contained some remaining red blood cells. However, their number usually was quite low compared to the number of platelets and thus did not disturb the experiments. Furthermore, the concentrates were leukocyte depleted. The different steps of this isolation are shown in figure 3.7. Platelet isolation was carried out in PIPES-Saline-Glucose (PSG)[v] and either HEPES Tyrode buffer (HT buffer)[vi] in the case of samples of non-fixed platelets or Medium 199 (Bio-Whittaker® Medium 199, with Earle's Balanced Salt Solution, with L-Glutamine and HEPES, Lonza, Basel, Switzerland) in the case of fixed platelets. The recipe of the HT buffer was taken from [18] and BSA was only added directly before the experiment. HT buffer was mixed with a BSA stock solution (10% BSA in PBS, Macs BSA stock solution, Miltenyi Biotech, Bergisch Gladbach, Germany) to yield a final concentration of $5\frac{\text{mg}}{\text{ml}}$ of BSA in the buffer.
To begin with, either Medium 199 (Bio-Whittaker® Medium 199, with Earle's Balanced Salt Solution, with L-Glutamine and HEPES, Lonza) or HT buffer as well as PSG were heated up to 37 °C and placed into an incubator (HeraCell 150, Thermo Scientific, Waltham, Massachusetts, USA) for CO_2-exchange (5% CO_2).[vii] Platelets

[v] 5 mM PIPES, 145 mM NaCl, 4 mM KCl, 50 μM $Na_2HPO_4 \cdot 12\ H_2O$, 1 mM $MgCl_2 \cdot 6\ H_2O$, 5 mM glucose, pH $\sim$ 6.8 after adjustment

[vi] 134 mM NaCl, 12 mM $NaHCO_3$, 2.9 mM KCl, 1 mM $MgCl_2$ (anhydrous), 5 mM HEPES, 5 mM glucose, 0.34 mM NaH_2PO_4, pH $\sim$ 7.4 after adjustment

[vii] If not in use the buffers/medium were stored in the incubator to keep them at 37 °C and allow for CO_2 exchange.

were extracted from the bag of platelet concentrate by a syringe and a needle. At first, 2 ml were discarded with a 2ml-syringe (BD Discardit™ II, Becton, Dickinson and Company, Franklin Lakes, New Jersey, USA) and a Nr.1-needle (∅ 0.90 × 40 mm, 100 Sterican®, B.Braun, Melsungen, Germany) to prevent contamination of the sample due to the opening of the bag. After this, 4 ml were extracted with the same needle and a 5ml-syringe (BD Discardit™ II, Becton, Dickinson and Company) and transferred into a Falcon tube (see figure 3.7 a)). 100 μl of prostaglandin E_1 (PGE_1) ($\sim 0.106 \frac{mg}{ml}$, Cayman Chemical Company, Ann Arbor, Michigan, USA) were added to the solution to keep the platelets quiescent. Then, the cell-plasma mixture was centrifuged at 480 g and $17 - 22\,^{\circ}C$ for 20 minutes in a centrifuge (Eppendorf Centrifuge 5810 R, Eppendorf, Hamburg, Germany). After centrifugation, the supernatant was discarded as is sketched in figure 3.7 b) and the cell pellet was resuspended again in 4 ml PSG (figure 3.7 c)).

The addition of PGE_1, the following centrifugation and the re-suspension of the pellet were repeated twice. In the first repetition, the cell pellet was dissolved in 4 ml PSG while in the second repetition it was dissolved in either 1 ml HT buffer (supplemented with $5 \frac{mg}{ml}$ of BSA) or in 1 ml Medium 199 (Bio-Whittaker® Medium

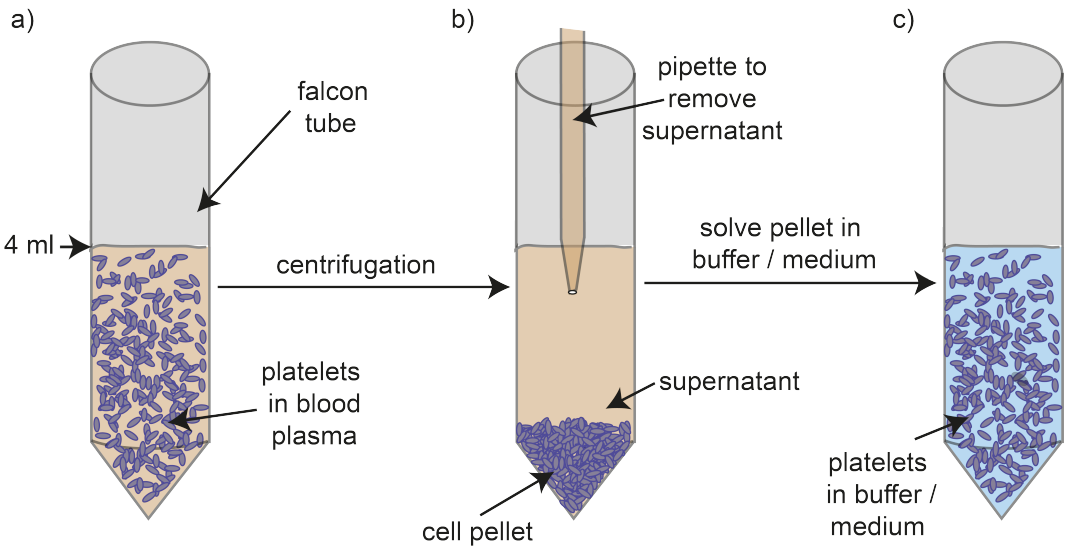

Figure 3.7.: Sketch of different steps in platelet isolation from platelet concentrates.
a) 4 ml of cell solution (platelets dissolved in blood plasma) were transferred into a Falcon tube.
b) The solution was centrifuged for 20 minutes at 480 g and $17 - 22\,^{\circ}C$ to separate the platelets from the plasma.
c) The resulting cell pellet was dissolved again in buffer/medium while the supernatant was discarded.

199, with Earle's Balanced Salt Solution, with L-Glutamine and HEPES, Lonza) (depending on the type of experiment, see above).
In order to yield reproducible cell numbers in the experiments, platelets were counted and diluted to the desired concentration. For counting, a hematocrit capillary (Heparinized Micro-Hematocrit Capillary Tubes, FisherBrand, Thermo Fisher Scientific Inc., Waltham, Massachusetts, USA) was filled with purified platelet solution and one end was sealed with clay sealant to prevent leakage. Then, the capillary was centrifuged for 10 minutes at 1000 g and $21 - 22\,^{\circ}\mathrm{C}$. The centrifugation separates the platelets from the liquid and allows the determination of cell number based on the height of the pellet and the height of the liquid column using a Reader Card (ZIPocrit, Microhematocrit Centrifuge, LW Scientific, Inc., Lawrenceville, Georgia, USA). A sketch of the hematocrit capillary with the platelets and the supernatant is shown in figure 3.8.

3.5 Platelet Staining and Sample Preparation

In instances were it is stated that all liquid is removed, this does not include the thin liquid film that remains each time after removal of liquid.

3.5.1 Actin Staining

Platelets were diluted to a concentration of $6 \times 10^7 \frac{\text{cells}}{\text{ml}}$ in Medium 199 (Bio-Whittaker® Medium 199, with Earle's Balanced Salt Solution, with L-Glutamine and HEPES, Lonza). The substrates (prepared as described in section 3.2.2) were washed three times with Medium 199 (Bio-Whittaker® Medium 199, with Earle's Balanced Salt Solution, with L-Glutamine and HEPES, Lonza) and stored with added Medium 199 (Bio-Whittaker® Medium 199, with Earle's Balanced Salt Solution, with L-Glutamine and HEPES, Lonza) until usage. Prior to the addition of

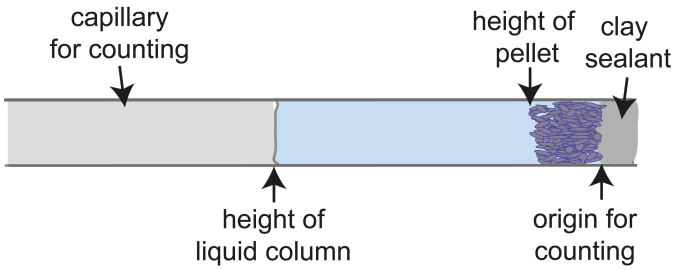

Figure 3.8.: Description of platelet counting with a microhematocrit capillary.
By reading out the height of the liquid column and the height of the pellet, the number of platelets can be determined with the help of a ZIPocrit, Microhematocrit Centrifuge Reader Card.

platelets all liquid was removed. The sketch in figure 3.9 shows the different steps of sample preparation in the case of fixed, actin-stained platelets.
150 μl of diluted platelet solution (prepared as described above, section 3.4) were added to each substrate and given 15 minutes to sediment onto the substrates[viii] (see figure 3.9 a)) before addition of 50 μl of thrombin solution (4 $\frac{u}{ml}$, thrombin from human plasma, $\geq$ 2800 NIH units/mg protein, Sigma-Aldrich). The substrates together with the platelet/thrombin-mixture were placed into an incubator (HeraCell 150, Thermo Scientific) at 37 °C and 5 % CO_2 for 60 minutes in order to let the platelets spread (see figure 3.9 b)). The platelets were fixed by adding

[viii] This yields a larger number of spread platelets.

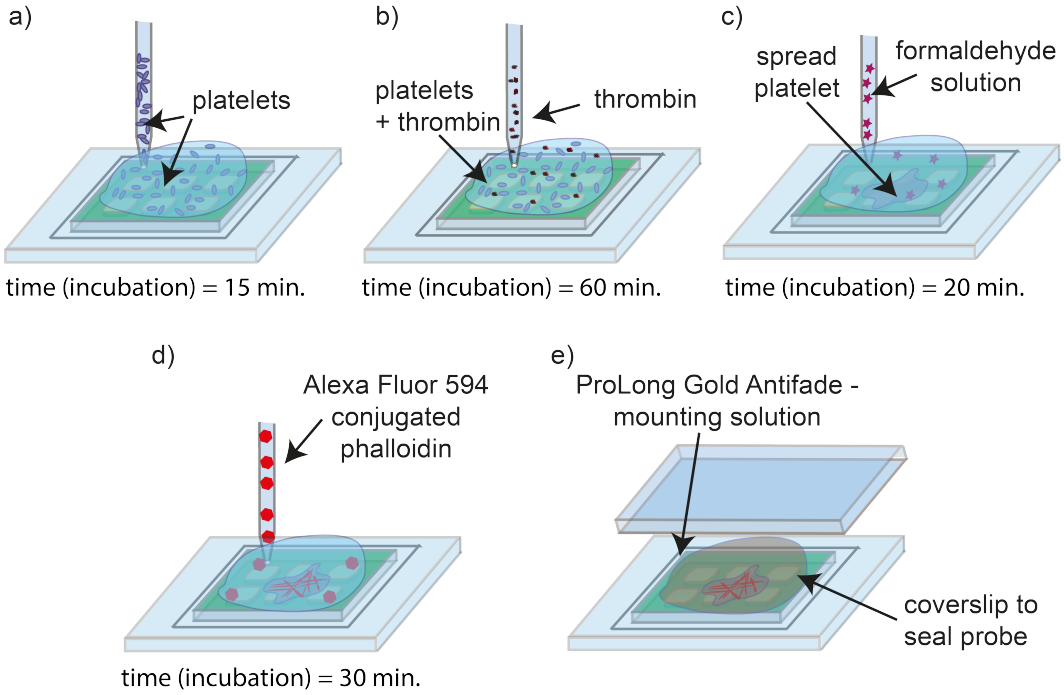

Figure 3.9.: Sketch of different steps in preparing the fixed, actin-stained platelet samples.
a) 150 μl of diluted platelet solution were added to a washed substrate.
b) Then, 50 μl thrombin solution were added after 15 minutes and the sample was incubated for 60 minutes in an incubator at 37 °C and 5% CO_2.
c) 200 μl of formaldehyde solution were added to fix platelets and the sample was incubated again for 20 minutes at 37 °C and 5% CO_2 and then washed three times with PBS.
d) Afterwards, 200 μl of Alexa Fluor® 594 phalloidin were added and incubated for 30 minutes at room temperature under the exclusion of light and subsequently washed again three times with PBS.
e) Most liquid was removed and the sample was sealed by addition of ProLong® Gold Antifade reagent and a cover slip, which was then attached to the underlying cover slip by nail polish.

200 μl of approximately 4 % formaldehyde (FA) solution ($\sim 4-8\,^{\circ}$C, diluted from min. 37 % formaldehyde (with 10 % methanol for stabilization), Merck KGaA, Darmstadt, Germany) to the platelet/thrombin mixture and incubating it again for 20 minutes at 37 °C and 5% CO_2 (see figure 3.9 c)). Subsequently, all liquid was removed and the substrates were washed three times with PBS. Again all liquid was removed and 200 μl Alexa Fluor® 594 phalloidin (approximately 4.9 $\frac{\text{u}}{\text{ml}}$, excitation: approximately 590 nm, emission: approximately 617 nm, Invitrogen) were added. The samples were incubated for 30 minutes at room temperature under the exclusion of light. Finally, all liquid was removed and the substrates were washed again three times with PBS (see figure 3.9 d)). The cover slip to which the substrate was attached, was transferred to a microscopic glass slide for easier handling and attached to it with nail polish. Most of the remaining liquid was removed from the cover slip and ProLong® Gold Antifade reagent (Invitrogen) was brought onto the substrate. This reagent helps to prevent photobleaching and cures so that long-term storage is possible. In order to finally seal the sample, a 18×18 mm cover slip (No.1, VWR) was put on top of the ProLong® Gold Antifade (Invitrogen) and fixed to the underlying cover slip with nail polish (see figure 3.9 e)). The sample was left for some time at room temperature to start the curing of the ProLong® Gold Antifade (Invitrogen) and then stored at $4-8\,^{\circ}$C.

3.5.2 Live Plasma Membrane Staining

Staining platelets with CellMask™ dye (Life Technologies GmbH, Darmstadt, Germany) has been conducted for example in [52]. The concentrations for BSA and platelets in the following protocol have been taken from this reference. The concentration of the CellMask™ dye (Life Technologies GmbH) has been chosen as proposed in [64]. A sketch of the different steps in membrane staining is depicted in figure 3.10.

A staining solution was prepared by mixing HT buffer (supplemented with $5\frac{\text{mg}}{\text{ml}}$ BSA) and CellMask™ DeepRed (excitation: approximately 649 nm, emission: approximately 666 nm, Life Technologies GmbH) to yield a final dye concentration of 2.5 $\frac{\mu\text{g}}{\text{ml}}$. Approximately 5 μl of unstained platelet solution were mixed with about 995 μl of this staining solution to yield a final platelet count of 2×10^7 $\frac{\text{cells}}{\text{ml}}$ in a total liquid amount of 1 ml (see figure 3.10 a)). This mixture was incubated for 6 minutes[ix]. At the end of incubation, 25 μl of PGE_1-solution ($\sim 0.106\frac{\text{mg}}{\text{ml}}$, Cayman

[ix] about 4 of the 6 minutes in an incubator (HeraCell 150, Thermo Scientific) at 37 °C and 5% CO_2

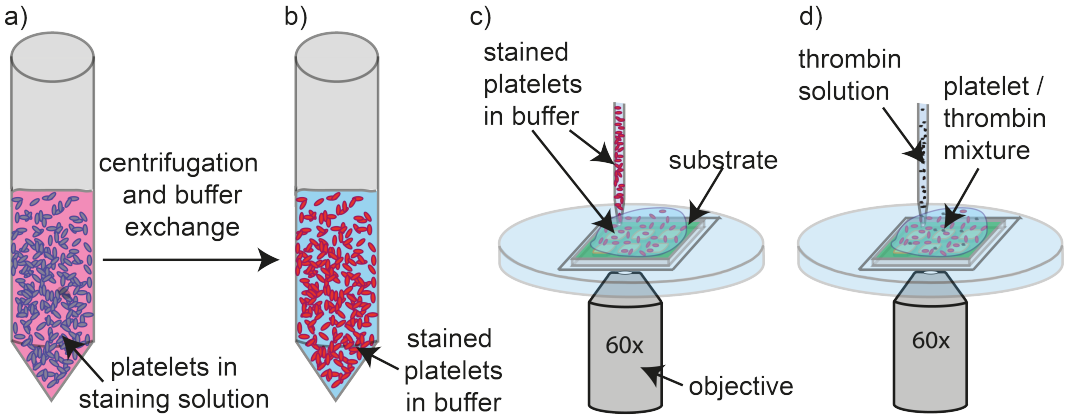

Figure 3.10.: Sketch of platelet preparation for live imaging of spreading.
a) Platelets were mixed with a staining solution containing CellMask™ DeepRed dye and incubated for 6 minutes ($\sim$ 4 of the 6 minutes in an incubator at 37 °C and 5% CO_2).
b) The solution was centrifuged for 5 minutes at 480 g and $20-21$ °C to separate platelets from liquid. Then, the cell pellet was re-diluted in HT buffer (supplemented with $5\frac{\text{mg}}{\text{ml}}$ BSA).
c) 150 μl of stained platelet solution were pipetted onto a washed substrate.
d) Shortly thereafter 50 μl of thrombin solution (16 $\frac{\text{u}}{\text{ml}}$) were added to the platelet solution.

Chemical Company) were added. Afterwards, the mixture was centrifuged for 5 minutes at 480 g and $20-21$ °C in a centrifuge (Eppendorf Centrifuge 5810 R, Eppendorf). The resulting cell pellet was resuspended in 1 ml HT buffer (supplemented with $5\frac{\text{mg}}{\text{ml}}$ BSA (see figure 3.10 b)). The BSA reduces background fluorescence [92]. A structured, completely fibrinogen-coated substrate (prepared as described in section 3.2.2) was washed three times with HT buffer (supplemented with $5\frac{\text{mg}}{\text{ml}}$ BSA). After the last washing step, the liquid was removed and HT buffer (supplemented with $5\frac{\text{mg}}{\text{ml}}$ BSA) was added for storage.
The following steps were performed on a microscope (see section 3.6 for details) equipped with an incubation-chamber (37 °C, 5% CO_2, model INUG2E-ONICS, Incubation System for Microscopes, Tokai Hit, Ltd., Gendoji-cho, Fujinomiya-shi, Shizuoka-ken, Japan). A washed substrate was placed into the incubation chamber and nearly all liquid was removed from the substrates. Then, 150 μl of membrane-stained platelet solution were added to the substrate (see figure 3.10 c)) and shortly thereafter 50 μl of thrombin solution (16 $\frac{\text{u}}{\text{ml}}$, thrombin from human plasma, $\geq$ 2800 NIH units/mg protein, Sigma-Aldrich) were added to trigger spreading (see figure 3.10 d)). Details of imaging can be found in the next section (section 3.6).

3.6 Imaging

All imaging was performed with an inverted research microscope (IX81, Olympus, Hamburg, Germany). This microscope is equipped with a digital charge-coupled device (CCD) camera ORCA-R2 C10600-10B (Hamamatsu Photonics Deutschland GmbH, Herrsching am Ammersee, Germany) and a 150W Xenon arc lamp for epi-fluorescence.

In the case of samples with fixed, actin-stained platelets, a 100× oil-immersion phase contrast objective UPLFLN 100XO2PH (numerical aperture (NA) 1.3, working distance (WD) 0.2 mm, Olympus) together with immersion oil Type-F (index of refraction: ne=1.518, dispersion: νe = 41 (23 °C) , Olympus) was used. A sketch of the imaging can be found in figure 3.11. Two fluorescence images (one of the substrate coating and one of the actin staining) as well as a phase contrast image were taken for each imaged position on the substrate. For both fluorescence channels an illumination time of 60 ms at a lamp power of 100% was applied, while for the phase contrast image the imaging parameters were set to 60 ms illumination time and 8.1 V lamp power. Here, a triple-band filter (U-M3DAFITR, Olympus) which is able to image fluorophores excitable around 350 nm (maximum, full width half maximum (FWHM) 50 nm (bandwidth)), 492 nm (maximum, FWHM 18 nm (bandwidth)) and 572 nm (maximum, FWHM 23 nm (bandwidth)) was used. Emission can be detected around 462 nm, 531 nm and 628 nm. The dichroic beam splitter lets light above approximately 449 nm, 510 nm and 586 nm pass through. The corresponding spectra of optical filters and dyes can be found in figure 3.12.

Confocal z-stacks were taken employing a FV-1000 confocal unit (Olympus) in-

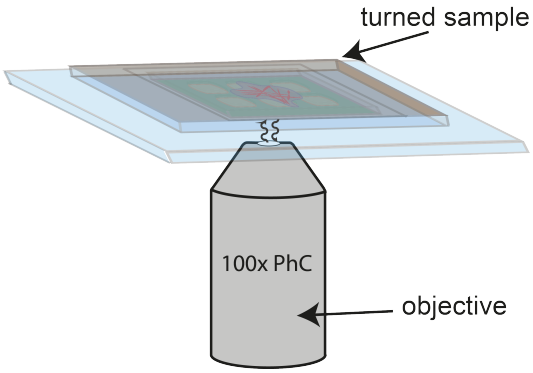

Figure 3.11.: Sketch of imaging of fixed samples.
The mounted sample was placed onto the microscope so that the cover slip that seals the probe lies directly on the objective. Fluorescence images of both fibrinogen coating and actin-staining (60 ms illumination time, 100% lamp power) were taken. Furthermore, a phase contrast image was also taken (60 ms illumination time, 8.1 V lamp power). All images were taken with the 100× oil-immersion phase contrast objective UPLFLN 100XO2PH.

corporated into the IX81-setup (Olympus, see above). Both, images of substrate coating with the 488 nm line of an argon laser and images of the actin-staining with

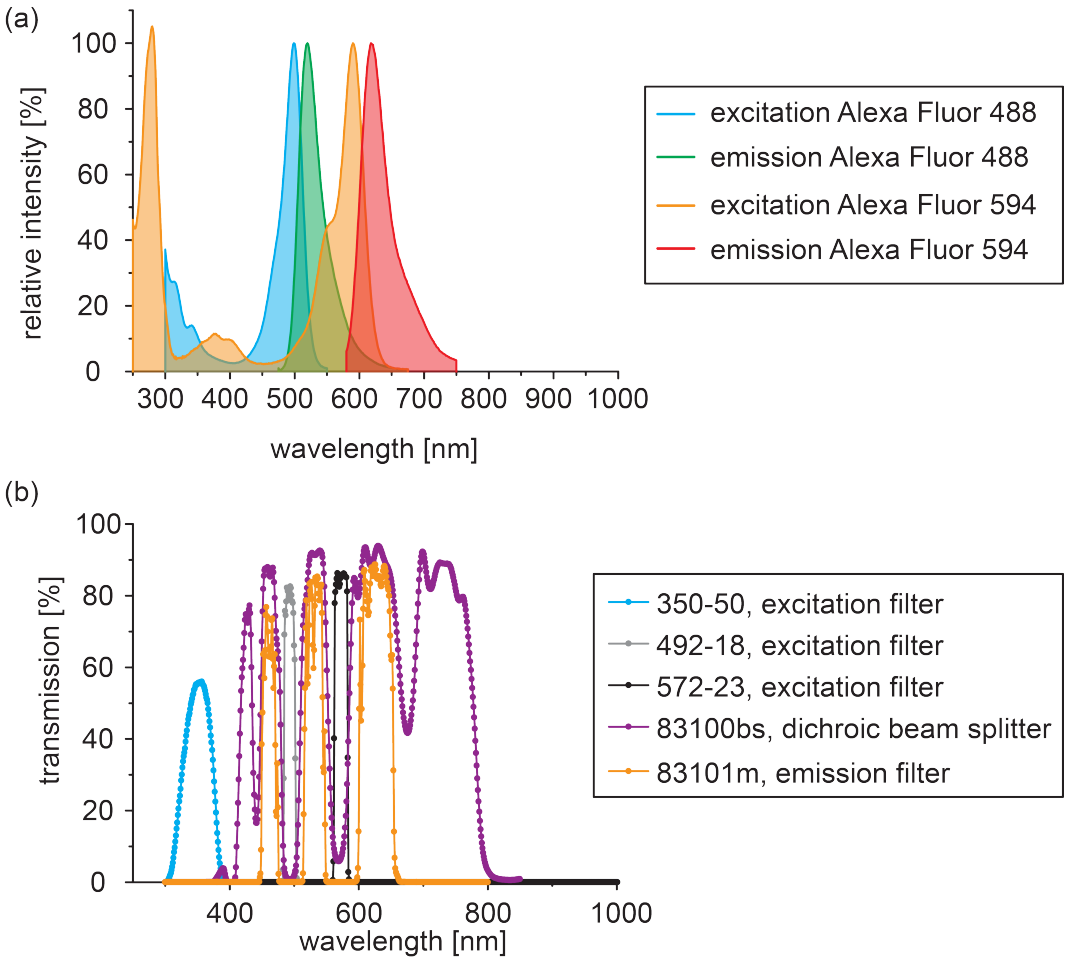

Figure 3.12.: Spectra of Alexa Fluor® 488 and 594 fluorophores (a)) as well as the spectra of the triple bandfilter (b)) used to image these fluorophores.
a) Excitation and emission spectra for Alexa Fluor® 488 (at pH 8) and 594 fluorophores (at pH 7.2). The shift in wavelength between excitation and emission is called "Stokes shift". This shift arises since not the whole excitation energy is turned into emitted radiation (fluorescence). The shift enables distinction between excitation and emission light. Data have been provided by Life Technologies GmbH (Molecular Probes® [65],[66]).
b) Spectra of triple bandfilter used in experiments to match the excitation and emission wavelength of Alexa Fluor® 488 and 594 fluorophores (a)). The triple band filter consists of a dichroic beamsplitter (purple), an emission filter (orange), as well as three excitation filters (light blue for DAPI, gray for FITC (or Alexa Fluor® 488) and black for TxRed (or Alexa Fluor® 594). Data have been provided by AHF analysentechnik AG / Dr. Ines Höfer (Olympus).

a diode laser at the wavelength 561 nm were taken every 0.25μm in z-direction at a total of 17 images. The following filters were used in this case: The excitation dichroic mirror DM405/488/561/633 was used together with the emission filter BA505 – 525 and the emission filter BA575 – 675.
In the case of non-fixed, membrane-stained platelets, time-lapse series of substrate coating and membrane staining were taken via epi-fluorescence. For this purpose a 60 x silicone-oil objective ULSAPO60XS2 (NA 1.3, WD 0.3 mm) together with silicone immersion oil (index of refraction: ne=1.406, dispersion: νe = 52 (23 °C), Olympus) was used. A sketch of the imaging can be found in figure 3.13.
In order to be able to switch fast between the two channels, a Cy5/FITC-dualband filter was employed. This filter consists of two bandpass filters: one that allows for excitation around 470 nm (maximum, FWHM 40 nm (bandwidth), 470/40 ET Bandpass, AHF analysentechnik AG, Tübingen, Germany, FITC) and a second one that allows for excitation around 628 nm (maximum, FWHM 40 nm (bandwidth), 628/40 BrightLine HC, AHF analysentechnik AG, Cy5).
Furthermore a beam splitter (497/655 H Dualband Strahlenteiler, AHF analysentechnik AG) which lets light above 497 nm and light above 655 nm pass through was employed. For emission, a dualband blocking filter (537/694 Dualband Sperrfilter H, AHF analysentechnik AG) that detects emission around 537 nm and around 694 nm was used. The Cy5 channel was used to image the cell membrane, whereas the FITC channel was used to image the substrate coating. The corresponding spectra of optical filters and dyes can be found in figure 3.14. The time lapse series consist of 1200 – 1800 pictures taken every 1.5 seconds in each of the two channels. The imaging parameters were set to 60 ms illumination time and

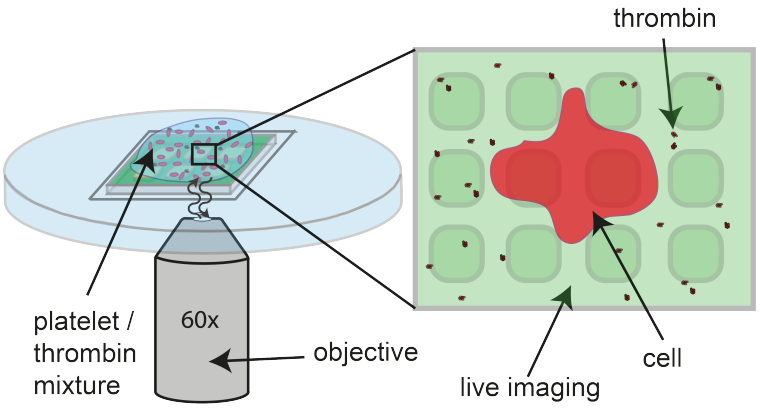

Figure 3.13.: Sketch of imaging of non-fixed samples. Time lapse series of the stained cell membrane as well as of the fibrinogen coating were taken every 1.5 seconds (60 ms illumination time, 7.72% lamp power). For this purpose, a 60× silicone-oil objective ULSAPO60XS2 was employed.

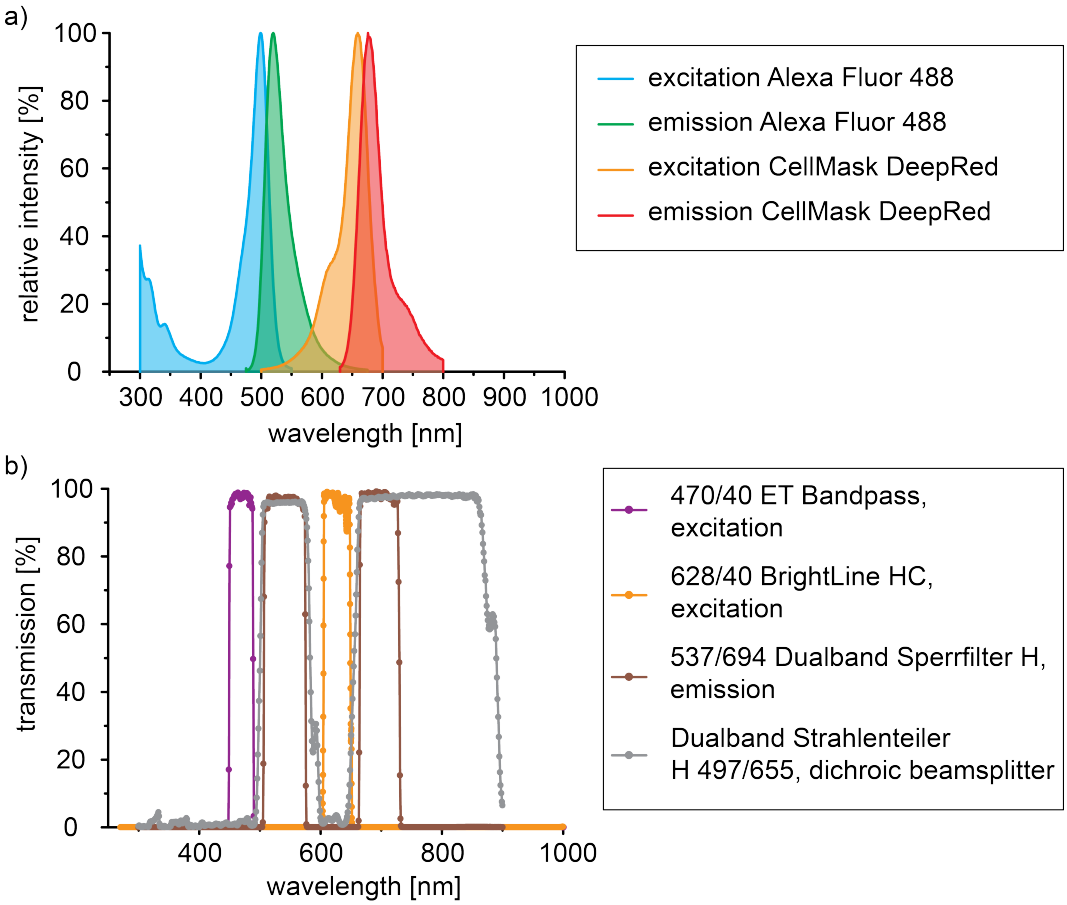

Figure 3.14.: Spectra of Alexa Fluor® 488 and CellMask™ DeepRed fluorophores (a)) as well as the spectra of the dual bandfilter (b)) used to image these fluorophores.
a) Excitation and emission spectra for Alexa Fluor® 488 (at pH 8) and CellMask™ DeepRed fluorophores (bound to zwitterionic detergent (CHAPS) micelles). Data have been provided by Life Technologies GmbH (Molecular Probes® [65],[67])
b) Spectra of dual bandfilter used in experiments to match the excitation and emission wavelength of Alexa Fluor® 488 and CellMask™ DeepRed fluorophores (a)). The dual bandfilter consists of a dichroic beamsplitter (gray), an emission filter (brown), as well as two excitation filters (purple for FITC (or Alexa Fluor® 488) and orange for Cy5 (or CellMask™ DeepRed)). Data have been provided by AHF analysentechnik AG ([1]).

7.72% lamp power.

4

Data Analysis

All analysis methods described below have been self-written in MATLAB® R2009b (MathWorks®, Natick, Massachusetts, USA), if it is not stated otherwise. Most of the parameters used below are given in pixels. For the fixed, actin-stained samples 1 pixel equals approximately 0.064 μm and the analysis specifically applied to these data is detailed in section 4.2 (results: chapter 5), while for the non-fixed membrane-stained samples 1 pixel equals approximately 0.108 μm and the analysis applied specifically to these data is shown in section 4.3 (results: chapters 6 and 7). Parts of this chapter have been published in Soft Matter [84].

4.1 Cell Outline Detection

In order to detect the cell outline, a program was employed that used the *edge* function. From this function the *canny* algorithm was used, which employed a Gaussian filter to reduce noise and afterwards detected edges by computing gradients of the image and detecting maxima in the magnitude of the gradients [15]. By using this algorithm, it was possible to include both edges arising from strong as well as from weak signal changes. To be able to include strong and weak edges is very helpful for the data analyzed here, since staining of cellular components is

not necessarily uniform over the volume/area of one platelet or between different platelets. In order to ensure that all parts of the cell were detected and the determined outline was consistent with the cell outline in the original fluorescence image, the resulting image produced by the *canny* algorithm was overlayed with the original fluorescence image in ImageJ [87] for visual control purposes. By this visual control, non-detected parts of the cell could be added manually based on the fluorescence image. This procedure is most helpful in the case of filopodia or other very thin parts of the cell that contain little stained material and thus usually show low fluorescence intensity and therefore shallower gradients, which are more difficult to detect. In figure 4.1 an illustration of the two different steps of cell outline detection is shown. This example shows a membrane-stained non-fixed platelet.

In the case of fixed, actin stained samples examined in this study, a low threshold of 0 and a high threshold of 0.05 as parameters for the *canny* algorithm are best suited to detect the cell outline. In the case of non-fixed platelets stained for their plasma membrane, first a Wiener filter was employed to the image. The *wiener2* function (neighborhood 7×7 pixels) helped to remove background noise that had

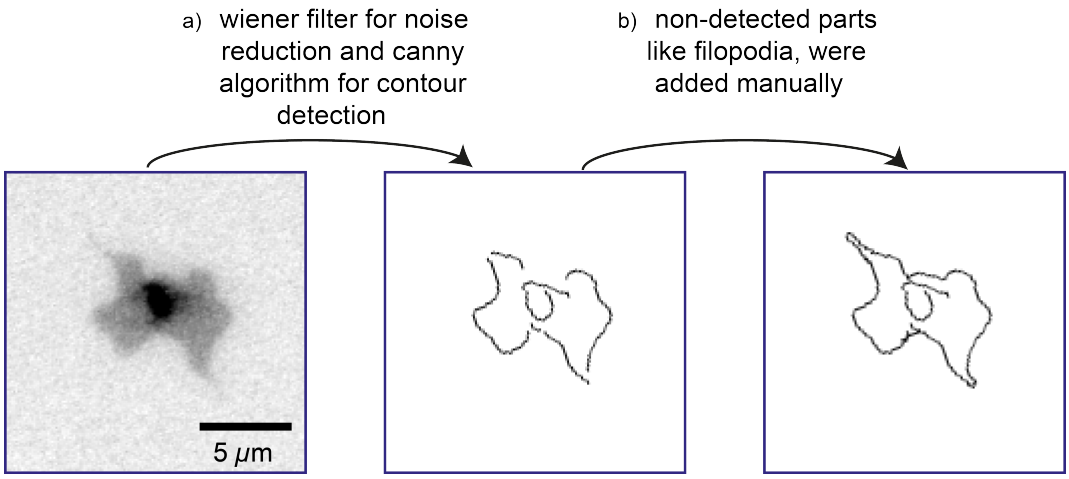

Figure 4.1.: Illustration of the two different steps of outline detection.
The images have been inverted to increase visibility and have been rotated in ImageJ [87] (bilinear interpolation) to align the rows of holes with the image borders.
a) Based on the original fluorescence image (left) the cell outline was detected automatically by noise reduction through a Wiener filter (*wiener2* function) and a subsequent edge detection through the *edge* function with the *canny* algorithm.
b) Parts of the outline that had not been detected in a) were manually added in ImageJ [87] in comparison with the original fluorescence image.

arisen due to the short exposure time and low lamp power needed to be able to image non-fixed blood platelets (see section 3.6). Short exposure times and low lamp powers help to decrease the amount of energy the platelets have to endure and thus can help the survival of platelets. For the subsequent *canny* algorithm step, a low threshold of 0.02 and a high threshold of 0.07 were used. Again the images of the detected outlines were overlaid with the original fluorescence images in ImageJ [87] as described above and missing parts of the cell were added manually.

4.2 Analysis of Fixed Samples

In the following, several pre-processing steps that were needed to sort out platelets that did not spread completely or might have been influenced by a distorted substrate, irregular fibrinogen coating or other platelets, are described and different conditions under which platelets were excluded from analysis are shown in figure 4.2. Platelets that did not spread completely were excluded from analysis (see figure 4.2 a)). Not completely spread platelets appeared darker in the phase contrast image, since they were thicker and therefore could be sorted out. Additionally, platelets lying on top of irregular fibrinogen coating were excluded from analysis. An example of irregular fibrinogen coating is shown in figure 4.2 b). Especially on selectively coated substrates, platelets were able to distort the fibrinogen coating of the substrate. In figure 4.2 c) an image of a distorted fibrinogen layer is shown. If any distortion of the fibrinogen layer was visible, the platelet that had distorted the layer, was excluded from analysis, since these interactions with the fibrinogen coating could have altered spread area and morphology of the platelet. Distorted substrate parts, *i.e.* the PDMS-layer itself is distorted, may arise, *e.g.*, when there are remaining dust particles on the coverslip to which the substrate is transferred (see section 3.2.1) or when the substrate is stretched while being transferred to the coverslip. The distortion of a substrate can be measured based on images of the substrate coating. To ensure an undistorted substrate, it was tested in ImageJ [87] whether simultaneous alignment of the horizontal and vertical rows of holes with the borders of the image was possible by rotation. If this simultaneous alignment was not possible, platelets lying on these parts of the substrate were omitted from analysis. A sketch of the alignment attempts is shown in figure 4.2 d). Furthermore, platelets were excluded from the analysis, that were in contact or too close to other platelets. Finally, platelets that were situated on a flat part of the substrate

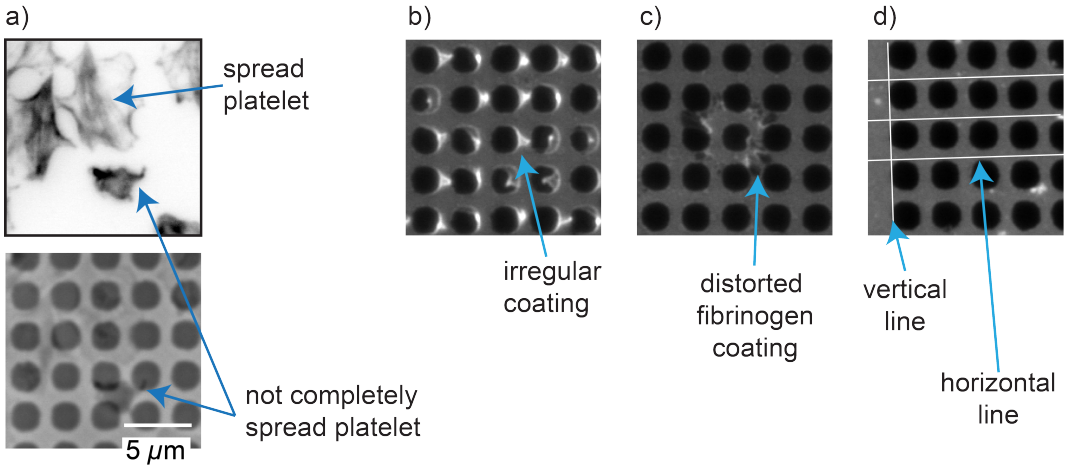

Figure 4.2.: Explanatory images for different cases in which platelets were not analyzed.
a) The upper image shows an inverted fluorescence image of stained actin. The lower image shows the corresponding phase contrast image. The images show an example of a not completely spread cell in contrast to a spread cell. In phase contrast microscopy images not completely spread platelets appear darker due to their higher thickness and thus can be sorted out.
b) Platelets lying on top of irregular fibrinogen coating were excluded from analysis to prevent uncontrollable influences due to the irregularity of the coating. An example for irregular coating can be seen in the fluorescence image of labeled fibrinogen.
c) Especially on selectively coated substrates platelets were able to distort the fibrinogen layer as can be seen in the fluorescence image of labeled fibrinogen. This distortion may in return also influence the cell (*e.g.* size, outline *etc.*). Thus, platelets that visibly distorted the fibrinogen coating were excluded from analysis.
d) Distortions of the substrate itself which may, for example, arise due to small dust particles on the underlying coverslip or stretching of the substrate, were detected by verifying whether the horizontal lines of holes formed a 90°-angle with the vertical lines. This is sketched in a fluorescence image of the labeled fibrinogen by a white vertical line following the vertical line of holes and several horizontal lines forming a 90°-angle with the vertical line. It is visible that the horizontal lines of holes deviate from the white horizontal lines. Platelets lying on this part of the substrate were excluded from analysis.

but lay too close to the neighboring structures or *vice versa* were sorted out.

4.2.1 Spread Area, Perimeter and Ellipse Measurements

After the cell outline had been detected as described in section 4.1, it was filled manually in ImageJ [87] creating a mask of the cell. Afterwards, this mask was selected and the area a_{cell}, as well as the perimeter p_{cell} were measured in ImageJ [87]. Furthermore, an ellipse (orientation, major and minor axis) that had the same area, orientation and eccentricity as the selection was calculated through the second moments (compare [114]) with the *Measure* function in ImageJ [87]. The results were

saved and further processed in OriginPro 8.5G (OriginLab, Northampton, Massachusetts, USA). The perimeter of the above mentioned ellipse was calculated via following equation in OriginPro 8.5G (OriginLab):

$$p_{\text{ellipse}} = \pi \cdot (a+b) \cdot (1 + (3 \cdot \lambda^2 / (10 + \sqrt{(4 - 3 \cdot \lambda^2)}))) \qquad (4.1)$$
$$\lambda = (a-b)/(a+b)$$

with a being the semi-major axis of the ellipse and b the semi-minor axis. This equation is an approximation of the perimeter of an ellipse as described in [99]. The *relative perimeter* of a cell was calculated in OriginPro 8.5G (OriginLab) as $p_{\text{cell}}/p_{\text{ellipse}}$. This relative perimeter shows how "rough" the outline of the cell is, since it takes the smallest value of 1 for a perfect ellipse and gets larger the more protrusions the cell has. Histograms of spread area a_{cell} and of *relative perimeter* $p_{\text{cell}}/p_{\text{ellipse}}$ were plotted in OriginPro 8.5G (OriginLab) with binsizes of $10\,\mu\text{m}^2$ for a_{cell} and 0.1 for $p_{\text{cell}}/p_{\text{ellipse}}$. In these histograms the percentage of values lying in a certain bin was denoted.

4.2.2 Curvature Calculation of Cell Outline

The curvature of the cell outline was analyzed in MATLAB® R2009b (MathWorks®) with a code written by Dr. Sarah Schwarz G. Henriques (PhD thesis, Institute for X-Ray Physics, University of Göttingen). The general program concept is also described in chapter VII of her doctoral thesis [88]. The exact steps of the program used for the data presented here, are described below. First, the platelets were labeled by *bwlabel* (4-connected objects[i]). Then, it was determined which pixels are part of the cell outline through the function *bwtraceboundary*. In this function, pixels that are part of the object have to be non-zero, while the background consists of pixels with the value zero and the connectivity was set to a 4-connected neighborhood[ii]. The found cell outline was then described through a spline, a composite of several polynomial functions each describing a part of the outline. This spline was parametrized via the arc length s along the cell outline. Parametrization with the arc-length was necessary, since the cell outline cannot be described via a function of $y(x)$ at all positions. A spline was calculate for each sequence of 7 points. As

[i] This means that a pixel belonged to the platelet if at least one of its neighboring pixels had a value of non-zero. Neighboring pixels were those pixels directly above/below or left/right of the pixel and not the ones diagonal to it.

[ii] Neighboring pixels were in this case again those pixels directly above/below or left/right of the pixel and not the ones diagonal to it.

the curvature was only calculated for static data here, no reference start-point on the cell outline had to be defined. The curvature of the calculated spline was obtained by $|\overrightarrow{c'}(s)| = \sqrt{\frac{\partial^2 x(s)}{\partial s^2} + \frac{\partial^2 y(s)}{\partial s^2}}$. After curvature calculation, the values were further processed in OriginPro 8.5 G (OriginLab). The curvature were sorted into bins of $0.2\,\mu\mathrm{m}^{-1}$. The percentages of values in the different bins was determined and the differences between the curvature of the cell outline on structured and flat substrates was obtained by subtracting the values on flat substrates from those on structured substrates.

4.3 Analysis of Non-Fixed Platelets

Preprocessing of data from non-fixed platelets spreading on structured and flat substrates is described below. If platelets still showed a large, bright spot in their middle after the time lapse series had been completed, they were excluded from further analysis. These platelets did most likely not spread completely with the bright spot displaying a lot of cell material still accumulated in the middle. An example of such a cell can be seen in figure 4.3. Note that in the beginning of spreading platelets usually showed this bright spot and thus also the cell in figure 4.1 a) still showed this spot. Furthermore, platelets that showed a persistent and clear contact to other platelets were sorted out. The time lapse series were only analyzed up to the point, where the platelets did not yet interact. Platelets that were situated on a flat part of the substrate but lay too close to the neighboring structures or vice versa were sorted out as well. Finally, if a cell was present in less than 400 images of the time lapse series or it could only be analyzed for less than 400 images due to interactions with other platelets, this platelet was not analyzed. The images were only analyzed if the cell was clearly visible, *i.e.* if the contrast was not too low. The contrast was usually sufficient in the first 1200 images of a time-lapse series, since cells take up the dye after a certain time [64]. However, the time point at which the contrast becomes too low, depends on the amount of time that has elapsed since staining. Consequently, not all time lapse series were analyzed until frame 1200. Very small distortions of substrates were allowed. If the angle between the horizontal and vertical lines deviated by no more than 2° from 90° (see figure 4.2 d) for a sketch of distortions), the platelets lying on top of the substrate were included in the further analysis.

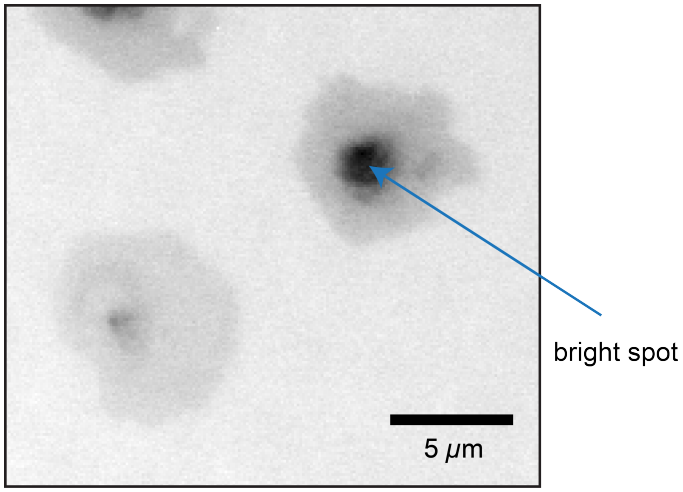

Figure 4.3.: Example of a cell still containing a large, bright spot after the time lapse series had been completed.
The image of the membrane-staining has been taken after the time lapse had ended with 60 ms illumination time and 41.86% lamp power (further description of imaging in section 3.6). The fluorescence image has been inverted for better visibility. The cell in the lower left is completely spread and no large, bright point in the middle is visible in contrast to the cell on the right.

4.3.1 Drift Correction

To be able to compare the position of the cell outlines between pictures in the time lapse studies, the time lapse series had to be corrected for drift. The drift and its correction were computed in MATLAB® R2009b (MathWorks®) based on a description on how to correlate two pictures provided by Mathworks® (Natick, Massachusetts, USA) in [94].
Drift detection was carried out based on the corresponding time lapse series of the fibrinogen coating of the substrate, since the coating did not change as strongly over time as the platelets. Drift detection was accomplished by determining the cross-correlations using the *normxcorr2* function [94]. Cross-correlations were calculated between one image (reference image) and each of the images of the stack. Usually, the reference image was taken from later points in the time lapse series, since these images were mostly better in focus than pictures in the beginning and thus drift correction was more reliable.[iii] The drift correction values for each image of the time lapse series were obtained by computing the maximum in cross-correlation between the reference image and this particular image [94]. In order to correct for the drift between images taken from the platelets, these images were corrected with the drift correction values calculated for the respective images of the substrate coating using the *imtransform* function. Translation was performed

[iii] Comparing succeeding images did not lead to the desired results in this case, since the drift between succeeding images can be smaller than one pixel and these small drifts could not be detected with this method.

as described in [34].

4.3.2 Filling of Platelet Outlines

For further analysis of the platelets, the cell outlines had to be filled and parts of the image not belonging to the cell of interest had to be removed. A sketch of the different main steps of this process is shown in figure 4.4.
To accelerate the algorithm, a region of interest (ROI) was defined around the cell by using a manual input option (*ginput*). All parts of this ROI that did not belong to the cell outline were removed by the function *bwareaopen* (threshold 90 pixels[iv]) and the remaining outline was filled by *imfill*. The processed ROI was then inserted into an empty image, which had the same size as the original image, at the position from which it had been taken in the original image. This procedure ensures that the cell is positioned exactly as it had been in the original image. Having the cell at the same position as in the original image is desirable, since it simplifies correlations to the underlying substrate imaged through the coating of the substrate.
In a last step, the processed images were again checked in ImageJ [87] in order to remove remaining objects that had not been filtered out by *bwareaopen* and to fill cell outlines manually that had not been closed and thus could not be filled by

[iv] All objects that contained less than 90 pixels are removed. The connectivity was set to 8 in this function, *i.e.* neighboring pixels were all pixels around the pixel.

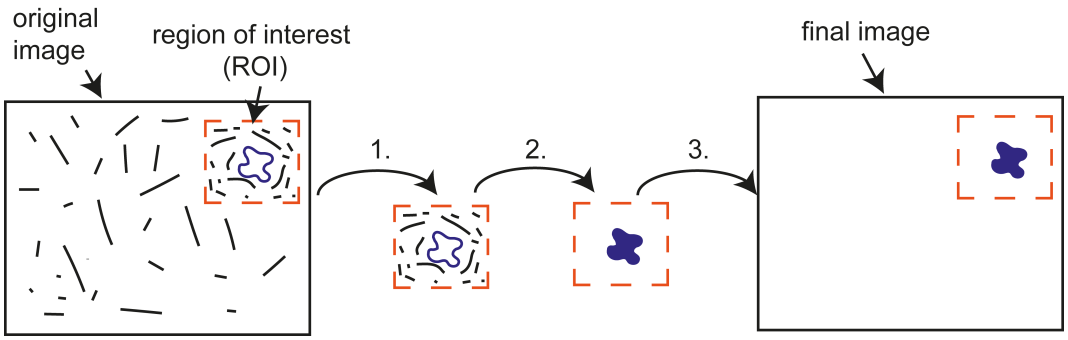

Figure 4.4.: Sketch of the three main steps of cell extraction.
1.) In a first step a region of interest (ROI, orange) was defined around the cell (blue).
2.) Filling of outlines and removal of parts outside the cell (black) only took place inside this ROI to improve algorithm performance.
3.) The processed ROI was inserted into an empty image having the same size as the original image at the position from which the ROI had been taken in the original image.

imfill. If the detected parts of the cell were shorter than 90 pixels in some images[v], these images were processed as described above, but with a smaller threshold for *bwareaopen* (same connectivity as above) of 10 pixels or 40 pixels (depending on cell size). In figure 4.5 an example for filling of cell outlines is shown.

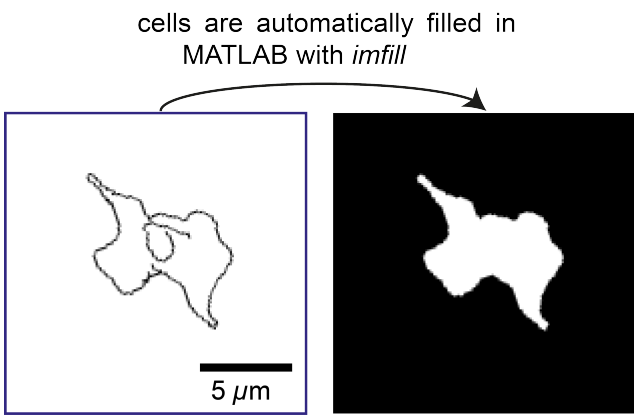

Figure 4.5.: An example of automatic filling of cell outlines. The images have been rotated in ImageJ [87] (bilinear interpolation) to align the rows of holes with the image borders. The left image has been inverted for better visibility. The detected cell outlines were filled automatically with the *imfill* function after parts outside the cell were removed by the *bwareaopen* function.

4.3.3 Spreading in Distinct Directions and Comparison to Ellipse

As the holes in the structured substrates alternate with interspaces, the cell encountered different conditions on these two regions of the substrate. Hence, the analysis has to describe the spreading behavior locally. One way to obtain a local description is to analyze the spreading along straight lines of different directions, which provides a *spreading length* depending on the position along the cell outline. One disadvantage of simply computing this spreading length is that, when comparing these lengths, effects due to cell shape superimpose smaller differences that may show alterations in spreading behavior. To compensate for these influences, an ellipse was calculated as reference that had the same orientation, eccentricity and area as the cell. To this end, first, the orientation as well as major and minor axis of an ellipse that has the same normalized second central moments as the cell were calculated. Secondly, the length of minor and major axis were scaled so that the ellipse adopted the same area as the cell while keeping the eccentricity constant. By comparing the spreading length with the extension of the ellipse along the straight lines, effects of overall cell shape (*e.g.* eccentricity) can be neglected.
The nomenclature for this analysis is as follows (see also table 4.1): Points lying on the ellipse are denoted as $q_{\text{ellipse}}(b,t)$, points lying on the cell outline as $q_{\text{cell}}(c,t)$, points lying on the straight lines as $q_{\text{line}}(d,\alpha)$, points of intersection between the

[v]This was only the case in the first images after attachment to the substrate.

straight lines and the cell outline as $p_{\text{cell}}(\beta, t)$ and points of intersection between the straight lines and the ellipse as $p_{\text{ellipse}}(\beta, t)$. $b \in [1, N_{\text{ellipse}}]$ defines a specific point on the ellipse with N_{ellipse} being the total number of points on the ellipse. $c \in [1, N_{\text{cell}}]$ defines a specific point on the cell outline with N_{cell} being the total number of points on the cell outline. Lastly, $d \in [1, N_{\text{line}}]$ defines a specific point on the straight lines with N_{line} being the total number of points on the line. $\alpha \in [0°, 165°]$ with 15° increments represents the angle the straight line encloses with the x-axis of the image and $\beta = \{\alpha, \alpha + 180°\}$[vi].

Table 4.1.: Abbreviations used in this section to describe variables needed to compute vectors from ellipse to cell outline.

$q_{\text{line}}(d, \alpha)$	points situated on the straight lines
$q_{\text{ellipse}}(b, t)$	points situated on the ellipse
$q_{\text{cell}}(c, t)$	points situated on cell outline
$p_{\text{ellipse}}(\beta, t)$	points of interception between the straight lines and the ellipse
$p_{\text{cell}}(\beta, t)$	points of interception between the straight lines and the cell outline
$\vec{v}_{\text{cell-ellipse}}(\beta, t)$	vector between the points $p_{\text{cell}}(\beta, t)$ and $p_{\text{ellipse}}(\beta, t)$
$l_{\text{cell-ellipse}}(\beta, t)$	signed length of vector $\vec{v}_{cell-ellipse}(\beta, t)$

For easier comparison, the images of time lapse series on structured substrates were rotated by the *imrotate* function (method: bilinear, bounding box: loose) to align the rows of holes in the underlying substrate with the image borders. The angle needed to align the substrate with the image borders was found as described in section 4.4. Afterwards, the images of the platelets were binarized again[vii]. Then, the cell area, the cell centroid as well as the length of major and minor axis and orientation of the above described ellipse that has the same normalized second central moments as the cell were computed using the functions *bwlabel* (4-connected objects[viii]) and *regionprops*. The major and minor axis of the ellipse were scaled so that the ellipse has the same area as the cell but the eccentricity was kept constant. Based on the centroid, the length of the major and minor axis and the orientation of the ellipse, points situated on the ellipse can be calculated following

[vi] If the straight lines go through any point that lies within the cell and not only touches the outline of the cell (see below), two points of interception were found and thus one was defined as belonging to α while the other one belonged to $\alpha + 180°$. The same holds true for the ellipse.

[vii] Due to the interpolation when rotating the binarized image, especially pixels at the cell outline can have values differing from 255.

[viii] This means that a pixel belonged to the cell if at least one of its neighboring pixels had a value of non-zero. Neighboring pixels were those pixels directly above/below or left/right of the pixel and not the ones diagonal to it.

the instruction given in [35]. The number of calculated points on the ellipse N_{ellipse} was set to 120.

The straight lines, along which the spreading was evaluated, were computed by the following equation:

$$y(x) = y_0 + (x - x_0) \cdot m \tag{4.2}$$

with $m = \tan(\alpha)$. Additionally, the lines went through the mean center of mass (centroid) of the cell (x_0, y_0). The mean center of mass was calculated by averaging the center of mass positions of the cell in all frames containing a binarized and filled cell. An example for these lines is shown in figure 4.6, where also the definition of the angles is shown.

To ensure that for $p_{\text{cell}}(\beta, t)$ only points were detected that were situated on the cell outline, this outline was extracted by the function *bwperim* (8-connected neighborhood[ix]) and used for further analysis. If all of the points $q_{\text{cell}}(c, t)$ in an image had at least a distance of 2 pixels to the mean center of mass and the mean center of mass lay within the cell, the image was analyzed. Other images were omitted, since the large movement of the center of mass of the cell would have influenced the results. The further analysis detected points of interception between the cell outline and the straight lines as well as points of interception between the ellipse and the straight lines ($p_{\text{cell}}(\beta, t)$ and $p_{\text{ellipse}}(\beta, t)$, respectively). A sketch of how the points $p_{\text{ellipse}}(\beta, t)$ were detected can be found in figure 4.7.

[ix] This means that a pixel belonged to the outline if at least one of its neighboring pixels had a value of zero. Neighboring pixels were all pixels around the pixel.

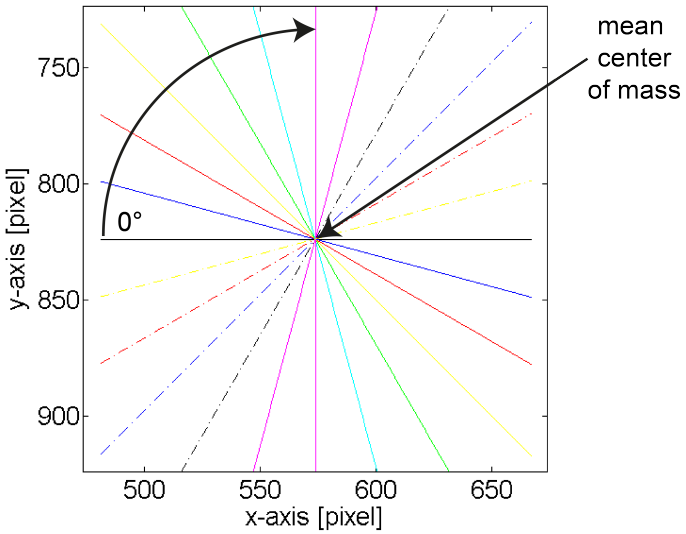

Figure 4.6.: Plot of the computed straight lines for one cell.
The line of 0° and the direction of following angles are marked. Furthermore, the mean center of mass is marked.

To maximize the number of points that were detected, the number of points on the lines N_{line} was increased by computing values for approximately every 0.2 pixel (in x-direction).
To detect $p_{\text{cell}}(\beta,t)$ and $p_{\text{ellipse}}(\beta,t)$, the x- and y-values of the points $q_{\text{cell}}(c,t)$ as well as of the points $q_{\text{ellipse}}(b,t)$ were compared to those on the lines $q_{\text{line}}(d,\alpha)$. To detect $p_{\text{cell}}(\beta,t)$, those values on the cell outline were searched that had the same x- and y-values as the rounded values on the straight lines[x]. The search was directly terminated after a point $p_{\text{cell}}(\beta,t)$ was detected and the same procedure was performed again to find the second point of interception on the opposite site of the cell outline. To detect $p_{\text{ellipse}}(\beta,t)$, the x- and y-values of the points $q_{\text{ellipse}}(b,t)$ were compared to those on the lines $q_{\text{line}}(d,\alpha)$. If the distance between the points $q_{\text{ellipse}}(c,t)$ and $q_{\text{line}}(d,\alpha)$ was smaller than 1.5 pixels,

[x]Due to the pixelated nature of the cell outline rounding to the nearest natural number was necessary.

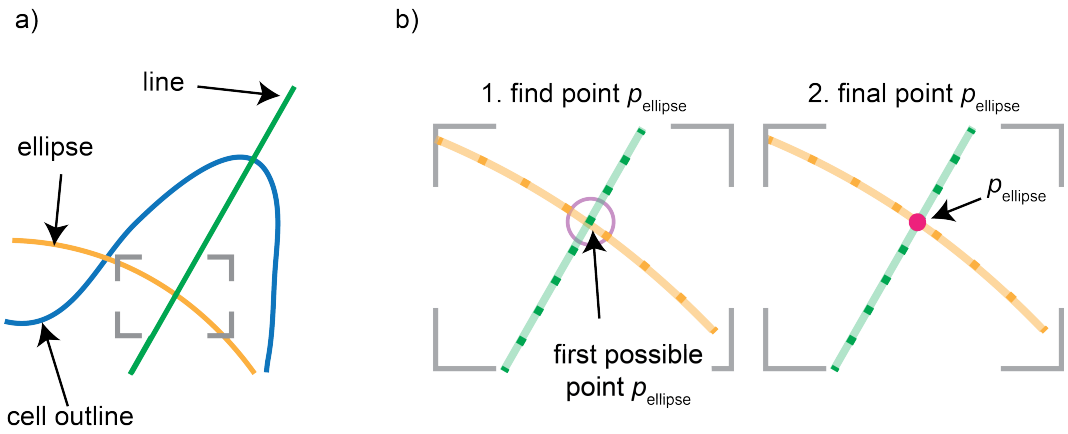

Figure 4.7.: Illustration of detection of the points $p_{\text{ellipse}}(\beta,t)$. The sketch shows the situation for one specific direction and one time point and illustrates how one point of interception was detected, the second point on the opposing site was detected accordingly.
a) The sketch shows a part of a cell outline (blue), a part of the corresponding ellipse (orange) and a part of the straight line (green) along which the points $p_{\text{ellipse}}(\beta,t)$ were detected.
b) Detail of the sketch in a) showing how a point $p_{\text{ellipse}}(\beta,t)$ was detected. 1. If a point on the line $q_{\text{line}}(d,\alpha)$ (green) lay less than 1.5 pixels (indicated by magenta circle) apart from a point on the ellipse $q_{\text{ellipse}}(c,t)$, a point $p_{\text{ellipse}}(\beta,t)$ was detected. 2. The search was terminated after a point (final point $p_{\text{ellipse}}(\beta,t)$ marked with pink circle) was detected and the same procedure was performed again to find the second point of interception on the opposing site of the ellipse. For $\alpha = 90°$ points on the ellipse were searched that did not deviate by more than 1 pixel from the x-position of the mean center of mass (not sketched here). In order to prevent detection of the same point, the detected points on opposite sites of the ellipse had to be spaced more than 2.5 pixels apart.

a point $p_{\text{ellipse}}(\beta, t)$ was detected. The search was directly terminated after a point $p_{\text{ellipse}}(\beta, t)$ was detected and the same procedure was performed again to find the second point of interception on the opposite site of the ellipse. In order to prevent detection of the same point, the detected points on opposite sites of the ellipse had to be spaced more than 2.5 pixels apart. As points $p_{\text{ellipse}}(\beta, t)$ the points on the straight line were given. In the case of $\alpha = 90°$[xi], points on the ellipse $p_{\text{ellipse}}(\beta, t)$ were detected that had an x-value that differed no more than 1 pixel from the x-value of the mean center of mass. Again, the detected points on opposite sites of the ellipse had to be spaced more than 2.5 pixels apart (see above). As $p_{\text{ellipse}}(\beta, t)$ the values for the points on the ellipse were given. For the cell outline and $\alpha = 90°$, points were searched that had the same x-value as the rounded x-value of the mean center of mass[xii]. In order to determine whether the detected points $\left(p_{\text{cell}}(\beta, t) \text{ and } p_{\text{ellipse}}(\beta, t)\right)$ belonged to the angle $\beta = \alpha$ or to the angle $\beta = \alpha + 180°$ (see figure 4.6), the position of the points in relation to the position of the mean center of mass was taken into account. Finally, the differences between $p_{\text{cell}}(\beta, t)$ and $p_{\text{ellipse}}(\beta, t)$ in x- and y-direction $\left(d_x(\beta, t)/d_y(\beta, t)\right)$ as well as the lengths of the corresponding vectors $\vec{v}_{\text{cell-ellipse}}(\beta, t)$ between $p_{\text{cell}}(\beta, t)$ and $p_{\text{ellipse}}(\beta, t)$ were calculated. An example of the result of this analysis is shown in figure 4.8. In this figure the ellipse is shown in black, the cell in blue, the points of interception between straight lines and cell outline $p_{\text{cell}}(\beta, t)$ are shown in red, the points of interception between straight lines and ellipse $p_{\text{ellipse}}(\beta, t)$ in cyan and the resulting vectors $\vec{v}_{\text{cell-ellipse}}(\beta, t)$ between the ellipse and cell outline are shown in magenta.

4.3.4 Further Data Analysis

Moving Average

The moving average of the above calculated cell area as well as of $d_x(\beta, t)$, $d_y(\beta, t)$ and the lengths of corresponding vectors $\vec{v}_{\text{cell-ellipse}}(\beta, t)$ were calculated. By this procedure, small errors that arised, *e.g.* from imprecisely detected cell outlines could be minimized, while preserving the overall result. Furthermore, missing values could be interpolated.

The moving average of a variable (see above) at a frame f_i was calculated by taking

[xi] For this direction the line was defined as $x = x(\text{mean center of mass})$.

[xii] Due to the pixelated nature of the cell outline rounding to the nearest natural number was necessary.

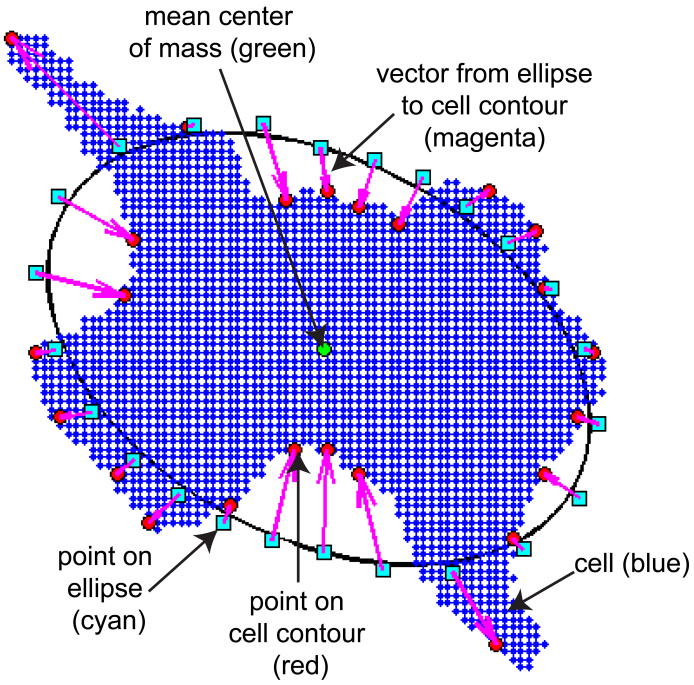

Figure 4.8.: Plot of points of interception between straight lines and cell outline $p_{\text{cell}}(\beta, t)$, points of interception between straight lines and ellipse $p_{\text{ellipse}}(\beta, t)$ as well as the resulting vectors.
The corresponding ellipse is shown in black, the cell in blue, the points of interception between straight lines and cell outline in red, the points of interception between straight lines and the ellipse in cyan and the resulting vectors $\vec{v}_{\text{cell-ellipse}}(\beta, t)$ in magenta.

the average of all values of this variable in an interval $[f_{i-10}, f_{i+10}]$[xiii]. Each frame represents one time point. The choice of the number of values that were averaged is discussed further in section 6.2. The sign of the vectors ($\vec{v}_{\text{cell-ellipse}}(\beta, t)$, magenta in figure 4.8) was calculated based on the moving average treated $d_x(\beta, t)$ and $d_y(\beta, t)$, *i.e.* the differences between cell outline and ellipse in x- and y-direction. If the cell outline lay inside of the ellipse, the sign of $\vec{v}_{\text{cell-ellipse}}(\beta, t)$ was denoted as negative, if it lay outside of the ellipse the sign was denoted as positive. The moving average of the signed length $l_{\text{cell-ellipse}}(\beta, t)$ was plotted via *imagesc* as can be seen in figure 4.9.

To describe the interdependencies of the different values of $\vec{v}_{\text{cell-ellipse}}(\beta, t)$, both the variance of $l_{\text{cell-ellipse}}(\beta, t)$ between the different angles/directions at fixed time points (see figure 4.6) var_{dir} as well as the variance of $l_{\text{cell-ellipse}}(\beta, t)$ between the different time points for a fixed angle/direction var_{time} were computed. The former describes the relations between, *e.g.* spreading over holes and on interspaces on structured substrates, the latter the dynamics along different directions. Additionally, the variances var_{dir} and var_{time} were calculated based on the original, *i.e.* not moving average treated values for the signed lengths $l_{\text{cell-ellipse}}(\beta, t)$. In figure

[xiii] For the first and last 10 frames the size of the interval was adjusted to the number of available frames on the site of the interval where there were fewer than 10 frames.

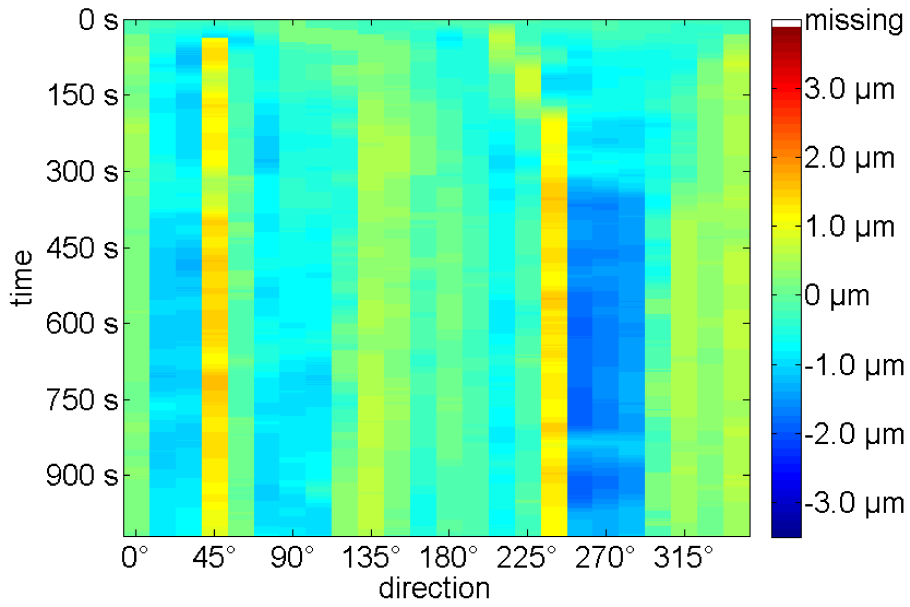

Figure 4.9.: Plot of the moving average of the signed lengths $l_{\text{cell-ellipse}}(\beta, t)$ of the cell shown in figure 4.8.
The values for different angles corresponding to the different lines (see figure 4.6) are shown on the x-axis and the evolution over time is shown on the y-axis. The signed lengths $l_{\text{cell-ellipse}}(\beta, t)$ are shown color-coded ranging from dark blue for the largest negative values, *i.e.* the cell outline lies inside the ellipse, to dark red for the largest positive values, *i.e.* the cell outline lies outside of the ellipse. A further discussion of these plots can be found in chapter 6. The missing values are shown in white.

4.10 an illustration of how the variances are calculated is shown. The area values in the last 50 images of all analyzed images were averaged for each platelet and plotted with the box-plot option in OriginPro 8.5 G (OriginLab). Furthermore, the mean values of var_{dir} were calculated and plotted, both in OriginPro 8.5 G (OriginLab). The mean areas and the mean var_{dir} values were calculated from the moving average treated data. Furthermore, the areas and variances were plotted in OriginPro 8.5 G (OriginLab).

Events of Retraction and Protrusion

Based on the moving average of the signed length $l_{\text{cell-ellipse}}(\beta, t)$, the spreading behavior was analyzed further by detecting events of large retraction or outgrowth. A further discussion of the choice of the parameters chosen here to detect retractions and outgrowth can be found in section 6.2.
To detect large retractions and outgrowth, the difference of each $l_{\text{cell-ellipse}}(\beta, t)$-value in frame $t = f_i$ with the corresponding value in frame $t = f_{i+120}$ was computed. This difference is denoted as $d(\beta, f_i, f_{i+120}) = |l_{\text{cell-ellipse}}(\beta, f_i) - l_{\text{cell-ellipse}}(\beta, f_{i+120})|$ in the following. If the absolute value of the above calculated difference was at least 0.75 μm and the differences $d(\beta, f_i, f_{i+x})$ with x lying in the interval $[i + 121\ ,\ i + 160]$ showed similar values as $d(\beta, f_i, f_{i+120})$, *i.e.* $d(\beta, f_i, f_{i+x}) \geq d(\beta, f_i, f_{i+120}) - 0.1\,\mu$m, this was defined as an event.[xiv] Furthermore, the sign of the differences $d(\beta, f_i, f_{i+120})$ and $d(\beta, f_i, f_{i+x})$ was required to stay the same. By comparing $l_{\text{cell-ellipse}}(\beta, t)$ in frame $t = t_i$ with $l_{\text{cell-ellipse}}(\beta, t)$ in frame $t = t_{i+120}$, *i.e.* 180 seconds later, and ensuring that the differences were maintained for at least 40 more frames, *i.e.* 60 seconds, simple fluctuations were excluded. Multiple detec-

[xiv] For the last 160 frames no events could be detected as comparable points later in time were missing.

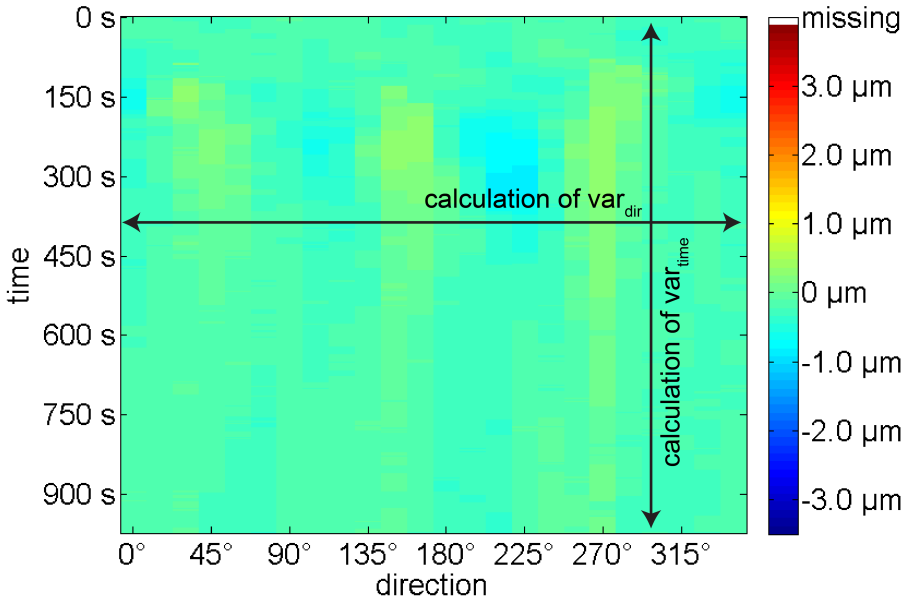

Figure 4.10.: Illustration of calculation of the two variances var_{dir} and var_{time}. The arrows show on basis of which values the variances were calculated.

tions of one event were sorted out by the condition that different events (along one direction) had to happen at least 50 frames, *i.e.* 75 seconds apart in time. As time point at which the event took place, the time of frame f_{i+120} was denoted. Furthermore, it was denoted whether the event signifies a protrusion or an invagination based on whether the cell outline lay within, outside or on the ellipse in the frame f_{i+120}. Finally, also the direction of the change was computed, *i.e.* whether the invagination was filled up/the protrusion grew or the invagination got larger/the protrusion retracted. These data are shown in chapter 6.

Display of Cell Outlines over Time

First, the images were rotated by the function *imrotate* (bilinear interpolation, bounding box: loose, see also section 4.3.3). The rotation alines the underlying rows of holes with the image borders. Then, the cell outline was found as described in section 4.2.2 by the functions *bwlabel* and *bwtraceboundary*. Thereafter, the outline in each frame was plotted in a color-coded way ranging from dark blue for early time points to dark red for later time points. Examples for this way of presentation can be found in figure 6.5 in chapter 6.

4.3.5 Tracing of Cellular Protrusions

In order to fully describe how the platelets sense and then deal with the underlying substrate in terms of spreading, the movement and positions of cellular protrusions were analyzed here. To this end, the endpoints of filopodia and broad, blunt protrusions were traced. The used algorithms are described in detail in the following.

The images were rotated by *imrotate* (bilinear interpolation, bounding box: loose, see also section 4.3.3) to align the rows of holes in the underlying substrate to the image borders. Then, points lying on the cell outline r were found as described in section 4.2.2 by the functions *bwlabel* and *bwtraceboundary*. Furthermore, the curvature of the cell outline was calculated as described in section 4.2.2 with a spline being fitted to 5 instead of 7 points due to differences in magnification.[xv] Furthermore, the lengths $l(r)$ from center of mass c_{mass} of the cell to the points lying on the cell outline were computed. A further discussion of the choice of the parameters chosen here to detect protrusions can be found in section 7.2.

[xv] The data analyzed in section 4.2.2 were recorded using a 100×-objective, while the data analyzed here were recorded with a 60×-objective.

Detection of Filopodia Endpoints

Filopodia were easier to identify than broad, blunt protrusions, like *e.g.* protruding lamellipodia, as filopodia are morphologically more distinct[xvi]. One possible means to identify filopodium endpoints was the high curvature at the endpoint of a filopodium. Additionally, filopodia protrude from the rest of the cell, so the length $l(r_1)$ from the center of mass to cell outline was higher than the length for the neighboring points on the cell outline. Here, a combination of these two characteristics was employed to find a stable way to track the endpoints of filopodia. The description of variables used in this section can be found in table 4.2.
In figure 4.11 a sketch of the points r_1, r_{left} and r_{right} as well as the lengths $l(r_1)$, $l(r_{\text{left}})$ and $l(r_{\text{right}})$ of the distances from these points to the center of mass of the cell can be found. Furthermore, the set of constraints employed in this analysis to find an endpoint of a filopodium is detailed in this figure.
Each point r_1 was compared to two other points, one lying 11 points left (r_{left}) and one lying 11 points right (r_{right}) along the outline from this point. To find reference points for the first and last points along the cell outline, periodic boundary conditions were employed. The length $l(r_1)$ had to be more than 5 pixels larger than the mean length of the vectors from center of mass to the points left and right ($l_{\text{mean, point}} = (l(r_{\text{left}}) + l(r_{\text{right}}))/2$) of point r_1 and had also to be larger than the individual lengths $l(r_{\text{left}})$ and $l(r_{\text{right}})$. If the cell was nearly completely spread,

[xvi] at least in fluorescence images of the cell membrane

Table 4.2.: Abbreviations used in this section to describe variables needed for the detection of endpoints of filopodia.

r_1	point on cell outline
r_{left}	reference point left of point r_1
r_{right}	reference point right of point r_1
$l(r_1)$	length of vector from center of mass to point r_1
$l(r_{\text{left}})$	length of vector from center of mass to point r_{left}
$l(r_{\text{right}})$	length of vector from center of mass to point r_{right}
l_{min}	minimal length from center of mass to cell outline for whole cell
l_{mean}	mean length from center of mass to cell outline for whole cell
A_{fin}	final area, *i.e.* area in last image
s	detected endpoint of filopodium
$c(s)$	curvature of detected endpoint of filopodium
c_{mean}	mean curvature for whole cell outline
c_{max}	maximal curvature for whole cell outline

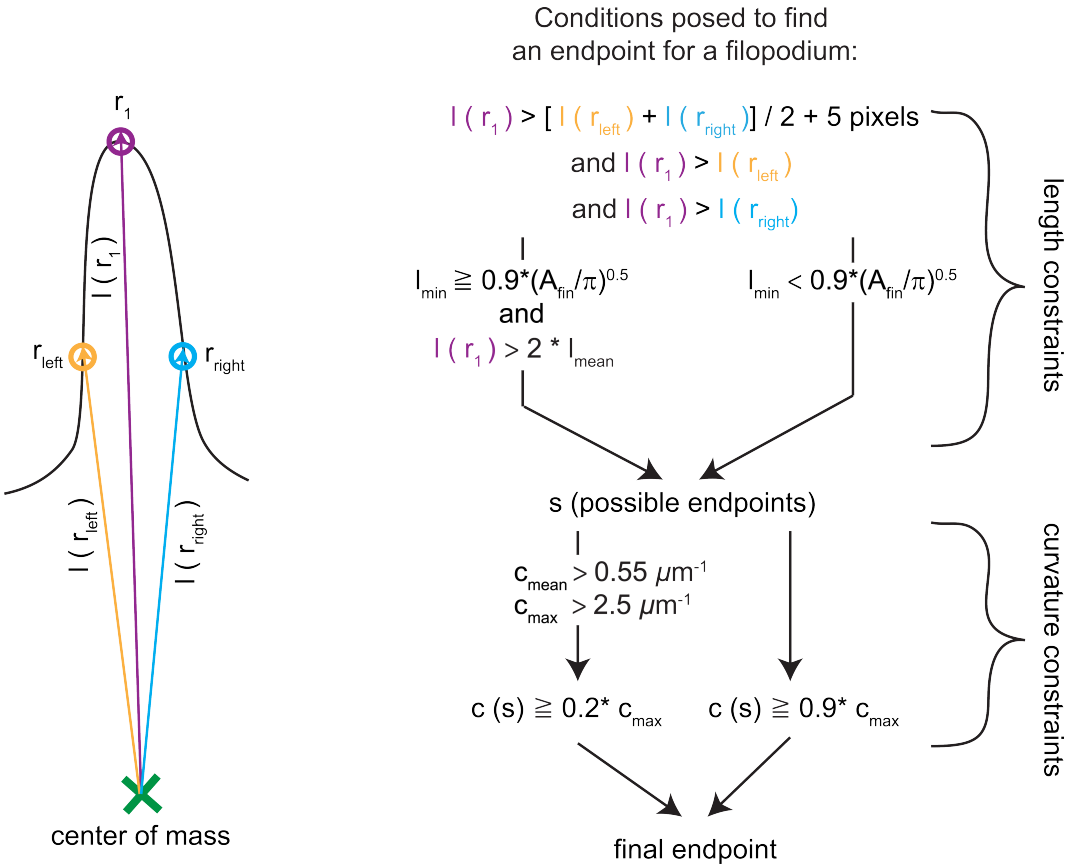

Figure 4.11.: Sketch showing the points r_1, r_{left} and r_{right} and the lengths of the vectors from center of mass of the cell to these points as well as a list of the set of constraints posed on the endpoints of filopodia.
(left) The point r_1 is shown in purple, the point r_{left} in dark yellow and the point r_{right} in light blue. The lengths of the vectors from the center of mass of the cell (green cross) to the points are shown in matching colors.
(right) The set of constraints posed to define an endpoint of a filopodium. The constraint that was posed on the distance between individual filopodia is not shown here. Definitions for the variables used here are given in table 4.2.

i.e. the minimal value l_{min} was at least as large as 90% of $(A_{\text{fin}}/\pi)^{0.5}$, with A_{fin} being the cell size[xvii] in the last image of the cell, the length $l(r_1)$ had to be more than twice as long as the mean length l_{mean} in this image. If l_{min} was smaller than 90% of $(A_{\text{fin}}/\pi)^{0.5}$, no condition for the minimal length from center of mass to cell outline was employed. Points that fulfilled these criteria were termed s.
Secondly, a constraint was posed on the curvature of the cell outline in point s. If the mean curvature for the whole platelet c_{mean} was higher than $0.55\,\mu\text{m}^{-1}$ and

[xvii] in pixel · pixel

the maximal curvature c_{max} was higher than 2.5 μm^{-1}, the curvature $c(s)$ at point s had to be at least 20% of c_{max}. Otherwise, the curvature $c(s)$ had to be at least 90% of c_{max}. Finally, in order to avoid multiple detections of filopodia endpoints, detected endpoints had to be situated at least 10 pixels apart from each other[xviii]. If more than one point was detected in too close vicinity, the point with the larger length $l(r_1)$ from center of mass to cell outline was designated as filopodium endpoint. A sketch of the found endpoints of protrusions can be seen in figure 4.12.

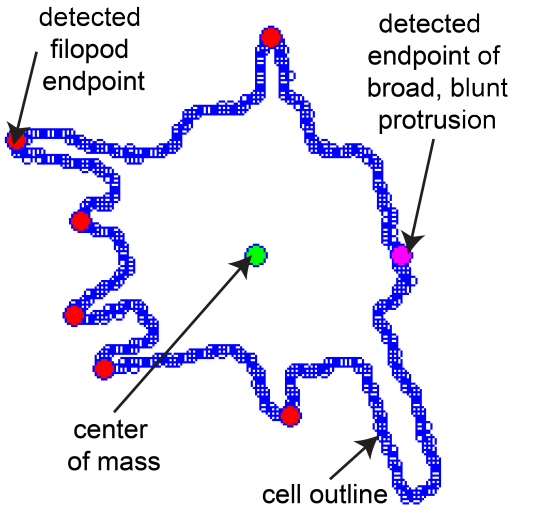

Figure 4.12.: Plot of detected protrusions for one time point in spreading.
Detected endpoints of filopodia are marked with red circles and the detected endpoint of a broad, blunt protrusion with a magenta circle. The center of mass of the cell in this image is marked with a green circle and the cell outline is plotted in blue. As can be seen for the protrusion in the lower right corner, the algorithm sometimes failed to detect protrusions. This is discussed further in section 7.2.

Detection of Endpoints of Broad, Blunt Protrusions

The detection of endpoints of broad, blunt protrusions followed the same scheme as the detection of endpoints of filopodia described above. The names of variables used in this section are shown in table 4.3.
In figure 4.13 a sketch of the points t_1, t_{left} and t_{right} as well as the lengths of the vectors from these points to the center of mass of the cell $l(t_1), l(t_{left})$ and $l(t_{right})$ can be found. Similarly as in figure 4.11 the set of constraints employed in this analysis to find an endpoint of a broad, blunt protrusion is detailed in figure 4.13. The reference points t_{left} and t_{right} lay 25 points left and right from the point t_1 along the outline. Again periodic boundary conditions were employed. In this case, however, as broad, blunt protrusions shall be detected, the length $l(t_1)$ had to be larger than the mean length of the points left and right ($l_{mean,\,point} = (l(t_{left}) + l(t_{right}))/2$) of point t_1. Additionally, the length $l(t_1)$ had to be also larger than the individual lengths $l(t_{left})$ and $l(t_{right})$.

[xviii] Also double detections of the same points were sorted out.

Table 4.3.: Abbreviations used in this section to describe variables needed for the detection of endpoints of broad, blunt protrusions

t_1	point on cell outline
t_{left}	reference point left of point t_1
t_{right}	reference point right of point t_1
$l(t_1)$	length of vector from center of mass to point t_1
$l(t_{\text{left}})$	length of vector from center of mass to point t_{left}
$l(t_{\text{right}})$	length of vector from center of mass to point t_{right}
l_{mean}	mean length from center of mass to cell outline for whole cell
l_{max}	maximal length from center of mass to cell outline for whole cell

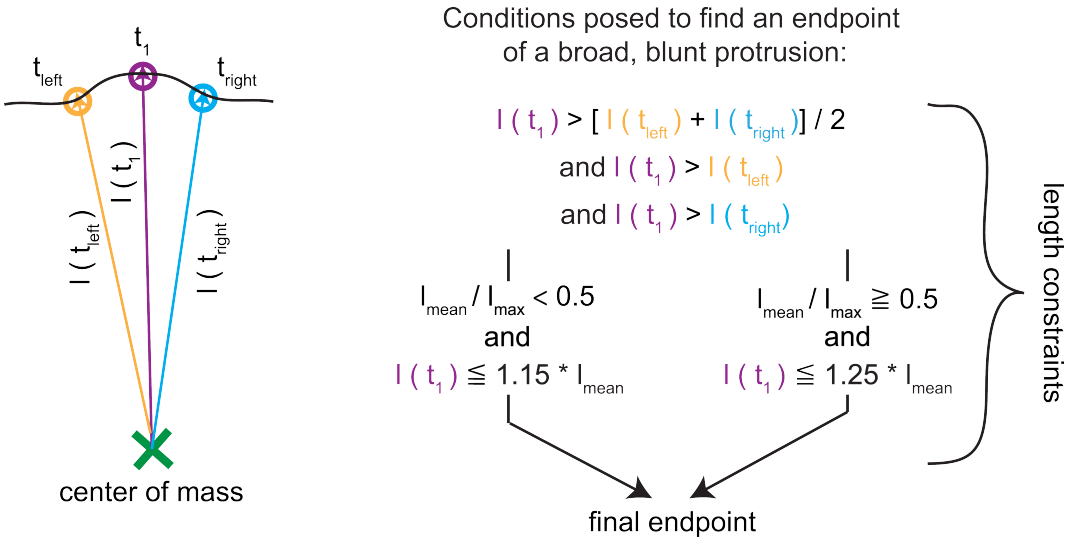

Figure 4.13.: Sketch of the points t_1, t_{left} and t_{right} and the lengths of the vectors from center of mass of the cell to these points as well as a list of the constraints posed here to the endpoints of broad, blunt protrusions.
(left) The point t_1 is shown in purple, the point t_{left} in dark yellow and the point t_{right} in light blue. The corresponding lengths of the vectors from the center of mass of the cell (green cross) to these points is shown in the same colors as the points.
(right) The set of constraints posed in this analysis to detect endpoints of broad, blunt protrusions. The definition of variables used in this analysis is shown in table 4.3. The constraint that was posed on the distance of a broad, blunt protrusion to other broad, blunt protrusions or to filopodia is not shown here.

In order to exclude filopodia, a condition was posed on the length $l(t_1)$. If the fraction $\frac{l_{\text{mean}}}{l_{\text{max}}}$ was smaller than 0.5, *i.e.* the maximal length was much larger than the mean value, $l(t_1)$ had to be smaller or equal to 115% of l_{mean}. If the maximal value was comparable to the mean value, *i.e.* $\frac{l_{\text{mean}}}{l_{\text{max}}} \geq = 0.5$, $l(t_1)$ had to be smaller or equal to 125% of l_{mean}. Furthermore, the protrusions detected in this analysis

had to be situated at least 25 pixels apart from the above detected filopodia. This condition partly avoided detection of points along the filopodium which otherwise would have met the conditions posed above. Finally, individual protrusions detected in this analysis had to be spaced at least 25 pixels apart to avoid multiple detections. If more than one point was detected in too close vicinity, the point with the larger length $l(t_1)$ from center of mass to cell outline was chosen as endpoint.

Tracing of Protrusion Endpoints over Time

In order to be able to follow the movement of endpoints of broad, blunt protrusions and endpoints of filopodia, the endpoints in different images had to be assigned to each other, *i.e.* traced. A sketch of how an endpoint was assigned is given in figure 4.14.
In order to trace a protrusion, the position of the endpoints were compared to the positions of the endpoints in all former images and grouped accordingly. To assign an endpoint to a filopodium, at least one endpoint of the group in the former images has to be as close as 8 pixels to the position of the endpoint. In the case of the broad, blunt protrusions this distance was set to 10 pixels. The endpoint was always assigned to the filopodium/protrusion that was closest in the former images but only if no other endpoint had already been assigned to the specific filopodium/protrusion in this image[xix]. If an endpoint could not be assigned to

[xix] The possibility of having two endpoints in one image for a single protrusion was not allowed for.

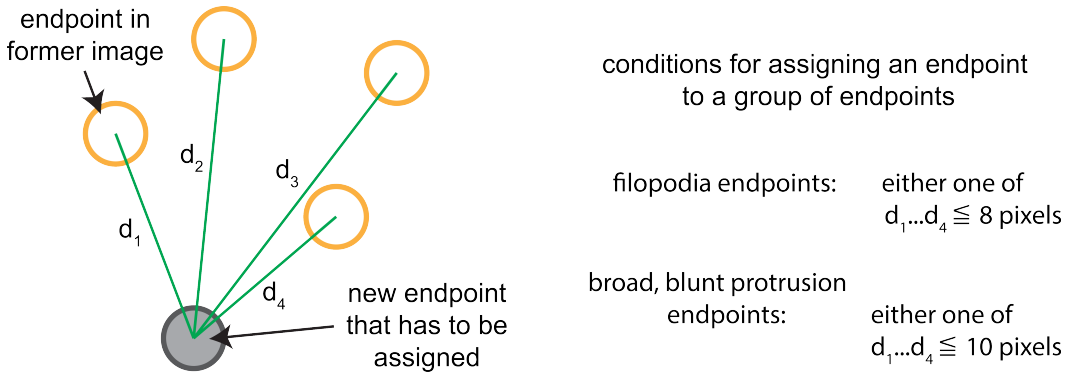

Figure 4.14.: Sketch of how endpoints of protrusions were assigned.
The endpoint that has to be assigned is shown as filled gray circle and endpoints belonging to one protrusion (from former images) are shown as open, dark yellow circles. The distances between the position of the endpoint that has to be assigned and the endpoints from former images are shown in green. On the right hand side, the constraints that were posed on the distances are denoted.

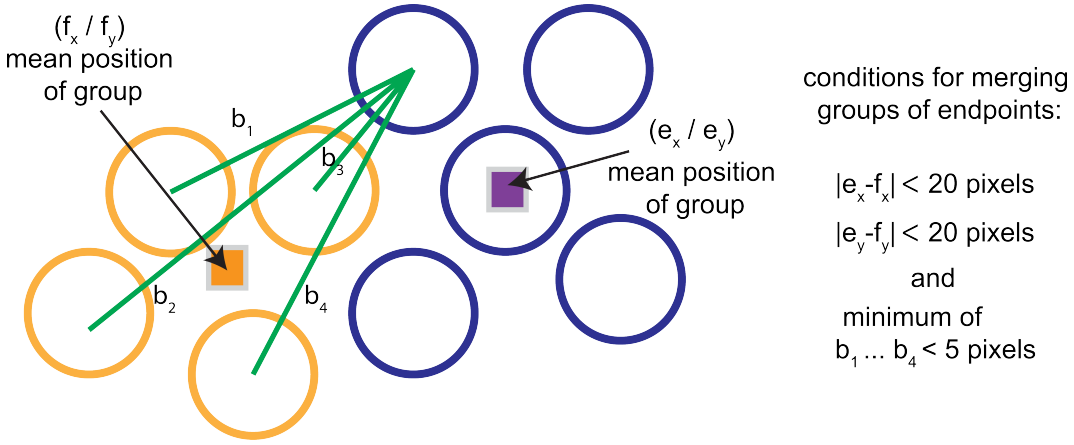

Figure 4.15.: Sketch showing under which conditions groups of endpoints were finally merged. Two groups of endpoints that may be merged (dark yellow and dark blue) are displayed. The lines connecting the endpoints of different groups are shown for one endpoint in the blue group. The mean positions of the groups of endpoints are shown as a dark yellow square (yellow group) and as a purple square (blue group). On the right hand side the constraint that was posed to determine whether two groups of endpoints could be merged is denoted. Additionally, the groups were only merged if no endpoint would have been deleted by this merging.

a filopodium/protrusion, a new group of endpoints was opened. Finally, the following steps were performed for both filopodia and broad, blunt protrusions to merge groups of protrusion endpoints belonging to one protrusion. Figure 4.15 sketches under which conditions groups of endpoints were merged.
If both the x- and y-position of the means of two groups were situated less than 20 pixels apart, it was determined whether they could be merged. If the smallest distance between points in the two groups was smaller than 5 pixels and no detected endpoint would have been deleted by merging the groups[xx], they were merged. Figure 4.16 shows an example for a final result of traced filopodia endpoints with endpoints belonging to one group shown in one color.

[xx] As already mentioned above, the possibility of having two endpoints in one image for a single protrusion was not allowed for.

Further Analysis

To compare the positions where the protrusions occurred on structured substrates to the positions of protrusions on a flat substrate, the mean angles under which protrusions occurred were calculated. A sketch of this mean angle for one group of endpoints can be found in figure 4.17 a).
The mean position of each group of endpoints was calculated and the vectors $\vec{v}$ from the mean center of mass to these mean positions were calculated. Then, the angles these vectors enclosed with the x-axis were calculated by $\alpha_{\text{mean}} = \tan(v_y/v_x)$ with v_x being the x-component of the vector and v_y being the y-component[xxi]. In order to describe the extension of the group of endpoints, the values for the extension in radial direction and the extension in the angular direction were calculated. To compute the extension in radial direction, the endpoints were projected onto the above calculated vectors $\vec{v}$ (see figure 4.17 b)). The projection was carried out using equation 4.3 with $\vec{r}$ describing the original position of the endpoint, $\vec{r}_{\text{proj}}$ the projected point and $\vec{r}_0$ the support vector (here the mean position of a group of endpoints).

$$\vec{r}_{\text{proj}} = \vec{r}_0 + \frac{(\vec{r} - \vec{r}_0) \cdot \vec{v}}{\vec{v} \cdot \vec{v}} \cdot \vec{v} \tag{4.3}$$

A line perpendicular to the line above was calculated by taking into account that the scalar product of two perpendicular vectors is zero:

[xxi] As the tangent has a limited codomain, additional information on where the endpoints were situated with respect to the mean center of mass were needed, so that the exact angle could be given.

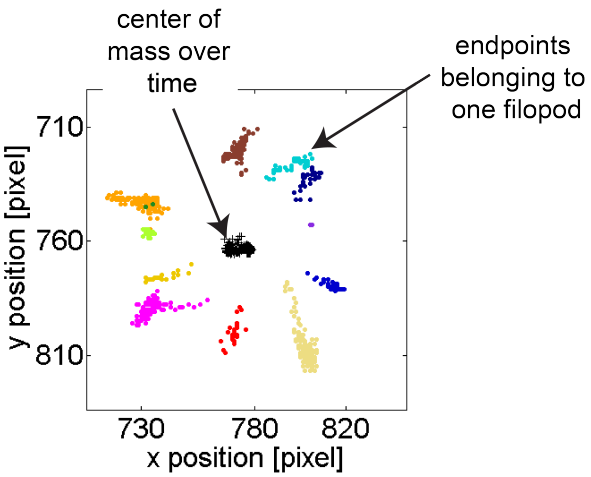

Figure 4.16.: Traced endpoints of filopodia displayed in a color-coded way. Endpoints belonging to one filopodium are plotted in the same color. The different centers of mass of the cell over time are shown as black crosses. This plot shows the endpoints for the whole time lapse series for the cell displayed in figure 4.12.

$$\vec{v} \cdot \vec{v}_{\text{perp}} = 0. \tag{4.4}$$

And thus

$$\vec{v} = (v_x, v_y) \quad \text{and} \quad \vec{v}_{\text{perp}} = (-v_y, v_x). \tag{4.5}$$

The projection of endpoints onto the vector $\vec{v}_{\text{perp}}$ was performed as described in equation 4.3. Then, the maximal distances between the projected points $\vec{r}_{\text{proj}}$ (in radial direction) and the maximal distance between the projected points $\vec{r}_{\text{proj, perp}}$ (in angular direction) were computed. By comparing these values, the elongation of the group of endpoints could be described. As a last parameter also the number of detected endpoints in each image, *i.e.* time point, was calculated. The mean angles and elongations of groups were further processed in OriginPro 8.5 G (OriginLab) by sorting them into bins of 30° and 0.75 μm, respectively and plotting them as histograms in which the percentage of values lying in a certain bin were denoted.

4.4 Characterization of Substrates

The hole sizes were measured by edge detection with the *canny* algorithm with a low threshold of 0 and a high threshold of 0.1 applied to the fluorescence image of fibrinogen coating. A further description of the *canny* algorithm is given in section 4.1. The processed images were rotated in ImageJ [87] in order to align the rows of holes with the image borders (bilinear rotation). Then, a brightness profile was measured in ImageJ [87] along a straight line through the center of a row of holes. The size of a hole was calculated from the mean positions of the left and right hole border. The sizes of the interspaces were calculated by computing the distances between the holes. The values for hole sizes given here were the sizes that were measured by analyzing the images of substrate coating on selectively coated substrates. A discussion of the values can be found in section 5.2.
The curvature of hole edges was determined for 2.1 μm large holes by manually fitting circles into the edge corners of a binarized image of the fibrinogen coating of a selectively coated substrate. The image was binarized by employing again the *canny* algorithm with a low threshold of 0 and a high threshold of 0.05 and then filling the holes manually in ImageJ [87]. The manual fitting was done in ImageJ [87] and the circle radii were denoted. Thus, an absolute value of 2.0 ($\pm$0.1) μm^{-1} was obtained for the curvature.

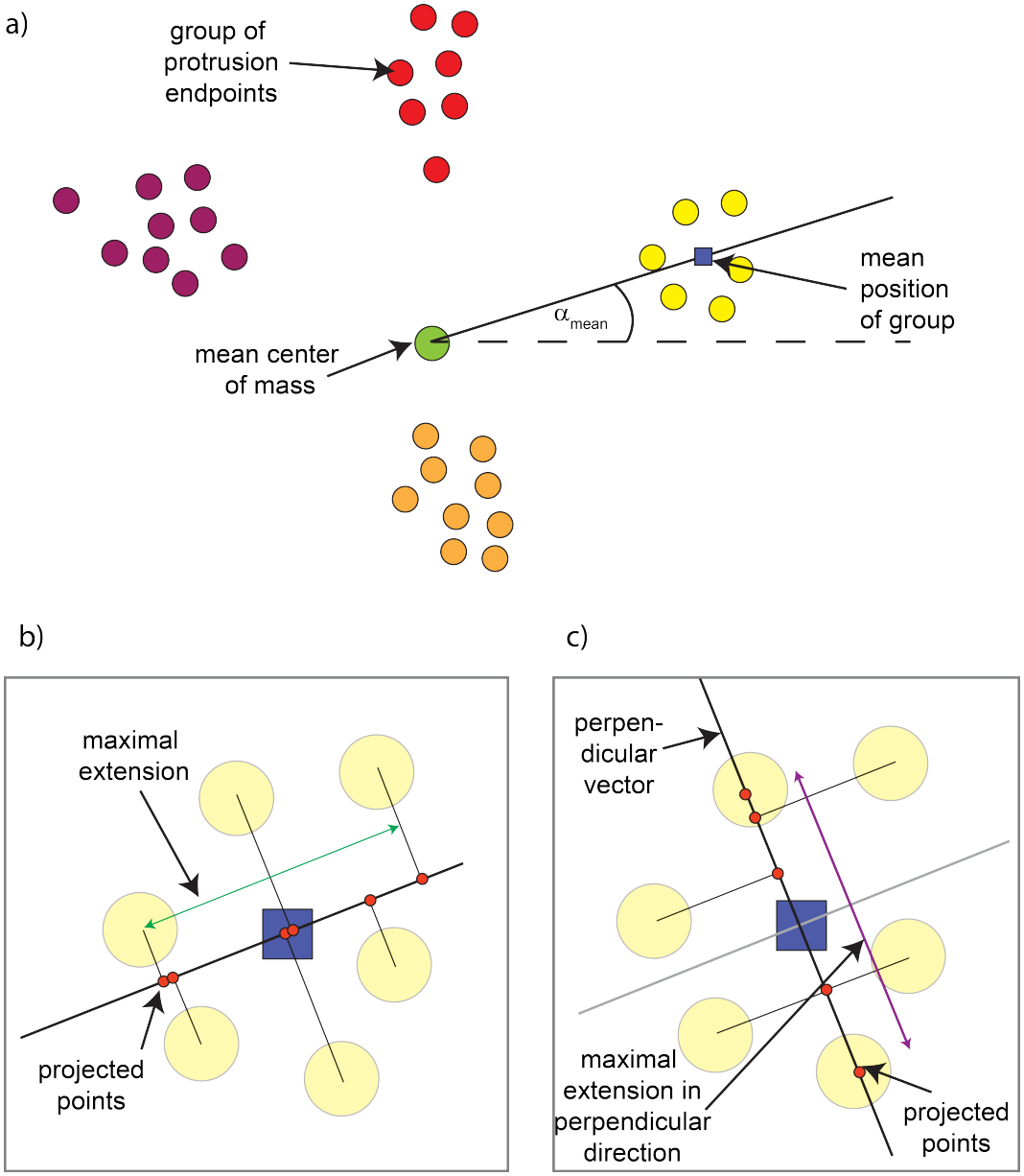

Figure 4.17.: Sketch of different parameters to describe the groups of endpoints.
a) Different groups of endpoints (yellow, orange, purple and red) as well as the mean center of mass (green) of the cell are illustrated. The mean angle α_{mean} for the group of yellow endpoints as well as the mean position of this group (blue square) are depicted.
b) Projection of endpoints onto the vector $\vec{v}$. The projected points $\vec{r}_{proj}$ are displayed in red and the vectors from original points (yellow) to projected point $\vec{r}_{proj}$ as black lines. The maximal distance the projected points lie apart from each other is depicted as a green double-headed arrow.
c) Projection of the endpoints onto the vector $\vec{v}_{perp}$ which is perpendicular to the vector $\vec{v}$ in b). The projected points $\vec{r}_{proj,perp}$ are displayed in red. The maximal distance of the projected points is illustrated as a purple double-headed arrow.

The angle by which an image of the fibrinogen coating and the corresponding cell image had to be rotated to align the horizontal and vertical lines of holes with the image borders was determined in ImageJ [87]. For this purpose, the image was rotated with bilinear interpolation until the horizontal and vertical lines of holes were oriented along the grid lines. If this simultaneous alignment was not possible, the underlying substrate was distorted and the platelets were excluded from analysis (see sections 4.2 and 4.3).

5

Morphological Changes Induced by Microstructured Substrates

Most of the results presented here have been published in Soft Matter [84]. Additional unpublished data have been added to detail some aspects. The terms used here to refer to different parts of the substrate as well as the definition of hole and interspace width are explained in figure A.1 in the appendix (chapter A).

To elucidate platelet behavior on structured substrates, area and morphology of platelets spread on smooth and on structured substrates were examined. The structured substrates contain a regular array of holes (2.1 ($\pm$0.1) μm wide holes and 0.9 ($\pm$0.1) μm wide interspaces or 2.8 ($\pm$0.1) μm wide holes and 1.1 ($\pm$0.1) μm wide interspaces, hole depth: about 500 nm (see 3.3.1)).

In figure 5.1 platelet morphology on selectively (left) and completely coated substrates[i] (right) is shown. The left-hand sides of the images show inverted fluorescence micrographs of the platelets' actin, while for the continuations of the images on the right-hand sides the phase contrast micrographs are shown. Thus, both substrate structures and cell outlines are visible in the images. The substrates shown in figure 5.1 contain 2.1 μm wide holes that appear dark gray in the phase

[i] produced as described in section 3.2

contrast image. In the phase contrast images, the interspaces appear light gray. The micrographs illustrate nicely that in both cases (selectively and completely coated substrates) platelets avoid the holes at their periphery. However, this reaction is stronger in the case of selectively coated substrates (left-hand side), while platelets on completely coated substrates sometimes span the holes at the periphery of the platelet. The effect, which the underlying substrate has on the platelets, becomes even more clear when looking at platelets that lie partly on a structured and partly on a smooth substrate (lower images): On the structured part, the cell periphery has adapted to the underlying substrate, while on the smooth part the platelet shows no adaptation and the cell outline is regular.

Similar adaptations to the underlying substrate can be observed for structures with hole sizes ranging from approximately 1.0 μm to 2.8 μm as can be seen in figure 5.2 (completely coated substrates). The images show an overlay of fluorescence images of fibrinogen coating (gray) and actin staining (red) in the upper row and inverted fluorescence images of the actin staining in the lower row. Interestingly, the platelet that lies on a substrate with 2.8 μm wide holes shows several straight

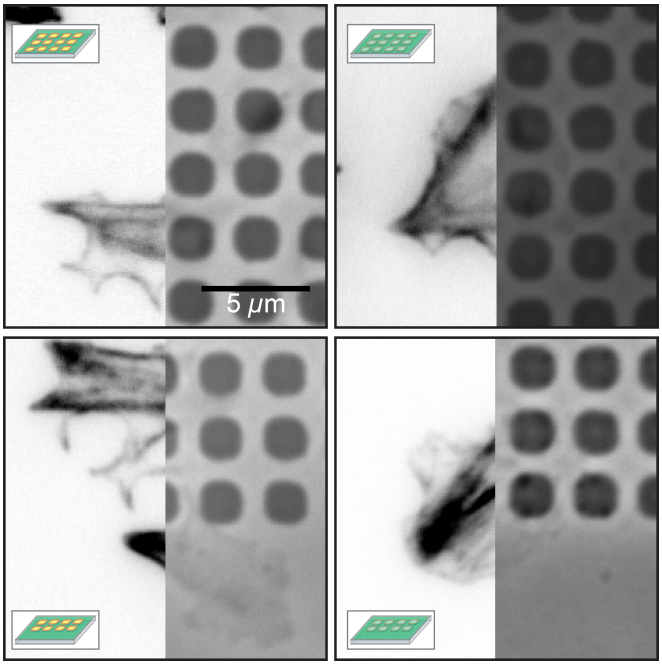

Figure 5.1.: Combined fluorescence and phase contrast micrographs of platelets stained for actin on selectively (left) and completely coated substrates (right). The images have been rotated in Adobe Illustrator CS5 (Adobe Systems Software Ireland Limited, Dublin, Republic of Ireland). The left half of each picture shows the inverted fluorescence image of stained actin, the right part shows the remaining part of the image as a phase contrast micrograph. As can be seen in the actin staining, platelets lying on a selectively coated substrate adapt more strongly to the underlying substrate than platelets lying on a completely coated substrate. The lower images show platelets partly lying on a structured and partly on a smooth substrate. Adaptation only occurs on the structured part while on the smooth part a regular morphology is observed.

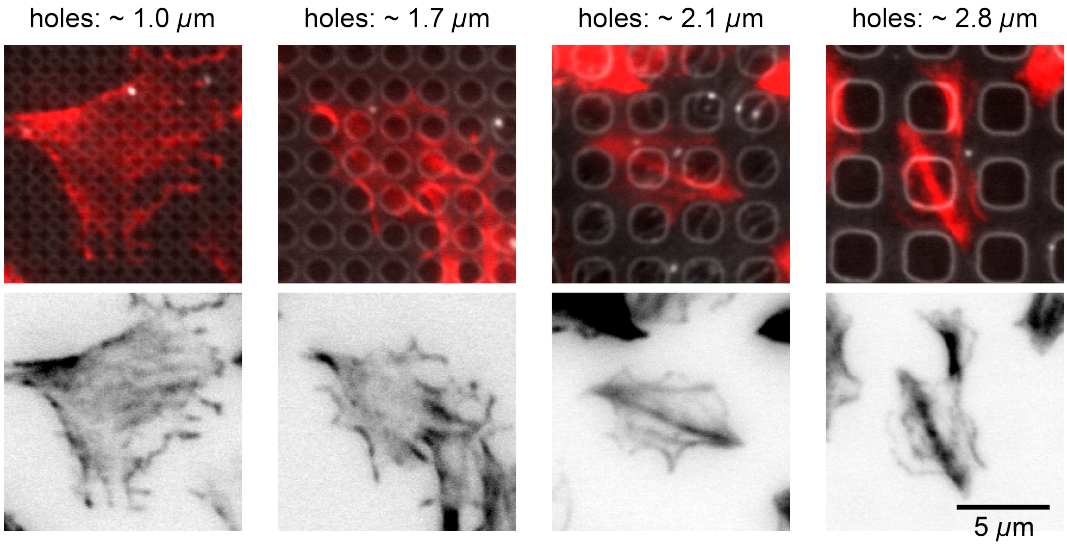

Figure 5.2.: Platelet morphology on completely coated substrates with different hole sizes. The upper images show a composite of a fluorescence image of the fibrinogen coating (gray) and the actin staining (red). The lower images show the actin staining alone in inverted grayscale. The platelets adapt to each hole size examined here (width: approximately 1.0 μm-2.8 μm). The figure has been adapted from [84] - Reproduced by permission of The Royal Society of Chemistry.

parts in its outline, which seem to be partly caused by the straight regions of the underlying holes.

From looking at the micrographs in figure 5.1 and figure 5.2, it is clear that the underlying structures influence the platelets even when the whole substrate is coated with fibrinogen and the platelets should in general be able to attach to any point of the substrate. But which parameters are influenced by the underlying substrate exactly?

To answer this question, first, the spread area of platelets was analyzed on structured substrates with 2.1 μm and 2.8 μm wide holes as well as on smooth substrates. Histograms of platelet spread area are shown in figure 5.3. In all cases the spread area lies around 30 μm^2 with neither the coating (completely or selectively) nor the underlying structure (smooth, structures with 2.1 μm or 2.8 μm wide holes) influencing the general distribution of cell area values. This finding suggests that the final size of platelets has to be influenced by other parameters than by the substrate topography or coating - at least in the regimes that are examined here. The most likely parameter to govern spread area is the substrate stiffness. Qui *et al.* [76] showed a dependency of spread area on the stiffness of the underlying substrate for platelets spreading on polyacrylamide substrates of varying stiffnesses.

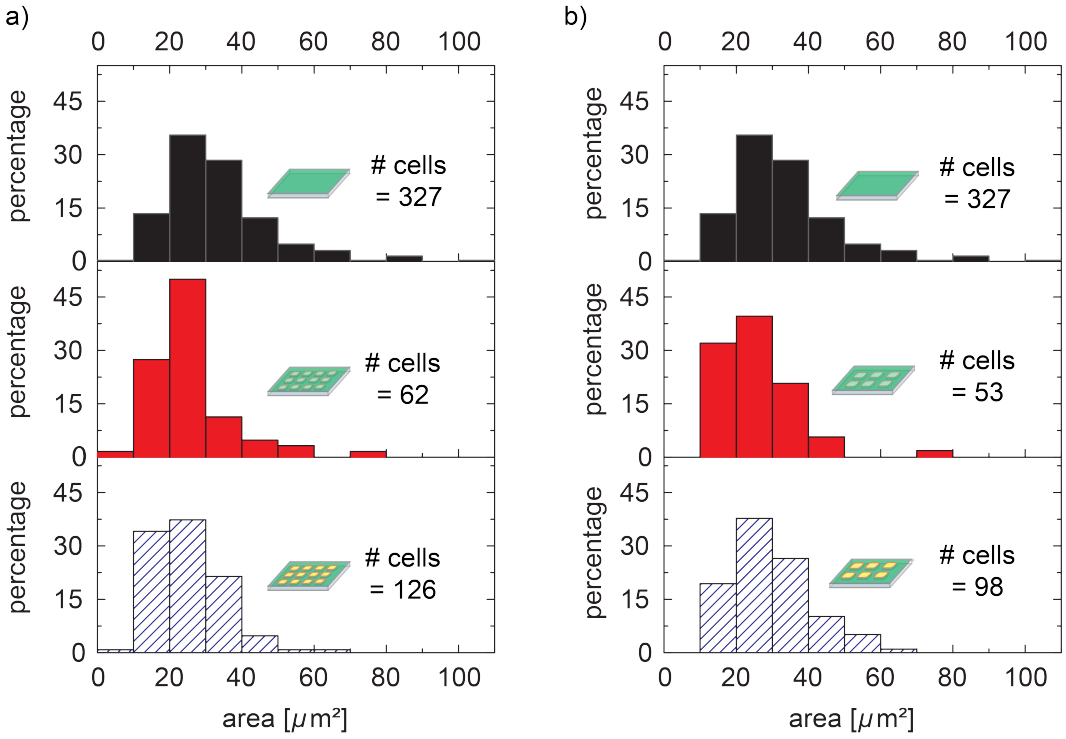

Figure 5.3.: Histograms of cell area on smooth substrates (same data for both plots), substrates with 2.1 μm-holes (a)) and substrates with 2.8 μm-holes (b)).
The upper histograms show cell area on smooth substrates, the histograms in the middle show cell area on structured, completely coated substrates, the lower histograms show cell area on structured, selectively coated substrates. Cell area lies in all cases around 30 μm^2 regardless of the size of holes or of the substrate's degree of coating. The figure has been adapted from [84] - Reproduced by permission of The Royal Society of Chemistry.

When taking into account the dimensions of quiescent platelets (about $2-5\,\mu$m in diameter and about $0.5\,\mu$m in height as given in [108]) and approximating platelets as circular discs, quiescent platelets have a volume of about $1.6-9.8\,\mu m^3$. Assuming a constant height of about 100 nm for the spread platelet (upper value given in [2] for the thickness of lamellipodia in spread platelets), cell areas of about $16-98\,\mu m^2$ are plausible for spread platelets if considering the volume to remain constant. These magnitudes also fit to an increase of exposed surface area during spreading of up to 420% as stated in [108]. Assuming this maximal increase, initial areas of $3.1-19.6\,\mu m^2$ (discs with diameters as stated above) would lead to final areas of about $13.2-83.5\,\mu m^2$. The ranges of values seen in the histograms in figure 5.3 agree with the range of possible area values for platelets calculated above from the initial volume and assuming a fixed cell height after spreading.

Thus, the parameter of final cell height may be fixed in spreading.
But how do the platelets manage to spread to a certain area despite the disturbances the holes provide? If the platelets are "prohibited" to spread over the holes at their periphery, they have to make up for the loss of area by increased spreading at other positions. Increased spreading, *e.g.*, on the interspaces between the holes together with avoidance of the holes would result in an elongated cell outline. In figure 5.4 inverted fluorescence micrographs of stained actin for platelets lying on smooth substrates, structured substrates with complete coating and structured substrates with selective coating are shown (structured substrates both consist of arrays of 2.1 μm wide holes). The platelet lying on a smooth substrate shows no protrusions while both platelets on structured substrates show protrusions albeit to different degrees. On the selectively coated substrate, the protrusions are more pronounced than on the completely coated substrate.

To examine whether the outlines of the platelets are indeed elongated for platelets that have to adapt to the underlying structure, the lengths of the outlines of platelets p_{cell} were measured. To account for different overall cell shapes, *i.e.* different cell eccentricities, the lengths of outlines of the platelets were normalized by the perimeter of an ellipse p_{ellipse} that has the same area, orientation and eccentricity as the cell. By computing the ratio of these two values, *i.e.* $\frac{p_{\text{cell}}}{p_{\text{ellipse}}}$, a measure of

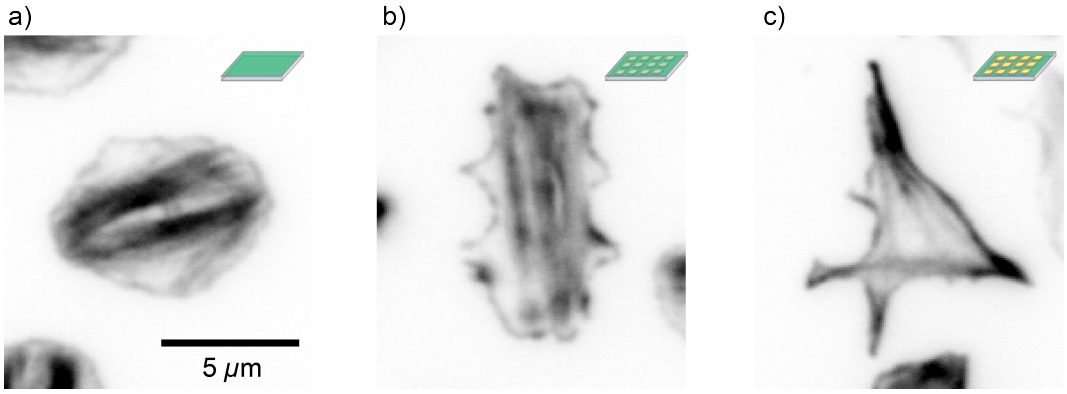

Figure 5.4.: Micrographs showing different degrees of protrusions on smooth substrates, structured substrates with complete coating and structured substrates with selective coating. The images consist of inverted fluorescence micrographs of stained actin.
a) On a smooth substrate no protrusions are visible.
b) On a completely coated, structured substrate several short protrusions are visible.
c) On a selectively coated, structured substrate protrusions are more pronounced than in b). The figure has been adapted from [84] - Reproduced by permission of The Royal Society of Chemistry.

how much the platelet deviates from an ellipse was obtained. If the platelet was a perfect ellipse, the fraction would take a value of 1. The values increase the more the platelet deviates from a perfect ellipse. In the following, the ratio $\frac{p_{\text{cell}}}{p_{\text{ellipse}}}$ will be termed *relative perimeter*. Histograms of these relative perimeters are plotted in figure 5.5.

For platelets lying on smooth substrates the relative perimeters assume the smallest values. For completely coated substrates the relative perimeters are shifted towards higher values, while the values for selectively coated substrates are even higher. This trend is evident for substrates with 2.1 μm wide holes and for substrates with 2.8 μm wide holes. In the case of substrates with 2.8 μm wide holes the effect is stronger than for substrates with 2.1 μm wide holes, very likely reflecting the need to compensate for more area loss due to larger holes.

The differences in relative perimeters between platelets lying on selectively coated and on completely coated substrates can be explained by the different degrees of adaptation to the substrates. The platelets adapt more strongly to the substrate by spreading, *e.g.*, more on the interspaces in between the holes to keep their area constant. This behavior would lead to a larger relative perimeter especially on structured substrates with selective coating where spanning over the holes at the periphery of platelets is reduced compared to structured substrates with complete coating and thus more area needs to be gained. As already shown in figure 5.1, platelets lying on a selectively coated substrate adapt more to the underlying substrate and seem to follow the outline of underlying holes at the periphery of platelets with more fidelity. One possible explanation for this higher fidelity lies in the differences in coating of hole edges and walls. On completely coated substrates the walls are coated with fibrinogen while on selectively coated substrates the walls are not coated. The hole edges are possibly coated to some extent on selectively coated substrates[ii] but most likely not as thoroughly as on completely coated substrates. Thus, it can be assumed that these differences in coating facilitate spreading over the holes at the cell periphery on completely coated substrates by providing more binding sites at the hole edges.

As described above and shown in figure 5.1, platelets on completely and selectively coated substrates show different degrees of adaptation to the underlying substrate. To quantify this adaptation, the curvature of the cell outline was calcu-

[ii] Partial coating of hole edges on selectively coated substrates can arise as neither stamp nor substrate are completely stiff and as a consequence both can bend slightly during the transfer of protein in microcontact printing.

lated. For the curvatures only absolute values are given. The curvature distribution on smooth substrates was used as a reference (see figure 5.6, inset in a)). The curvature values on smooth substrates decay fast towards higher values and thus point to an energy minimization on smooth substrates.
To visualize the adaptations of platelets on structured substrates in comparison to a regular distribution of curvature values on smooth substrates, the differences between the distributions were calculated, *i.e.* the histogram values on smooth

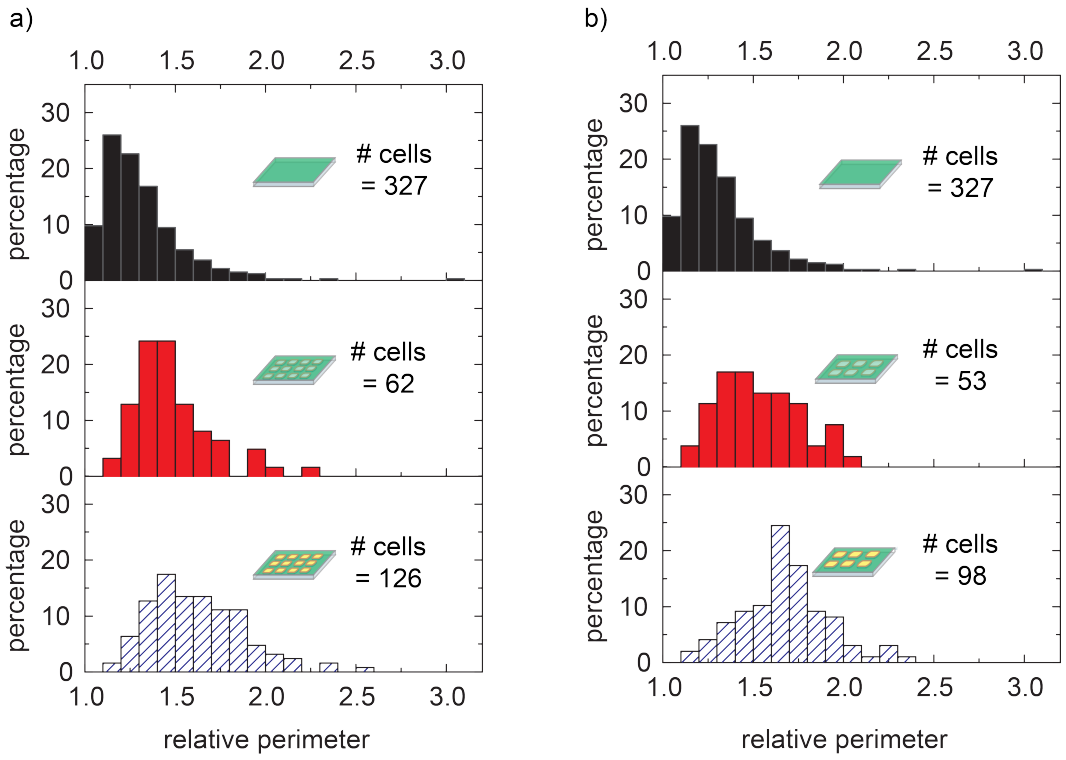

Figure 5.5.: Histograms of relative perimeters on smooth substrates (same data for both plots), substrates with 2.1 μm-holes (a)) and substrates with 2.8 μm-holes (b)).
The upper histograms show the relative perimeters on smooth substrates, the histograms in the middle show the relative perimeters on structured, completely coated substrates, the lower histograms show the relative perimeters on structured, selectively coated substrates.
a) The relative perimeters assume the smallest values on smooth substrates and are shifted towards larger values on completely coated, structured substrates. For selectively coated, structured substrates the relative perimeters are shifted to even larger values.
b) On substrates with 2.8 μm-holes the trend described in a) is even stronger and the relative perimeters on structured substrates are shifted to larger values than on substrates with 2.1 μm-holes. The figure has been adapted from [84] - Reproduced by permission of The Royal Society of Chemistry.

substrates were subtracted from the values on structured substrates. These differences are denoted as Δ *percentage* and are shown as histograms in figure 5.6. On substrates with 2.1 μm wide holes, small curvature values occur less often than on smooth substrates resulting in negative values for the differences on both completely and selectively coated substrates. On both types of structured substrates curvature values around 1 μm^{-1} and around 2 μm^{-1} occur more often than on smooth substrates and are thus positive. The curvature values around 2 μm^{-1} are probably caused by adaptation to the hole corners, since these corners were measured to have a curvature of about 2.0 ($\pm$0.1) μm^{-1} (see section 4.4). In figure A.2 in the appendix (chapter A) the curvature values along the cell outline are displayed for platelets showing values around 2 μm^{-1} at parts of their outline on selectively coated substrates with 2.1 μm wide holes. Values around 2 μm^{-1} can be observed in the concave corners of invaginations (over underlying holes). The endpoints of protrusions show relatively high curvature values of up to 5 μm^{-1}. However, depending on the shape of protrusions, the protrusions can also account for parts of the curvature values around 2 μm^{-1}. This reflects an increased adaptation to the underlying substrate in the case of selectively coated substrates.

In general, the curvature values on selectively coated substrates are shifted towards higher values compared to the values on completely coated substrates. These higher values suggest an increased adaptation to the underlying substrate in the case of selectively coated substrates. On completely coated substrates curvature values around 1 μm^{-1} show the highest elevation. This peak probably corresponds to the mean curvature of the holes calculated by their radius r_{hole} to be $c_{\text{mean}} = 1/r_{\text{hole}}$.

On completely coated substrates with 2.8 μm wide holes, Δ percentage shows two peaks: One around 1 μm^{-1} and again a second smaller one around 2 μm^{-1}. These peaks suggest a similar adaptation as in the case of completely coated substrates with 2.1 μm wide holes. On selectively coated substrates (2.8 μm wide holes) the situation is, however, different. The smaller values are more pronounced on the structured substrates and values around 1 μm^{-1} are more pronounced on smooth substrates than on structured, selectively coated substrates. This distribution can be explained by the shape of the holes. The 2.8 μm wide holes show longer straight regions at their edges than the 2.1 μm wide holes (see inset phase contrast micrographs of holes, straight parts marked in orange and corners in cyan). These longer straight regions likely result in more straight parts in the cell outline and thus lead to smaller curvatures.

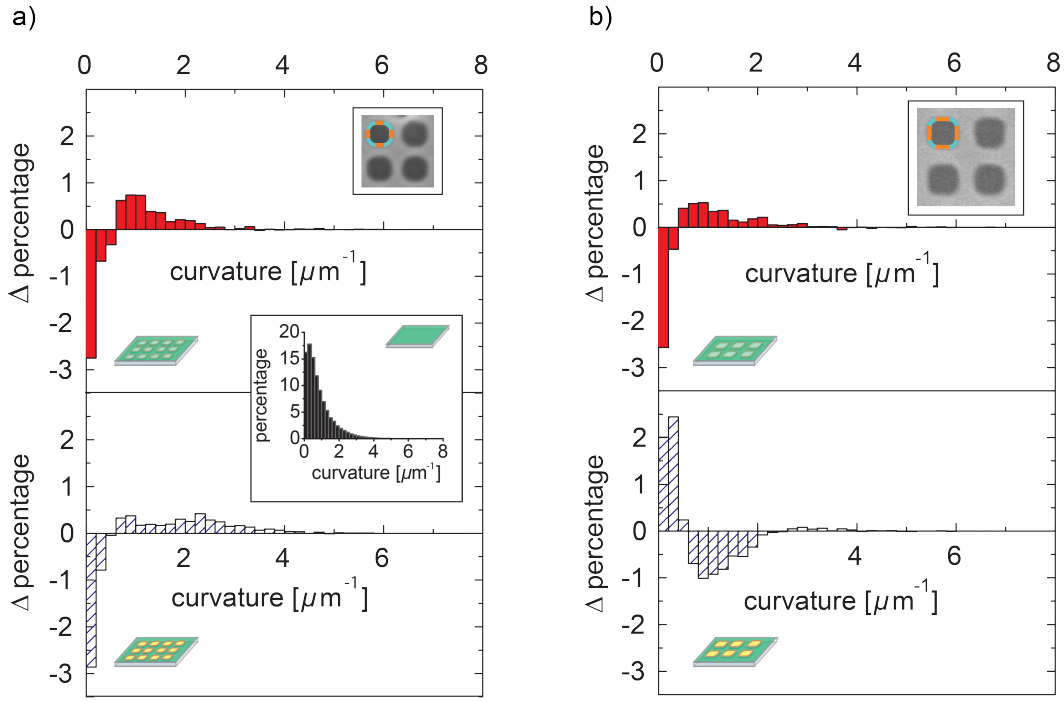

Figure 5.6.: Histograms of differences in curvature of the cell outline on selectively and completely coated, structured substrates with 2.1 μm-holes (a)) and with 2.8 μm-holes (b)) as compared to smooth substrates as well as the curvature distribution of the cell outline on smooth substrates (inset a)). For the curvatures only absolute values are given.
The upper insets show phase contrast micrographs of the different substrates in which the straight parts of the holes are marked in orange while the curved corners are marked in cyan. The micrograph in (b) has been rotated in ImageJ [87] (bilinear interpolation) to align the lines of holes with the image borders. The upper histograms show the differences between structured, completely coated substrates and smooth substrates. The lower histograms show the differences between structured, selectively coated substrates and smooth substrates.
a, inset) The curvature distribution on smooth substrates decays towards higher curvature values being in line with energy minimization.
a) In both histograms, smaller curvature values occur more often on smooth substrates while on structured substrates values around 1 μm^{-1} and 2 μm^{-1} are elevated. The distinct distribution is different: On completely coated substrates the first peak around 1 μm^{-1} is larger, while on selectively coated substrates the second peak around 2 μm^{-1} is larger.
b) In the upper histogram (completely coated), smaller curvature values occur more often on smooth substrates, while on the structured substrates values around 1 μm^{-1} and 2 μm^{-1} are elevated. For selectively coated substrates in the lower histogram the situation is different, smaller curvature values are more elevated on structured substrates, while on smooth substrates values around 1 μm^{-1} are elevated compared to the structured substrates. This distribution likely arises due to longer straight parts of the platelet that may occur on selectively coated substrates with 2.8 μm-holes. Figure has been adapted from [84] - Reproduced by permission of The Royal Society of Chemistry.

Taking all this into account, one can conclude a higher degree of adaptation of platelets on selectively coated substrates than on completely coated substrates. Possible reasons for the different degrees of adaptation have been described above in the context of the different relative perimeters.

But why do the platelets adapt at all to the underlying substrate? One possible explanation for this behavior is that bending into the holes at the periphery costs more energy than bending around the holes. When bending into the hole bending energy would have to be invested to deform the platelet, while by bending around the holes the cell outline would have to be elongated slightly. In figure A.3 in the appendix (chapter A) a profile extracted from the atomic force microscopy image in figure 3.6 is shown. This profile illustrates by how much the platelet would have to bend to extend into the holes. In figure A.4 in the appendix (chapter A) a sketch compares the height dimensions of a completely spread platelet to the height dimension of the structures used here. Although a structure depth of about 500 nm does not appear very deep, a comparison between platelet height for a completely spread platelet and structure depth shows pronounced differences in dimensions. As can be seen in figure A.3 the hole walls are not perfectly vertical but still quite steep. This steepness is discussed further in section 5.2. For small holes the platelets would have to follow the hole geometry quite precisely, since there is only a limited space for the platelet to attach to. It can be assumed that the larger the hole gets, the easier it is for the platelet to bend inside the hole.

For the hole sizes examined here, one can sometimes observe platelets bending into the holes. Micrographs of a z-stack of a platelet lying on a substrate with slightly larger and more round holes than used here (about 3 μm in diameter) extending protrusions into holes are shown in the appendix (chapter A) in figure A.5. The protrusions attach to the center of the hole's bottom and thus the curvature needed to bend into the holes might be reduced.

Further insights into the behavior of platelets on structured substrates can be obtained by the following observations. Platelets lying on structured substrates (both on selectively and completely coated substrates) sometimes show actin accumulation at the hole edges underneath the inner parts of the platelet visible as higher signals in actin fluorescence staining (see figure A.6 in the appendix (chapter A)). The actin accumulation seems more pronounced on selectively coated substrates. Furthermore, in figure A.7 (appendix chapter A) a membrane-stained platelet spreading on a completely coated substrate shows a higher fluorescence signal at the position of the hole edges beneath the inner parts of the platelet. The po-

sitions of the underlying holes with respect to the cell are shown by fluorescence micrographs of the staining of the plasma membrane and the fibrinogen coating of the substrate in figure A.8 in the appendix (chapter A).
Together, these accumulations of actin and cell membrane staining indicate that the platelet enters the holes beneath its central region. If the platelet enters a hole cellular material can be situated near the hole wall and its fluorescence signal is projected onto the x-y-plane and thus leads to a higher signal. However, entering the hole is unlikely in the case of selectively coated substrates, since no binding sites are present inside the hole. In this case, actin accumulation at the hole edges is probably caused by new actin fibers originating from focal adhesions formed at the hole edge to stabilize the platelet. Focal adhesion formation at edges of topographies or at borders to non-adhesive substrate parts were observed for example by Dunn and Heath [33] and Rossier *et al.* [81], respectively (see also section 2.5).
Even though the platelets avoid the holes at their periphery as shown above, groups of platelets can cover the holes completely in a collective attempt. Examples of such groups can be seen in figure A.9 in the appendix (chapter A). It can be assumed that this behavior represents the behavior *in vivo* where many platelets cooperate to close a wound. Possible explanations for platelets being able to completely span the holes collectively are that binding to other spread platelets may be stronger than to the fibrinogen coating of the substrate or that the spread platelets have already spanned parts of the hole so that the following platelet only needs to span smaller parts. Alternatively, spread platelets may be more elastic than the substrate and thus help the new platelet to span the hole by pulling the other platelets closer together which would lead to a smaller distance the new platelet would have to span. When comparing the numbers of platelets in the groups on selectively coated substrates to that in a group on a completely coated substrate, it seems that the number of platelets in such a group is larger on completely coated substrates probably due to the existence of more binding sites.

5.1 Discussion of Results with Regard to Existing Literature

Several points discussed here also apply to the next chapters (chapter 6 and 7). If the following reference [2] is given, the termini filopodia and lamellipodia are used instead of the termini pseudopodia and hyalomer as given by the authors. For further notes on this usage of termini see section 2.3.2.

The histograms of cell area in figure 5.3 show only few platelets above $60\,\mu m^2$. These larger platelets very likely represent so-called preplatelets in the blood (see section 2.1.2 for references on preplatelets and further explanations). If the larger platelets are preplatelets, this also explains why these larger platelets are lesser in number, since only about 4% of the platelet/preplatelet/proplatelet mixture in the blood are preplatelets [96]. The occurrence of preplatelets is further discussed in section 6.1. A study by Park *et al.* [72] has shown the final spread area of platelets on fibrinogen coated glass to be about $50\,\mu m^2$. Differences to the values in figure 5.3 can be explain by both a smaller stiffness of PDMS ($750\,(\pm 170)$ kPa for a ratio of 10:1 of base to crosslinker baked for 1 hour at 60°C [93][iii]) compared to glass (> 45 GPa [46]) as well as different concentrations of fibrinogen as both substrate stiffness and fibrinogen coating have been shown to alter spread area in platelets [76].

Although single platelets avoid the holes at their periphery, platelets are able to collectively cover the holes completely (see figure A.9). A similar collective behavior has been observed for fibroblasts but not for endothelial cells and thus depends on the cell type [83]. From a physiological point of view, collective coverage of holes makes sense for blood platelets, as *in vivo* many platelets cover a wound collectively. An important feature for this collective coverage could be that lamellipodia of spreading platelets can overlap [2]. Furthermore, platelets attaching to already spread platelets and not to the underlying substrate extend filopodia which interconnect the single platelets further [2]. Taken all into account, the observations indicate that blood platelets use their neighboring cells as support to further cover a hole similarly to what has been observed in fibroblasts [83]. It has been shown that on microtextured implant surfaces multilayers of platelets form [71] which fits to the observed collective behavior of platelets on our structured substrates.

Several studies have shown that platelets adapt to micropatterns when the follow-

[iii] The stiffness of the PDMS substrates used here is very likely higher, since it is cured at a higher temperature of 80°C.

ing conditions occur: they encounter a border to a non-adhesive/uncoated region, the adhesive pattern is large enough for the platelets to spread on and the non-adhesive/uncoated regions are large enough to enforce adaptation [25, 29, 52]. Thus, the adaptation to micropatterns very likely is similar to what is observed here on topographically structured substrates (see figure 5.1 and figure 5.2). Experiments with BHK21 C13 cells trying to distinguish between the effects of micropattern and microtopography revealed that cells can sense both cues simultaneously [12]. For the experiments presented here, the micropattern and topography are overlaid (see figure 3.5), so that conflicting cues from pattern and topography only arise for completely coated substrates. By coating the whole substrate it becomes clear that topography accounts for the reaction seen here, *i.e.* avoidance of the holes at the periphery of platelets. However, this reaction is amplified if both micropattern and topography are presented together, as on selectively coated substrates platelets adapt more strongly to the substrate (see figures 5.1 and 5.6). The amplifying effects of topographies accompanied by fitting micropatterns have also been observed for BHK21 C13 cells on ridges/grooves [12].

In figure A.6 actin accumulation at the edges of holes has been described. This actin accumulation has also been observed for other cells at edges of topographic features [83, 110] and is accompanied by focal adhesions [83]. Dunn and Heath [33] found focal adhesions near the edge of topographic features where actin filaments of chick heart fibroblasts end and thus do not cross the border. Also Britland *et al.* [12] found actin filaments that ended near the edge of topographic features in BHK21 C13 cells. Hence, actin accumulation in platelets at the edges of holes as seen in figure A.6 indicates that the platelets react to discontinuities in topography similarly as other cells. On micropatterned substrates, *i.e.* chemical patterns, actin accumulation at the border of the pattern is found for platelets as well [52] further indicating a role of actin accumulation at discontinuities.

Filopodia of platelets are thought to sense the coating of the underlying substrate [52]. Thus, the increased relative perimeters on structured substrates compared to smooth substrates (as shown in figure 5.5) indicate that the platelets search for binding sites and thus produce more filopodia. On structured substrates with selective coating, the number of binding sites is reduced compared to smooth substrates, while on structured substrates with complete coating the binding sites in the holes lie in a different plane than those on the interspaces and thus are not available for platelets not extending into the holes. The role of filopodia in platelet spreading is discussed further in chapter 7.

The reaction of cells to edges of topographic structures is thought to rely on the bending angle the cytoskeletal filaments would have to endure when bending to overcome the edges [33, 91]. The bending angle needed to overcome an edge can be reduced if the cell does not encounter the edges perpendicularly [33]. This aspect is sketched in figure 5.7 by showing a cell encountering the edge of a ridge perpendicularly or nearly parallel. However, the reducing effect is small when the extension of the indentation is equal in the direction parallel and perpendicular to the edge as it is the case for holes in the substrates used here.

Additionally, it is assumed that the attached parts of the cell on each side of the discontinuity need to have a certain size to be able to support the bending [91]. Furthermore, the existence of a critical length that the cells are still able to span is considered [91]. As platelets are able to span non-adhesive regions of up to $4-5\,\mu$m on micropatterned substrates [52], the critical spanning distance for platelets can be assumed to lie in this range. The sizes of holes examined in our studies fall within this range underlining that platelets are able to span the holes. However, at the cell periphery spanning seems to be harder to accomplish, as platelets avoid the holes at their periphery (see figure 5.1). This suggests that a minimum of adhesion sites is needed to support the spanning. This argument is supported by the finding that platelets seem to span holes at their periphery more easily on completely coated substrates on which very likely more binding sites exist at the hole edges. Bending into the holes at the periphery of platelets is hindered likely because bending in the sheet consisting of membrane and cytoskeleton would

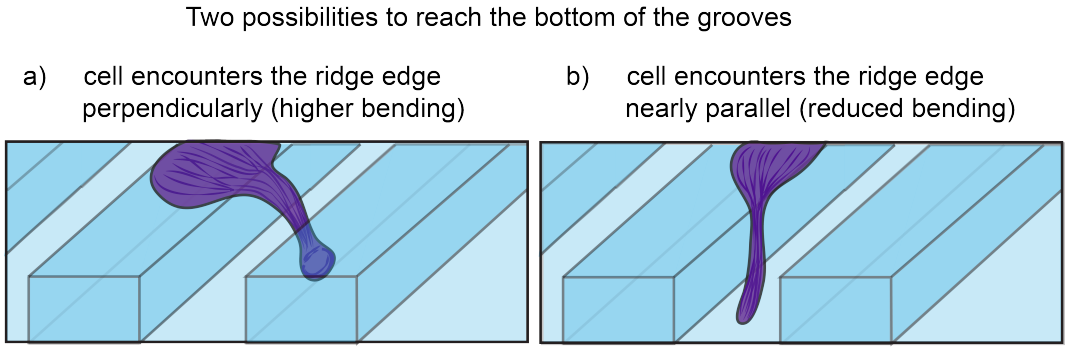

Figure 5.7.: Sketch of two possibilities of bending into a groove if the cell lies on top of a ridge. a) If the cell encounters the edge perpendicularly, bending can only be slightly reduced by attaching near the wall of the opposite ridge and not following the outline of the structure with high fidelity.
b) If the cell encounters the edge under a different angle, bending can be reduced by attaching farther along the groove and thus accomplishing bending into the groove over a longer distance.

be too high. As discussed above, the situation for bending into a hole can be assumed to be more acute than for bending into a groove, since the cell cannot minimize its bending angle strongly. Only if the platelet does not follow the hole wall but attaches to the bottom of the hole near the opposite edge it can reduce the bending slightly. As the holes get larger, bending into the holes is facilitated, since the bending angle can be reduced more due to more available space over which the bending can take place. A sketch of bending into differently sized holes is shown in figure 5.8.

The larger available space has the potential to influence adhesion sites as has been stated by Ohara and Buck [69] and this, in turn, can influence the behavior of the cells [69]. Similarly, as has been observed by Clark *et al.* [21] for crossing borders of steps with different heights by other cells, in our studies extension of protrusions into holes by platelets is not completely prohibited.
Cell area seems to be influenced differently by underlying topography for different cell types as can be seen for example in [86, 110] and [32]. How the cell area is influenced by the underlying structure likely depends on the structure itself, since both positive influences and negative influences on cell area have been observed for different kinds of macrophages in [110] (positive influences, larger area on structured substrates than on smooth substrates) and [86] (negative influences, smaller area on structured substrates than on smooth substrates). The influences of diminished binding sites which can also affect cell area [58], are likely neglectable for our data as a surface coverage of above 15 % is sufficient to achieve 80% of maximal spreading in mouse B16F1 melanoma cells and NIH 3T3 fibroblasts [58]. It has to be noted however, that also the distribution of these binding sites seems

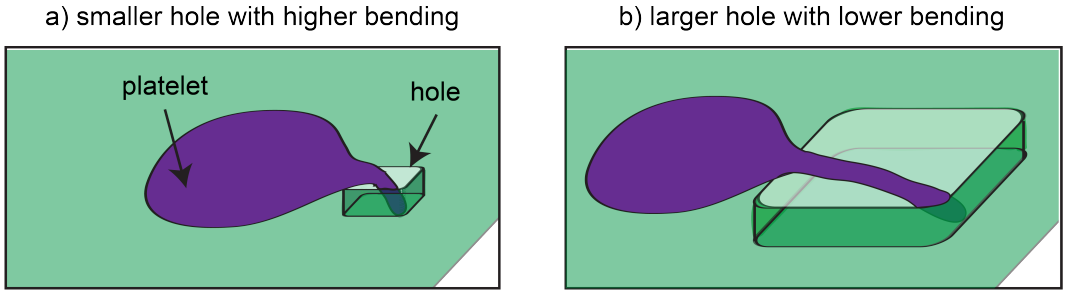

Figure 5.8.: Sketch of platelet bending into a small hole (a)) and into a larger hole (b)).
a) When bending into a small hole the platelet has to bend quite strongly.
b) The larger the hole gets, the more bending into it is facilitated, since bending can be distributed over a larger distance.

to play a role as Corum *et al.* [25] found that platelets do not spread largely on substrates covered by 20 % with fibrinogen consisting of randomly placed patches (average size 5.3 ($\pm$0.4) μm^2).
Differences in platelet behavior on structured substrates compared to smooth substrates have been attributed to differences in protein adsorption [20, 53]. The substrates used here, however, have been precoated with fibrinogen and the fluorescence micrographs of the labeled fibrinogen indicate that its distribution is mostly even on the length scale of the resolution (see figure 3.5). Although platelets are able to secrete fibrinogen [38], the effects of protein adsorption are likely neglectable for precoated substrates used in our experiments.
One has to keep in mind for all our results that cell behavior on topographically structured substrates likely depends on the specific cell type as has been stated by Clark *et al.* [21] and Salem *et al.* [83].

5.2 Discussion of Analysis and Experimental Methods

Several points discussed here also apply to the next chapters (chapters 6 and 7).
The hole sizes were measured for the selectively coated substrates. The selectively coated substrates have the advantage that the fibrinogen coating shows a defined hole edge, since the hole walls are not coated in this case. As can be seen in figure 3.5 b) and c) the completely coated substrates show a broader hole edge most likely due to the coating of the not perfectly straight walls. Measurements of distances for completely coated substrates between the outer boundaries of the edges for the largest holes used here, show a slightly larger hole size (around 3.0 ($\pm$0.1) μm) than measured on the selectively coated substrates but lie nearly in the error interval of the values measured for the selectively coated substrates. However, a slight accumulation of fibrinogen on completely coated substrates at the edges of interspaces due to the discontinuity similarly as has been described in [20] cannot be ruled out. This accumulation could also enlarge the bright region seen in the fibrinogen coating and thus account for the slightly larger hole sizes. Therefore, the sizes measured on selectively coated substrates were given here. The height of the structures is measured on the silicon wafers. PDMS shows only a shrinkage ratio of about 1.5% during baking at 80°C for 3 hours for a PDMS layer with a height of 1.2 mm [57]. Thus, the depth of the structures in the PDMS substrates should be similar to those on the wafers.
One may argue that fixation with formaldehyde changes the structure of platelets

and thus potentially led to artifacts in the data presented in this chapter. In fact, it has been shown for SK8/18-2 cells that formaldehyde fixation changes structural details in the cytoskeleton on length scales between about $15 - 60$ nm [103]. These length scales are, however, beyond the resolution limit of conventional light microscopy [54] as used here. Furthermore, experiments with non-fixed platelets in the next chapter (chapter 6) confirm the observations made here concerning general cell morphology and cell area. Thus, it is reasonable to assume that the effects of fixation are neglectable here.

In order to avoid some steps of preprocessing in which platelets that distort the fibrinogen layer have to be sorted out, as described in section 4.2 (see figure 4.2 c)), one could use chemical linkers like aminopropyltrimethoxysilane (APTMES) and disuccinimidyl suberate (DSS) to immobilize the fibrinogen as described in [16]. Feuerstein *et al.* [37] also observed an interaction of platelets with fibrinogen coatings. As they further reported a decrease of platelet area over time [37], all platelets that distorted the fibrinogen layer visibly in our experiments were sorted out as described in section 4.2 to prevent influences on the cell area and cell morphology.

Drying of fibrinogen for some experiments on completely coated, structured substrates did result in irregular fibrinogen coating. However, as only those platelets were analyzed that did not lie on top of irregular fibrinogen coating and slight irregularities do not seem to alter platelet behavior as described in section 3.3.2, also data on dried fibrinogen were used here.

As can be seen in figure A.3 in the appendix (chapter A) the hole walls are not perfectly vertical. It has been pointed out by von Recum and van Kooten [78] that the curvature at the edges of topographies plays an important role in cell behavior. Once, however, the cells span the discontinuities, the angle of the edge and the structure height are thought to be unimportant [91]. Thus, the not perfectly vertical hole walls most likely have no influence on the experiments presented here, since the platelets avoid the holes at their periphery. More vertical hole walls can be created by further optimization of the photolithography process.

6

Dynamics of Spreading and Retraction on Microstructured Substrates

All quantities described below have been calculated for all analyzable cell images in the time-lapse series. This chapter recapitulates how the dynamics of platelet spreading lead to the morphology shown and characterized in the former chapter (chapter 5). The structured substrates used here were all completely coated (containing 2.8 ($\pm$0.1) μm wide holes with a depth of about 500 nm (see 3.3.1) and 1.1 ($\pm$0.1) μm wide interspaces). In order to visualize the dynamics of platelet spreading on structured and smooth substrates, time lapse series of membrane-stained platelets (see section 3.5.2 for staining protocol) were recorded as described in section 3.6. In figure 6.1 examples of different time points in spreading for a platelet on a smooth substrate (upper) and for a platelet on a structured substrate that has adapted to the underlying substrate (lower) are shown. The positions of the underlying holes in the case of the platelet on the structured substrate are shown in figure B.1 in the appendix (chapter B). Spreading occurs in both cases on a time-scale of several minutes. Different overall brightnesses of the micrographs probably result from different times elapsed since staining[i] or from different free

[i]The dye is taken up from cells after a while [64].

dye concentrations. However, since the detection of cell outlines is based on contrast rather than on overall brightness (see section 4.1), this does not influence our results.

Even at early time points, as can be seen for the micrographs at 300 seconds in figure 6.1, differences in morphology between platelets on smooth and on structured substrates are apparent. On smooth substrates, platelets spread evenly outwards. On structured substrates however, spreading over the holes is diminished and overall spreading seems to be more dynamic. This more dynamic behavior shows for example in possible retractions over the holes at the cell periphery. An example for a retraction can be seen in the image at time point 450 seconds in comparison to the former time point of 300 seconds in figure 6.1. Interestingly, in this example an outgrowth over a hole can be observed later on in spreading (time point 750 seconds in figure 6.1). However, this outgrowth does not seem to be stable, since it is retracted afterwards (compare figure 6.1, time point 900 seconds). Based on these observations, spreading behavior was studied in more detail to describe the different strategies by which platelets spread on structured and smooth substrates. The analysis was performed using the methods described in sections 4.3.3

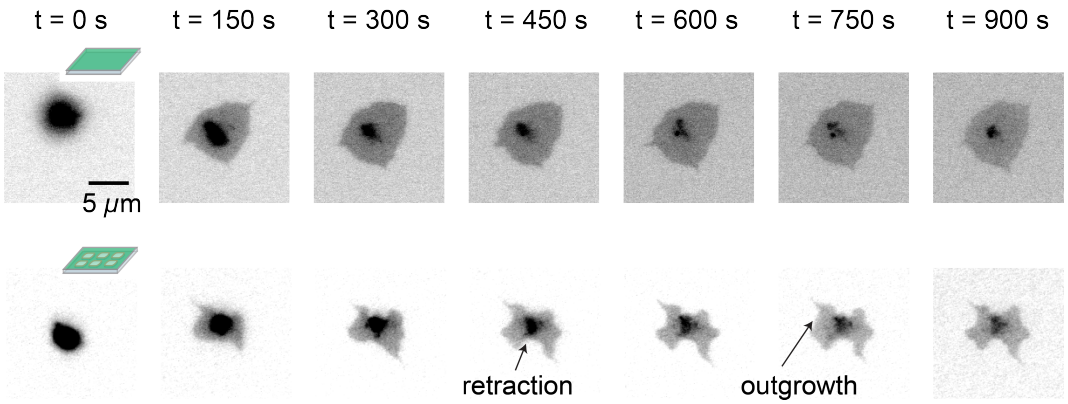

Figure 6.1.: Inverted fluorescence images of different time points in spreading on a smooth (upper) and on a structured (lower) substrate.
The lower images show a platelet that has adapted to the substrate. Platelets spread on a time-scale of several minutes both on smooth and on structured PDMS-substrates. Differences in morphology for the platelets on the two different substrate types are clearly apparent for early time points, *e.g.* for the micrographs at 300 seconds. Spreading on smooth substrates appears to be simple outward spreading, whereas spreading over holes in the structured substrate is diminished and even occasional retractions over holes can be observed. Interestingly, the reaction of platelets to structured substrates seems to be very dynamic, since an outgrowth over a hole can also be observed in late spreading (see image at 750 seconds). The lower images have been rotated in ImageJ [87] (bilinear interpolation) to align the lines of holes with the image borders.

and 4.3.4.

As a first parameter, cell area at different time points was calculated. By computing the cell area, the global spreading behavior of platelets can be characterized, since contributions to spreading in all directions are taken into account by the spread area. The resulting spread area over time for platelets on structured and smooth substrates is shown in figure 6.2. The spreading shows a first, fast spreading phase while spreading in the second phase slows down. As could also be observed in the images in figure 6.1, global spreading on smooth substrates appears undisturbed. On structured substrates though, global spreading appears to be more dynamic with occasional dips (local minima) and subsequent gains of area. Examples for these area losses and gains are marked in figure 6.3 by arrows. However, additional retractions are likely masked by simultaneous outgrowth at other positions of the platelet.

In both cases (smooth and structured) the mean final spread area shows a distribution over a similar range as can be seen by the outermost points of the whiskers in the box-plots in figure 6.4. The interquartile range is defined as the range below and above which 25 % of the values lie. The average values of the mean final area are about 33 μm^2 in the case of platelets on smooth substrates and about 41 μm^2 on structured substrates as is also indicated by the squares inside the boxes in figure

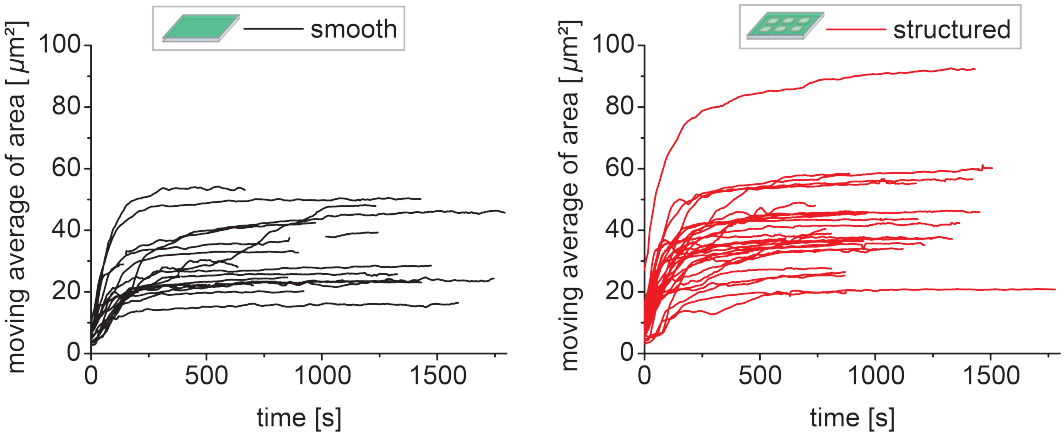

Figure 6.2.: Moving average of cell area on smooth (left, black) and on structured (right, red) substrates.
The mean final spread area lies in both cases around $30 - 40\,\mu$m^2 (see also figure 6.4). However, similar to what can be observed in figure 6.1 spreading on structured substrates seems to be more dynamic. Occasionally, dips and subsequent gains in area can be observed on structured substrates corresponding to retractions and subsequent spreading of the platelet (see also figure 6.3).

6.4. The outermost points of the whiskers are the biggest (upper whisker) and the smallest (lower whisker) values that lie in the interval [upper border of the box + 1.5 · interquartile range, lower border of the box - 1.5 · interquartile range]. However, since the statistics are not very large with 29 platelets for the structured and 16 platelets for the smooth case, the average is not very representative and looking at the range of data instead is more meaningful. Still, the average of the mean final

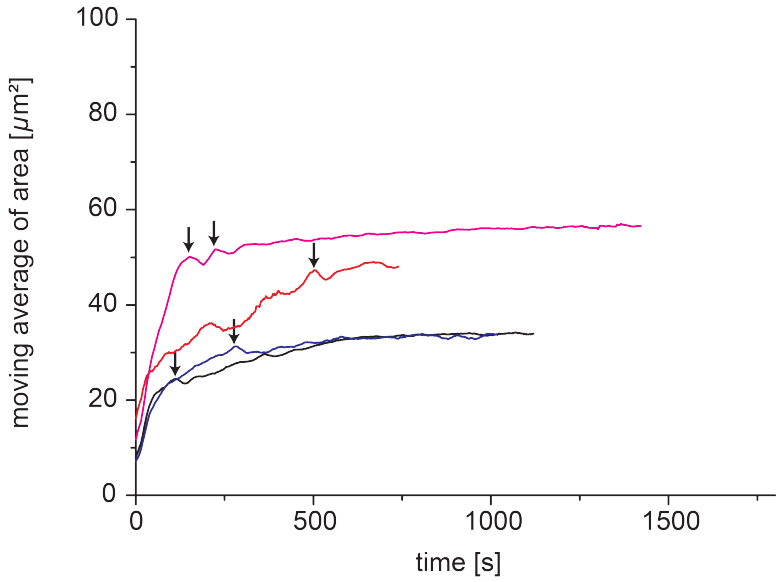

Figure 6.3.: Examples of area curves on structured substrates in which retractions are visible through area dips (local minima). The values at which the area starts to dip are marked with arrows.

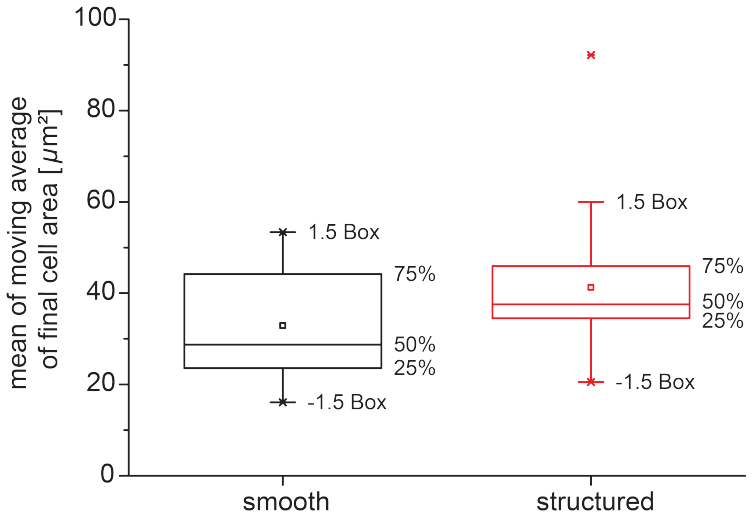

Figure 6.4.: Mean area of the last 50 time points (already treated by the moving average) of all analyzed time points on smooth (black, left) and on structured substrates (red, right) visualized via a box plot. The squares inside the boxes indicate the mean, the lines the median and the whole box is defined as the interquartile range. The range of values as can be seen by the outermost points of the whiskers is quite similar for both substrate types.

area lies in the same range as for the static experiments with much larger statistics (see chapter 5). The similar distributions on structured and smooth substrates for mean final spread areas in the case of membrane-stained living platelets further suggest that final spread area does not depend on the underlying structure at least not for structures as used here which has been shown as well in chapter 5.
But what characterizes local spreading? A first hint can be found in the plots of color-coded overlays of cell outlines over time. Examples for this way of visualizing spreading are shown in figure 6.5. Outlines originating from early time points are shown in dark blue, while outlines from late time points are shown in dark red. The arrows indicate the movement at certain positions. The platelet lying on the smooth substrate spreads evenly outwards and a very dynamic behavior can only be observed at the positions of the three filopodia (see figure 6.5, left). On the structured substrate, however, several retractions can be observed (see figure 6.5, right). Directly next to the retracting parts, the platelet protrudes smoothly outwards as is indicated by the arrows.

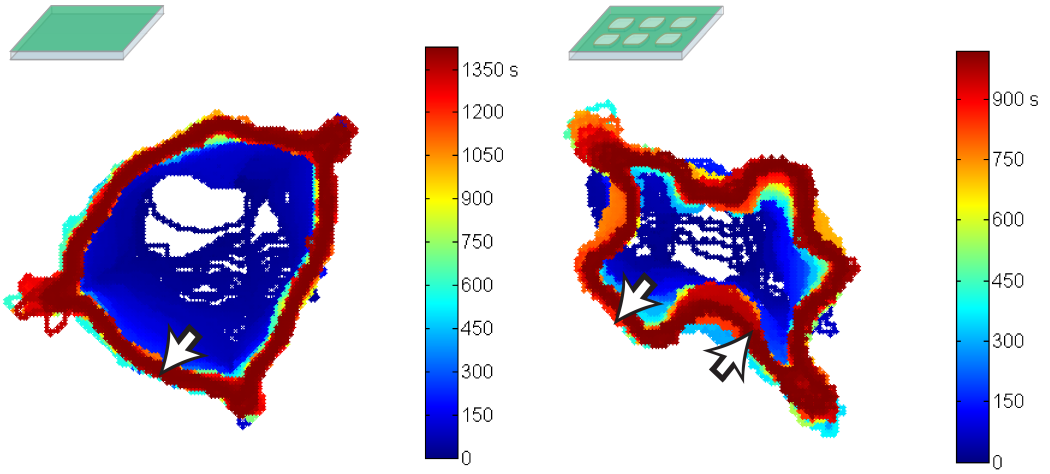

Figure 6.5.: Color-coded overlay of cell outlines ranging from dark blue for the first time points to dark red for the last time points on smooth (left) and structured substrates (right). In figure B.1 (appendix, chapter B) a micrograph of the underlying substrate for the platelet on the structured substrate is shown. The movements at certain positions are indicated by the arrows.
(left) Plot of a platelet lying on a smooth substrate and showing smooth outwards spreading. Strong dynamics are only visible at the position of the three filopodia.
(right) Plot of a platelet lying on a structured substrate that has adapted to the underlying substrate. Several points of retractions are visible. The arrows here indicate the different directions of movement at two adjacent positions. The platelet retracts at the position of the hole but spreads evenly outward next to it. The outward spreading next to the hole indicates that the platelet compensates for retractions over the holes by enhanced spreading over the interspaces.

To analyze local spreading more systematically, platelet spreading along different lines was analyzed in comparison to the extension of an ellipse with the same orientation, eccentricity and area as the platelet. By computing the spreading along different lines local phenomena like retractions over the holes can be made visible better than via the cell area, as area dips caused by a retraction over a hole can be compensated by outgrowth at other positions. A description on how spreading was analyzed along different lines is given in section 4.3.3.
In figure 6.6 two plots each of the moving average of the signed lengths $l_{\text{cell-ellipse}}(\beta, t)$ of vectors between the cell outline and a corresponding ellipse that has the same orientation, eccentricity and area as the cell are shown for platelets on structured (a) and b)) and on smooth substrates (c) and d)). The sign is negative if the platelet lies inside the ellipse and positive otherwise. These plots show two categories of platelets both on structured and on smooth substrates. In a) and c) platelets with alternating protrusions and invaginations can be seen, whereas in b) and d) the signed lengths $l_{\text{cell-ellipse}}(\beta, t)$ of the vectors only fluctuate around zero with no larger order. This finding indicates that on structured substrates two different cases can take place, either the platelets adapt to the underlying substrate and show alternating protrusions and invaginations due to the structure or they do not adapt and show a similar behavior as on smooth substrates. The differences in adaptation probably arise from the way of spreading, *i.e.* whether spreading is achieved only via lamellipodia or is started by filopodia. This aspect is examined and discussed further in chapter 7. The main difference between the plots shown in a) and c) of figure 6.6 is the temporal evolution of the signed lengths $l_{\text{cell-ellipse}}(\beta, t)$ of vectors between cell and ellipse. On the structured substrate, the differences between alternating protrusions and invaginations become amplified over time, whereas on the smooth substrate these differences even out over time and the platelet adapts a state of lower membrane curvature and thus lower energy.

The interdependency between the signed lengths $l_{\text{cell-ellipse}}(\beta, t)$ of the vectors between cell and ellipse along different directions can be visualized by computing the variance of the moving averages of these signed lengths for a fixed time point. The resulting variances var_{dir} for platelets on smooth substrates (left, black) and on structured substrates (right, red) over time are shown in figure 6.7. In these plots two types of platelets on structured substrates (red lines) can be distinguished. Several platelets show high variances var_{dir} due to adaptations to the underlying substrate. However, there are also platelets on structured substrates that show

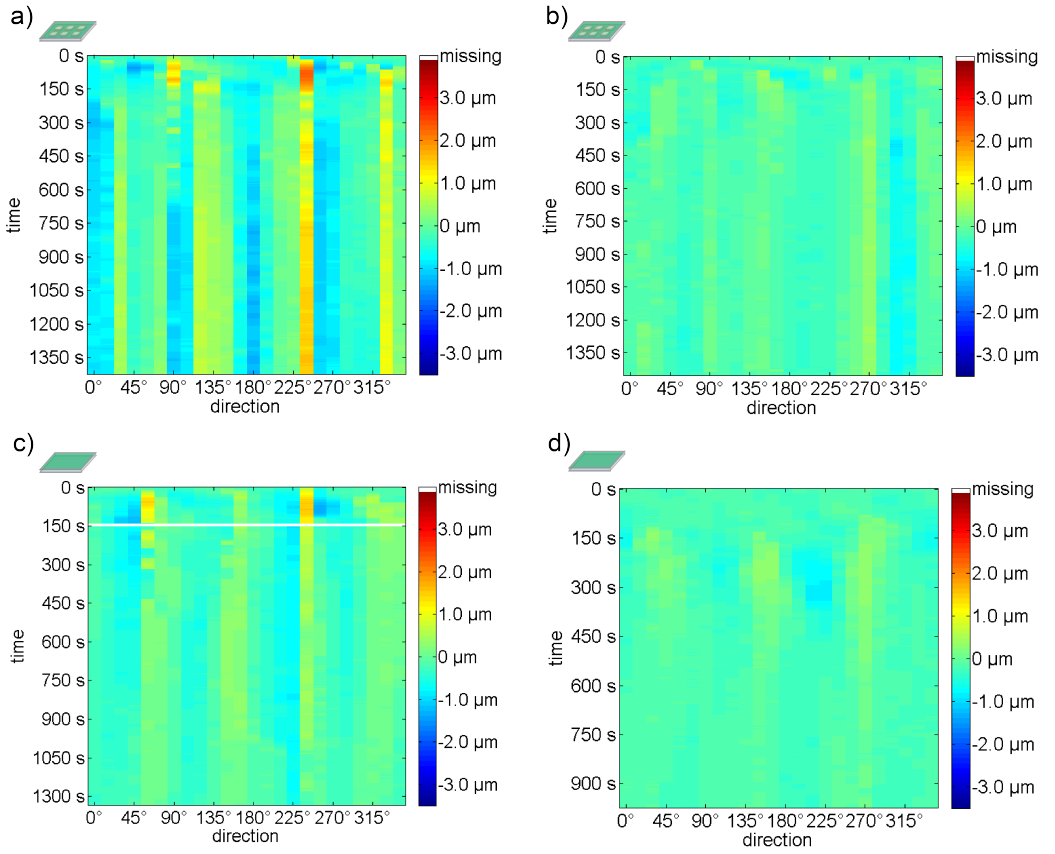

Figure 6.6.: Examples of the color-coded moving average of signed lengths $l_{\text{cell-ellipse}}(\beta, t)$ of the vectors between platelet and ellipse on structured (upper) and smooth substrates (lower). The signed lengths are shown for the different directions from 0° to 345° (left to right) and from the first to the last time point (top to bottom). The plots show two different categories of platelets on structured and smooth substrates. a) and c) show plots for platelets that display alternating protrusions and invaginations, whereas in b) and d) the values fluctuate around zero with no larger order. The main difference between a) and c) is that on the smooth substrate the differences between the directions even out with time, whereas on the structured substrate they grow.

variances var_{dir} corresponding to the variances of platelets on smooth substrates. To quantify the differences on smooth and structured substrates, the mean of var_{dir} (computed from the var_{dir} values of moving average treated data) was analyzed. 13 out of 29 platelets on the structured substrates show a mean var_{dir} that is higher than 0.18 μm^2. On smooth substrates only 1 out of 16 platelets shows a mean var_{dir} that is higher than 0.18 μm^2. The mean values of var_{dir} are shown in figure B.2 in the appendix (chapter B). Interestingly, also in the very beginning of spreading higher variances can be observed on structured substrates. A plot of var_{dir} at early

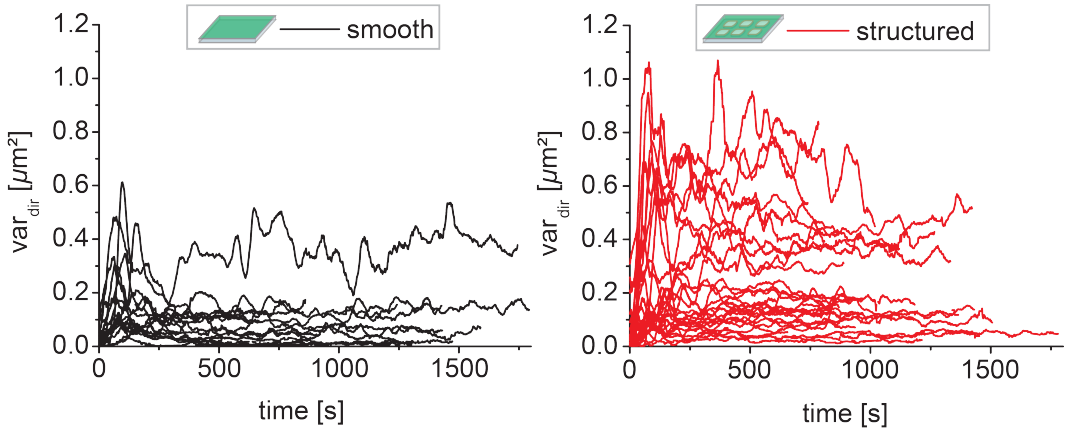

Figure 6.7.: Variances between different directions var_{dir} over time for platelets on smooth (left, black) and on structured (right, red) substrates. Var_{dir} was calculated based on the moving average of the signed lengths $l_{\text{cell-ellipse}}(\beta, t)$ of vectors between cell and ellipse.
On structured substrates several platelets show higher variances var_{dir} than platelets on smooth substrates from the beginning of spreading on. However, also platelets showing a variance similar to the variance on smooth substrates can be observed. 13 out of 29 platelets on structured substrates show a mean var_{dir} of more than $0.18\,\mu\text{m}^2$, while only 1 out of 16 platelets on the smooth substrates shows a mean var_{dir} of more than $0.18\,\mu\text{m}^2$. A high variance suggests a diverse spreading behavior in different directions.

time points can be found in the appendix (chapter B) in figure B.3. These differences in var_{dir} at earlier time points probably arise from filopodia. This aspect is discussed further in chapter 7.

The different dynamics during spreading along different directions can be visualized by computing the variance in time for a fixed direction var_{time}. The values for var_{time} can be seen in figure 6.8 for platelets on smooth substrates (black, left) and on structured substrates (red, right). For structured substrates higher values of var_{time} can be found. These higher values indicate a more dynamic spreading behavior for some platelets on structured substrates. Again, these higher values do not occur for all platelets on structured substrates similar to what can be observed for var_{dir}.

Finally, events of large outgrowth and retractions as have been shown in figure 6.1 were quantified. A description of the analysis of large retractions and outgrowth can be found in section 4.3.4. The results of this analysis are shown in figure 6.9. Yellow markers show large changes in protrusions and blue markers show large changes in invaginations. Filled markers show growing invaginations and protrusions. Open markers show retracting protrusions and filling of invaginations. Single plots showing only the events for protrusions or invaginations can be found

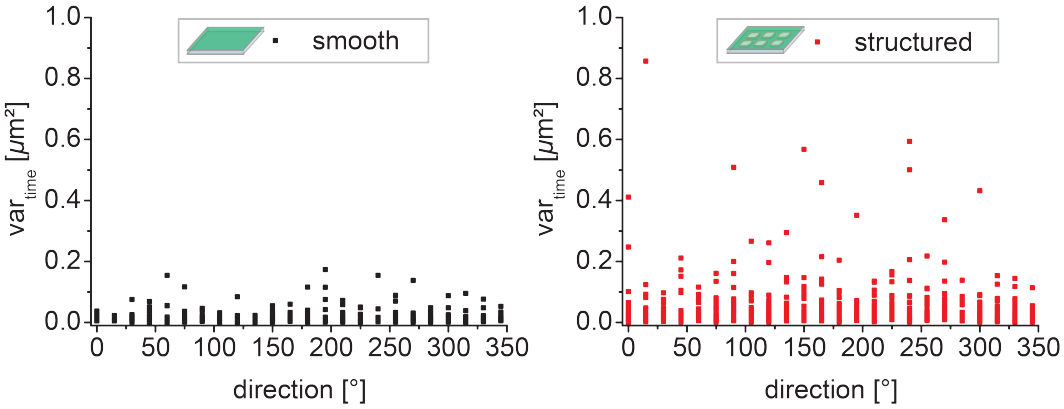

Figure 6.8.: Variances in time var_{time} for different directions on smooth (left, black) and on structured (right, red) substrates. Var_{time} was calculated based on the moving average of the signed lengths $l_{\text{cell-ellipse}}(\beta, t)$ of vectors between cell and ellipse.
Higher variances var_{time} can be observed on structured substrates than on smooth substrates. These higher variances point to a more dynamic spreading behavior on structured substrates than on smooth substrates.

in figure B.4 in the appendix (chapter B).
On smooth substrates (left) several events of growing protrusions can be observed, whereas invaginations are both being filled up and grow. On structured substrates (right), on the other hand, many more growing protrusions but also many growing invaginations can be seen. Even when taking into account the different numbers of platelets on smooth and structured substrates (smooth: 16 platelets, structured 29 platelets), the higher numbers in large changes in protrusions and invaginations on structured substrates compared to those on smooth substrates are still pronounced.
This result confirms the picture of a more dynamic spreading behavior on structured substrates. Furthermore, it underlines that the structure perturbs simple outward spreading in some cases so that the platelet has to find a way of dealing with the perturbations and still reach its desired spreading area. In the light of these numerous growing invaginations it is even more astonishing that the platelets manage to keep their final spreading area more or less constant. However, the finding that the number of growing protrusions is also larger on structured substrates compared to smooth substrates, hints at how platelets cope with the perturbations. These data suggest that the platelets compensate the area losses due to retractions or hindered spreading over holes by spreading more over other positions of the substrates, *e.g.* at the interspaces between the holes. This finding also explains why retractions cannot always be detected in the plots of spread

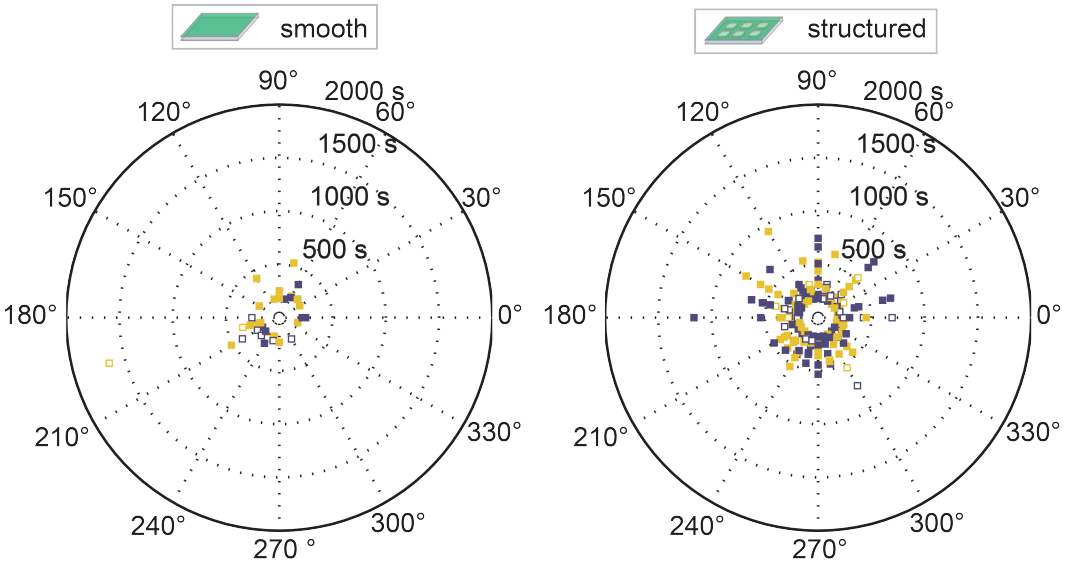

Figure 6.9.: Events of large changes in invaginations (blue symbols) and protrusions (yellow symbols) on smooth (left) and on structured substrates (right).
The polar plots show the different directions in azimuthal direction, while the time is shown in radial direction. Filled symbols show growing invaginations (■) and growing protrusions (■). Open symbols show filling invaginations (□) and retracting protrusions (□). On smooth substrates several events of large protrusion growth can be observed (■), whereas invaginations are both being filled up and grow (□ and ■). On structured substrates, on the contrary, both more growing protrusions (■) and more growing invaginations (■) can be observed.

area over time, as has already been discussed above. A connection between retractions/outgrowth and particular directions is not visible which is most likely a result of the platelets lying differently on the structured substrates and thus encountering the underlying holes in different directions.
One possible explanation for the retractions over the holes are different contributions of actin and myosin during spreading. A sketch of the possible mechanism of cell retraction over the holes is shown in figure 6.10 and takes into account general findings on the mechanism of spreading as found by others (see [43, 81], which have been summarized in sections 2.3.1 and 2.5). A further discussion of this mechanism with regard to the existing literature can be found in section 6.1.
In the first fast phase of spreading actin polymerization is assumed to outweigh retractions due to myosin (see figure 6.10 a)-b)). Myosin forces are then up-regulated and since the platelets are likely not attached to the substrate over the holes the resistance to forces build up by myosin is very low, so that the platelet is retracted over the holes (see figure 6.10 c)-e)). However, if a platelet is able to span a hole

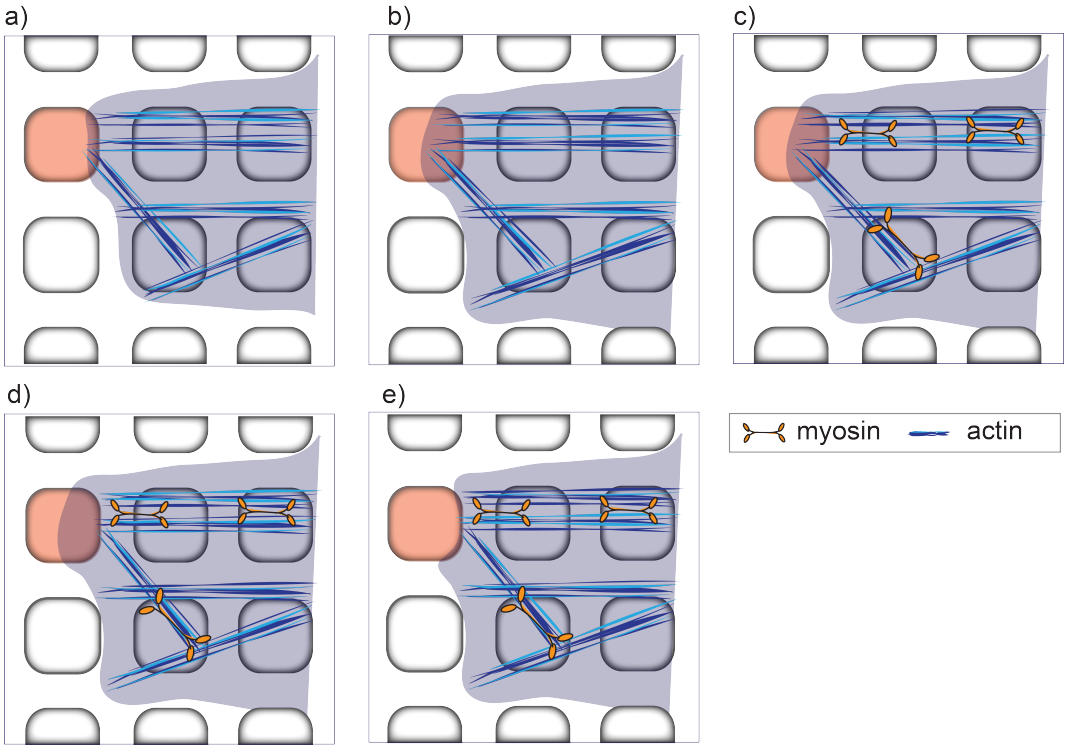

Figure 6.10.: Sketch of possible mechanism to explain retraction over the holes.
The hole above which the retraction occurs is sketched in orange. a)-b) The platelet spreads over the holes by actin polymerization. c)-d) Myosin exerts forces on the lammelipodium and thus the actin is retracted. e) The membrane is retracted over the hole as well, since the cell likely is not attached to the substrate over the hole.

completely, it can establish binding sites at the other side of the hole and thus stabilize itself.

For some platelets several retractions and subsequent outgrowth over the holes can be observed which indicates oscillating contributions of actin and myosin. An example for a series of retractions and outgrowth is shown in figure 6.11. The yellow stars approximately indicate the beginning of retractions, whereas the blue stars show a nearly complete return to the original form. To illustrate the position of the underlying holes, fluorescence images of the fibrinogen coating of the substrate as well as of the plasma membrane of the platelet are shown in figure B.5 in the appendix (chapter B). It would be interesting to see for how long the platelet can perform cycles of retractions and outgrowth. Unfortunately, it is not possible to visualize the complete process with our experimental methods, as one

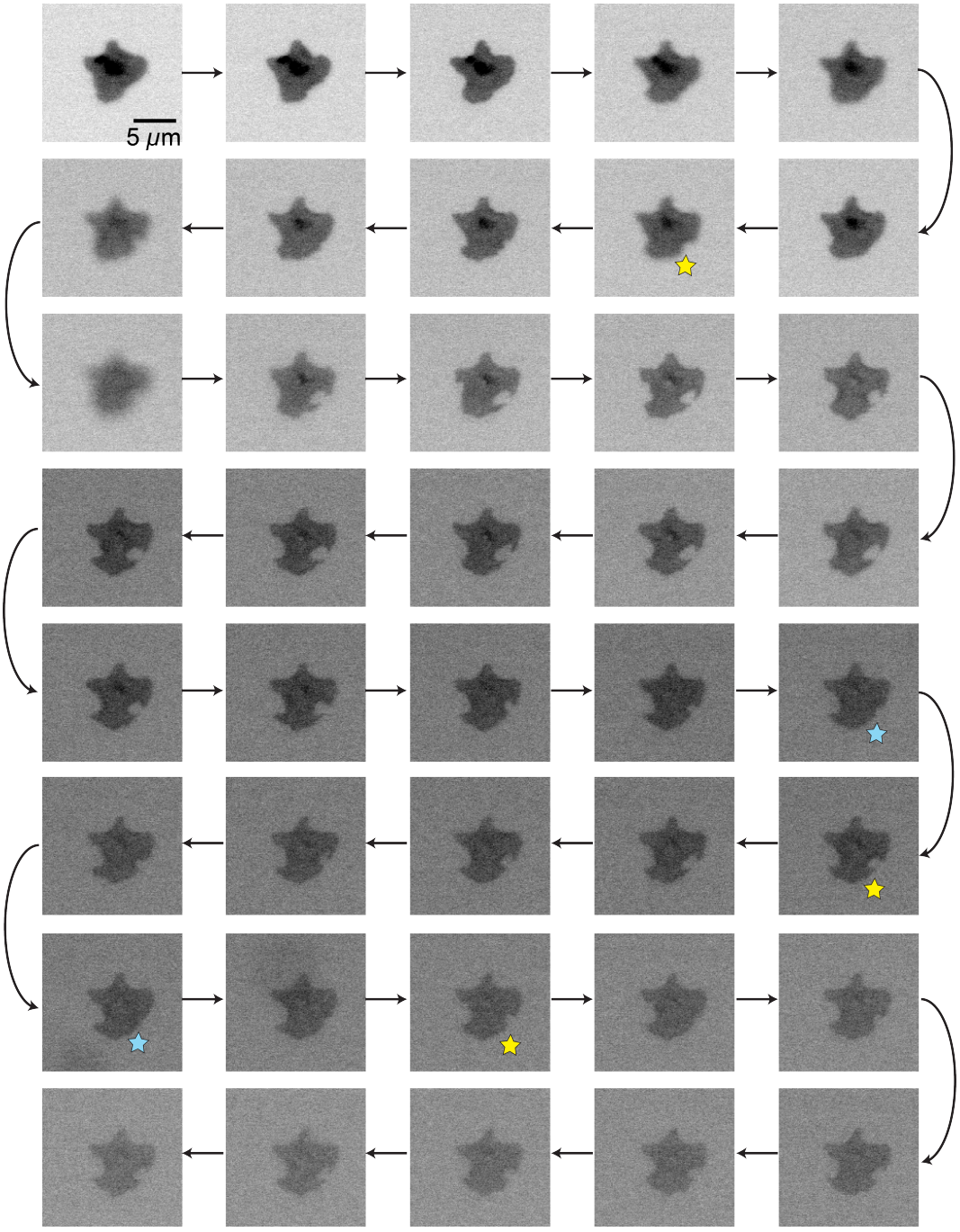

Figure 6.11.: Inverted fluorescence images of a platelet on a structured substrate that shows repeating retractions and outgrowth over a hole.
The micrographs represent snapshots from a time lapse series and lie 45 seconds apart from each other. Yellow stars indicate the approximate beginning of retractions and blue stars indicate nearly complete returns to the original form. Retractions and outgrowth can be observed multiple times hinting at a oscillating contribution of actin and myosin in spreading.

would need to be able to visualize spreading over a longer time period[ii]. However, visualizing platelets over a longer time may be possible using a new dye (SiR actin) that can stain actin in living cells [62]. This option is discussed further in chapter 8. The cell shown in figure 6.11 was not included in our former analysis as the beginning of spreading was not captured in the time-lapse series.
Two different groups of platelets show clearly in the values of var_{dir} (figure 6.7 and figure B.2) on structured substrates. One group of platelets adapts to the substrate as can be seen by mean values of var_{dir} of higher than $0.18\,\mu\mathrm{m}^2$ (in the following defined as adapted platelets) and one group does not adapt or not as well to the substrate as can be seen by mean values of var_{dir} of less than $0.18\,\mu\mathrm{m}^2$ (in the following defined as unadapted platelets). The finding that two groups of platelets with different levels of adaptation to the substrate exist on completely coated, structured substrates can explain why the differences in relative perimeter and cell outline curvature between platelets on smooth and completely structured substrates (see figures 5.5 and 5.6 in chapter 5) are not larger. Differences in adaptation between different platelets may also be present on selectively coated substrates but are probably not as distinct as for completely coated substrates since spanning over holes at the cell periphery is already reduced compared to completely coated substrates (see chapter 5). If some of the platelets behave similarly as those on smooth substrates, the differences between smooth and structured substrates are not as large as if all platelets adapted strongly to the structured substrate. In line with the different adaptation levels on completely coated substrates observed in this chapter, platelets have been observed to span holes at their periphery in the case of completely coated substrates as described in chapter 5.

6.1 Discussion of Results with Regard to Existing Literature

If the following reference [2] is given, the termini filopodia and lamellipodia are used instead of the termini pseudopodia and hyalomer as given by the authors. For further notes on this usage of termini see section 2.3.2.
As has already been mentioned in section 5.1, larger platelets in our studies are very likely preplatelets (see section 2.1.2 for references on preplatelets and further explanations) which also explains why larger platelets occur seldomly in our studies. Spreading behavior and reaction to the structured substrate was found to

[ii] As already mentioned above, the CellMask™ dye is taken up by cells after a while. See the data sheet for details [64].

be similar as for smaller platelets (see also figure 6.13) and thus the possible existence of preplatelets in our samples does not influence the results - except for the occasional occurrences of larger cell areas. Preplatelets can be distinguished from platelets by size, initial shape and by whether the cells are able to undergo transitions to proplatelets [96]. The initial shape could not be evaluated in our time lapse series since in the first images the cell outline usually is not well visible. Furthermore, also transitions to proplatelets were not observed for the platelets analyzed in this chapter since platelets rapidly spreaded and did not stay in the quiescent state. For the largest platelet observed here that spreads to about 90 μm^2 on a structured substrate (see figure 6.2), cell size is elevated from the beginning on suggesting that this cell is a preplatelet. However, the initial areas of platelets as shown in figure 6.2 are likely overestimated since the cell area is a very fast changing quantity in the beginning of spreading and the moving average thus does not represent the initial values accurately. For our further analysis however, the moving average does not influence the results as is discussed further in section 6.2.

The time needed for spreading observed here is about 10 minutes as shown in figure 6.2, similar to what has been observed by Allen *et al.* [2] for platelet spreading on glass at 29°C. Park *et al.* [72], however, saw almost complete spreading on fibrinogen-coated glass after 60 minutes at room temperature. As the temperature employed during our experiments resembles more that employed for the experiments presented by Allen *et al.* [2], the spreading time found here seems plausible. Rossier *et al.* [81] observed similar alterations in spreading for fibroblasts on micropatterned glass coverslips as described here for platelets on microstructured PDMS substrates. Firstly, the initial fast spreading phase they observed is also accompanied by enhanced outgrowth at adhesive regions compared to non-adhesive regions [81]. Secondly, in their studies contractions after this first phase lead to retractions over the non-adhesive parts of the substrate which are followed by cycles of contractions and protrusions leading to further growth of cell area [81].

Although most aspects of these two observations summarized above fit nicely to the results presented here for platelets, it is plausible that cellular bridge formation as described in [81] is different due to the geometry of the underlying substrate used for our experiments. On our substrates, regions with non-available binding sites are interspersed with adhesive regions in all directions, whereas for patterned lines interspersed with non-adhesive lines as in [81] binding sites are missing completely for certain directions. Thus, it can be assumed for our exper-

iments that when the platelet retracts over the holes, the retraction is stopped at the next interspace. However, as mentioned in chapter 5, some spanning of the holes at the periphery of cells can be observed for platelets on completely coated substrates. For our data on platelet spreading on microstructured substrates, concave parts of the cell outline can also be induced by the specific geometry of the underlying substrate, *i.e.* the holes, instead of being a manifestation of cellular bridges as seen for fibroblasts in [81].

The finding that platelets on microstructured substrates, as examined in the studies presented in this thesis (chapter 5 and 6), behave similarly as fibroblasts on micropatterned substrates as described by Rossier *et al.* [81], underlines the results presented in chapter 5. If platelets do not enter the holes at their periphery, they are not able to sense the binding sites provided at the walls and bottoms of the holes (see figure A.1 for terminology) and thus show spreading restricted to the $2D$-plane at their periphery similar to fibroblasts spreading on micropatterned substrates. This conclusion fits also to the notion that the specific 3D geometry of the substrate becomes unimportant once the cells bridge the topographic discontinuities as has been mentioned by Stevenson *et al.* [91]

The model proposed here (see figure 6.10) to explain the retractions and outgrowth observed for platelets spreading on structured substrates takes into account several aspects of other models of cell spreading [43, 81]. Retraction over the holes upon myosin force exertion due to missing binding sites (missing in the plane in which the interspaces lie) is an important part of our model.

Ruffling over non-adhesive parts of substrates can be explained by forces exerted by myosin on adhesion points at the tip of the lamellipodium [43]. If the adhesions are not present or too weak, the cell detaches from the substrate and displays ruffling, otherwise force dependent growth of adhesions takes place [43]. Rossier *et al.* [81] observed retractions over non-adhesive substrate parts caused by contractions due to myosin II as well. Retractions or ruffling of lamellipodia of platelets having spread on siliconized glass have been observed by Allen *et al.* [2]. Myosin plays an important role for platelets during spreading, as hole formation in platelets spreading on collagen can be observed when myosin is inhibited [13]. Possible oscillating contributions of myosin and actin leading to the cycles of retraction and protrusion as shown in figure 6.11, fit to the observations and suggestions of others (see [31, 42, 43, 81]). Giannone *et al.* [43] proposed that rearward translocating actin from the lamellipodium initiates a new cycle of myosin force generation.

6.2 Discussion of Analysis and Experimental Methods

The number of values based on which the moving average was calculated was chosen to be 21. When averaging over too many values, changes in cell morphology would be averaged out while for too few values the data would still be noisy and missing points could not be interpolated. As the interest here lies in long-term changes in the cell morphology, the value of 21 is justified. Furthermore, computing the variances on basis of the raw data without any moving average, does not alter the general result of higher values for var_{dir} and var_{time} on structured substrates compared to smooth substrates. For comparison, the variances calculated based on the raw data are shown in figures B.6 and B.7 in the appendix (chapter B). By the choice of 21 points feeding into the moving average most missing values can be interpolated.
In figure 6.12 detected events, *i.e.* large changes in protrusions and invaginations, and the color-coded signed lengths of the vectors between cell and ellipse are shown for a reference platelet.

The parameters used in the analysis to detect events are chosen such that in particular the retractions around 270° that are well visible in the plot of the color-coded signed lengths $l_{\text{cell-ellipse}}(\beta, t)$ (and also in the corresponding time lapse series of the platelet) are faithfully detected for this particular platelet. The large differences between the time points that were compared (120 images, *i.e.* 180 seconds in between) were chosen to detect long-term changes of the position of the cell outline, *i.e.* changes that persist for a longer time. Taking the moving averages of the signed lengths $l_{\text{cell-ellipse}}(\beta, t)$ of the vectors between cell and ellipse to compute the events and not the raw data makes sense, since long-term changes in cell morphology shall be detected. Further details of why specific constraints were chosen have already been discussed in section 4.3.4. For all analyzed platelets the same parameters were used to ensure comparability. The choice of different parameters will lead to slightly different results as other types of events, *e.g.* more long-lasting or more short-lasting events, would be detected. However, the parameters used here describe the differences between smooth and structured substrates, as seen in the time lapse movies of platelet spreading on the different substrate types.
The number of straight lines, along which spreading was analyzed, was chosen to be 12, *i.e.* 24 different angles with increments of 15°. As can be seen in figure 4.8 and in figure 6.15, invaginations are detected by $1-4$ lines depending on the exact geometry of the cell outline. In figure 6.13 the distributions of points on the

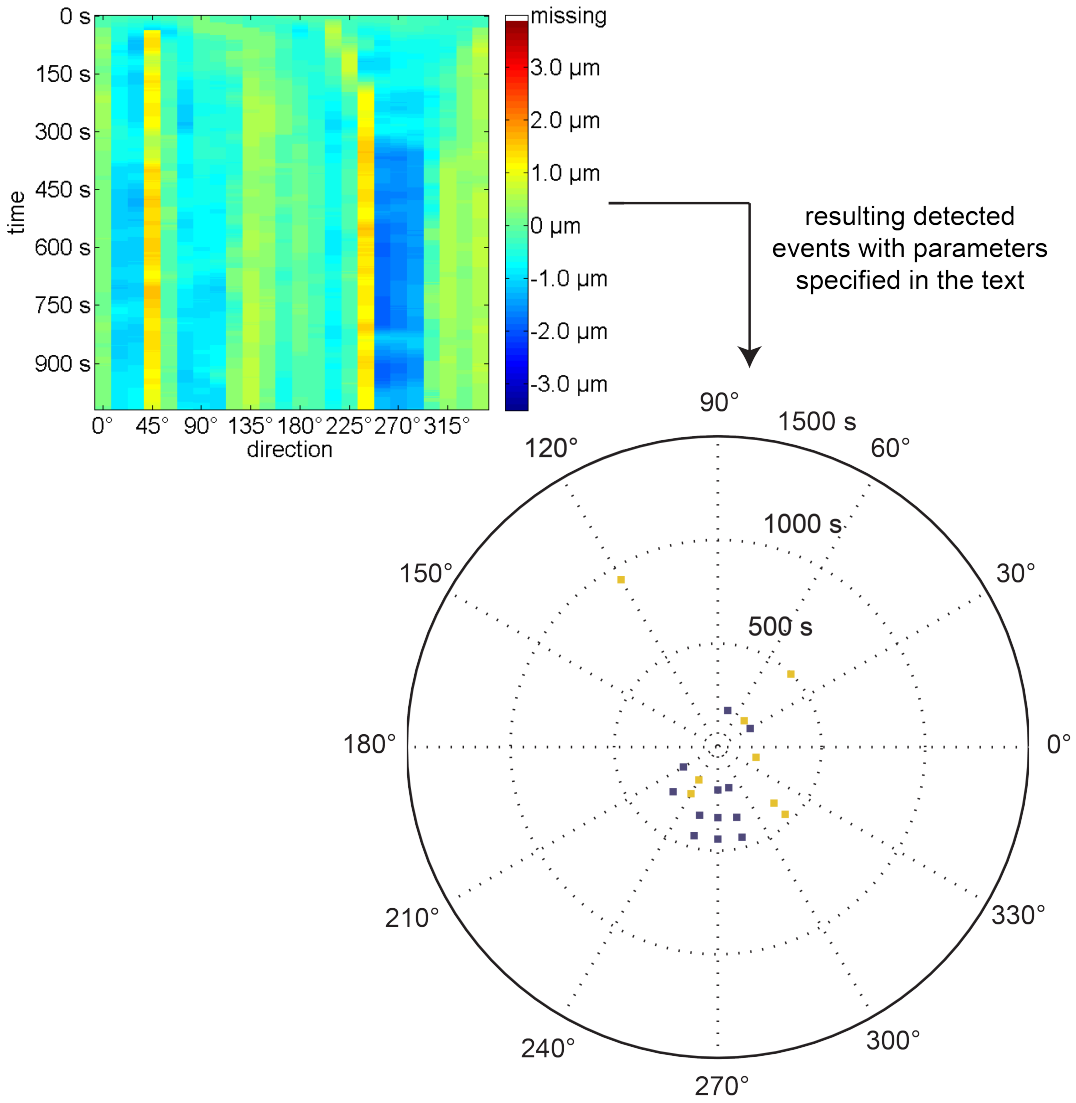

Figure 6.12.: Plot of color-coded moving average of signed lengths of vectors between cell and ellipse (upper, left) as well as detected events for this platelet shown in a polar plot (lower, right). (left, upper) The color-coding ranges from dark blue for the largest negative values to dark red for the largest positive values. The direction is shown on the x-axis while the time is shown on the y-axis. (right, lower) The time of events is denoted in radial direction in the polar plots whereas the direction in which the event takes place is denoted in azimuthal direction. Filled symbols show growing of invaginations (■) and protrusions (■). The choice of parameters used here allows for detection of events visible in the upper left plot.

cell outline (red points) for the last analyzed time point are shown for the largest (figure 6.13 a)) and second largest platelet (figure 6.13 b)) examined here. Even for the largest platelet examined here, which is with a final area about $90\,\mu m^2$ much

larger than the average platelet, the points on the cell outline are situated close enough to describe changes in cell morphology. The platelet shown in figure 6.13 b) is the second-largest platelet and represents, with a final spread area of about $60\,\mu m^2$, a more realistic upper limit for the average platelet examined here. As a scale reference the positions on the x- and $y-$axis are given in pixels with 1 pixel corresponding to about 108 nm. Thus, although the spreading could be examined along more lines, the spacing of the lines seems sufficient to detect changes in overall cell morphology.

In figure 6.14 changes in the sign over time for vectors between cell and ellipse near a filopodium are shown. These changes most likely result from movements of the filopodium itself and can in part be responsible for the high dynamics seen along some lines (see figure 6.8). Additionally, some of the faster changes in var_{dir}

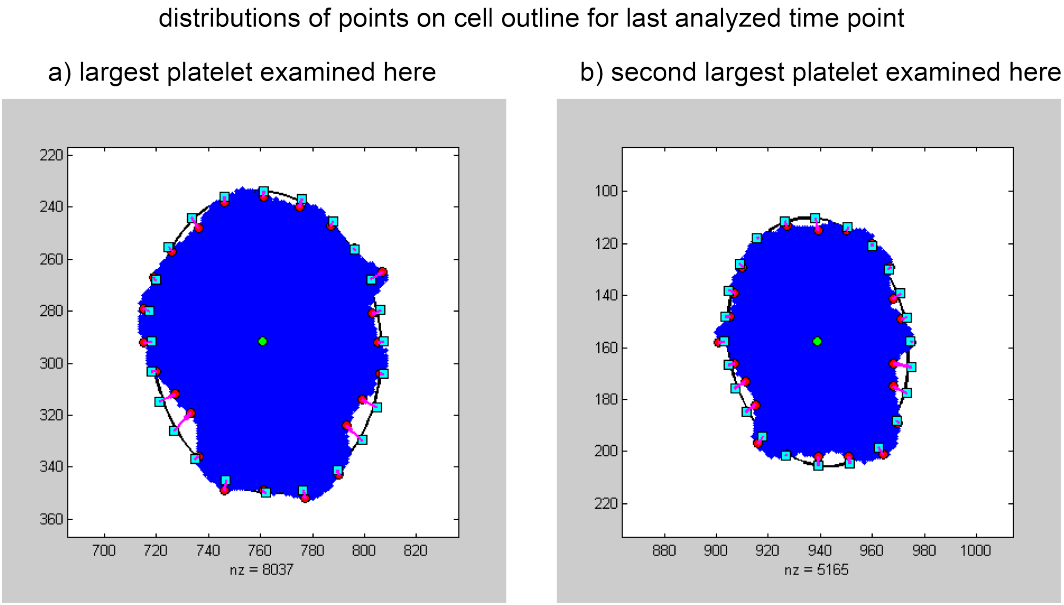

Figure 6.13.: Distribution of points on cell outline and ellipse for the largest (a)) and second largest platelet (b)) examined in this dynamic study at the last analyzed time point. The points on the cell outline are shown in red and the points on the ellipse in cyan, the cell is shown in blue. The positions along the x- and $y-$axis are denoted in pixels to give a scale ($1\,\mathrm{pixel} \approx 108$ nm).
a) The platelet shown here has a final area of about $90\,\mu m^2$ and thus is much larger than the average platelet examined here. Even in this case, the distances between the points on the cell outline are not large.
b) This platelet has a final area of about $60\,\mu m^2$ and thus represents a more realistic upper limit for the average platelet and shows that points along the cell outline are situated close enough to detect changes in cell morphology.

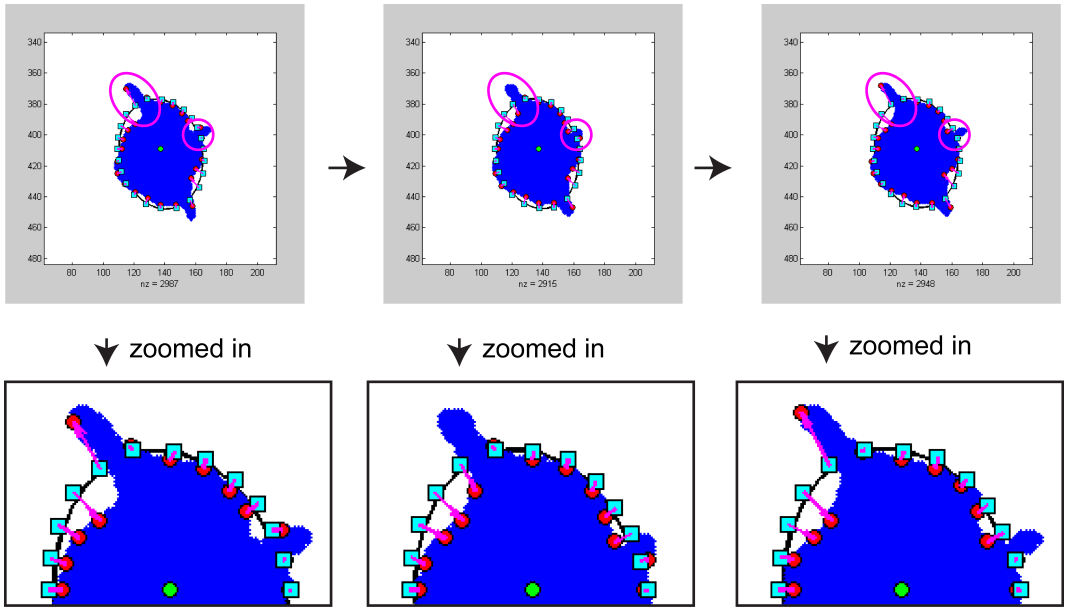

Figure 6.14.: Changes in sign for vectors between cell and ellipse (shown in magenta) over time. The time evolution is shown from left to right. The positions of changes in sign are marked with magenta ellipses/circles and occur near filopodia whose movements seem to be responsible for the changes in sign.

(see figure 6.7) likely result from these filopodia movements. However, it is reasonable to assume that in the events of large changes in protrusions and invaginations these short-lived changes in sign do not play a large role, since for the detection of these large changes in invaginations or protrusions the changes have to persist for at least 60 seconds.
In figure 6.15 a protrusion is shown that lies inside the ellipse and thus is designated as invagination. A protrusion lying inside of the ellipse usually occurs if this protrusion is much shorter than the other protrusions. This can slightly influence the number of detected events in protrusions and invaginations.

Errors in drift correction have the potential to influence the results. However, no large drift is visible in drift-corrected images of the substrate coating. Further errors can lie in the detection of the cell outline and the way how points of interception between ellipse and straight lines are found. Slight errors in the detection of the cell outline can arise when adding not automatically detected parts of the cell manually. Also, when automatically detecting edges errors of 1 pixel can occur. The detection of points of interception of cell outline and straight lines is

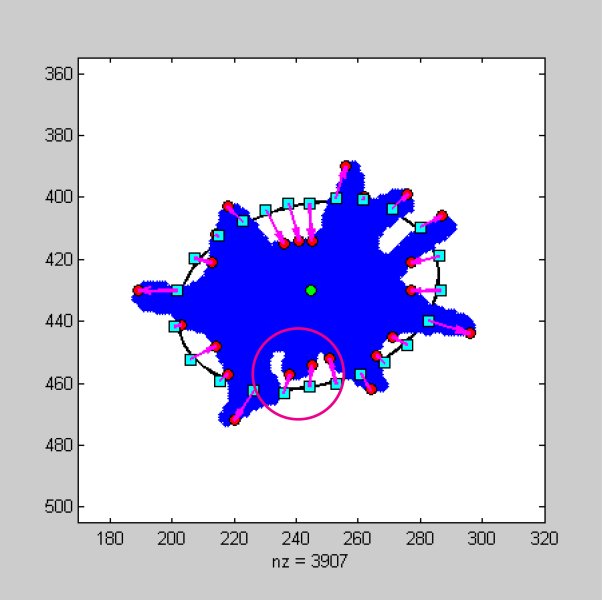

Figure 6.15.: Plot of a short protrusion (marked by a magenta circle) that lies inside the ellipse and thus is detected as invagination. Usually only very short protrusions lie inside the ellipse and are detected as invaginations rather than as protrusions.

accurate except for rounding errors[iii]. For points of interception of the ellipse and the straight lines a deviation of less than 1.5 pixels is allowed. However, since the points have to lie on the straight lines, the error mainly overestimates or underestimates the size of the ellipse slightly. For the vertical line of 90°/270° the maximum error can be 1 pixel and as point of interception the point on the ellipse is given so that slight deviations from the line can occur. The values of the points on the ellipse are given in this case, since only the x-value of the point of interception can be defined by the line. By applying the moving average to the data all these small errors can be reduced. Errors in drift correction would especially influence the detection of events, since these rely on the comparison of single values. Therefore, the condition that the difference has to be kept for 40 more frames, *i.e.* 60 seconds, was introduced to ensure that no short-lived changes were detected. Maybe the strongest argument for a small influence of errors is that when assuming similar values for the errors for all data sets, these errors should not largely influence the values with respect to each other.

Rotating the binarized images to align the underlying holes with the image borders and subsequently binarizing the images again, changes the cell outline slightly and can enlarge the thickness of the protrusions while reducing the width of invaginations. These effects, however, mostly influence the regions in which an

[iii] The values on the line have to be rounded to the next natural number due to the pixelated nature of the cell outline

invagination merges into a protrusion. The ellipse as reference for spreading allows comparison of values for platelets with different eccentricities. Furthermore, it sets a definition for protrusions and invaginations depending on whether the values lie inside the ellipse or outside of the ellipse.
In early spreading, cell area and cellular protrusions grow fast. These fast growing protrusions also influence the position and size of the ellipse, so that the difference between the ellipse and the cell outline in between the protrusions also grows. Those regions are classified as invaginations, if they lie inside of the ellipse, and since the distances to the ellipse also grow by the growth of the protrusions, early large changes in invaginations can be caused by growth of protrusions. Retractions will thus mostly be detected in the later occurring events.
The idea that the avoidance of holes at the periphery can change cell area is plausible when taking into account that the platelet encounters many of these holes at its periphery. But have retractions over single holes the potential to influence cell area? The area of one of the holes in the substrates used in this chapter lies around 7-8 μm^2 [iv]. Thus, a complete retraction over one hole or slight retractions over several holes can indeed influence the cell area. Another argument for the influences of retractions on cell area is shown in figure 6.3 where retractions are visible in the area curves. However, for this plot one has to take into account that all other regions of the platelet are not fixed in position so that simultaneous outgrowth can reduce the effects retractions have on the cell area. Note that the losses in area as shown in figure 6.3 are regained within several minutes. The hole size in this chapter was chosen to allow for the maximal effect of retractions over these holes while simultaneously keeping the holes so small that quiescent platelets cannot simply enter the holes and spread inside them.

[iv] It is assumed here that the hole is basically a square with a side length of 2.8 μm. The area for such a square has to be slightly revised downwards due to the rounded corners.

7

Dynamics of Cellular Protrusions

All quantities described below have been calculated for all analyzable cell images in the time-lapse series. To examine whether the numbers and paths of filopodia influence the spreading on structured substrates and are connected to the different levels of adaptation for the data examined in chapter 6, platelets that show high values for the mean of var_{dir} were examined separately from the rest of the platelets lying on structured substrates. Here, mean values of var_{dir} larger than $0.18\,\mu\mathrm{m}^2$ are considered as platelets *adapted* to the substrate, while platelets with a lower mean value for var_{dir} are considered as *unadapted*. The values for the mean of var_{dir} are shown in figure B.2 in the appendix (chapter B). Given the plots of var_{dir} for early time points (see figure B.3 in the appendix, chapter B), it seems that some platelets spread differently compared to others on structured substrates, *i.e.* with a higher variation between different directions. Filopodia can account for these differences, since they can be formed very early in spreading and their formation would result in high values of var_{dir}.

Considering the examples for color-coded groups of filopodia endpoints in figure 7.1 a), it can be expected that adapted platelets lying on structured substrates show a high number of filopodia and that these filopodia are also more persistent. In this figure each point describes an endpoint of a protrusion at one time point

of the time-lapse series. The platelet shown in figure 7.1 a) (I.) lying on a smooth substrate does show more persistent filopodia than the unadapted platelet on the structured substrate (IV.) and resembles more the adapted platelet on the structured substrate (III.) than the second platelet on the smooth substrate (II.). The second platelet on a smooth substrate (II.), however, shows a duration and paths of filopodia resembling more those of the unadapted platelet on the structured substrate (IV.).

For broad, blunt protrusions the situation is different, both the first platelet on the smooth substrate (I.) as well as the adapted platelet on the structured substrate (III.) show more separated broad, blunt protrusions than the unadapted platelet (IV.) (see figure 7.1 b)). In the case of the unadapted platelet (IV.), it seems as if single broad, blunt protrusions merge into each other similar as for the second platelet on the smooth substrate (II.). Merging of broad, blunt protrusions indicates a smooth outline. Taking all this into account, platelets showing more persistent filopodia on structured substrates during the time lapse series seem to adapt more to the substrate than platelets spreading mostly via other pathways like lamellipodia. Interestingly, the results suggest that there are two different types of platelets both on smooth and structured substrates - one showing more persistent filopodia and one mostly lacking filopodia. These differences seem to be reflected in the broad, blunt protrusions as well.
To analyze the influences of filopodia further, the mean number of filopodia as well as the standard deviation of the number of filopodia were calculated for each time point of the time-lapse series for platelets lying on smooth substrates and platelets lying on structured substrates (divided into adapted and unadapted). The results are shown in figure 7.2. The mean numbers of filopodia are higher for adapted platelets on structured substrates (b)) than for platelets on smooth substrates (a)). The difference between adapted platelets and unadapted platelets (c)) is even larger than that between adapted platelets and platelets on smooth substrates. For platelets lying on smooth substrates and unadapted platelets lying on structured substrates the mean number of filopodia increases strongly in the beginning of spreading and drops after several tens of seconds. If the platelets are adapted to the underlying structured substrate however, the mean number of filopodia increases in the beginning of spreading and then stays at a value of between $2-3$. This behavior indicates that filopodia remain even at later time points in spreading. However, due to their morphology also the cellular extensions along the interspaces between the holes are prone to be detected as filopodia. A fur-

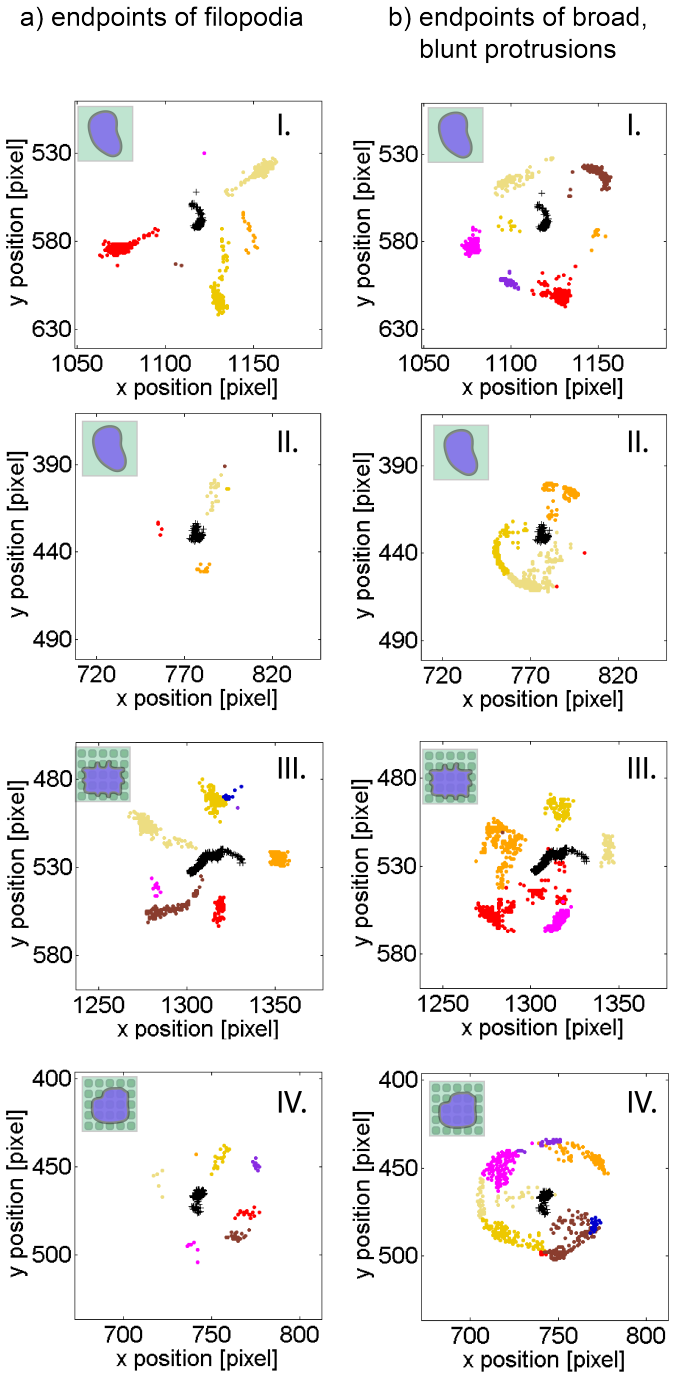

Figure 7.1.: Plots of differently colored groups of endpoints for filopodia (a)) and broad, blunt protrusions (b)) of individual platelets lying on smooth substrates (I., II.), for an adapted platelet lying on a structured substrate (III.) and an unadapted platelet lying on a structured substrate (IV.). The platelets shown for filopodia and for broad, blunt protrusions are the same and the black crosses show the center of mass over time.
a) The adapted platelet on the structured substrate (III.) shows many groups of endpoints of filopodia. These groups are also more elongated than for the unadapted platelet lying on a structured substrate (IV.). For the upper platelet on the smooth substrate (I.) the groups of endpoints are also elongated, but not for the lower one (II.) which also shows very few endpoints of filopodia.
b) For the adapted platelet lying on a structured substrate (III.), the groups of endpoints are more defined than for the unadapted platelet lying on a structured substrate (IV.). For the latter one the groups of endpoints seem to blend into each other and form a smooth outline, similar as for the second platelet (II.) on the smooth substrate. The platelet on the smooth substrate that shows distinct filopodia (I.) also shows more distinguishable broad, blunt protrusions (I.). 1 pixel corresponds to about 108 nm here.

ther discussion of whether the detected filopodia at later time points are really filopodia can be found in section 7.2.

The divergent values for later time points in all three cases very likely arise from

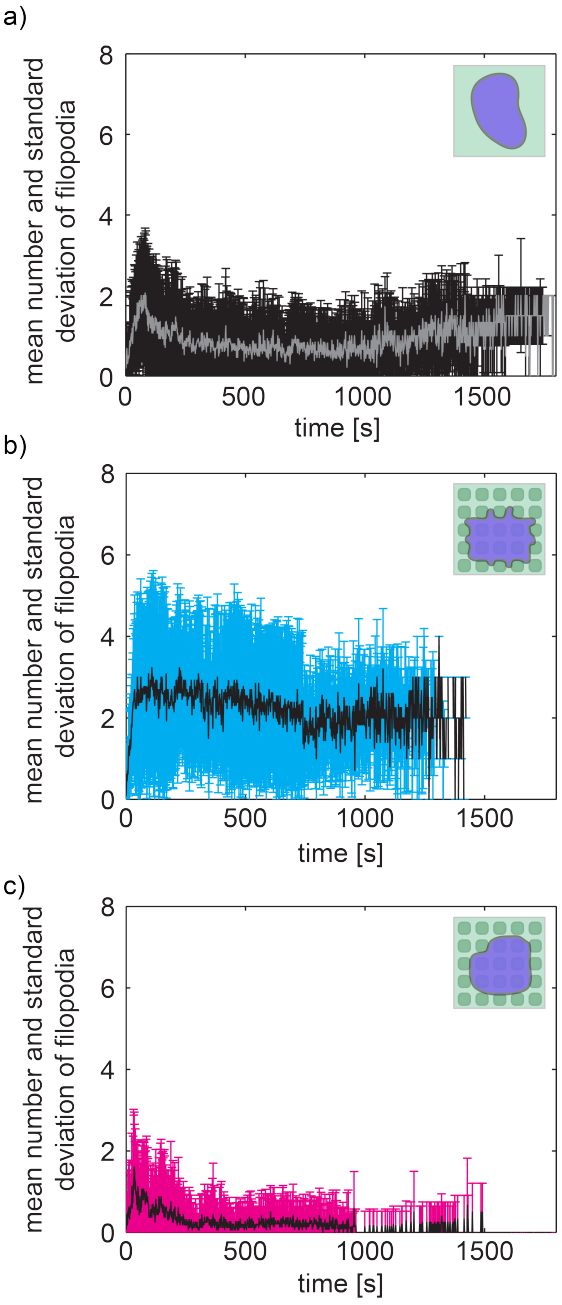

Figure 7.2.: Plots showing the mean number as well as the standard deviation of the number of filopodia as a function of time for platelets lying on smooth substrates (a)), for adapted platelets lying on structured substrates (b)) and unadapted platelets lying on structured substrates (c)). The fluctuations at the end arise very likely from the reduced number of platelets contributing to these values.
a) The mean is shown in gray while the standard deviation is shown in black. The mean number of filopodia first sharply increases and then decreases over time starting from about 2 to approximately 1. The range of the standard deviation shows that platelet behavior is not completely uniform and platelets with more or fewer filopodia exist.
b) The mean is shown in black while the standard deviation is shown in light blue. The mean number of filopodia is increasing in the beginning of spreading and then stays at around $2-3$. The standard deviations are much higher than for the smooth substrates in a). These large standard deviations indicate a greater variety in filopod number than on smooth substrates.
c) The mean is shown in black while the standard deviation is shown in magenta. The mean shows a steep increase in the beginning and than decreases fast to values around 0. The mean numbers of filopodia are much smaller than for the other two cases - especially compared to the adapted platelets on structured substrates. The standard deviations are smaller than in the two other cases as well.

the reduced number of platelets averaged for these values, since the time lapse series do not all have the same duration. The standard deviations are largest for adapted platelets lying on structured substrates, indicating a large variation in the number of filopodia. The large standard deviations can also arise from different

time points at which each platelet forms its filopodia. Furthermore, errors in detection of filopodia can lead to high standard deviations. The different reasons for higher standard deviations are discussed further in section 7.2. However, the mean numbers of filopodia still suggest a different behavior for the three cases. The result that the mean numbers of filopodia are quite different for the three cases from the beginning of spreading on, indicates that these differences are an inherent feature of the platelets and not induced by the substrate. The mean number and standard deviation of the number of filopodia as a function of time for all platelets on structured substrates taken together are shown in figure C.1 in the appendix (chapter C). When all platelets on structured substrates are averaged for the number of filopodia, the difference in mean numbers between smooth and structured substrates is much smaller than when comparing platelets that are adapted to the underlying structured substrate to platelets on smooth substrates. This finding suggests that two populations of platelets exist showing different degrees of filopodia formation and when averaged similar numbers of filopodia seem to occur on structured and smooth substrates. A comparison between the mean numbers and standard deviations of the number of filopodia for the different cases (smooth, structured (adapted), structured (unadapted) and structured (all)) is shown in table 7.1. The mean numbers and standard deviations of the number of endpoints of broad, blunt protrusions are shown in figures C.2 and C.3 as well as table C.1 in the appendix (chapter C). In general, detecting those broad, blunt protrusions is more difficult than detecting filopodia as has been discussed already in section 4.3.5. Thus, the mean number of broad, blunt protrusions is not as reliable as the mean number of filopodia and is therefore not discussed further here.

On smooth substrates, the whole population was analyzed together, since there is no means except for the number of filopodia to distinguish between possible groups of platelets because the average morphology during the time lapse series is similar for all platelets (see figure 6.7 in the previous chapter). However, occasionally remaining very small filopodia can be seen for platelets having spread on smooth substrates (see section 7.2 and figure 7.7 for further discussion). It is reasonable to assume that smaller differences in the average morphology during the time lapse series on smooth substrates between the two possible populations result from the lack of disturbances on smooth substrates, so that both ways of spreading (including filopodia versus mainly using lamellipodia) are equally effective.

The results suggest that the situation is different on structured substrates. In figure 7.3, possible differences between the two different ways of spreading on structured substrates are shown. If the platelet uses filopodia (figure 7.3 a)), these filopodia (drawn in gray) grow, *e.g.*, on the interspaces. To cover the hole, cell material has to be dragged forward between the two filopodia (drawn in red). Complete coverage of the hole may be especially hard to accomplish this way in the second slow phase of spreading[i], so that the part drawn in red is not tightly connected to the substrate on one side and thus instable (see also figure 6.10). If the platelet spreads mainly via lamellipodia, the situation is different (see figure 7.3 b)). The platelet can establish more connections to the substrate from the beginning on, as it spreads in a broader way. Broad spreading has the potential to facilitate spreading over the holes, and thus lead to complete coverage of the hole.

Furthermore, it was suggested by Kita *et al.* [52] (see also section 2.6) that filopodia have sensory tasks while platelets spread on micropatterned substrates. Thus, it can be assumed that filopodia-forming platelets sense the distribution of binding sites on the substrate and adapt their spreading behavior accordingly. The role of filopodia in spreading on structured substrates is further discussed in section 7.1.

On smooth substrates, it can be assumed that the first way of spreading (with contribution of filopodia) is easier to accomplish than on structured substrates, since connections to the substrate can be established everywhere. However, occasionally remaining tiny filopodia ends can be observed for spread platelets on smooth substrates hinting at a similar mechanism of spreading as described in figure 7.3 a). As the morphologies during the time lapse series on smooth substrates

[i] The two phases of spreading are discussed in the previous chapter 6.

Table 7.1.: Table summarizing the mean numbers and standard deviations of the number of filopodia on different substrates.
The magnitudes of the quantities in question are depicted with symbols ranging from +++ to +. The symbols serve only to visualize the relationships of the magnitudes on the different substrates and do not show the absolute values.

	$\text{structured}_{\text{adapted}}$	$\text{structured}_{\text{unadapted}}$	$\text{structured}_{\text{all}}$	smooth
mean number of filopodia	+++	+	++	++
standard deviation of filopodia	+++	+	+++	++

are not very different, there is no reliable way of separating the sub-populations of platelets on smooth substrates[ii] as described above. The lack of a possibility to distinguish between sub-populations on smooth substrates also explains why the mean number of filopodia is higher for platelets on smooth substrates than for unadapted platelets on structured substrates (see figure 7.2). Thus, the results suggest that the structured substrates provide a means to distinguish between the different ways of spreading. Although the number of filopodia increases rapidly in the beginning as can be seen in figure 7.2, and it is thus hypothesized that the potential to form filopodia is platelet inherent and not caused by the substrate, it is still possible that there are very fast adaptation mechanisms of the platelets that lead to more filopodia formation. Very fast adaptation mechanisms are probably difficult to detect in the experiments performed here, as the cell outline is usually not perfectly visible in the first images of cell spreading. However, since platelets with different filopodia forming capacities can be found as well on smooth substrates, it is reasonable to suggest that inherent capacities of the platelets or signals

[ii] except for the number of filopodia itself

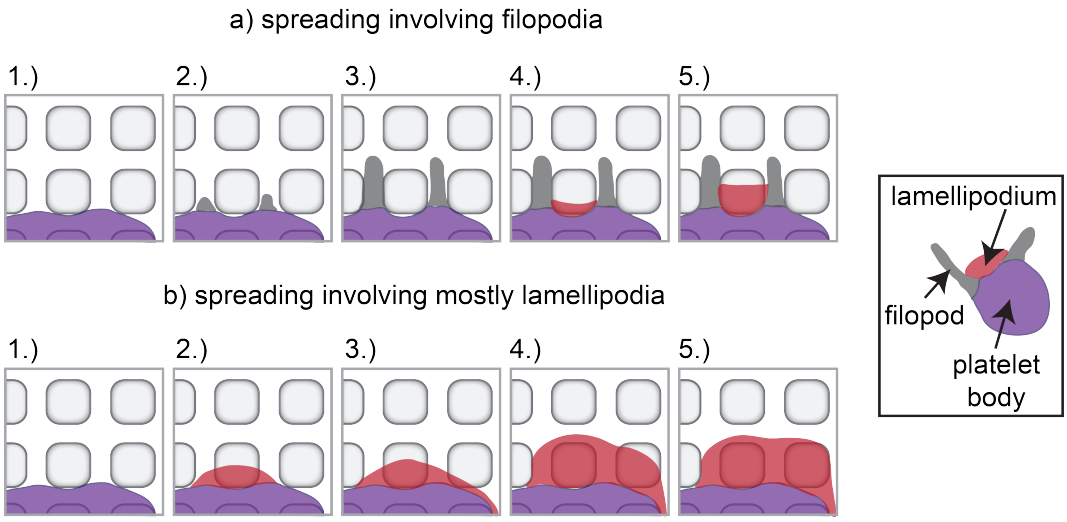

Figure 7.3.: Sketch showing possible spreading strategies over holes involving filopodia (a)) as well as spreading achieved mainly via lamellipodia (b)). As can be seen in the sketch on the right filopodia are shown in gray, the platelet body in purple and lamellipodia in red.
a) Filopodia emerge and spread, *e.g.*, on the interspaces (1. and 2.). These filopodia grow (3.) and a lamellipodium starts to grow between the filopodia (4.). The lamellipodium grows but cannot cover the hole completely and thus remains unstable (5.).
b) Spreading is achieved mostly by an outwards growing lamellipodium (1.-5.). Finally, the lamellipodium has covered both holes and is stably attached to the interspaces (5.).

the platelets sensed in solution before attaching to the substrate cause the differences in behavior. Taking all results into account, the degree of filopodia formation seems to depend more on the specific platelet itself than on the underlying substrate.

If the number of filopodia is different for the three cases, is the behavior of those filopodia also different? To answer this question, the groups of endpoints as shown in figure 7.1 were analyzed and their extension was described in radial and angular direction. Plots showing examples of this extension can be found in figure 7.4. The plots show the lines in radial direction and angular direction going through the mean positions of the groups of endpoints in magenta and cyan, respectively. The endpoints that were projected onto the lines are shown in gray for the radial lines and in black for the angular lines. In these examples, a platelet lying on a smooth substrate (I.) and an adapted platelet (III.) on a structured substrate show several groups of endpoints for filopodia that are extended in radial direction (see figure 7.4 a)). The other platelet on a smooth substrate (II.) and the unadapted platelet (IV.) on a structured substrate show filopodia whose paths are not as extended as in the other two plots. As comparison, also the extensions of endpoints of broad, blunt protrusions are shown in figure 7.4 b) and these appear to be more extended in angular direction than the endpoint distributions of filopodia.

The extension of the groups of endpoints of filopodia was analyzed more systematically for all platelets and is shown in histograms in figure 7.5. Again, since the broad, blunt protrusions are more difficult to detect than filopodia and thus not as reliable, similar data for broad, blunt protrusions can be found in figure C.4 and table C.2 in the appendix (chapter C) but are not discussed here.

For adapted platelets on structured substrates (figure 7.5 a), middle) the maximal distance of projected points in radial direction is shifted towards higher values indicating more elongated filopodia paths. The larger values of the maximal distance indicate a more pronounced spreading along the interspaces between the holes and thus support the suggestion (chapter 6) that the final spread area is held constant by spreading further over the interspaces when spreading over the holes is diminished. Platelets on smooth substrates (upper) and unadapted platelets (lower) on structured substrates show only slight differences with the former showing minimal higher values.

The values for maximal distances of filopodia endpoints projected onto a line in angular direction (see figure 7.5 b)) are overall smaller than the values found for

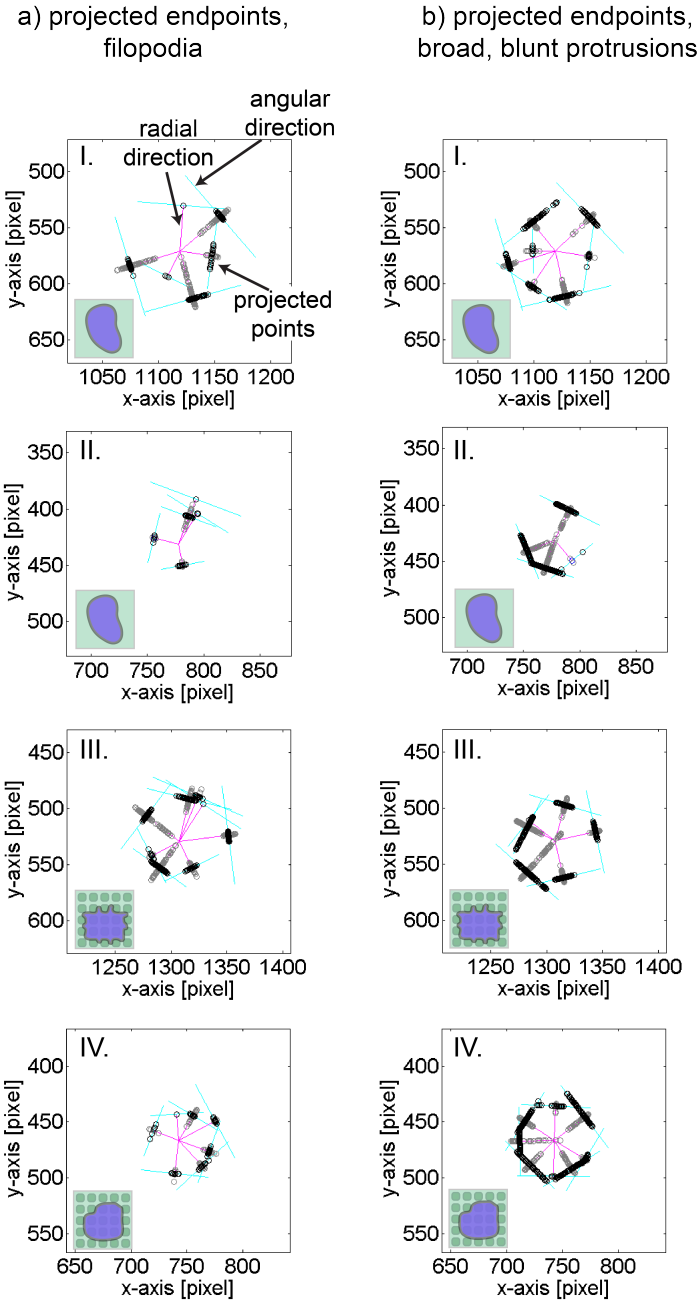

Figure 7.4.: Plots showing the endpoints projected onto lines in radial direction (magenta lines, gray points) and onto angular lines (cyan lines, black points) on smooth substrates (I., II.) and structured substrates (III.: adapted, IV.: unadapted) for filopodia (a)) and broad, blunt protrusions (b)). The platelets shown here are the same that have been shown in figure 7.1 and each plot shows the projected points for an individual platelet. 1 pixel corresponds to about 108 nm here.
a) The upper platelet on the smooth substrate and the adapted platelet on the structured substrate (I. and III.) show several quite extended (in radial direction) groups of endpoints as can be seen by the distance of the projected endpoints. The second platelet on the smooth substrate and the unadapted platelet (II. and IV.) show filopodia that are not as extended as in the other two plots.
b) The groups of projected endpoints of broad, blunt protrusions are more extended in angular direction than in the case of filopodia in a).

the radial direction. These differences indicate that the filopodia paths are more elongated in radial direction than in angular direction, suggesting that filopodia help in outward spreading by moving along the radial direction. Again, the values for platelets on smooth substrates (upper) and for unadapted platelets (lower) on

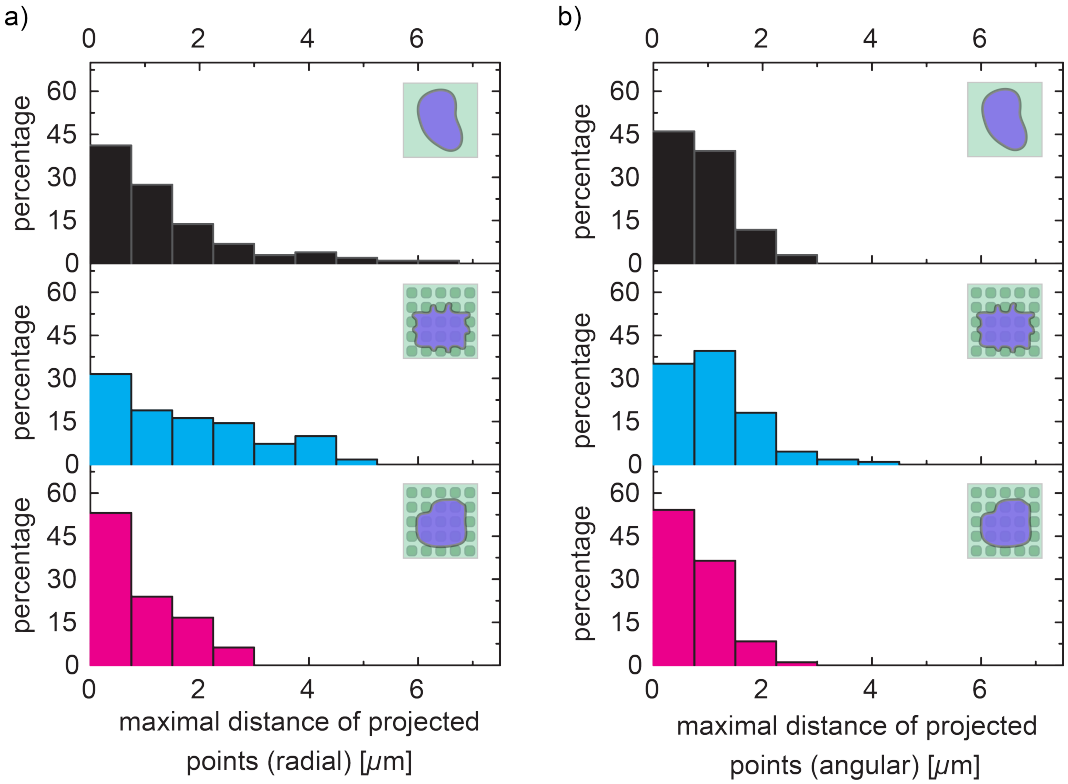

Figure 7.5.: Histograms of the maximal distance between projected endpoints of filopodia in radial (a)) and angular direction (b)) on smooth substrates (upper) and structured substrates (middle: adapted, lower: unadapted).
a) Adapted platelets on structured substrates show larger values than unadapted platelets on structured substrates and platelets on smooth substrates. The larger values for adapted platelets on structured substrates point to more elongated paths of filopodia.
b) The values on smooth substrates are quite similar to those of unadapted platelets on structured substrates with the former showing only minimal larger values. The adapted platelets on structured substrates show slightly higher values for the maximal distance of projected points in angular direction than the two other groups. The values for the maximal distance of projected points in angular direction are smaller than those in radial direction. These differences point to elongated filopodia paths in radial direction.

structured substrates are fairly similar with the former being only slightly higher. For adapted platelets (middle) on structured substrates the values are slightly shifted towards higher values. The difference between adapted platelets on structured, unadapted platelets on structured and platelets on smooth substrates can result from the regular arrays of holes in the structured substrates. Once a filopod is not confined by neighboring holes any more, it can move more or less undisturbed in horizontal and vertical direction on the interspaces. However, the

confinements caused by structured substrates do not seem to influence the mean angle of the filopodia paths as can be seen in figure 7.6. The lack of mean angle dependence on the topography of the substrate can be attributed to the fact that the platelets do not all start to spread at similar positions of the substrate (*e.g.* each at the center of a hole). Thus, the position of the filopodium determines the angles at which it finds the interspaces and the angles cannot be generalized for all platelets. A similar plot for broad, blunt protrusions can be found in the appendix (chapter C, figure C.5) but the results are not detailed here as has been discussed for other plots for the behavior of broad, blunt protrusions above. A comparison between the extensions of the groups of filopodia as well as the directions of filopodia for the different cases (smooth, structured (adapted) and structured (unadapted)) is shown in table 7.2.

The elongated filopodia paths fit to the elevated relative perimeter (see figure 5.5)

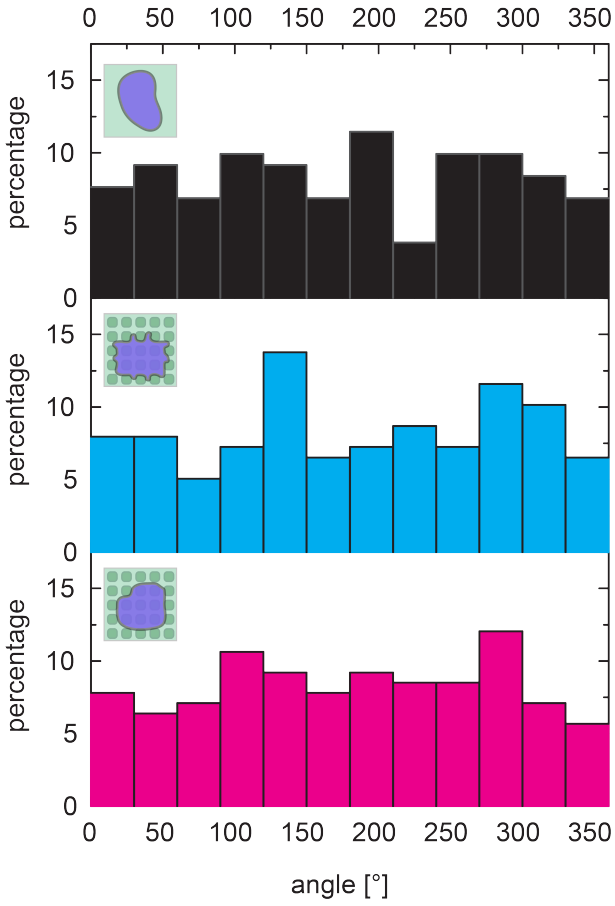

Figure 7.6.: Histograms of mean angle of groups of filopodia endpoints for platelets on smooth (upper, black) and platelets on structured substrates (middle, light blue: adapted; lower, magenta: unadapted).
The histograms show no preferred directions in any of the three conditions. This lack of dependence on the topography of substrates can be attributed to the geometry of the underlying substrate as mostly the position of the filopod determines in which direction it finds interspaces.

Table 7.2.: Table summarizing the maximal extensions in radial and in angular direction as well as the mean angle for groups of filopodia endpoints on different substrates.
The magnitudes of the quantities in question are depicted with symbols ranging from +++ to +. The symbols serve only to visualize the relationships of the magnitudes on the different substrates and do not show the absolute values.

	$\text{structured}_{\text{adapted}}$	$\text{structured}_{\text{unadapted}}$	smooth
maximal radial projection	+++	+ to ++	++
maximal angular projection	+++, smaller than in radial direction	++, smaller than in radial direction	++, smaller than in radial direction
angle	no preferred direction	no preferred direction	no preferred direction

and also to the higher number of large events in protrusions on structured substrates (see figure 6.9) as compared to smooth substrates. Furthermore, differences in spreading between different directions for platelets on smooth substrates have already been shown in figure 6.6 in the former chapter. These differences even out over time and thus a similar final morphology is obtained for all platelets on smooth substrates. This observation fits nicely to the ideas presented here how platelets spread with contribution of filopodia on smooth substrates.

7.1 Discussion of Results with Regard to Existing Literature

If the following reference [2] is given, the termini filopodia and lamellipodia are used instead of the termini pseudopodia and hyalomer as given by the authors. For further notes on this usage of termini see section 2.3.2.
In this chapter, the existence of two groups of platelets differing in filopodia formation is proposed. Different spreading behaviors either with or without contribution of filopodia have also been observed by Dubin-Thaler *et al.* [31] and Giannone *et al.* [42] for fibroblasts. The different cells are part of the same cell line but growth conditions (amount of serum) change the percentages of the different cells [31]. Allen *et al.* [2] also discussed differences in filopodia formation for platelets spreading on siliconized glass and stated that platelets can also spread without any filopodia. PAR4 is a thrombin receptor [11]. Filopodia formation in

murine platelets has been shown to be influenced by activation of this thrombin receptor [56]. Both, the number of filopodia as well as the duration of filopodia formation are influenced by the activation PAR4 [56]. Without activation of the receptor more filopodia are formed and formation occurs over a longer period of time [56]. Thus, the two groups of platelets described in this chapter may arise from different levels of thrombin stimulation. This interpretation would also explain the longer presence of filopodia for platelets that show extensive filopodia formation (see figure 7.2 b)), as in the absence of activation of PAR4 platelets show more filopodia as well as an increased time in which new filopodia are formed [56]. The timescales on which filopodia were present as can be seen in figure 7.2 fit well to those that have been presented by Lee *et al.* [56]. With activation of a thrombin receptor, filopodia are present for about 4 minutes [56] similar to what can be seen for unadapted platelets in figure 7.2 c). When comparing filopodia formation for adapted platelets shown in this chapter (see figure 7.2 b)) to platelets without an activated thrombin receptor that reach their maximal number of filopodia within 4 minutes as has been shown by Lee *et al.* [56], it is obvious that the plateau in filopodia number is reached much faster for adapted platelets. However, in both cases the number of filopodia is kept more or less constant after the plateau is reached.

If differences in thrombin stimulation are indeed the cause for the differences between adapted and unadapted platelets, one can conclude that stimulation with thrombin helps platelets to overcome irregularities in the underlying substrates and that thrombin plays an important role in spreading on structured substrates.

The differences in mean numbers of filopodia presented in this chapter to those in the study presented in [56] can arise either from different experimental conditions, *e.g.* different substrate stiffnesses or from the use of thrombin instead of an activator of PAR4 as used by Lee *et al.* [56]. Additionally, the imaging techniques differ (reflection interference contrast microscopy in contrast to fluorescence microscopy) so that differences in accuracy of filopodia detection can also cause differences in mean numbers. As thrombin was added via a pipette for the experiments presented in this thesis, and as the concentration of thrombin thus depended on diffusion and convection, it is plausible that platelets could have experienced different thrombin levels in our studies. Also, secretion of various factors by other platelets [9, 38, 79] in the vicinity may slightly alter local thrombin concentration in our experiments. However, differences in thrombin stimulation may not only be due to different thrombin concentrations, but can also arise from a natural vari-

ation of numbers of thrombin receptors on individual platelets. Differences in receptor numbers then could lead to differences in intracellular signaling.
Platelets use filopodia to attract other platelets to the wounded site [44] so that there are probably different roles *in vivo* for platelets showing different degrees of filopodia formation.
Platelets can also display simultaneously different types of spreading (with filopodia/without filopodia) at different positions of the platelet [2]. Thus, adaptation can also be a local phenomenon.
In general, filopodia formation in cells can be regulated by different proteins, *e.g.* capping protein and Ena/VASP [63] or Ena and Dia [5] (see section 2.2 for details). Platelets can synthesize proteins during *ex vivo* storage [89] and single platelets possibly have different levels of proteins.
Taking all these observations into account, it seems plausible that there are differences in the capability of platelets to form filopodia.
Filopodia are thought to search for binding sites and trigger movement of platelets onto adhesive stripes when coming in contact with them on micropatterned substrates [52]. Similarly, platelets which are situated on top of other platelets only spread on the substrate when their filopodia come into contact with the siliconized glass surface [2]. Thus, platelets that form filopodia can in all likelihood sense the underlying substrate and recognize the missing binding sites (missing in the plane in which the binding sites of the interspaces lie) at the position of the holes. Additionally, the filopodia probably sense the 3D structure of our substrates, since filopodia are speculated to be able to recognize curvature [27]. In figure B.1 in the appendix (chapter B) a membrane-stained platelet can be seen on a structured substrate. This platelet shows two filopodia whose endpoints are situated near the holes. Where exactly the filopodia end is hard to say because the signal-to-noise ratio is low[iii]. However, the close relationship of filopodia endpoints and hole edges still indicates a sensing of the holes by the filopodia. Taken all this into account, it can be assumed that adaptation to the substrate is an active process triggered by the filopodia that sense the underlying substrate. However, the adaptation to the substrate can also have a mechanical component as is suggested in figure 7.3. The adhesion sites on the substrate may be altered by the presence of filopodia as has been discussed by Schäfer *et al.* [85] for keratinocytes and thus

[iii] The micrographs were taken after the time lapse series had ceased and thus the platelet have most likely already taken up some of the dye as described in [64] which would explain why the signal-to-noise ratio is worse than in the time lapse series.

alter the behavior of platelets.
The angle distribution in figure 7.6 shows no directional preferences for filopodia formation which fits to the observation Lee *et al.* [56] made for murine platelets on smooth fibrinogen covered glass. Reasons for the lack of directionality of protrusion formation on structured substrates have been already discussed above.

7.2 Discussion of Analysis and Experimental Methods

As already mentioned in the former section 7.1, the observation that filopodia numbers on structured substrates for adapted platelets do not or only slightly decrease over time can also be caused by the analysis, since protrusions over the interspaces can also be detected as filopodia due to their shape. Figure 7.7, however, shows that there can be remaining filopodia on structured as well as on smooth substrates after the time-lapse series has ceased. The remaining filopodia on a smooth substrate after spreading suggest that this cell has spread by contribution of filopodia and the interspaces between filopodia have been filled up by lamellipodia during spreading.

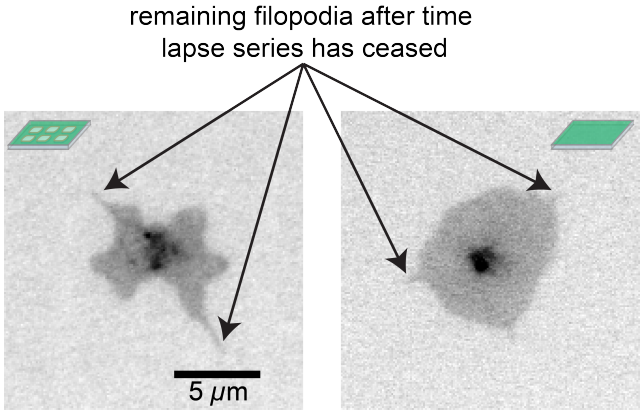

Figure 7.7.: Inverted fluorescence images of a platelet on a structured substrate and a platelet on a smooth substrate that still show filopodia after the time lapse series has ceased. Except for the illumination power of 41.86% imaging was performed as described in section 3.6. The micrograph for the platelet on the structured substrate has been rotated (bilinear interpolation) in ImageJ [87] to align the underlying rows of holes with the image borders.

As can be seen in figures 7.2 and C.1 the standard deviations of the number of filopodia for adapted platelets and all platelets on structured substrates taken together are higher than for unadapted platelets on structured substrates and for platelets on smooth substrates. These high standard deviations can arise from filopodia that were not detected in some images but were detected in others. An example of a filopodium that has not been detected can be seen in figure 4.12.

However, the standard deviations can also be a result of a high variability between different platelets and/or diverse time points for the formation of filopodia. Furthermore, some filopodia have very likely not been detected from the fluorescence micrographs as they appear faint due to their tiny width. Especially in the beginning of spreading, small filopodia can be hard to detect, since the platelet has not yet flattened over the substrate and thus it is possible that filopodia are out of focus. However, single missing endpoints do not have a large effect on the results presented here. For the mean number of endpoints per time all analysed cells were averaged so that single missing endpoints do not result in a huge error. For the analysis of the extension of groups of endpoints, missing endpoints are only of importance if their position is extremely different from the other endpoints. For the angles, under which groups occur, the positions of all endpoints belonging to one group are averaged so that single missing endpoints do not contribute strongly if enough endpoints belong to the group. For the extension of endpoints only those groups were analyzed that have more than one endpoint since for the computation of distances at least two endpoints are needed. It is particularly important to keep this in mind for the cases in which protrusions vanish fast and thus some groups only consists of one endpoint. Groups of endpoints consisting only of one endpoint likely especially occur for unadapted platelets on structured substrates for which a short live time of filopodia can be observed as shown in figure 7.2 c). Thus, some of the filopodia were not considered in the calculation of maximal distances between endpoints.

In order to detect the filopodia and the broad, blunt protrusions constraints were applied that are adaptable to the specific situation. These sets of constraints showed the best detection of protrusions. However, other conditions can also be employed to detect protrusions. A further explanation of why certain constraints have been employed is given in section 4.3.5.

An alternative way to analyze filopodia was proposed by Tsygankov *et al.* [97]. The software they developed has the advantage that it can also detect curved filopodia, since it detects the filopodia by investigating the length of a path inside of the cell [97]. Furthermore, tracing of filopodia lying close together is facilitated by using the whole path inside the filopodium as reference for tracing [97]. To be able to sort the protrusions in the analysis applied to our data (as described in section 4.3.5), constraints were posed that defined the maximal distance two endpoints were allowed to have to belong to one filopodium. Curved filopodia were seldomly observed in the data presented in this chapter so that failing to detect these

filopodia does not result in big errors. However, very short filopodia are not easily detected by the analysis method used for the results in this chapter and thus can be missing. Furthermore, the shape of the filopodia can hinder detection. If filopodia had a blunt, broad tip similar to that of the undetected filopodium in the lower right corner in figure 4.12, they were not detected due to the posed constraints (see figure 4.11 for the detailed constraints). However, these constraints were needed to exclude other types of protrusions and only detect filopodia. Lamellipodia are not as morphologically distinct in fluorescence images of a stained cell membrane as filopodia which show as protrusions from the cell that have a limited width. Thus, other forms of protrusions like lamellipodia are not as well detectable as filopodia.

In tracing of filopodia by the analysis applied here (see section 4.3.5), errors can arise due to the fact that the endpoints can only be compared to the endpoints in the former images. Furthermore, the fact that an endpoint was always assigned to the nearest group of endpoints can also introduce some errors if groups of endpoints overlap. Thus, merging of groups after all endpoints were assigned was introduced with the condition that groups can only be merged if this would not lead to more than one endpoint being assigned to the same group at one time point. Taken all into account, the analysis applied here has some drawbacks for specific situations like very close filopodia or curved filopodia but has a sufficient accuracy to analyze the data presented here.

8

Summary, Conclusions and Outlook

Spread platelets lying on smooth substrates display an undisturbed cell outline mostly without numerous protrusions. If the substrate underneath, however, has a microtopography, platelets adapt to it by avoiding the holes in the underlying substrate at their periphery. Two types of structured substrates were employed in our studies, a selectively coated substrate on which the insides of the holes are blocked and fibrinogen coating is confined to the interspaces and a completely coated substrate on which both holes and interspaces are coated with fibrinogen. By comparing the behavior of platelets on the different substrates (smooth, structured with complete coating, structured with selective coating), one can distinguish between the effects of topography (biophysical cues) and the effects of binding site distribution (biochemical cues). Comparison reveals that adaptation is stronger on selectively coated substrates compared to completely coated substrates. Taking the distribution of the binding sites into account, it can be assumed that platelets do not find as many binding sites at the hole edges on selectively coated substrates and thus cannot span the holes at their periphery as easily. As has been suggested by Britland *et al.* [12], higher adaptation can also be explained by the non-conflicting cues that are presented to the cells by micropattern and microtopography, *i.e.* both keep the cell from entering the holes at its periphery and

thus, when acting together, very likely amplify the effect. Bending into the holes at the cell periphery is restricted by the topography used here (hole sizes: about $1.0 - 2.8\,\mu$m, about 500 nm in depth) and this restriction can be assumed to arise from energy minimization of the system. Bending into the holes very likely costs more energy than bending around the holes which enforces a slight elongation of the cell outline. Thus, bending around the holes is favored to reduce the energy of the system. However, although the platelets conform to the underlying substrate, the final cell areas are comparable to those of platelets on smooth substrates. The constant final area is achieved through enhanced spreading at other positions of the substrate, *e.g.* in between the holes, leading to a prolonged cell outline. Thus, the disturbances provided by the holes during spreading decouple the optimization of spread area from the optimization of cell outline.

The finding that cell area is similar on smooth and structured substrates is even more striking when observing the dynamics of spreading on completely coated, structured substrates. Platelets on structured substrates even show retractions at their periphery over the underlying holes after the first, fast spreading phase. However, they are still able to compensate for the area losses by enhanced spreading at other positions on the substrate and thus show higher dynamics compared to platelets on smooth substrates. Retraction over the holes is most likely caused by the inability of the platelet to reach the binding sites inside of the hole. Therefore, binding between platelet and substrate is likely not possible at the position of the hole. Thus, if forces are exerted by myosin on the lamellipodia after the first, fast spreading phase, the platelets are prone to retract over the holes.

However, not all platelets react in the same way to the structured substrates. Analysis of local spreading behavior reveals two types of platelets, one group adapts to completely coated substrates and one does not adapt as strongly or not at all. Differences in spreading between the platelets can be seen early on in spreading and seem to occur on smooth substrates as well, although the differences are much less distinct and lead to similar final results in spreading. Differences in early spreading can be assumed to be caused by filopodia, as several platelets show a high variance between spreading in different directions early on and the development of filopodia would result in such behavior.

Following the endpoints of filopodia over time reveals that adapted platelets on structured substrates indeed show more filopodia and the paths are more elongated compared to the behavior found for unadapted platelets on structured substrates. Additionally, filopodia persist most likely longer for adapted platelets on

structured substrates. On smooth substrates, it seems that two types of platelets with different degrees of filopodia formation exist as well but, as mentioned above, the final result in spreading is very similar for the two types on smooth substrates. Since the number and behavior of filopodia seems to depend more on the platelet itself than on the underlying substrate, the degree of filopodia formation appears to be an inherent characteristic of the single platelet. PAR4 is a thrombin receptor [11]. Lee *et al.* [56] showed that activation of this thrombin receptor influences the degree and the duration of filopodia formation in murine platelets. As the differences in duration and numbers of filopodia observed here for adapted and unadapted platelets fit nicely to the differences caused by activation of PAR4 which have been shown in [56], it is reasonable to assume that unadapted platelets may have experienced more thrombin stimulation than adapted platelets. Differences in thrombin stimulation may arise through both differences in thrombin distribution in the solution or different numbers of thrombin receptors on individual platelets. Taking all into account, activation by thrombin may help the platelets to cover irregular regions in a wound or an implant. However, differences in the ability to form filopodia can also be caused by different levels of proteins that influence actin filament assembly as has been shown for other cells [5, 63].

Adaptation to the substrate seems to be connected to the ability of forming filopodia and may either be caused by filopodia sensing the substrate or it can have a mechanical component. Sensing of the substrate by filopodia has also been proposed by Kita *et al.* [52] for platelets on micropatterned substrates. For the mechanical component spreading including filopodia may lead to adaptation to the substrate, since in order to cover a hole cell material has to be dragged over the holes after filopodia have formed, *e.g.* over the interspaces. Spreading by lamellipodia thus seems advantageous when spreading over a hole, since more binding sites can be established early on. Therefore, the cell is very likely more stable and able to cover a hole even if forces are exerted on the lamellipodium by myosin. These two possible interpretations would also explain why platelets spreading on smooth substrates show nearly no differences in final morphology for the two different spreading modes (filopodial/lamellipodial). On smooth substrates, lamellipodia that spread in between filopodia can attach to the substrate at any position. It follows that the platelet is stable, irrespective of the involvement of filopodia in the initial spreading. Thus, apart from having found a possible reason why two groups of platelets with different degrees of adaptation to the substrate exist, we found a means to distinguish between platelets that spread

with contribution of filopodia and those that spread mostly without filopodia by means of studying spreading dynamics. These findings not only illustrate details of spreading also applicable to other cell types, but furthermore likely present a means to influence the behavior of platelets on structured substrates.
Since blood directly comes into contact with implants placed into the bone [28, 71], platelets can influence the later events of implant incorporation [71]. Hence, the ability to influence platelet behavior on structured substrates may in turn provide the possibility to regulate how an implant is incorporated into the body. The adaptations on structured substrates do not include the final cell area and thus indicate a fixed final height platelets adapt on substrates of the same material composition. This fixed height could help the platelet to obtain a defined state of its cytoskeleton and may be important for its physiological function.
To conclude, we have shown that platelets conform to structured substrates with enhanced spreading on interspaces and decreased spreading and/or retractions over the holes. The degree of adaptation is determined by the available biochemical cues, *e.g.* coating, while the topography hinders the platelet to enter holes at their periphery. Even when adapted, platelets keep their final area constant which seems to be achieved by a more dynamic spreading process. Finally, we suggest that differences in adaptation on completely coated, structured substrate arise due to different ways of spreading (with contribution of filopodia or mainly via lamellipodia) that may have their origin in differences of stimulation with thrombin. Not only would this dependency on thrombin provide a means to regulate platelet behavior. It would also implicate that structured implant surfaces should be investigated under addition of a range of physiologically relevant thrombin levels, as differences in thrombin concentration may alter platelet behavior on structured substrates. However, also different levels of proteins that influence actin filament assembly (like Ena/VASP and capping proteins [63] or Ena (Enabled) and Dia (Diaphanous, a formin) [5]) in cells may contribute to differences in filopodia formation.
In order to proof our hypothesis that the activation of thrombin receptors leads to differences in adaptation, possible next experiments can be performed using photo-activatable thrombin [45, 70, 98]. Since this thrombin can be activated by incidence of light [45, 70, 98], it can be released in a controlled way into a microfluidic device in direct vicinity of a platelet, similarly as caged cAMP is used to study *Dictyostelium discoideum* during chemotaxis [104]. When placing structured substrates, as used in the studies presented in this thesis, into a microfluidic de-

vice and letting platelets settle on these substrates before activating the thrombin, one has a means to directly observe the reaction of platelets to thrombin and the alterations in the spreading process on structured substrates. If thrombin is simply added to the platelet solution even in a microfluidic device, intial reactions to thrombin may already take place before platelets have settled onto the substrate. The time during which the platelets are still suspended may regulate the amount of thrombin the platelets experience before spreading. Thus, photo-activatable thrombin provides the opportunity to control both the amount of thrombin and the time point at which the platelets get into contact with thrombin.

Additionally, it will be helpful to stain the platelets with SiR-actin [62] which would allow for direct imaging of actin during spreading. Furthermore, the usage of this dye would enable a longer imaging than using CellMask™ dyes which are slowly taken up by the cells [64]. Signal-to-noise ratios may also be improved by SiR actin compared to CellMask™, since fluorescence of SiR actin has been shown to be upregulated by a factor of more than 100 when it binds to actin *in vitro* [62]. A better signal-to-noise ratio would facilitate imaging of filopodia. Furthermore, imaging actin directly during spreading could be used to verify the model we proposed for platelet spreading on structured substrates.

Moreover, one might test the influence of flow on platelet reaction to structured substrates in order to mimic the physiological situation more closely. In the context of a more physiological situation, also softer substrates could be employed to test whether platelets react differently to holes in softer substrates than to holes in stiffer substrates. If substrates are sufficiently soft, platelets may even be able to ”close“ smaller holes by pulling on the edges of the hole. Finally, platelet reaction to nanostructures should be tested as well in detail as implants may not only have a microstructure but also exhibit a nanostructure. Furthermore, the extracellular matrix itself inherently provides a nanostructure [49].

Bibliography

[1] AHF analysentechnik AG. 628/40 BrightLine HC, 470/40 ET Bandpass, 537/694 Dualband Sperrfilter H, 497/655 H Dualband Strahlenteiler. URL `http://www.ahf.de/spectren/F39-628.txt,http://www.ahf.de/spectren/F57-200.txt,http://www.ahf.de/spectren/F58-200.txt,http://www.ahf.de/spectren/F49-470.txt`. last checked: September 26, 2014. (cited on page 41)

[2] R. D. Allen, L. R. Zacharski, S. T. Widirstky, R. Rosenstein, L. M. Zaitlin, and D. R. Burgess. Transformation and motility of human platelets: details of the shape change and release reaction observed by optical and electron microscopy. *The Journal of Cell Biology*, 83(1):126–142, 1979. doi: 10.1083/jcb.83.1.126. (cited on page 14, 15, 16, 74, 82, 101, 102, 103, 122, 124, and 165)

[3] C. C. Berry, G. Campbell, A. Spadiccino, M. Robertson, and A.S.G. Curtis. The influence of microscale topography on fibroblast attachment and motility. *Biomaterials*, 25(26):5781–5788, 2004. doi: 10.1016/j.biomaterials.2004.01.029. (cited on page 19)

[4] C. J. Bettinger, R. Langer, and J. T. Borenstein. Engineering substrate topography at the micro- and nanoscale to control cell function. *Angewandte Chemie (International ed. in English)*, 48(30):5406–5415, 2009. doi: 10.1002/anie.200805179. (cited on page 1 and 19)

[5] C. G. Bilancia, J. D. Winkelman, D. Tsygankov, S. H. Nowotarski, J. A. Sees, K. Comber, I. Evans, V. Lakhani, W. Wood, T. C. Elston, D. R. Kovar, and M. Peifer. Enabled negatively regulates diaphanous-driven actin dynamics in vitro and in vivo. *Developmental Cell*, 28(4):394–408, 2014. doi: 10.1016/j.devcel.2014.01.015. (cited on page 12, 124, 131, and 132)

[6] I. B. Bischofs, F. Klein, D. Lehnert, M. Bastmeyer, and U. S. Schwarz. Filamentous network mechanics and active contractility determine cell and tissue shape. *Biophysical Journal*, 95(7):3488–3496, 2008. doi: 10.1529/biophysj.108.134296. (cited on page 17)

[7] L. Blanchoin, R. Boujemaa-Paterski, C. Sykes, and J. Plastino. Actin dynamics, architecture, and mechanics in cell motility. *Physiological Reviews*, 94(1):235–263, 2014. doi: 10.1152/physrev.00018.2013. (cited on page 18)

[8] T. Bornschlögl. How filopodia pull: what we know about the mechanics and dynamics of filopodia. *Cytoskeleton*, 70(10):590–603, 2013. doi: 10.1002/cm.21130. (cited on page 11)

[9] B. A. Bouchard, J. R. Silveira, and P. B. Tracy. Chapter 21 - Interactions between platelets and the coagulation system. In A. D. Michelson, editor, *Platelets*. Elsevier/Academic Press, London, 3rd edition, 2013. (cited on page 5, 6, and 123)

[10] D. Brambley, B. Martin, and P. D. Prewett. Microlithography: An overview. *Advanced Materials for Optics and Electronics*, 4(2):55–74, 1994. doi: 10.1002/amo.860040203. (cited on page 1, 16, and 23)

[11] L. F. Brass. Thrombin and platelet activation. *CHEST Journal*, 124(3_suppl):18S–25S, 2003. doi: 10.1378/chest.124.3_suppl.18S. (cited on page 6, 15, 21, 122, and 131)

[12] S. Britland, H. Morgan, B. Wojiak-Stodart, M. Riehle, A. Curtis, and C. Wilkinson. Synergistic and hierarchical adhesive and topographic guidance of BHK cells. *Experimental Cell Research*, 228(2):313–325, 1996. doi: 10.1006/excr.1996.0331. (cited on page 18, 83, and 129)

[13] S.D.J. Calaminus, J. M. Auger, O.J.T. McCarty, M.J.O. Wakelam, L. M. Machesky, and S. P. Watson. MyosinIIa contractility is required for maintenance of platelet structure during spreading on collagen and contributes to thrombus stability. *Journal of Thrombosis and Haemostasis*, 5(10):2136–2145, 2007. doi: 10.1111/j.1538-7836.2007.02696.x. (cited on page 10 and 103)

[14] L. A. Cameron, P. A. Giardini, F. S. Soo, and J. A. Theriot. Secrets of actin-based motility revealed by a bacterial pathogen. *Nature Reviews. Molecular Cell Biology*, 1(2):110–119, 2000. doi: 10.1038/35040061. (cited on page 13)

[15] J. Canny. A computational approach to edge detection. *IEEE Transactions on Pattern Analysis and Machine Intelligence*, 8(6):679–698, 1986. doi: 10.1109/TPAMI.1986.4767851. (cited on page 43)

[16] E.C.J Carriveau, H. Kaur, and B. Mutus. Method and apparatus to conduct kinetic analysis of platelet function in whole blood samples: United States Patent Application Publication: US 2011/0086363 A1, 2011. (cited on page 87)

[17] R. C. Carroll, R. G. Butler, P. A. Morris, and J. M. Gerrard. Separable assembly of platelet pseudopodal and contractile cytoskeletons. *Cell*, 30(2): 385–393, 1982. doi: 10.1016/0092-8674(82)90236-7. (cited on page 15)

[18] A. H. Charafeddine, E. J. Kim, D. M. Maynard, H. Yi, T. A. Weaver, M. Gunay-Aygun, M. Russell, W. A. Gahl, and A. D. Kirk. Platelet-derived CD154: ultrastructural localization and clinical correlation in organ transplantation. *American Journal of Transplantation : Official Journal of the American Society of Transplantation and the American Society of Transplant Surgeons*, 12 (11):3143–3151, 2012. doi: 10.1111/j.1600-6143.2012.04241.x. (cited on page 32)

[19] J. L. Charest, M. T. Eliason, A. J. García, and W. P. King. Combined microscale mechanical topography and chemical patterns on polymer cell culture substrates. *Biomaterials*, 27(11):2487–2494, 2006. doi: 10.1016/j.biomaterials.2005.11.022. (cited on page 18)

[20] H. Chen, W. Song, F. Zhou, Z. Wu, H. Huang, J. Zhang, Q. Lin, and B. Yang. The effect of surface microtopography of poly(dimethylsiloxane) on protein adsorption, platelet and cell adhesion. *Colloids and Surfaces. B: Biointerfaces*, 71(2):275–281, 2009. doi: 10.1016/j.colsurfb.2009.02.018. (cited on page 21 and 86)

[21] P. Clark, P. Connolly, A. S. Curtis, J. A. Dow, and C. D. Wilkinson. Topographical control of cell behaviour. I. Simple step cues. *Development*, 99(3): 439–448, 1987. (cited on page 19, 85, and 86)

[22] P. Clark, P. Connolly, A. S. Curtis, J. A. Dow, and C. D. Wilkinson. Topographical control of cell behaviour: II. Multiple grooved substrata. *Development*, 108(4):635–644, 1990. (cited on page 17)

[23] K. J. Clemetson. Platelets and primary haemostasis. *Thrombosis Research*, 129 (3):220–224, 2012. doi: 10.1016/j.thromres.2011.11.036. (cited on page 7)

[24] I. Cohen and A. de Vries. Platelet contractile regulation in an isometric system. *Nature*, 246(5427):36–37, 1973. doi: 10.1038/246036a0. (cited on page 10)

[25] L. E. Corum, C. D. Eichinger, T. W. Hsiao, and V. Hlady. Using microcontact printing of fibrinogen to control surface-induced platelet adhesion and activation. *Langmuir : the ACS Journal of Surfaces and Colloids*, 27(13):8316–8322, 2011. doi: 10.1021/la201064d. (cited on page 1, 20, 83, and 86)

[26] A.S.G. Curtis and C.D.W. Wilkinson. Reactions of cells to topography. *Journal of Biomaterials Science. Polymer Edition*, 9(12):1313–1329, 1998. doi: 10.1163/156856298X00415. (cited on page 1)

[27] M. J. Dalby, N. Gadegaard, M. O. Riehle, C.D.W. Wilkinson, and A.S.G. Curtis. Investigating filopodia sensing using arrays of defined nano-pits down to 35 nm diameter in size. *The International Journal of Biochemistry & Cell Biology*, 36(10):2005–2015, 2004. doi: 10.1016/j.biocel.2004.03.001. (cited on page 19 and 124)

[28] J. E. Davies. In vitro modeling of the bone/implant interface. *The Anatomical Record*, 245(2):426–445, 1996. doi: 10.1002/(SICI)1097-0185(199606)245:2<426::AID-AR21>3.0.CO;2-Q. (cited on page 21 and 132)

[29] P. Davydovskaya, M. Janko, F. Gaertner, Z. Ahmad, Ö. Simsek, S. Maßberg, and R. W. Stark. Blood platelet adhesion to printed von Willebrand factor. *Journal of Biomedical Materials Research. Part A*, 2(100A):335–341, 2012. doi: 10.1002/jbm.a.33275. (cited on page 20, 21, and 83)

[30] B. Diagouraga, A. Grichine, A. Fertin, J. Wang, S. Khochbin, and K. Sadoul. Motor-driven marginal band coiling promotes cell shape change during platelet activation. *The Journal of Cell Biology*, 204(2):177–185, 2014. doi: 10.1083/jcb.201306085. (cited on page 9 and 10)

[31] B. J. Dubin-Thaler, G. Giannone, H.-G. Döbereiner, and M. P. Sheetz. Nanometer analysis of cell spreading on matrix-coated surfaces reveals two distinct cell states and STEPs. *Biophysical Journal*, 86(3):1794–1806, 2004. doi: 10.1016/S0006-3495(04)74246-0. (cited on page 13, 103, and 122)

[32] G. A. Dunn and A. F. Brown. Alignment of fibroblasts on grooved surfaces described by a simple geometric transformation. *Journal of Cell Science*, 83:313–340, 1986. (cited on page 20 and 85)

[33] G. A. Dunn and J. P. Heath. A new hypothesis of contact guidance in tissue cells. *Experimental Cell Research*, 101(1):1–14, 1976. doi: 10.1016/0014-4827(76)90405-5. (cited on page 18, 81, 83, and 84)

[34] S. Eddins. Spatial transformations: Translation confusion: Matlab Central, Steve on Image Processing, 2006. URL `http://blogs.mathworks.com/steve/2006/07/07/spatial-transformations-translation-confusion/?s_tid=Blog_Steve_Category`. last checked: June 2014. (cited on page 50)

[35] S. Eddins. Visualizing regionprops ellipse measurements: Matlab Central, Steve on Image Processing, 2010. URL `http://blogs.mathworks.com/steve/2010/07/30/visualizing-regionprops-ellipse-measurements/`. last checked: July 2014. (cited on page 53)

[36] H. Falet, K. M. Hoffmeister, R. Neujahr, J. E. Italiano, T. P. Stossel, F. S. Southwick, and J. H. Hartwig. Importance of free actin filament barbed ends for Arp2/3 complex function in platelets and fibroblasts. *Proceedings of the National Academy of Sciences of the United States of America*, 99(26):16782–16787, 2002. doi: 10.1073/pnas.222652499. (cited on page 15)

[37] I. A. Feuerstein and J. I. Sheppard. States in adherent platelet morphology and the processing of adsorbed protein on biomaterials. *Biomaterials*, 14(2):137–147, 1993. doi: 10.1016/0142-9612(93)90228-T. (cited on page 16 and 87)

[38] R. Flaumenhaft. Chapter 18 - Platelet Secretion. In A. D. Michelson, editor, *Platelets*. Elsevier/Academic Press, London, 3rd edition, 2013. (cited on page 5, 86, and 123)

[39] R. G. Flemming, C. J. Murphy, G. A. Abrams, S. L. Goodman, and P. F. Nealey. Effects of synthetic micro- and nano-structured surfaces on cell behavior. *Biomaterials*, 20(6):573–588, 1999. doi: 10.1016/S0142-9612(98)00209-9. (cited on page 1)

[40] J. E. Fox, J. K. Boyles, C. C. Reynolds, and D. R. Phillips. Actin filament content and organization in unstimulated platelets. *The Journal of Cell Biology*, 98(6):1985–1991, 1984. doi: 10.1083/jcb.98.6.1985. (cited on page 10)

[41] J. E. Fox, C. C. Reynolds, J. S. Morrow, and D. R. Phillips. Spectrin is associated with membrane-bound actin filaments in platelets and is hydrolyzed

by the Ca2+-dependent protease during platelet activation. *Blood*, 69(2):537–545, 1987. (cited on page 9)

[42] G. Giannone, B. J. Dubin-Thaler, H.-G. Döbereiner, N. Kieffer, A. R. Bresnick, and M. P. Sheetz. Periodic lamellipodial contractions correlate with rearward actin waves. *Cell*, 116(3):431–443, 2004. doi: 10.1016/S0092-8674(04)00058-3. (cited on page 13, 103, and 122)

[43] G. Giannone, B. J. Dubin-Thaler, O. Rossier, Y. Cai, O. Chaga, G. Jiang, W. Beaver, H.-G. Döbereiner, Y. Freund, G. Borisy, and M. P. Sheetz. Lamellipodial actin mechanically links myosin activity with adhesion-site formation. *Cell*, 128(3):561–575, 2007. doi: 10.1016/j.cell.2006.12.039. (cited on page 13, 14, 98, and 103)

[44] J. H. Hartwig. Chapter 8 - The Platelet Cytoskeleton. In A. D. Michelson, editor, *Platelets*. Elsevier/Academic Press, London, 3rd edition, 2013. (cited on page 5, 6, 7, 9, 10, 14, 15, and 124)

[45] C.-L Hsu, S.-C. Wei, J.-W. Jian, H.-T. Chang, W.-H. Chen, and C.-C. Huang. Highly flexible and stable aptamer-caged nanoparticles for control of thrombin activity. *RSC Advances*, 2(4):1577–1584, 2012. doi: 10.1039/c1ra00344e. (cited on page 132)

[46] S. Inaba, S. Fujino, and K. Morinaga. Young's modulus and compositional parameters of oxide glasses. *Journal of the American Ceramic Society*, 82(12): 3501–3507, 1999. doi: 10.1111/j.1151-2916.1999.tb02272.x. (cited on page 82)

[47] J. E. Italiano jr. and J. H. Hartwig. Chapter 2 - Megakaryocyte Development and Platelet Formation. In A. D. Michelson, editor, *Platelets*. Elsevier/Academic Press, London, 3rd edition, 2013. (cited on page 5, 6, 7, and 8)

[48] J. E. Italiano jr., P. Lecine, R. A. Shivdasani, and J. H. Hartwig. Blood platelets are assembled principally at the ends of proplatelet processes produced by differentiated megakaryocytes. *The Journal of Cell Biology*, 147(6):1299–1312, 1999. doi: 10.1083/jcb.147.6.1299. (cited on page 8)

[49] I. A. Janson and A. J. Putnam. Extracellular matrix elasticity and topography: Material-based cues that affect cell function via conserved mechanisms. *Journal of Biomedical Materials Research. Part A*, 2014:00A:000-000, 2014. doi: 10.1002/jbm.a.35254. (cited on page 1 and 133)

[50] R. S. Kane, S. Takayama, E. Ostuni, D. E. Ingber, and G. M. Whitesides. Patterning proteins and cells using soft lithography. *Biomaterials*, 20(23-24): 2363–2376, 1999. doi: 10.1016/S0142-9612(99)00165-9. (cited on page 1)

[51] L. Kikuchi, J. Y. Park, C. Victor, and J. E. Davies. Platelet interactions with calcium-phosphate-coated surfaces. *Biomaterials*, 26(26):5285–5295, 2005. doi: 10.1016/j.biomaterials.2005.01.009. (cited on page 2 and 21)

[52] A. Kita, Y. Sakurai, D. R. Myers, R. Rounsevell, J. N. Huang, T. J. Seok, K. Yu, M. C. Wu, D. A. Fletcher, and W. A. Lam. Microenvironmental geometry guides platelet adhesion and spreading: a quantitative analysis at the single cell level. *PloS ONE*, 6(10):e26437, 2011. doi: 10.1371/journal.pone.0026437. (cited on page 1, 17, 20, 36, 83, 84, 116, 124, and 131)

[53] L. B. Koh, I. Rodriguez, and S. S. Venkatraman. The effect of topography of polymer surfaces on platelet adhesion. *Biomaterials*, 31(7):1533–1545, 2010. doi: 10.1016/j.biomaterials.2009.11.022. (cited on page 21, 22, and 86)

[54] R. Kopelman and W. Tan. Near-field optics: imaging single molecules. *Science*, 262(5138):1382–1384, 1993. doi: 10.1126/science.262.5138.1382. (cited on page 87)

[55] M. Krause, E. W. Dent, J. E. Bear, J. J. Loureiro, and F. B. Gertler. Ena/VASP proteins: regulators of the actin cytoskeleton and cell migration. *Annual Review of Cell and Developmental Biology*, 19:541–564, 2003. doi: 10.1146/annurev.cellbio.19.050103.103356. (cited on page 12)

[56] D. Lee, K. P. Fong, M. R. King, L. F. Brass, and D. A. Hammer. Differential dynamics of platelet contact and spreading. *Biophysical Journal*, 102(3):472–482, 2012. doi: 10.1016/j.bpj.2011.10.056. (cited on page 14, 15, 123, 125, and 131)

[57] S. W. Lee and S. S. Lee. Shrinkage ratio of PDMS and its alignment method for the wafer level process. *Microsystem Technologies*, 14(2):205–208, 2008. doi: 10.1007/s00542-007-0417-y. (cited on page 86)

[58] D. Lehnert, B. Wehrle-Haller, C. David, U. Weiland, C. Ballestrem, B. A. Imhof, and M. Bastmeyer. Cell behaviour on micropatterned substrata: limits of extracellular matrix geometry for spreading and adhesion. *Journal of Cell Science*, 117(Pt 1):41–52, 2004. doi: 10.1242/jcs.00836. (cited on page 20 and 85)

[59] J. Levin. Chapter 1 - The Evolution of Mammalian Platelets. In A. D. Michelson, editor, *Platelets*. Elsevier/Academic Press, London, 3rd edition, 2013. (cited on page 5 and 6)

[60] X. M. Liang, S. J. Han, J.-A. Reems, D. Gao, and N. J. Sniadecki. Platelet retraction force measurements using flexible post force sensors. *Lab on a Chip*, 10(8):991–998, 2010. doi: 10.1039/b918719g. (cited on page 16 and 27)

[61] J. Y. Lim and H. J. Donahue. Cell sensing and response to micro- and nanostructured surfaces produced by chemical and topographic patterning. *Tissue Engineering*, 13(8):1879–1891, 2007. doi: 10.1089/ten.2006.0154. (cited on page 1 and 17)

[62] G. Lukinavičius, L. Reymond, E. D'Este, A. Masharina, F. Göttfert, H. Ta, A. Güther, M. Fournier, S. Rizzo, H. Waldmann, C. Blaukopf, C. Sommer, D. W. Gerlich, H.-D. Arndt, S. W. Hell, and K. Johnsson. Fluorogenic probes for live-cell imaging of the cytoskeleton. *Nature Methods*, 11(7):731–733, 2014. doi: 10.1038/nmeth.2972. (cited on page 101 and 133)

[63] M. R. Mejillano, S. Kojima, D. A. Applewhite, F. B. Gertler, T. M. Svitkina, and G. G. Borisy. Lamellipodial versus filopodial mode of the actin nanomachinery: pivotal role of the filament barbed end. *Cell*, 118(3):363–373, 2004. doi: 10.1016/j.cell.2004.07.019. (cited on page 12, 124, 131, and 132)

[64] Molecular Probes by Life Technologies GmbH. CellMask™ Plasma Membrane Stains: Revision A.0: MAN0001956, MP10045, . URL `https://tools.lifetechnologies.com/content/sfs/manuals/CellMask_Plasma_Membrane_Stains_PI.pdf`. last checked: Dezember 21, 2014. (cited on page 36, 48, 89, 101, 124, and 133)

[65] Molecular Probes by Life Technologies GmbH. Fluorescence Ex/Em spectra of Alexa Fluor® 488 in pH 8 buffer., . URL `http://www.lifetechnologies.com/content/dam/LifeTech/Documents/spectra/plotfiles/11001ph8.txt`. last checked: September 26, 2014. (cited on page 39 and 41)

[66] Molecular Probes by Life Technologies GmbH. Fluorescence Ex/Em spectra of Alexa Fluor® 594 in pH 7.2 buffer., . URL `http://www.lifetechnologies.com/content/dam/LifeTech/Documents/`

spectra/plotfiles/11005p72.txt. last checked: September 26, 2014. (cited on page 39)

[67] Molecular Probes by Life Technologies GmbH. Fluorescence Ex/Em spectra of CellMask™ Deep Red plasma membrane stain bound to zwitterionic detergent (CHAPS) micelles., . URL http://www.lifetechnologies.com/content/dam/LifeTech/Documents/spectra/plotfiles/10046.txt. last checked: September 26, 2014. (cited on page 41)

[68] B. Nöding. *Dynamic measurements of individual intermediate filaments*. Diploma Thesis, Courant Research Centre Nano-Spectroscopy and X-Ray Imaging, Georg-August-Universität Göttingen, Göttingen, 06/2010. (cited on page 23)

[69] P. T. Ohara and R. C. Buck. Contact guidance in vitro. A light, transmission, and scanning electron microscopic study. *Experimental Cell Research*, 121(2): 235–249, 1979. doi: 10.1016/0014-4827(79)90002-8. (cited on page 17, 19, and 85)

[70] P. Pan and H. Bayley. Caged cysteine and thiophosphoryl peptides. *FEBS Letters*, 405(1):81–85, 1997. doi: 10.1016/S0014-5793(97)00165-8. (cited on page 132)

[71] J. Y. Park, C. H. Gemmell, and J. E. Davies. Platelet interactions with titanium: modulation of platelet activity by surface topography. *Biomaterials*, 22 (19):2671–2682, 2001. doi: 10.1016/S0142-9612(01)00009-6. (cited on page 1, 2, 3, 21, 82, 132, and 149)

[72] K. Park, F. W. Mao, and H. Park. Morphological characterization of surface-induced platelet activation. *Biomaterials*, 11(1):24–31, 1990. doi: 10.1016/0142-9612(90)90047-T. (cited on page 15, 16, 82, and 102)

[73] S. Patel-Hett, J. L. Richardson, H. Schulze, K. Drabek, N. A. Isaac, K. Hoffmeister, R. A. Shivdasani, J. C. Bulinski, N. Galjart, J. H. Hartwig, and J. E. Italiano. Visualization of microtubule growth in living platelets reveals a dynamic marginal band with multiple microtubules. *Blood*, 111(9): 4605–4616, 2008. doi: 10.1182/blood-2007-10-118844. (cited on page 15)

[74] A. C. von Philipsborn, S. Lang, A. Bernard, J. Loeschinger, C. David, D. Lehnert, M. Bastmeyer, and F. Bonhoeffer. Microcontact printing of axon guidance molecules for generation of graded patterns. *Nature Protocols*, 1(3): 1322–1328, 2006. doi: 10.1038/nprot.2006.251. (cited on page 28)

[75] A. Ponti, M. Machacek, S. L. Gupton, C. M. Waterman-Storer, and G. Danuser. Two distinct actin networks drive the protrusion of migrating cells. *Science*, 305(5691):1782–1786, 2004. doi: 10.1126/science.1100533. (cited on page 13)

[76] Y. Qiu, A. C. Brown, D. R. Myers, Y. Sakurai, R. G. Mannino, R. Tran, B. Ahn, E. T. Hardy, M. F. Kee, S. Kumar, G. Bao, T. H. Barker, and W. A. Lam. Platelet mechanosensing of substrate stiffness during clot formation mediates adhesion, spreading, and activation. *Proceedings of the National Academy of Sciences of the United States of America*, 111(40):14430–14435, 2014. doi: 10.1073/pnas.1322917111. (cited on page 1, 73, and 82)

[77] H. Raslova, L. Roy, C. Vourc'h, J.P. Le Couedic, O. Brison, D. Metivier, J. Feunteun, G. Kroemer, N. Debili, and W. Vainchenker. Megakaryocyte polyploidization is associated with a functional gene amplification. *Blood*, 101(2): 541–544, 2003. doi: 10.1182/blood-2002-05-1553. (cited on page 7)

[78] A.F. von Recum and T.G. van Kooten. The influence of micro-topography on cellular response and the implications for silicone implants. *Journal of Biomaterials Science. Polymer Edition*, 7(2):181–198, 1996. doi: 10.1163/156856295X00698. (cited on page 19 and 87)

[79] F. Rendu and B. Brohard-Bohn. The platelet release reaction: granules' constituents, secretion and functions. *Platelets*, 12(5):261–273, 2001. doi: 10.1080/09537100120068170. (cited on page 123)

[80] R. Rodvien and C. H. Mielke jr. Role of platelets in hemostasis and thrombosis. *The Western Journal of Medicine*, 125(3):181–186, 1976. (cited on page 1 and 6)

[81] O. M. Rossier, N. Gauthier, N. Biais, W. Vonnegut, M.-A. Fardin, P. Avigan, E. R. Heller, A. Mathur, S. Ghassemi, M. S. Koeckert, J. C. Hone, and M. P. Sheetz. Force generated by actomyosin contraction builds bridges between adhesive contacts. *The EMBO Journal*, 29(6):1055–1068, 2010. doi: 10.1038/emboj.2010.2. (cited on page 17, 81, 98, 102, and 103)

[82] S. A. Ruiz and C. S. Chen. Microcontact printing: A tool to pattern. *Soft Matter*, 3(2):168–177, 2007. doi: 10.1039/b613349e. (cited on page 1, 16, and 27)

[83] A. K. Salem, R. Stevens, R. G. Pearson, M. C. Davies, S.J.B Tendler, C. J. Roberts, P. M. Williams, and K. M. Shakesheff. Interactions of 3T3 fibroblasts and endothelial cells with defined pore features. *Journal of Biomedical Materials Research*, 61(2):212–217, 2002. doi: 10.1002/jbm.10195. (cited on page 19, 82, 83, and 86)

[84] R. Sandmann, S. Schwarz G. Henriques, F. Rehfeldt, and S. Köster. Microtopography influences blood platelet spreading. *Soft Matter*, 10(14):2365–2371, 2014. doi: 10.1039/c3sm52636d. URL `http://pubs.rsc.org/en/content/articlelanding/2014/sm/c3sm52636d#!divAbstract`. (cited on page 23, 30, 31, 43, 71, 73, 74, 75, 77, 79, 161, and 165)

[85] C. Schäfer, B. Borm, S. Born, C. Möhl, E.-M. Eibl, and B. Hoffmann. One step ahead: role of filopodia in adhesion formation during cell migration of keratinocytes. *Experimental Cell Research*, 315(7):1212–1224, 2009. doi: 10.1016/j.yexcr.2008.11.008. (cited on page 11 and 124)

[86] J. A. Schmidt and A. F. von Recum. Macrophage response to microtextured silicone. *Biomaterials*, 13(15):1059–1069, 1992. doi: 10.1016/0142-9612(92)90138-E. (cited on page 20 and 85)

[87] C. A. Schneider, W. S. Rasband, and K. W. Eliceiri. NIH Image to ImageJ: 25 years of image analysis. *Nature Methods*, 9(7):671–675, 2012. doi: 10.1038/nmeth.2089. (cited on page 44, 45, 46, 50, 51, 67, 69, 79, 90, 125, 166, 168, 169, 172, and 175)

[88] S. Schwarz G. Henriques. *Biophysics of Blood Platelet Contraction*. Dissertation, Georg-August-Universität, Göttingen, 21.05.2013. URL `http://hdl.handle.net/11858/00-1735-0000-001C-21C5-C`. (cited on page 32 and 47)

[89] H. Schwertz, S. Köster, W.H.A. Kahr, N. Michetti, B. F. Kraemer, D. A. Weitz, R. C. Blaylock, L. W. Kraiss, A. Greinacher, G. A. Zimmerman, and A. S. Weyrich. Anucleate platelets generate progeny. *Blood*, 115(18):3801–3809, 2010. doi: 10.1182/blood-2009-08-239558. (cited on page 8 and 124)

[90] J. V. Small, T. Stradal, E. Vignal, and K. Rottner. The lamellipodium: where motility begins. *Trends in Cell Biology*, 12(3):112–120, 2002. doi: 10.1016/S0962-8924(01)02237-1. (cited on page 11)

[91] P. M. Stevenson and A. M. Donald. Identification of three regimes of behavior for cell attachment on topographically patterned substrates. *Lang-*

muir : the ACS Journal of Surfaces and Colloids, 25(1):367–376, 2009. doi: 10.1021/la802859v. (cited on page 17, 18, 19, 84, 87, and 103)

[92] T.T.T. Tan, C. Khaw, and M.M.L. Ng. Challenges and recent advances in live cell bioimaging. In A. Méndez-Vilas and J. Díaz, editors, *Microscopy: Science, Technology, Applications and Education*, volume 2 of *Microscopy Book Series, Number 4*, pages 1495–1505. Formatex Research Center, Badajoz, 2010. ISBN 8461461905. (cited on page 37)

[93] A. I. Teixeira, S. Ilkhanizadeh, J. A. Wigenius, J. K. Duckworth, O. Inganäs, and O. Hermanson. The promotion of neuronal maturation on soft substrates. *Biomaterials*, 30(27):4567–4572, 2009. doi: 10.1016/j.biomaterials.2009.05.013. (cited on page 82)

[94] Inc The MathWorks. Registering an Image Using Normalized Cross-Correlation. URL `http://www.mathworks.de/products/demos/image/cross_correlation/imreg.html`. last checked: June 2014. (cited on page 49)

[95] J. N. Thon, A. Montalvo, S. Patel-Hett, M. T. Devine, J. L. Richardson, A. Ehrlicher, M. K. Larson, K. Hoffmeister, J. H. Hartwig, and J. E. Italiano. Cytoskeletal mechanics of proplatelet maturation and platelet release. *The Journal of Cell Biology*, 191(4):861–874, 2010. doi: 10.1083/jcb.201006102. (cited on page 8)

[96] J. N. Thon, H. Macleod, A. J. Begonja, J. Zhu, K.-C. Lee, A. Mogilner, J. H. Hartwig, and J. E. Italiano. Microtubule and cortical forces determine platelet size during vascular platelet production. *Nature Communications*, 3:852, 2012. doi: 10.1038/ncomms1838. (cited on page 8, 82, and 102)

[97] D. Tsygankov, C. G. Bilancia, E. A. Vitriol, K. M. Hahn, M. Peifer, and T. C. Elston. CellGeo: a computational platform for the analysis of shape changes in cells with complex geometries. *The Journal of Cell Biology*, 204(3):443–460, 2014. doi: 10.1083/jcb.201306067. (cited on page 12 and 126)

[98] A. D. Turner, S. V. Pizzo, G. W. Rozakis, and N. A. Porter. Photochemical activation of acylated α -thrombin. *Journal of the American Chemical Society*, 109(4):1274–1275, 1987. doi: 10.1021/ja00238a062. (cited on page 132)

[99] M. B. Villarino. A note on the accuracy of Ramanujan's approximative formula for the perimeter of an ellipse. *Journal of Inequalities in Pure and Applied Mathematics*, 7(1):article 21, 2006. (cited on page 47)

[100] T. Wakatsuki, R. B. Wysolmerski, and E. L. Elson. Mechanics of cell spreading: role of myosin II. *Journal of Cell Science*, 116(Pt 8):1617–1625, 2003. doi: 10.1242/jcs.00340. (cited on page 15)

[101] Y. L. Wang. Exchange of actin subunits at the leading edge of living fibroblasts: possible role of treadmilling. *The Journal of Cell Biology*, 101(2):597–602, 1985. doi: 10.1083/jcb.101.2.597. (cited on page 13)

[102] N. Watanabe and T. J. Mitchison. Single-molecule speckle analysis of actin filament turnover in lamellipodia. *Science*, 295(5557):1083–1086, 2002. doi: 10.1126/science.1067470. (cited on page 13)

[103] B. Weinhausen, O. Saldanha, R. N. Wilke, C. Dammann, M. Priebe, M. Burghammer, M. Sprung, and S. Köster. Scanning x-ray nanodiffraction on living eukaryotic cells in microfluidic environments. *Physical Review Letters*, 112(8), 2014. doi: 10.1103/PhysRevLett.112.088102. (cited on page 87)

[104] C. Westendorf, J. Negrete, A. J. Bae, R. Sandmann, E. Bodenschatz, and C. Beta. Actin cytoskeleton of chemotactic amoebae operates close to the onset of oscillations. *Proceedings of the National Academy of Sciences of the United States of America*, 110(10):3853–3858, 2013. doi: 10.1073/pnas.1216629110. (cited on page 132)

[105] J. G. White. Interaction of membrane systems in blood platelets. *The American Journal of Pathology*, 66(2):295–312, 1972. (cited on page 9)

[106] J. G. White. Separate and combined interactions of fibrinogen-gold and latex with surface-activated platelets. *The American Journal of Pathology*, 137 (4):989–998, 1990. (cited on page 9)

[107] J. G. White. Platelets are covercytes, not phagocytes: uptake of bacteria involves channels of the open canalicular system. *Platelets*, 16(2):121–131, 2005. doi: 10.1080/09537100400007390. (cited on page 9)

[108] J. G. White. Chapter 7 - Platelet Structure. In A. D. Michelson, editor, *Platelets*. Elsevier/Academic Press, London, 3rd edition, 2013. (cited on page 5, 6, 9, 10, 32, and 74)

[109] J. G. White and G. Escolar. Current concepts of platelet membrane response to surface activation. *Platelets*, 4(4):175–189, 1993. doi: 10.3109/09537109309013215. (cited on page 9)

[110] B. Wójciak-Stothard, Z. Madeja, W. Korohoda, A. Curtis, and C. Wilkinson. Activation of macrophage-like cells by multiple grooved substrata. Topographical control of cell behaviour. *Cell Biology International*, 19(6):485–490, 1995. doi: 10.1006/cbir.1995.1092. (cited on page 18, 20, 83, and 85)

[111] R. Woolley, Ú. Prendergast, B. Jose, D. Kenny, and C. McDonagh. A rapid, topographical platelet activation assay. *Analyst*, 138(16):4512–4518, 2013. doi: 10.1039/c3an00046j. (cited on page 20 and 21)

[112] Y. Xia and G. M. Whitesides. Soft Lithography. *Annual Review of Materials Science*, 28(1):153–184, 1998. doi: 10.1146/annurev.matsci.28.1.153. (cited on page 1, 16, 17, and 23)

[113] C. Yang, L. Czech, S. Gerboth, S. Kojima, G. Scita, and T. Svitkina. Novel roles of formin mDia2 in lamellipodia and filopodia formation in motile cells. *PLoS Biology*, 5(11):e317, 2007. doi: 10.1371/journal.pbio.0050317. URL `http://journals.plos.org/plosbiology/article?id=10.1371/journal.pbio.0050317`. (cited on page 11 and 149)

[114] A. Zemel, F. Rehfeldt, A.E.X Brown, D. E. Discher, and S. A. Safran. Optimal matrix rigidity for stress-fiber polarization in stem cells. *Nature Physics*, 6(6):468–473, 2010. doi: 10.1038/nphys1613. (cited on page 46)

[115] M. Zhou, J. H. Yang, X. Ye, A. R. Zheng, G. Li, P. F. Yang, Y. Zhu, and L. Cai. Blood platelet's behavior on nanostructured superhydrophobic surface. *Journal of Nano Research*, 2:129–136, 2008. doi: 10.4028/www.scientific.net/JNanoR.2.129. (cited on page 2 and 21)

List of Figures

List of Tables

List of Publications

- Rabea Sandmann, Sarah Schwarz G. Henriques, Florian Rehfeldt, and Sarah Köster. Micro-topography influences blood platelet spreading. Soft Matter, 10(14):2365-2371, 2014.
- Christian Westendorf, Jose Negrete, Jr., Albert J. Bae, Rabea Sandmann, Eberhard Bodenschatz and Carsten Beta. Actin cytoskeleton of chemotactic amoebae operates close to the onset of oscillations. Proceedings of the National Academy of Sciences of the United States of America, 110(10): 3853-3858, 2013.
- Sarah Schwarz Henriques, Rabea Sandmann, Alexander Strate, and Sarah Köster. Force field evolution during human blood platelet activation. Journal of Cell Science, 125(10):3914-3920, 2012.

Danksagung

An dieser Stelle möchte ich mich bei zahlreichen Menschen bedanken, die mich während der letzten dreieinhalb Jahre bei der Durchführung meiner Doktorarbeit unterstützt haben und unerlässlich für den Erfolg dieser Arbeit waren.
Zuallererst möchte ich mich bei **Sarah Köster** für die Möglichkeit eine Doktorarbeit in ihrer Gruppe anzufertigen sowie für ihre Unterstützung und Beratung während der gesamten Doktorarbeit bedanken. Regelmäßige Diskussionen über meine Ergebnisse und die weitere Vorgehensweise haben immer sehr zum Fortkommen dieser Arbeit beigetragen. Außerdem danke ich ihr für die Möglichkeit einen Forschungsaufenthalt in einer medizinischen Forschungsgruppe in den USA durchzuführen. Weiterhin bot sie mir die Gelegenheit an zahlreichen Konferenzen und Workshops teilzunehmen.
Florian Rehfeldt danke ich für die zahlreichen hilfreichen Diskussionen, in denen ich von seinem umfangreichen Wissen, unter anderem in der zellulären Biophysik und der Datenanalyse, profitieren konnte. Zusätzlich halfen er und **Susanne Karsch** mir bei Aufnahmen meiner Substrate am „atomic force microscope "(AFM). Außerdem möchte ich ihm noch für sein Engagement als Zweit-Gutachter dieser Arbeit danken.
Oskar Hallatschek danke ich für die theoretischen Aspekte, die er mir während der Thesis Committee Meetings näher brachte.
Andreas Janshoff, Iwan Schaap und **Detlev Schild** danke ich dafür, dass sie meiner Verteidigung beiwohnen werden.
Des Weiteren möchte ich allen meinen früheren und derzeitigen Kollegen für die vielen Gespräche, kleineren und größeren Hilfestellungen, sowie die gute Atmosphäre innerhalb der Gruppe danken.
Besonders möchte ich hier **Sarah Schwarz** hervorheben. Von ihr erlernte ich einige der angewendeten Protokolle zum Umgang mit Thrombozyten. Außerdem stellte

sie das hier verwendete MATLAB-Programm zur Krümmungsberechnung der Zellkontur zur Verfügung. Die Zusammenarbeit mit ihr an den Thrombozyten-Projekten war stets eine Freude. Auch meinen alten und neuen Bürokollegen möchte ich besonders danken. **Johanna Block, Gerrit Brehm, Christian Dammann** und **Britta Weinhausen** sorgten immer für ein gutes Büroklima. Vor allem bei **Christian** möchte ich mich für die Diskussionen über meine Ergebnisse und Auswertungen bedanken. Aber auch mit **Britta, Johanna** und **Gerrit** habe ich oft Aspekte meiner Arbeit diskutiert.
Susanne Karsch half mir neben den Messungen am AFM durch ihre zahlreichen kritischen Auseinandersetzungen mit meinen Ergebnissen.
Bernd Nöding stellte mir das Protokoll zur Herstellung der strukturierten Siliziumwafer zur Verfügung und war bei kleineren und größeren Fragen im Labor stets eine Hilfe. **Jens Nolting** ließ mich an seinem umfangreichen Wissen über Analysemethoden und speziell MATLAB-Programmierung teilhaben. Er war vor allem in den letzten Monaten der Doktorarbeit ein unermüdlicher Diskussionspartner. Weitere Hilfe im Labor kam von **Susanne Bauch**, die zahlreiche Aliquots für mich herstellte und auch sonst immer zur Stelle war wenn ich Rat brauchte. **Valeria Piazza** beriet mich bei Anfärbeprotokollen und mit **Martha Brennich** fand stets ein reger Gedankenaustausch über die neusten Ergebnisse statt.
Gerrit Brehm, Jana Hanke, Aishwarya Paknikar und **Christiane Ranke** brachten neue Ideen in die Thrombozyten-Gruppe und sorgten fortwährend für einen sehr anregenden Gedankenaustausch besonders was Labor- und Analysetechniken anbelangte. Für das Korrekturlesen dieser Arbeit möchte ich **Johanna Block, Gerrit Brehm, Rita Graceffa, Jana Hanke, Clément Hémonnot, Jens Nolting, Aishwarya Paknikar, Oliva Saldanha** und **Viktor Schröder** danken.
Auch meinem ehemaligen Bachelorarbeits-Betreuer **Christian Westendorf** von dem ich die Grundlagen für jede weitere experimentelle Arbeit erlernt habe und von dessen guter damaliger Betreuung ich noch heute profitiere möchte ich hiermit nochmals meinen Dank aussprechen.
Dem Team der Abteilung für Transfusionsmedizin der Universitätsmedizin und besonders **Joachim Riggert, Tobias Legler** und **Andreas Strate** möchte ich an dieser Stelle noch einmal einen herzlichen Dank für die Bereitstellung der Thrombozyten-Konzentrate aussprechen. Ohne diese Konzentrate hätten die Experimente nicht durchgeführt werden können. **Jochen Herbst** und **Jörg Maliendretos** halfen mir bei Problem im Reinraum und sorgten immer für reibungslose Abläufe in diesem.

Für zahlreiche gute Ideen und Gedankenaustäusche über mögliche Verbindungen meiner Ergebnisse zu theoretischen Modellen danke ich **Reiner Kree** und **Assaf Zemel**.
Der Forschungsaufenthalt in der Gruppe von **Andrew Weyrich** und **Guy Zimmerman** in Utah war spannend, lehrreich und wurde vor allem durch ihre herzliche Art und die freundschaftliche Gruppen-Atmosphäre zu einem unvergesslichen Erlebnis. **Hansjörg Schwertz**, der mich in dieser Zeit betreute, brachte mir die medizinische Seite meines Projekts näher und lehrte mich viele neue biochemische Techniken und vor allem den Umgang mit Megakaryozyten. Zusätzlich ist er bis heute ein wichtiger Ansprechpartner bei Fragen zu medizinischen und biologischen Hintergründen und beriet uns so auch bei Protokollen. Auch für die zahlreichen schönen Stunden, die ich an Wochenenden oder abends mit ihm und seiner Familie in Salt Lake City verbringen durfte, möchte ich mich nochmals bedanken.
Meine Freunde waren auch in schwierigen Zeiten immer eine große Stütze. Mit dem ein oder anderen Kaffee und langen Gesprächen haben sie mir immer den Tag verschönert. Zuletzt möchte ich mich noch bei meinen **Eltern, Geschwistern, Kåre** und vor allem bei **Jörn** bedanken. Ihre Unterstützung war wohl nach der oben erwähnten fachlichen Beratung der wichtigste Faktor für das Gelingen dieser Arbeit. **Jörn** hat mich vor allem in sehr stressigen Phasen in jeder möglichen Art und Weise unterstützt. Nicht nur für die fachlichen Diskussionen sondern vor allem auch für die alltäglichen Dinge, die er mir abgenommen hat, kann ich ihm gar nicht genug danken.

A

Supplementary Data - Morphological Changes Induced by Microstructured Substrates

Parts of this appendix have been published in Soft Matter [84]. In figure A.1 the different terms used in this thesis to describe different parts of the holes in the substrate as well as the definition of hole and interspace width are sketched.

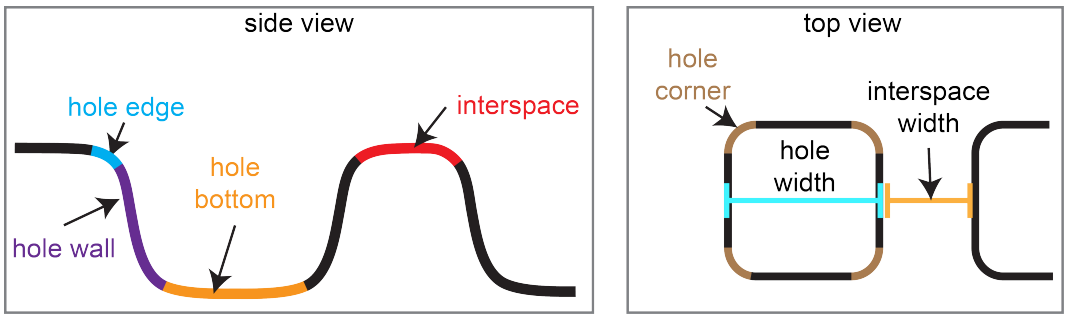

Figure A.1.: Sketch showing the different terms used to describe different parts of the substrate. (side view) The hole edge is drawn in light blue, the hole wall in purple, the hole bottom in orange and the interspace in red. (top view) The hole corners are marked in brown, the width of the holes is marked in cyan and the width of the interspaces in orange.

In figure A.2 cell outline curvatures on selectively coated substrates (2.1 μm wide

holes) are shown. The concave edges of invaginations show curvatures around $2.0\,\mu m^{-1}$ and thus confirm the tight adaption of platelets on selectively coated substrates.

A profile of the structures extracted from the atomic force microscopy image in figure 3.6 can be found in figure A.3. The hole walls are not perfectly vertical but nevertheless quite steep. A discussion of the influence of this steepness can be found in chapter 5.2.

The relations of platelet height and structure height are sketched in figure A.4. For this sketch a platelet height of about 100 nm was assumed and the cell is shown in purple, while the structure height is sketched to be about 500 nm and shown in orange.

Platelets extending protrusions into the holes can sometimes be seen. It is reasonable to assume that the numbers of platelets that bend into the holes will be elevated as hole sizes increase. In figure A.5 micrographs of a confocal z-stack are shown for a cell extending protrusions into the holes. The actin staining is shown in red while the fibrinogen coating is shown in gray. The holes shown here are slightly larger and more circular (about $3\,\mu m$ in diameter) than the biggest holes used for the experiments. In this case, the cell attaches to the center of the hole's bottom and thus probably can reduce the curvature induced by bending into the hole. Figure A.6 further elucidates cell behavior on structured substrates by showing regions of actin accumulation at the hole edges both on selectively coated and completely coated substrates. It can be seen that the accumulation is visible for both hole sizes displayed ($2.8\,\mu m$ and $2.1\,\mu m$ wide holes) and for both substrate types. However, the accumulation seems to be stronger on selectively coated substrates, which can result from a more selective representation of binding sites at the hole edges.

An additional observation that elucidates the reaction of platelets to the underlying substrate is shown in figure A.7. In this figure, inverted fluorescence images of a platelet stained for its membrane are shown. The arrows point at bright regions in the plasma membrane that appear during spreading.

The shape of these regions resembles the underlying holes and thus indicates an accumulation of membrane material at the edges of the holes. The positions of the underlying holes are illustrated in figure A.8. This figure shows micrographs of the stained plasma membrane of the platelet shown in figure A.7 as well as a fluorescence micrograph of the fibrinogen coating of the substrate.

The accumulation of membrane at the hole edges can result from the cell entering

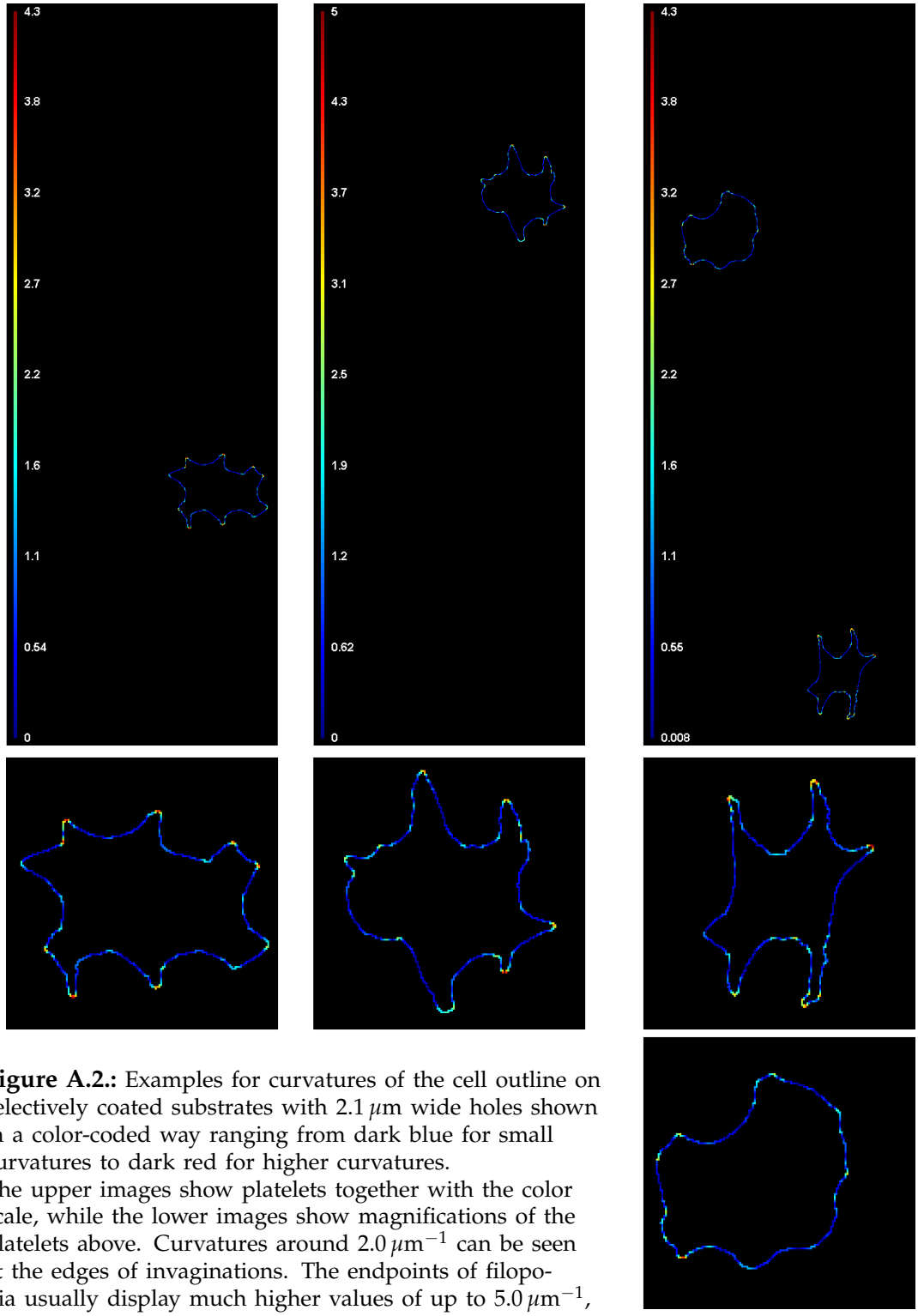

Figure A.2.: Examples for curvatures of the cell outline on selectively coated substrates with 2.1 μm wide holes shown in a color-coded way ranging from dark blue for small curvatures to dark red for higher curvatures.
The upper images show platelets together with the color scale, while the lower images show magnifications of the platelets above. Curvatures around 2.0 μm^{-1} can be seen at the edges of invaginations. The endpoints of filopodia usually display much higher values of up to 5.0 μm^{-1}, while straight parts show very small curvatures.

the holes in its middle during spreading. Entering the holes would result in a higher fluorescence signal at the position of the hole walls if the cell attaches to the wall.[i] Platelets entering the hole although not at their periphery during spreading would underline that the platelets in principle are able to enter the holes. However, they enter the holes only if no more favorable options are available

[i]Unfortunately, no z-stack of this cell is available as this behavior was only noticed after the experiment had been terminated.

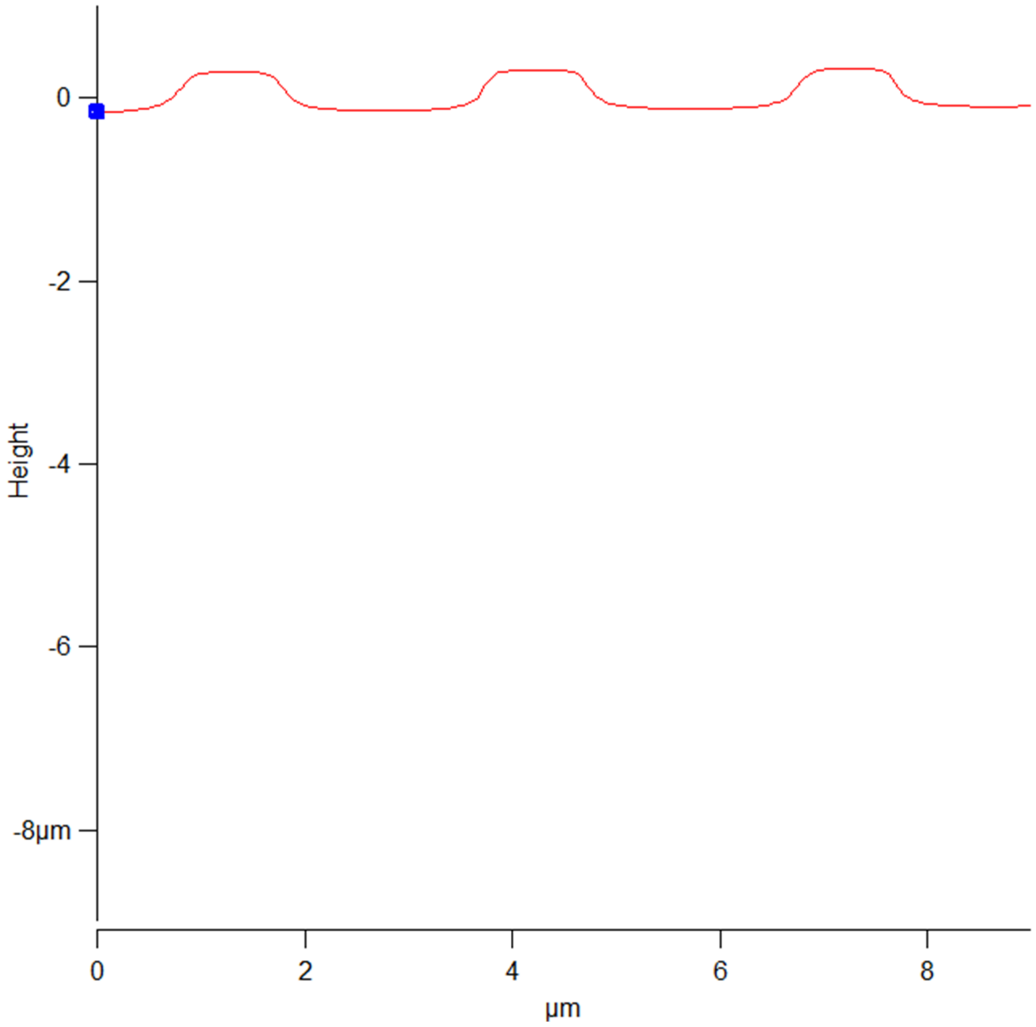

Figure A.3.: Profile of the atomic force microscopy image shown in figure 3.6.
The profile shows the height retrace channel of the measurement. The height is denoted on the y-axis while the distance is denoted on the x-axis. The hole walls are not perfectly straight, but nevertheless quite steep. A discussion of the steepness of the hole walls can be found in section 5.2.

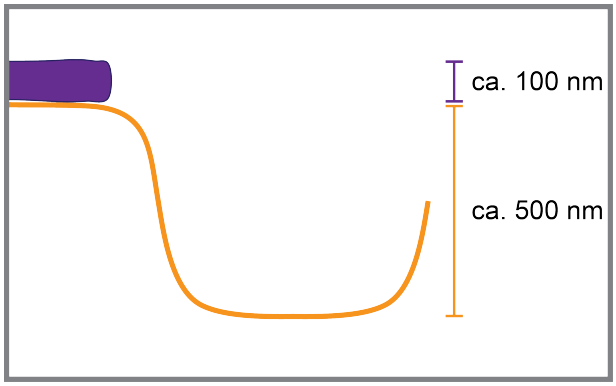

Figure A.4.: The height dimensions of the structures as well as those of completely spread platelets are shown in side view. The structure height is sketched to be about 500 nm and the cell height is assumed to be about 100 nm (see [2] for the height of lamellipodia of completely spreaded platelets). The structure is shown in orange and the cell is shown in purple.

and in the inner parts of the cell more contact sites can only be developed inside the hole. By comparing figure A.6 and figure A.7, possible explanations for the

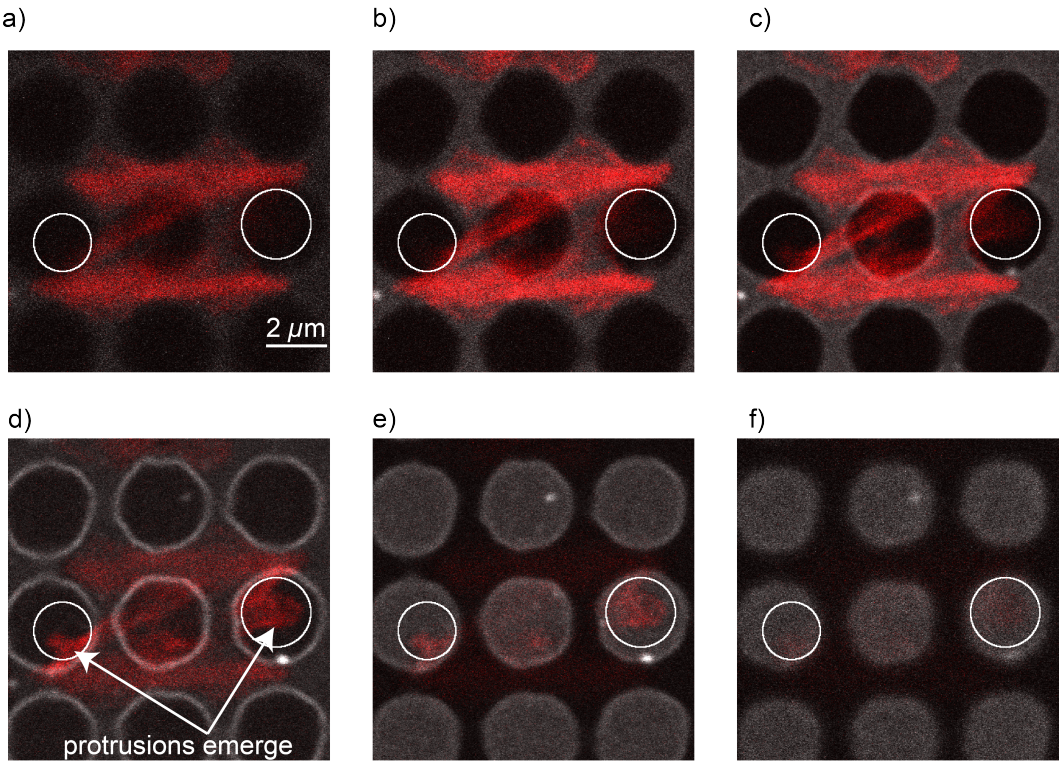

Figure A.5.: Micrographs of a confocal z-stack for a cell extending protrusions into the holes on a completely coated substrate (actin: red, fibrinogen: gray).
The holes are about $3\,\mu$m wide. Pictures a) to f) show different planes from above the cell to below the cell ($\Delta z = 0.25\,\mu$m). Protrusions extend into the holes and are marked with white circles. Figure has been adapted from the supplementary movie in [84] - Reproduced by permission of The Royal Society of Chemistry.

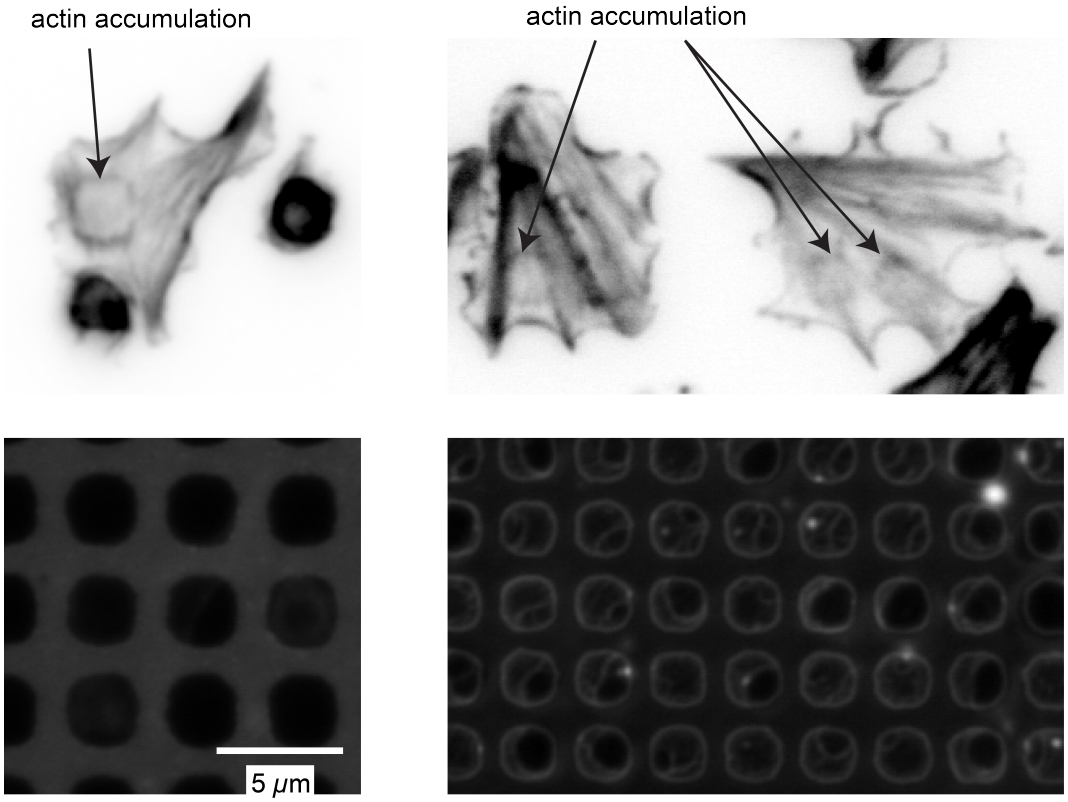

Figure A.6.: Fluorescence images of actin staining (upper, inverted) and fibrinogen coating (lower) showing actin accumulation at the hole edges on a selectively coated (left, 2.8 μm wide holes) as well as on a completely coated substrate (right, 2.1 μm wide holes). Images have been rotated (bilinear interpolation) in ImageJ [87] to align rows of holes with image borders.
Actin accumulation can be seen for both hole sizes and on both substrates types but the accumulation seems more pronounced on selectively coated substrates probably due to a different distribution of binding sites at the hole edge.

actin accumulation in figure A.6 arise. Membrane and actin accumulation at the hole edges hint to platelets entering the holes. In this case higher signal in actin and membrane staining would arise due to more material at the hole walls whose fluorescence signal is projected onto the x-y-plane. However, entering the holes seems unlikely in the case of selectively coated substrates, since no binding sites are present inside the hole. Therefore, on selectively coated substrates more actin may assemble due to focal adhesions that possibly assemble at the hole edges to stabilize the cell, while on completely coated substrates the cell probably enters the holes. These differences probably also explain the differences in actin signal strength at the hole edges.

The results detailed in chapter 5 show that single platelets adapt to the underlying

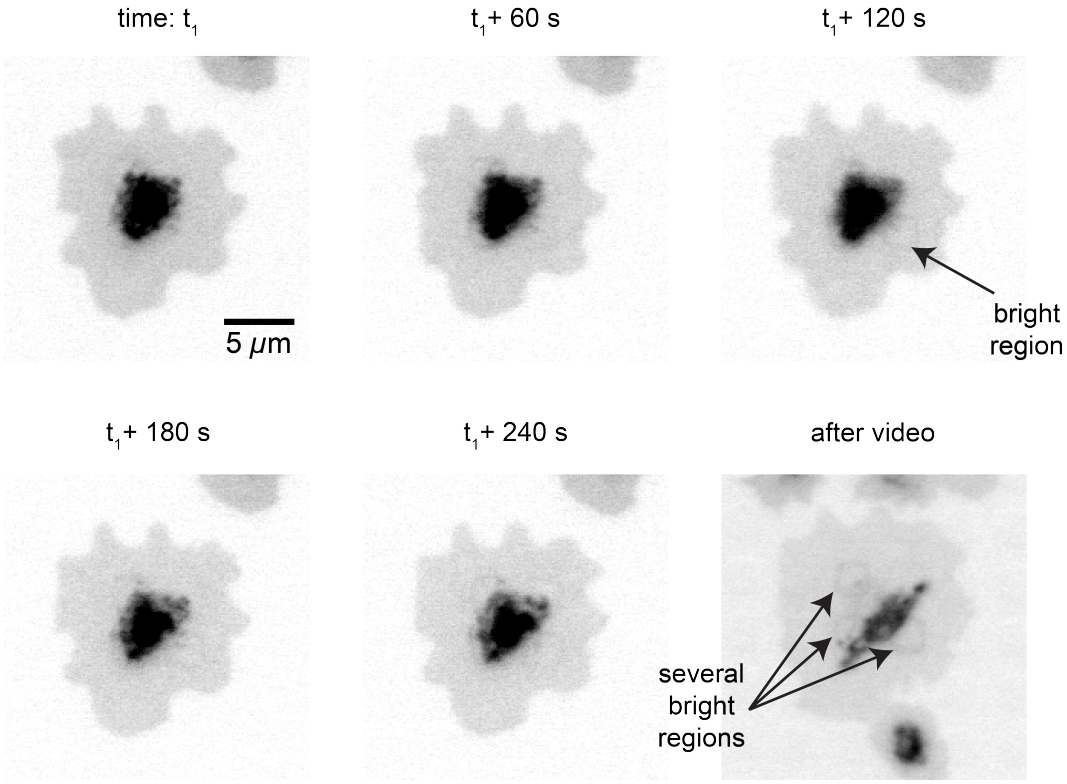

Figure A.7.: Inverted fluorescence images of a membrane stained cell spreading on a structured substrate with complete coating.
The different time points are indicated above the images. The last image was taken after the time-lapse series had ended with a higher illumination power of 100% in contrast to an illumination power of 7.72% for the other images. Details of the imaging are presented in section 3.6. Bright regions in membrane staining whose positions correspond to the borders of the underlying holes can be observed during spreading. In the last image there are clearly 3 bright regions visible that resemble the outline of the underlying holes. These bright regions indicate that the platelets enter the holes in their middle during spreading which would lead to an accumulation of cell membrane at the hole walls.

substrates by avoiding holes at their periphery. However, it has to be noted that a group of platelets is still able to cover the holes completely in a collective effort. Examples for this behavior are shown in figure A.9. It is probably easier for the platelets to span over holes in the layer of underlying spread platelets, since the binding strength to other platelets may be higher than to a layer of fibrinogen on a substrate. Furthermore, the underlying platelets may be much more deformable than the PDMS substrate. Maybe the spread platelets have already spanned parts of the substrate and thus the distance the newly arriving platelets have to span is reduced.

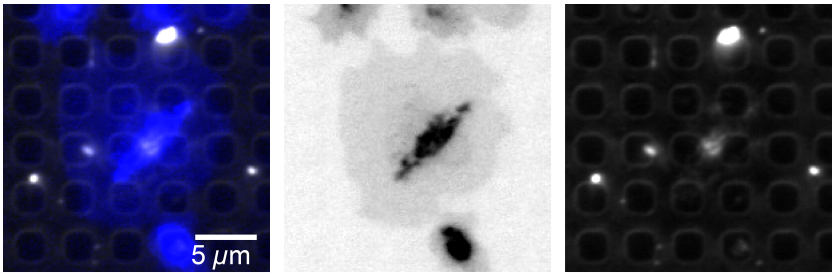

Figure A.8.: Fluorescence micrographs of membrane staining of the platelet shown in figure A.7 and corresponding fibrinogen coating of the substrate (completely coated, hole width: about $2.8\,\mu$m). In order to align the rows of holes with the image borders, the micrographs have been rotated in ImageJ [87] (bilinear interpolation). The micrographs have been recorded after the time lapse series ceased with a lamp power of 41.86% and an illumination time of $60\,$ms. For further imaging parameters see section 3.6.
(left) Composite of fluorescence images of membrane staining (blue) and fibrinogen coating (gray).
(middle) Inverted fluorescence micrograph of plasma membrane staining.
(right) Fluorescence micrograph of fibrinogen coating of underlying substrate.

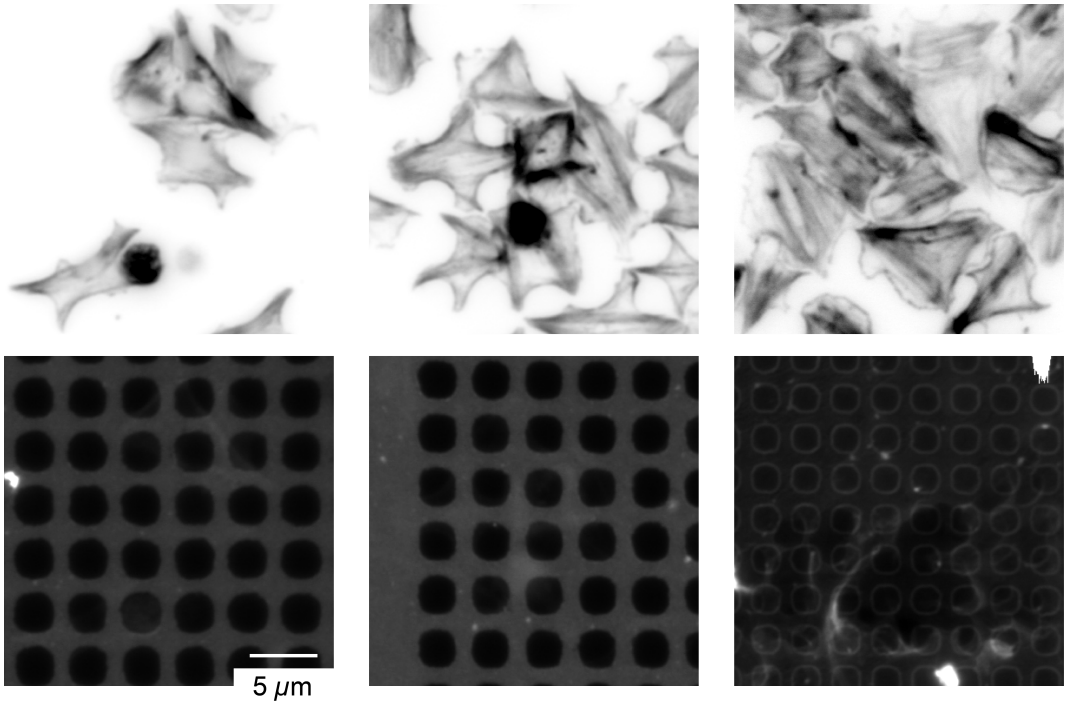

Figure A.9.: Fluorescence images of actin staining (upper, inverted) and fibrinogen coating (lower) showing groups of platelets that collectively are able to cover the holes in selectively coated substrates (left, middle) as well as in a completely coated substrate (right). On the completely coated substrate, more platelets seem to form the group. Images have been rotated (bilinear interpolation) in ImageJ [87] to align rows of holes with image borders. Irregularities in the lower image on the right result from irregular fibrinogen coating but do not seem to influence the platelets.

B

Supplementary Data - Dynamics of Spreading and Retraction on Microstructured Substrates

In figure B.1 a micrograph of the membrane-stained platelet on a structured substrate displayed in figure 6.1 and the corresponding micrograph of the fibrinogen coating of the underlying substrate are shown. The left micrograph shows a composite of the fluorescence image of a membrane-stained platelet (blue) and of the fibrinogen coating of the substrate (gray). The middle and right image show the single micrographs of the membrane-stained platelet (middle, inverted) and of the fibrinogen coating of the substrate (right). The images show the position of the holes with respect to the platelet.

In figure B.2 the mean values of var_{dir} (computed from the var_{dir} values of moving average treated data) are shown for platelets on structured and platelets on smooth substrates. On structured substrates 13 out of 29 platelets show mean values above $0.18\,\mu\mathrm{m}^2$, while on smooth substrates only 1 out of 16 platelets shows a mean value of higher than $0.18\,\mu\mathrm{m}^2$.

Variations of figures 6.7 and 6.9 from chapter 6 are shown here for better visibility of details (figure B.3 and figure B.4). Figure B.3 shows a zoom-in into early time points of var_{dir} depicting the differences between platelets on smooth (left, black)

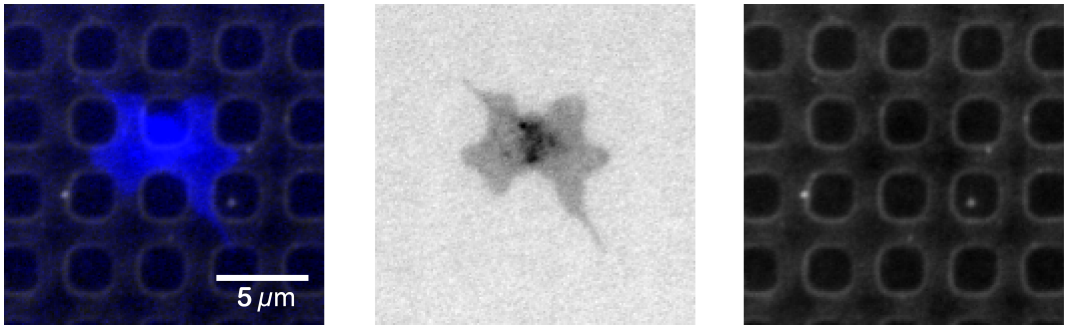

Figure B.1.: Fluorescence micrographs of the platelet displayed in figure 6.1 and of the fibrinogen coating of the underlying structured substrate. All micrographs have been rotated (bilinear interpolation) in ImageJ [87] to align the holes in the underlying substrate with the image borders. Except for the illumination power which was set to 41.86% imaging was performed as described in section 3.6. The micrographs have been taken after the time-lapse series from which the images in figure 6.1 were obtained had ceased.
(left) Composite of fluorescence micrographs of membrane-stained platelet (blue) and fibrinogen coating (gray).
(middle) Inverted fluorescence micrograph of membrane-stained platelet.
(right) Fluorescence micrograph of fibrinogen coating of the substrate.

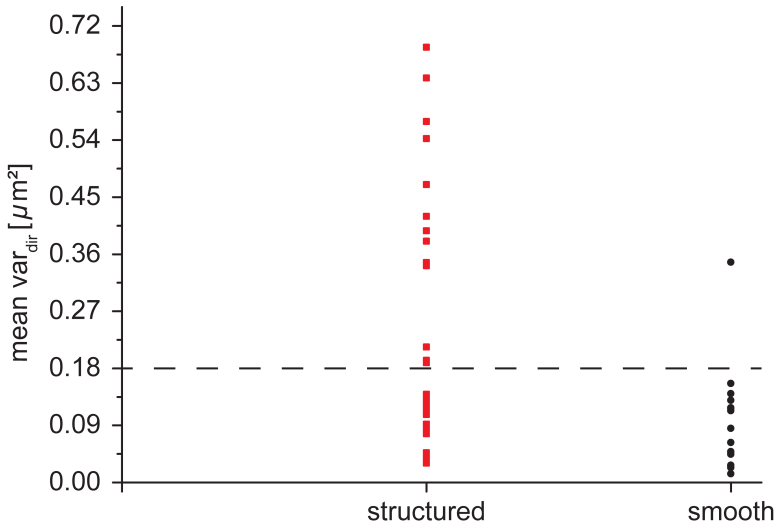

Figure B.2.: Plot of the average values of var_{dir} (calculated from the moving average treated data) for platelets on structured (left, red) and smooth (right, black) substrates. The value of $0.18\,\mu\mathrm{m}^2$ is marked with a dashed line.
The mean of var_{dir} is higher than $0.18\,\mu\mathrm{m}^2$ for about half (13 out of 29 platelets) of the platelets investigated on structured substrates here. For platelets lying on smooth substrates only 1 of 16 platelets shows a mean value for var_{dir} that is higher than $0.18\,\mu\mathrm{m}^2$.

and on structured substrates (right, red) in early spreading.

Differences between the two substrate types are visible as early as 50 seconds after

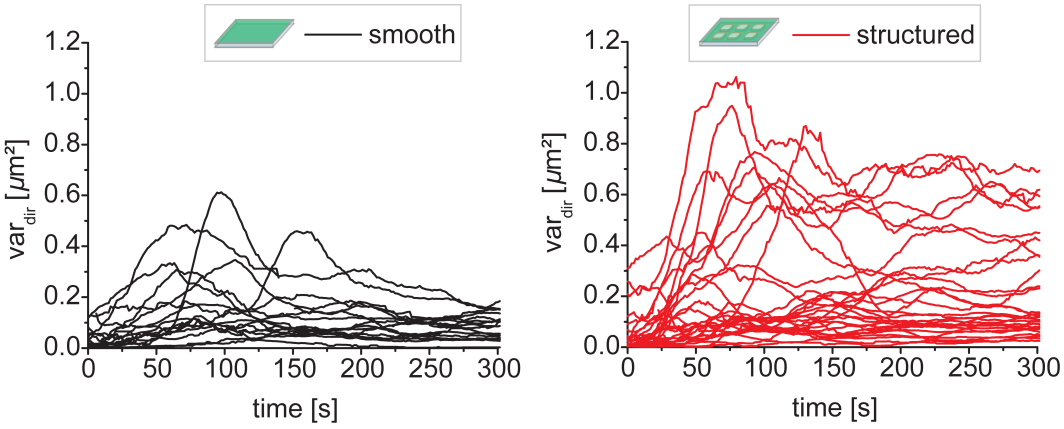

Figure B.3.: Plot of var_{dir} at early time points on smooth (left, black) and structured substrates (right, red). Var_{dir} is calculated based on the moving average of the signed lengths $l_{\text{cell-ellipse}}(\beta, t)$ of vectors between cell and ellipse.
Even 50 seconds after the onset of spreading, first differences between smooth and structured substrates are visible and several platelets on structured substrates show a higher value for var_{dir}.

spreading has started with several platelets on structured substrates showing high values of var_{dir}. These differences can be attributed to the formation of filopodia as is discussed in chapter 7.

To visualize the differences between platelets on smooth substrates and platelets on structured substrates for both large changes in protrusions and large changes in invaginations better, figure B.4 shows single plots for protrusions (upper, yellow) and invaginations (lower, blue). A clear difference in the number of large changes can be observed for both invaginations and protrusions. On smooth substrates only few large changes are present, while on structured substrates many more large changes occur with mainly growing protrusions and invaginations hinting at an adaptation to the substrate.

In figure B.5 fluorescence micrographs of the plasma membrane staining for the platelet shown in figure 6.11 and the fibrinogen coating of the underlying substrate are shown.

Figures B.6 and B.7 show the variances var_{dir} and var_{time} calculated on basis of the original data (no moving average). These data show the same trends as the variances that are calculated based on the moving average of the signed lengths $l_{\text{cell-ellipse}}(\beta, t)$ of the vectors between cell and ellipse (see figure 6.7 and 6.8).

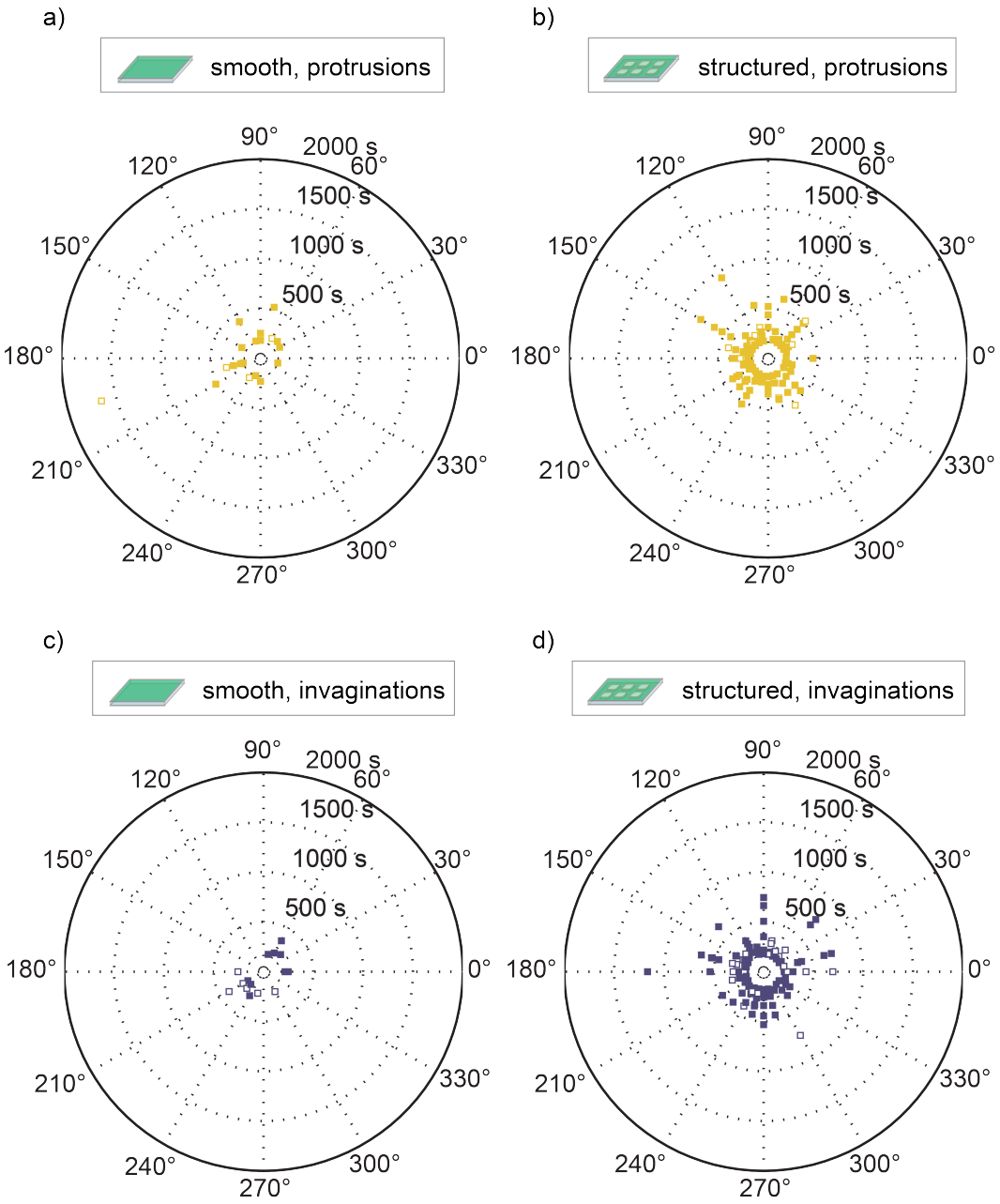

Figure B.4.: Single plots of large changes in protrusions (on smooth substrates a) and on structured substrates b)) and invaginations (on smooth substrates c) and on structured substrates d)). The polar plots show the different directions in azimuthal direction, while the time is shown in radial direction. Filled symbols show growing invaginations (■) and growing protrusions (■). Open symbols show filling invaginations (□) and retracting protrusions (□).
a) Some protrusions are growing on smooth substrates and nearly none are retracted.
b) Many more protrusions are growing on structured substrates than on smooth substrates and again nearly none are retracted.
c) Some invaginations are growing and some are being filled up on smooth substrates.
d) Many more invaginations are growing on structured substrates than on smooth substrates. Some invaginations are being filled up.

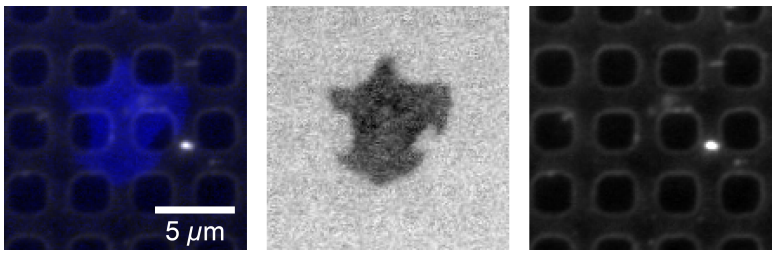

Figure B.5.: Fluorescence micrographs of membrane staining of platelet shown in figure 6.11 and corresponding fibrinogen coating of substrate. The micrographs have been rotated in ImageJ [87] (bilinear interpolation) to align the rows of holes with the image borders. The micrographs have been taken after the time lapse series had ended with a lamp power of 41.86% and an illumination time of 60 ms. Further imaging parameters are detailed in section 3.6.
(left) Composite of fluorescence image of membrane staining (blue) and fibrinogen coating (gray).
(middle) Inverted fluorescence micrograph of plasma membrane staining.
(right) Fluorescence micrograph of fibrinogen coating of the underlying substrate.

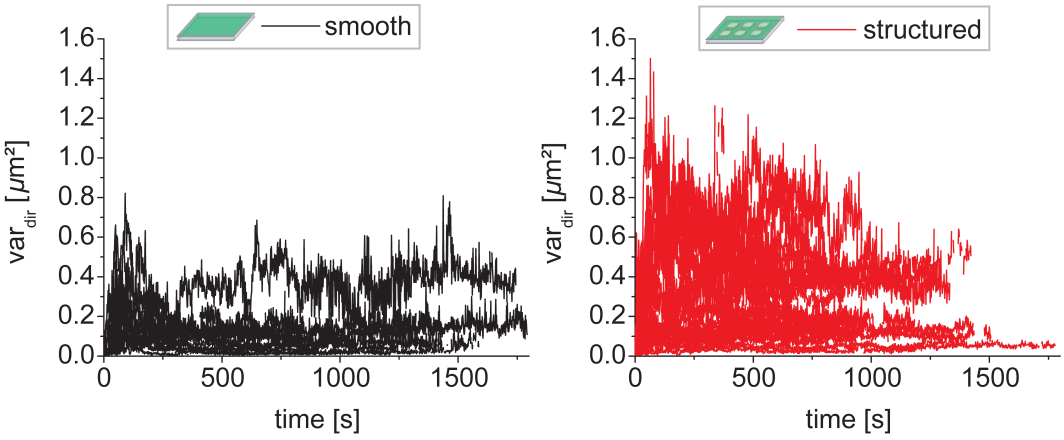

Figure B.6.: Plots of var_{dir} over time for platelets on smooth (left, black) and structured (right, red) substrates computed on the basis of the original (without moving average) signed lengths $l_{\text{cell-ellipse}}(\beta, t)$ of the vectors between cell and ellipse.
The values are more noisy than the variances calculated from the averaged data (see figure 6.7) but show the same differences between platelets on smooth and structured substrates with higher variances for some platelets on structured substrates.

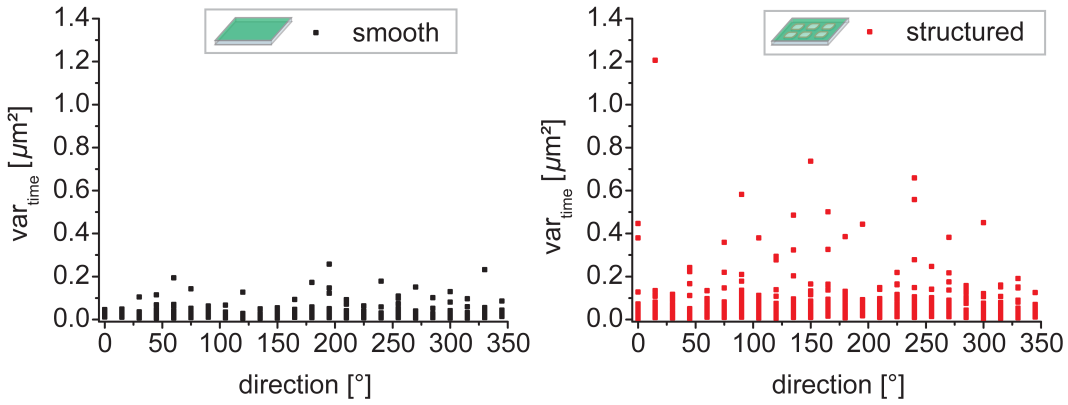

Figure B.7.: Plots of var_{time} over time for platelets on smooth (left, black) and structured (right, red) substrates computed on the basis of the original (without moving average) signed lengths $l_{\text{cell-ellipse}}(\beta, t)$ of the vectors between cell and ellipse.
Values are higher than for the variances calculated from the averaged data (see figure 6.8) but the general trend of several higher values on structured substrates compared to smooth substrates is conserved. The differences towards the variances calculated from the averaged data can arise from noise in the data that is reduced by averaging.

C

Supplementary Data - Dynamics of Cellular Protrusions

This chapter contains additional data belonging to chapter 7. To distinguish platelets lying on structured substrates and having a mean value for var_{dir} of more than $0.18\,\mu\mathrm{m}^2$ from those having a mean value for var_{dir} of less than $0.18\,\mu\mathrm{m}^2$, the former are called *adapted* to the substrate while the latter are called *unadapted*.
For completeness, plots of the mean number and standard deviation of the number of broad, blunt protrusions over time as well as histograms of the mean angle and maximal distance between projected points in radial direction and in angular direction for broad, blunt protrusions are shown here. Furthermore, the mean number and the standard deviation of the number of filopodia as a function of time for all platelets on structured substrates together (adapted and unadapted) in comparison to the mean number and the standard deviation of the number of filopodia as a function of time on smooth substrates are shown.
In figure C.1, the mean number and standard deviation of the number of filopodia as a function of time on smooth (upper) and on structured substrates (lower) is depicted. Here, platelets lying on structured substrates comprise both adapted platelets and unadapted platelets. The mean number of filopodia for platelets on

smooth substrates is discussed in chapter 7. Contrasting to the mean number of filopodia over time for platelets that are adapted to the structured substrate (see figure 7.2 in chapter 7), the mean number of filopodia over time for all platelets on structured substrates is not as different from the mean number of filopodia over time on smooth substrates. However, the mean number of filopodia for all platelets on structured substrates still shows a much slower decay than for smooth substrates and shows higher standard deviations than on smooth substrates, suggesting more variety between the platelets.

The mean number and standard deviation of the number of broad, blunt protrusions as a function of time on smooth substrates (black, upper) and on structured substrates, divided into adapted platelets (middle, light blue) and unadapted platelets (lower, magenta), are shown in figure C.2. In figure C.3, the respective plots for all platelets on structured substrates (not subdivided, lower, red)

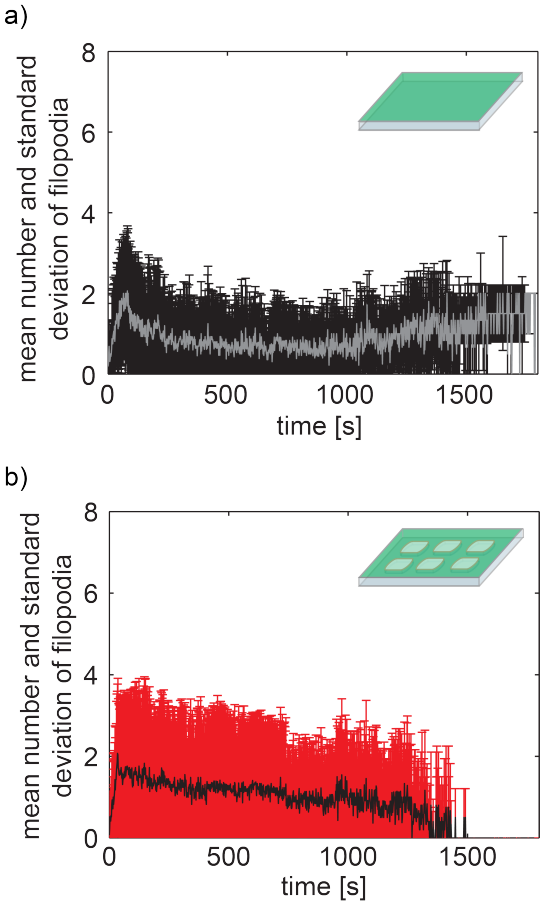

Figure C.1.: Plots showing the mean number as well as the standard deviation of the number of filopodia as a function of time for platelets lying on smooth substrates (a)) and for all platelets on structured substrates (b), adapted and unadapted platelets). The fluctuations at the end arise in all cases very likely from the reduced number of platelets contributing to these values.
a) The mean is shown in gray while the standard deviation is shown in black. The mean number of filopodia first sharply increases and then decreases over time starting from about 2 to approximately 1. The wide range of the standard deviation shows that cell behavior is not completely uniform and platelets with more or less filopodia exist.
b) The mean is shown in black while the standard deviation is shown in red. The mean number of endpoints is sharply increasing in the beginning of spreading and decays slower than on smooth substrates (a)). However, the mean number of filopodia over time is not as different from the smooth substrate as in the case of adapted platelets (see figure 7.2). The standard deviations are in general higher than for the smooth substrates in a). The higher standard deviations indicate a greater variety of filopod number than on smooth substrates.

and again for platelets on smooth substrates (upper, black) are shown. Adapted platelets on structured substrates and platelets on smooth substrates show similar mean numbers of broad, blunt protrusions of about 2. The unadapted platelets on structured substrates show higher mean numbers of broad, blunt protrusions that lie between 3 and 4.

The higher mean numbers of broad, blunt protrusions probably hint to a spreading that is governed by these broad, blunt protrusions in the case of unadapted platelets. However, also a slight adaptation can be reflected in this feature, since an alternation of slight protrusions and invaginations can lead to a higher detection of broad, blunt protrusions. If the platelets on structured substrates are not subdivided, the mean numbers of broad, blunt protrusions are more similar to that on smooth substrates. The standard deviations are similar in all cases.

The maximal distance between projected endpoints of broad, blunt protrusions shows in all three conditions - platelets on smooth substrates (black, upper), adapted platelets on structured substrates (light blue, middle) and unadapted platelets on structured substrates (magenta, lower) - a shift towards higher values for the angular direction as compared to the radial direction (see figure C.4). These differences between radial and angular direction could reflect the broad nature of the broad, blunt protrusions examined here. Adapted platelets on structured substrates show slightly higher values in radial direction than unadapted platelets on structured substrates and platelets on smooth substrates. For the angular direction, the adapted platelets show smaller values than the unadapted platelets on structured substrates and the platelets on smooth substrates. This finding can be attributed to a stronger confinement to the interspaces when platelets adapt to the underlying substrate and avoid the holes at their periphery. In table C.1 the mean numbers and standard deviations of the number of broad, blunt protrusions are summarized.

The mean angles of broad, blunt protrusions in figure C.5 show no preferred direction for this type of protrusions similar to what can be seen in figure 7.6 for filopodia.

A comparison between the quantities of broad, blunt protrusions for the different cases (smooth, structured (adapted) and structured (unadapted)) can be found in table C.2.

Table C.1.: Table summarizing the mean numbers and standard deviations of the number of broad, blunt protrusion endpoints on different substrates.
The magnitudes of the quantities in question are depicted with symbols ranging from +++ to +. The symbols serve only to visualize the relationships of the magnitudes on the different substrates and do not show the absolute values.

	$\text{structured}_{\text{adapted}}$	$\text{structured}_{\text{unadapted}}$	$\text{structured}_{\text{all}}$	smooth
mean number of broad, blunt protrusions	+ to ++	+++	++	++
standard deviation of broad, blunt protrusions	++	++	++ to +++	++

Table C.2.: Table summarizing the maximal extensions in radial and in angular direction as well as the mean angle for groups of broad, blunt protrusion endpoints on different substrates.
The magnitudes of the quantities in question are depicted with symbols ranging from +++ to ++. The symbols serve only to visualize the relationships of the magnitudes on the different substrates and do not show the absolute values.

	$\text{structured}_{\text{adapted}}$	$\text{structured}_{\text{unadapted}}$	smooth
maximal radial projection	+++	++	++
maximal angular projection	++, larger than in radial direction	+++, larger than in radial direction	+++, larger than in radial direction
angle	no preferred direction	no preferred direction	no preferred direction

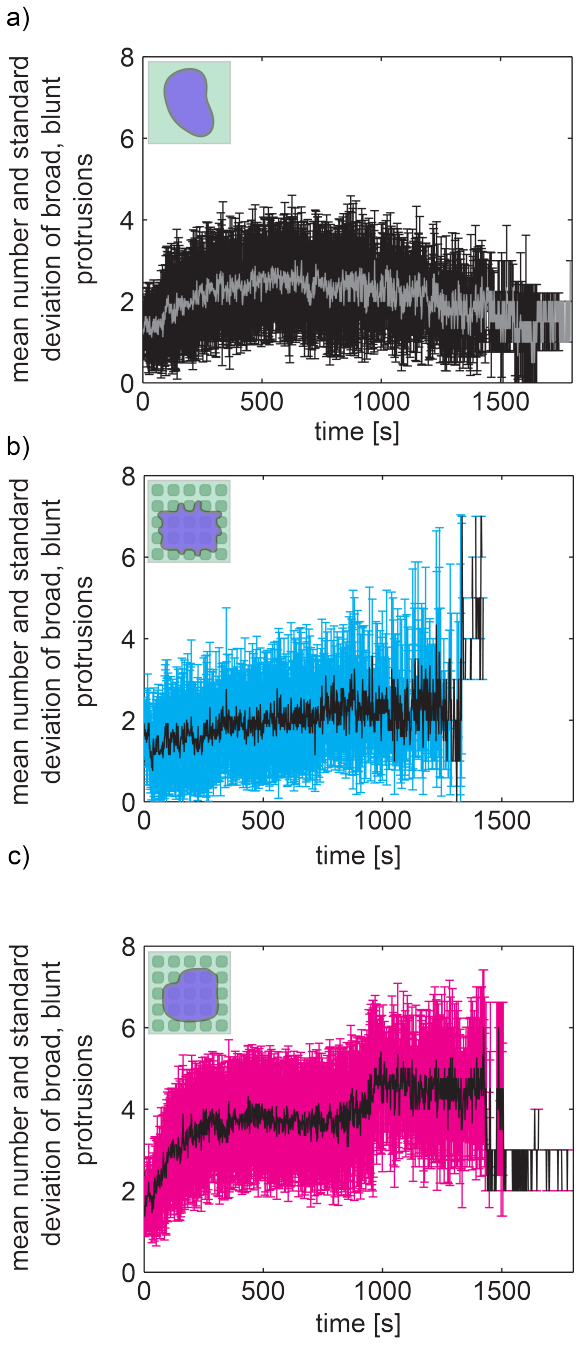

Figure C.2.: Plots showing the mean number as well as the standard deviation of the number of broad, blunt protrusions as a function of time for platelets lying on smooth substrates (a)), for adapted platelets lying on structured substrates (b)) and unadapted platelets lying on structured substrates (c)). The deviations at the late time points occur very likely due to the reduced number of platelets contributing to these values.
a) The mean number is shown in gray while the standard deviation is shown in black. The mean number of broad, blunt protrusions is about 2 and does not change strongly over time. The wide range of the standard deviation shows that cell behavior is not completely uniform and platelets with more or less broad, blunt protrusions exist.
b)The mean number is shown in black while the standard deviation is shown in light blue. The mean numbers and the standard deviations are comparable to those on smooth substrates (a)). The numbers do not change strongly except for the last time points.
c) The mean number is shown in black while the standard deviation is shown in magenta. The mean number of broad, blunt protrusions increases during the first minutes of spreading to about $3-4$. The standard deviations are comparable to those in a) and b). The second increase in mean number arises very likely from the reduced number of platelets contributing to these values.

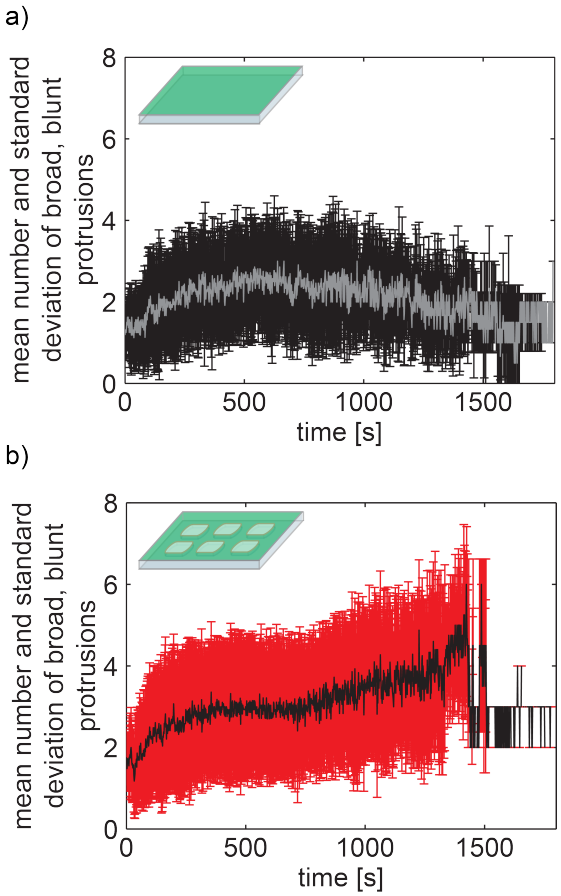

Figure C.3.: Plots showing the mean number as well as the standard deviation of the number of broad, blunt protrusions as a function of time for platelets lying on smooth substrates (a)) and for all platelets on structured substrates (b), adapted and unadapted platelets). The fluctuations at the end arise in all cases very likely from the reduced number of platelets contributing to these values.
a) The mean number is shown in gray while the standard deviation is shown in black. This plot has already been described in figure C.2.
b) The mean number is shown in black while the standard deviation is shown in red. Both, the mean numbers and standard deviations of broad, blunt protrusions of all platelets on structured substrates are similar as on smooth substrates with the mean numbers lying between 2 and 3.

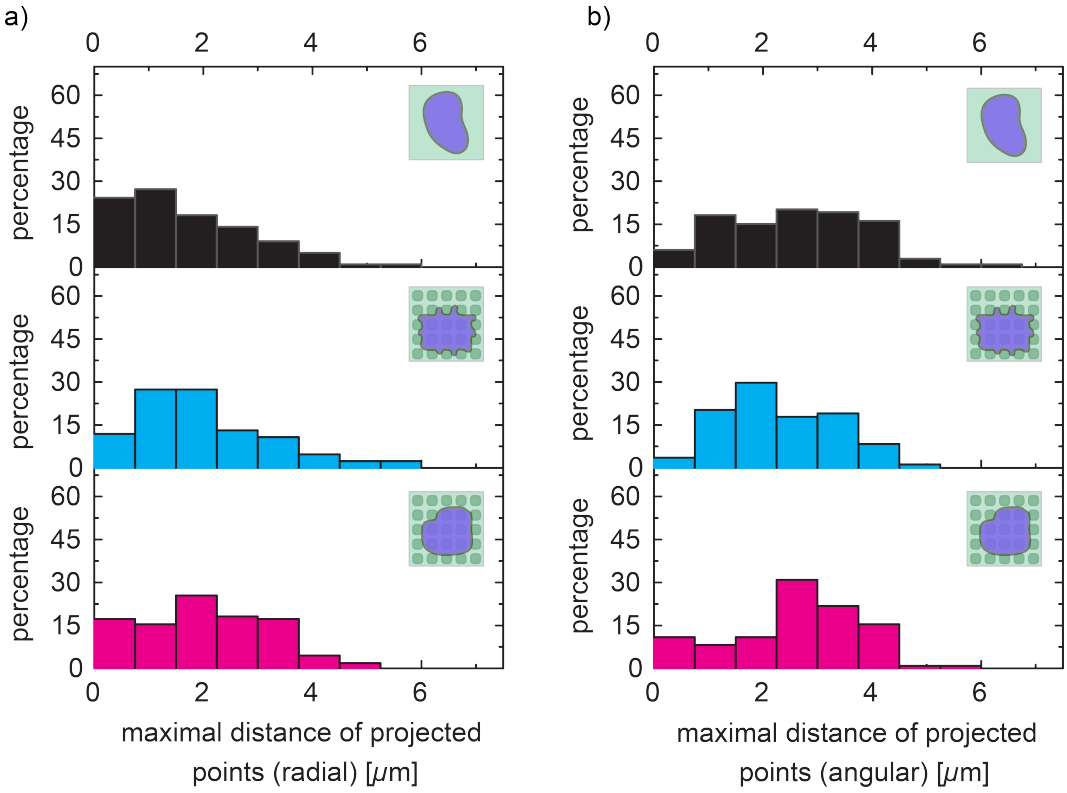

Figure C.4.: Histograms of the maximal distance between projected endpoints of broad, blunt protrusions in radial (a)) and in angular direction (b)) on smooth substrates (upper) and structured substrates (middle: adapted, lower: unadapted).
a) The maximal distances of projected endpoints in radial direction for broad, blunt protrusions do not show big differences for the three cases. For adapted platelets on structured substrates (middle), larger values are slightly more frequent than for the other two cases.
b) The maximal distances of projected endpoints in angular direction for broad blunt protrusions are slightly smaller for adapted platelets lying on structured substrates than for the other two cases. The values in angular direction are in general larger than the values in radial direction shown in a).

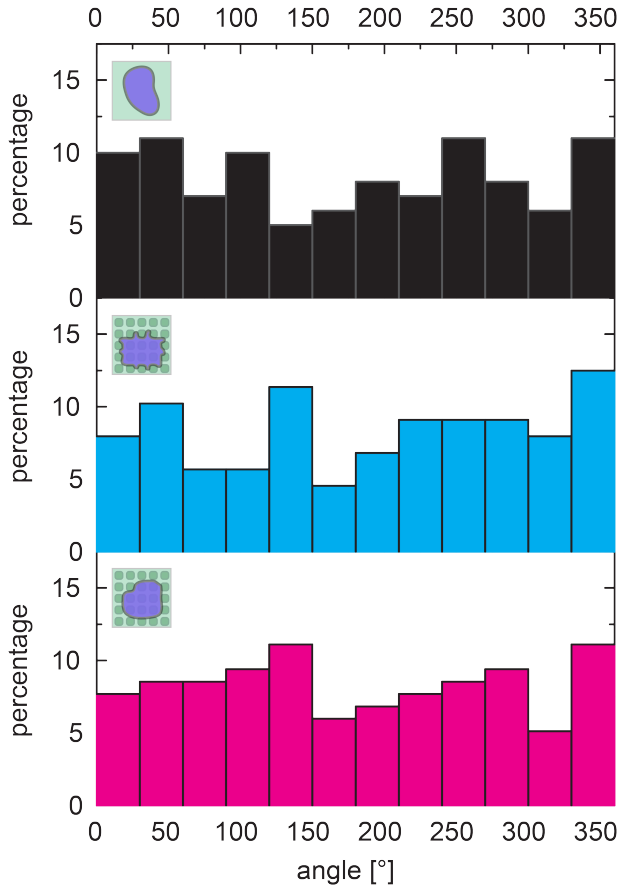

Figure C.5.: Histograms of mean angle of groups of broad, blunt protrusion endpoints for platelets on smooth (upper, black) and platelets on structured substrates (middle, light blue: adapted; lower, magenta: unadapted). Similarly to the distribution of angles of filopodia no preferred directions can be seen for neither condition. For an explanation of this behavior see chapter 7.